UNIVERSIDAD MICHOACANA DE SAN NICOLÁS DE HIDALGO

DIVISIÓN DE ESTUDIOS DE POSGRADO DE LA FACULTAD DE INGENIERÍA ELÉCTRICA

"A SECURITY BOUNDARY CONSTRAINED DIRECT CURRENT OPTIMAL POWER FLOW"

BY

MIGUEL CHÁVEZ LUGO

THESIS

REQUERIMENT FOR THE DEGREE OF

DOCTOR IN SCIENCES IN ELECTRICAL ENGINEERING

ADVISOR

CLAUDIO RUBÉN FUERTE ESQUIVELPhilosophiaeDoctorem

MORELIA, MICHOACÁN FEBRUARY 2015

Acknowledgments

I would firstly like to thank and acknowledge my advisor Prof. Claudio Rubén Fuerte Esquivel, for his support and guidance during this Ph.D. research work, but also during my master degree studies. In all our meetings he has provided appreciated attention, experience, knowledge and friendship, always encouraging me to carry out my research work.

My acknowledgment is also due to the members of the doctoral committee, for the support they provided to improve the level of this thesis report. Their valuable suggestions were very helpful to finish this thesis.

Tothe División de Estudios de Posgrado de la FIE de la UMSNH, where I hadthegreat opportunity of carrying out posgraduate studies.

I thank and acknowledge to the ConsejoNacional de Ciencia y Tecnología (CONACyT) of Mexico by the financial support received through the grant No. 218560.

Dedication

To my father

Miguel Chávez Ramírez

To my mother

Caritina Lugo Ramírez

To my sisters and brothers

Maria, Esmeralda, Pedro and Julian

Contents

Acknowledgments……i
Dedication……ii
Contents……iii
List of figures……vi
List of tables……viii
List of publications……x
Resumen……xi
Abstract……xii
Nomenclature……xiii
Acronyms……xv

1 Introduction 1

1.1 Research Motivation……1
1.2 State of the art……3
1.3 Objectives……5
1.4 Main Contribution……6
1.5 Organization of the Thesis……6

2 Theoretical concepts 8

2.1 Introduction……8
2.2 Formulation of the power system DAE model……8
2.2.1 Synchronous generator model……9
2.2.2 Excitation system model……10
2.2.3 Load model……11
2.2.4 Network power equations……12
2.3 Voltage stability……13
2.4 Feasibility region and bifurcation concepts……14
2.4.1 Equilibrium solutions and stability analysis……15
2.4.2 Saddle-node bifurcation……17
2.4.3 Limit induced bifurcation (LIB)……18

2.4.4 Hopf bifurcation……19
2.5 Numerical computation of bifurcations……..……..20
2.6 Numerical computation of the feasibility region and its boundary……..23
2.6.1 Study case …….28
2.7 Conclusions……..…….31

3 Linearization of the Feasibility Boundary 32
3.1 Introduction……...……32
3.2 Definitions…….32
3.3 Hyperplane definition…….……..33
3.4 Linear representation of the feasibilities' boundary……...……..34
3.5 Linear inequalities……...…..39
3.6 Reduction of the number of approximant hyperplanes……...39
3.7 Study cases……....41
3.7.1 IEEE 3-machine 9-bus system …….42
A. Two areas' study case: stability boundary……....42
B.1 Three areas' study case: stability boundary……..44
B.2 Three areas' study case: security boundary……..46
3.7.2 IEEE 54-machine 118-bus test system…….……48
A. Two areas study case……...48
B. Three areas study case……..……...50
3.8 Conclusions……...……52

4 Stability/security boundary-constrained DC optimal power flow 53
4.1 Introduction……..…….53
4.2 Security constrained DC-OPF…….…….....53
4.3 SBC DC-OPF nonlinear model…….55
4.4 Proposed SBC DC-OPF linear model……..….56
4.5 Study cases…….……...57
4.5.1 IEEE 3-machine 9-bus test system…….……..58

4.5.1.1 Two control areas: stability boundary…….….59
4.5.1.2 Three control areas……....61
A. Stability analysis……..…..61
B. Security analysis……..…..63
4.5.2 IEEE 54-machine 118-bus test system……..…....66
4.6 Conclusions……...69

5 Conclusions and contributions 71
5.1 Conclusions……..……..……..71
5.2 Contributions……72
5.3 Future Work…….73

A Hyperplanes' coefficients…….74
A.1 IEEE 3-machine 9-bus test system……..74
A.1.1 Two control areas……....74
A.1.2 Three control areas, stability boundary…….……..74
A.1.3 Three control areas, security boundary……..….82
A.2 IEEE 54-machine 118-bus test system……89
A.2.1 Two control areas……89
A.2.2 Three control areas…….…….90

B Critical dispatches…….……98
C IEEE 3-machine 9-bus System Data……..110
D Numerical examples illustrating the proposed linearization algorithms…..112
E IEEE 54-machine 118-bus System Data……..……..121
Bibliography……..……125

List of figures

Figure 2.1 Dynamic and static stability margin…….……14

Figure 2.2 Flowchart to obtain the feasibility boundary……..27

Figure 2.3 On-line diagram of the IEEE 3-machine 9-bus test system…….……..28

Figure 2.4 Voltage magnitude at node 4 in the (P_G+jQ_G)-parameter space (generation area A)……..….29

Figure 2.5 Voltage magnitude at node 4 in the (P_G+jQ_G)-parameter space (generation area B)……..….29

Figure 2.6 Voltage magnitude at node 4 in the (P_G+jQ_G)-parameter space (generation area C)……...29

Figure 2.7 Isolated equilibrium point of the feasibility boundary in the P_G-parameter space……..…30

Figure 2.8 Isolated equilibrium point of the feasibility boundary in the Q_G-parameter space……..……30

Figure 2.9 Stability boundary for the IEEE 9-bus system……..31

Figure 3.1 Plane through $\boldsymbol{p}$ with normal vector $\boldsymbol{\eta}$……..…….34

Figure 3.2 Hyperplane with vertices $\boldsymbol{P}_{\boldsymbol{G}_1}^{c,i}$, $\boldsymbol{P}_{\boldsymbol{G}_2}^{c,i}$ and $\boldsymbol{P}_{\boldsymbol{G}_3}^{c,i}$ ……..36

Figure 3.3 Flowchart to obtain the linearization of the feasibility boundary…….38

Figure 3.4 On-line diagram of the IEEE 3-machine 9-bus test system……..…42

Figure 3.5 Stability boundary of the IEEE 9-bus test system: two areas……...43

Figure 3.6 Approximation of stability boundary of the IEEE 9-bus test system: two areas…….……..43

Figure 3.7 Stability boundary of the IEEE 3-machine 9-bus test system: areas…….44

Figure 3.8 Absolute error with the boundary points' approximation of the IEEE 9-bus stability boundary…….……45

Figure 3.9 Absolute error with the inner product approach approximation of the IEEE 9-bus stability boundary…….……...……46

Figure 3.10 Security boundary of the IEEE 3-machine 9-bus test system: three areas...47

Figure 3.11 Absolute error with the boundary points' approximation…….47

Figure 3.12 Absolute error with the inner product approach……...…48

Figure 3.13 Security boundary of the IEEE 118-bus test system: two control areas……49

Figure 3.14 Linear approximation of the security boundary of the IEEE 118-bus test system: two control areas……..49
Figure 3.15 Security boundary of the IEEE 118-bus test system, three areas…….50
Figure 3.16 Absolute error with the boundary points' approximation of the IEEE 118-bus test system…….51
Figure 3.17 Absolute error with the inner product approach of the IEEE 118-bus test system……..51
Figure 4.1 Flowchart of the process to solve the proposed linear SBC DC-OPF model……58
Figure 4.2 Dispatch solutions for the IEEE 9-bus system: loading Case 1……..60
Figure 4.3 Dispatch solutions for the IEEE 9-bus system: loading Case 2……..60
Figure 4.4 Stability boundary and DC-OPF dispatch solutions for the IEEE 9-bus system: Case 3……62
Figure 4.5 Stability boundary and DC-OPF dispatch solutions for the IEEE 9-bus system: Case 4……62
Figure 4.6 Security boundary and DC-OPF dispatch solutions for the IEEE 9-bus system……64
Figure 4.7 Security boundary and DC-OPF dispatch solutions for the IEEE 118-bus system…….67
Figure 4.8 Security boundary and DC-OPF dispatch solutions for the IEEE 118-bus system with modified generation costs……69

List of tables

Table 3.1 Number of $\sum^{hy}$ for the IEEE 3-machine 9-bus system: stability boundary...45

Table 3.2 Number of $\sum^{hy}$ for the IEEE 3-machine 9-bus system: security boundary...46

Table 3.3 Number of $\sum^{hy}$ for the IEEE 54-machine 118-bus system $\sum$ security boundary……...…….51

Table 4.1 DC-OPF dispatch results for the IEEE 9-bus system: Case 1……..59

Table 4.2 DC-OPF dispatch results for the IEEE 9-bus system: Case 2……..59

Table 4.3 DC-OPF dispatch results for the IEEE 9-bus system: Case 3……..61

Table 4.4 DC-OPF dispatch results for the IEEE 9-bus system: Case 4……..63

Table 4.5 Linear SBC DC-OPF dispatch results for the IEEE 3-machine 9-bus system……63

Table 4.6 Security DC-OPF dispatch solutions for the IEEE 9-bus system……64

Table 4.7 Secure linear SBC DC-OPF dispatch results for the IEEE 3-machine 9-bus system……...…….65

Table 4.8 CPU times for the security-based DC-OPF models……..65

Table 4.9 CPU times for the linear SBC DC-OPF approaches…….65

Table 4.10 Linear SBC DC-OPF dispatch results for the IEEE 118-bus system……...66

Table 4.11 DC-OPF solutions for the IEEE 118-bus system……..66

Table 4.12 CPU times for the security-based DC-OPF models for the 118-bus system……....67

Table 4.13 CPU times for the linear SBC DC-OPF approaches for the 118-bus system……....67

Table 4.14 Generation costs of control areas for the IEEE 118-bus system……..68

Table 4.15 DC-OPF solutions for the IEEE 54-machine 118-bus system……..68

Table A.1 Brute force approximation for the IEEE 9-bus, stability boundary: Two control areas……..74

Table A.2 Brute force approximation for the IEEE 9-bus, stability boundary, three control areas……..74

Table A.3 Boundary points' approximation for the IEEE 9-bus, stability boundary, three control areas…….…….……81

Table A.4 Inner product reduction for the IEEE 9-bus, stability boundary, three control areas……..……82
Table A.5 Brute force approximation for the IEEE 9-bus, security boundary, three control areas…….82
Table A.6 Boundary points' approximation for the IEEE 9-bus, security boundary, three control areas…….88
Table A.7 Inner product reduction for the IEEE 9-bus, security boundary, three control areas…….89
Table A.8 Brute force approximation for the IEEE 118-bus, two control areas…….89
Table A.9 Brute force approximation for the IEEE 118-bus, three control areas..….90
Table A.10 Boundary points' approximation for the IEEE 118-bus, three control areas…….95
Table A.11 Inner product reduction for the IEEE 118-bus, three control areas……97
Table B.1 Critical dispatches for the Figure 3.4…….……..98
Table B.2Critical dispatches for the Figure 3.6……...……..…..98
Table B.3 Critical dispatches for the Figure 3.9……...……...102
Table B.4 Critical dispatches for the Figure 3.12……106
Table B.5 Critical dispatches for the Figure 3.14…….……..…..106
Table C.1 Transmission line parameters IEEE 9-bus system…….……..…110
Table C.2 Load parameters IEEE 9-bus system……..110
Table C.3 Generator parameters…….……110
Table C.4 Exciter parameters……...…110
Table C.5 Power generation bids for the IEEE 9-bus…….111
Table D.1 Hyperplane Parameters……..112
Table D.2 Boundary points……....113
Table D.3 Arrangement of hyperplanes……....116
Table D.4. Parallel vectors……..119
Table E.1 Transmission line parameters…….……121
Table E.2 Transformer parameters……..122
Table E.3 Load parameters……...……123
Table E.4 Shunt capacitors……...123
Table E.5 Power generation bids for the IEEE 118-bus……..123

List of publications

Chávez-Lugo M. and Fuerte-Esquivel C.R., "Computation of the Voltage Oscillatory Stability Boundary by a Direct Method," 2014 IEEE International Autumn Meeting on Power, Electronics and Computing (ROPEC 2014) , ISBN: 978-1-4799-2370-0, 5-7, November, 2014, Ixtapa, Gro, Mex., pp. 88-93. DOI: ()

Chavez-Lugo M., Fuerte-Esquivel C.R. and Pizano-Martínez A., "Computation of available transfer capability considering transient stability constraints," 2014 IEEE International Autumn Meeting on Power, Electronics and Computing (ROPEC 2014) , ISBN: 978-1-4799-2370-0, 5-7, November, 2014, Ixtapa, Gro, Mex., pp 29-34. DOI: ()

Chávez-Lugo, M., Fuerte-Esquivel, C. R., Cañizares, C. A., and Gutierrez-Martinez, V. J., "*Practical Security Boundary-Constrained DC Optimal Power Flow for Electricity Markets*", submitted to the **IEEE *Transactions on Power Delivery***, **ISSN 0885-897**, Manuscript ID: **TPWRS-01185-2014.R1**, at present in second review.

Resumen

Hoy en día, los sistemas de potencia están siendo operados cada vez más cerca de sus límites de control y de operación debido al incremento en la demanda de energía y a los mercados eléctricoscompetitivos, que junto con otros requerimientos regulatorios hacen más difícil la construcción de nuevas infraestructuras de transmisión. Como consecuencia, los problemas de colapso de voltaje y de inestabilidad oscilatoria de voltaje ocurren con mayor frecuencia, y han sido una de las principales causas de los apagones que han ocurrido en los Estados Unidos y Europa. Por otra parte, muchas aplicaciones en tiempo real, tales como en los mercados eléctricos de Nueva York, Nueva Inglaterra, el medio oeste de Estados Unidos y PJM, utilizan flujos óptimos de potencia (OPF) basado en corriente directa (DC) para determinar los despachos óptimos de generación. Sin embargo, ya que los OPF basados en DC no consideran las magnitudes de voltaje, no hay una manera de considerar restricciones de voltaje en la formulación de problema,tal que las unidades de generación sean despachadas de la manera más económica mientras se satisfacen los límites de todas las restricciones de seguridad de voltaje que impone el sistema.

Con base en lo anterior, esta tesis proporciona un enfoque sistemático para abordar la cuestión fundamental sobre la forma de incluir las restricciones de seguridad de voltaje en un modelo de OPF basado en DC. Una contribución de nuestra propuesta corresponde a la representación lineal de la frontera no lineal de seguridad de voltaje con base en un conjunto de hiperplanos. Finalmente, y con base a la representación lineal,se obtiene un conjunto de restricciones lineales de la frontera de seguridad de voltaje a partir del conjunto de hiperplanosaproximantes, y las restricciones resultantes se incluyen en el modelo DC-OPF.

Por último, se presentan casos de estudio para demostrar que el despacho de potencia resultante del modelo de optimización propuesto se encuentra dentro de la región segura de voltaje de operación.

Palabras clave: Flujos de potencia óptimos, frontera de seguridad, potencia de despacho.

Abstract

Nowadays, power systems are operating increasingly closer to their control and operational limits because of the increase of power demand and highly competitive electricity markets, which together with other regulatory requirements make new transmission facility construction more difficult. As a consequence voltage collapse and voltage oscillatory instability problems occur with some frequency and have been one of the primary reasons for the blackouts that have been witnessed in US and Europe. On the other hand, many real-time applications, such as several day-ahead New York, New England, Midwest, and PJM electricity markets, use a form of the direct current (DC)-based optimal power flow (OPF) to determine optimal generation dispatches. Since the DC-based OPF does not take into account voltage magnitudes, however, there is no direct way of having voltage constraints in the formulation in order to dispatch generating units in the most economical manner while keeping within bounds all the voltage security constraints imposed on the system.

Based on the mentioned above, this thesis provides a systematic approach to address the fundamental question regarding how to include voltage security constraints into a DC OPF-based model in order to avoid an operation condition where an optimal equilibrium point loses its voltage stability for small changes in system parameters. The proposed approach consists of three main stages. The first is aimed at computing the nonlinear secure region of operation and its associated boundary beyond which the system loses its voltage stability; this boundary is only represented in the generator active power-parameter space due to the fact that these powers are the main control variables in a DC-based OPF model. The second and new contribution of our proposal corresponds to the linear representation of the nonlinear voltage security boundary by an appropriate piecewise approximation based on a set of hyperplanes. Finally, the third stage consists in deriving a set of linear voltage security boundary constraints from the set of approximants hyperplanes and adding this set of constraints to the DC-OPF model.

Lastly, case studies are presented to demonstrate that the power dispatch resulting from the proposed linear security boundary-constrained DC OPF is within the voltage secure region of operation.

Keywords: Optimal power flow, security boundary, power dispatch.

Nomenclature

Sets

n_b	Number of buses in the electrical system
n_G	Number of generators
n_{dd}	Number of dispatch directions
n_{hy}	Number of hyperplanes
n_{G_A}	Number of generation control areas

Definitions

F	Feasibility region
Σ	Feasibility boundary
Σ^{hy}	Feasibility region bounded by hyperplanes
H	Hyperplane

Parameters

C_{Gi}	Cost of the *i*-th generator's bid power ($/MWh)
$P_{Gi}^{\min}$	Lower active power limit of *i*-th generator (MW)
$P_{Gi}^{\max}$	Upper active power limit of *i*-th generator (MW)
$P_{km}^{\min}$	Lower active power flow limit (MW)
$P_{km}^{\max}$	Upper active power flow limit (MW)
P_{L_k}	Active power demand at the *k*-th bus (MW)
$P_{G_{i,0}}$	Base active power of the *i*-th generator (MW)
$Q_{G_{i,0}}$	Base reactive power of the *i*-th generator (MW)
b_{km}	Susceptance of transmission element connecting buses *k* and *m* (pu)

g_{km} Conductance of transmission element connecting buses *k* and *m* (pu)

$\alpha_{km}(\ell)$ Slope of the ℓ-th segment of the piecewise linear approximation of system losses

$d_{i,k}$ *k*-th dispatch direction of the *i*-th generator (dimensionless)

Variables

P_{G_i} Dispatched active power of *i*-th generator (MW)

P_{G_k} Active power generation at the *k*-th bus (MW)

$P_{G_j}^{A_k}$ Active power produced by the *j*-th generator embedded at the *k*-th control area (MW)

$P_{G_{i,k}}^{c}$ Critical active power produced by the *i*-th generator in its *k*-th dispatch direction (MW)

$Q_{G_{i,k}}^{c}$ Critical reactive power produced by the *i*-th generator in its *k*-th dispatch direction (MVARs)

δ_k, δ_m Nodal voltage angle at buses *k* and *m* (rad)

α Generation increasing factor (dimensionless)

$\eta_{i,j}$ *j*-th element of the normal vector to its corresponding *i*-thhyperplane

C^i Constant term of *i*-thhyperplane

Acronyms

AC	Alternating Current
AVR	Automatic Voltage Regulator
BPNN	Back-Propagation Neural Network
DAE	Differential-Algebraic Equations
DC	Direct Current
DC-OPF	Direct Current Optimal Power Flow
HB	Hopf Bifurcation
LIB	Limit-Induced Bifurcation
ODE	Ordinary Differential Equations
OPF	Optimal Power Flow
SB	Security Boundary
SBC	Security Boundary-Constrained
SBC DC-OPF	Security Boundary-Constrained Direct Current Optimal Power Flow
SC-OPF	Security-Constrained Optimal Power Flow
SC DC-OPF	Security-Constrained Direct Current Optimal Power Flow
SNB	Saddle-Node Bifurcation
VSC-OPF	Voltage Stability-Constrained Optimal Power Flow

Chapter 1

Introduction

1.1 Research Motivation

Nowadays, power systems are operating increasingly closer to their control and operational limits because of the increase of power demand and highly competitive electricity markets, which together with other regulatory requirements make new transmission facility construction more difficult. As a consequence voltage collapse and voltage oscillatory instability problems occur with some frequency and have been one of the primary reasons for the blackouts that have been witnessed in US and Europe [Besanger et al., 2013]. This has led to concerns on the part of system operators regarding the secure operation of power networks, particularly in the new competitive electricity market environment.

The effect of operating so close to these limits on the overall operating costs of the power system is typically studied by formulating an optimal power flow (OPF) problem. The solution of this problem is used to dispatch generating units in the most economical manner, while satisfying operational and physical constraints of the power system; this solution, however, may not be secure, i.e. the solution does not guarantee avoiding or overcoming emergency conditions in the pre- or post-contingency operating states. Hence, the operational limits should be properly represented in a security-constrained optimal power flow (SC-OPF) problem [Martínez-Ramos and Quintana, 2009]; currently, the practice is to use constraints based on nodal power balances and the operating limits imposed by nodal voltages, branch flows, control limits, as well as power transfers over transmission corridors[Martínez-Ramos and Quintana, 2009].

In the context of electricity markets, security is measured in terms of “system congestion” levels, which have a direct effect on market transactions and electricity prices, and are represented by means of power transfer limits on main transmission corridors between operating areas. The problem with these limits is that they do not always represent

the actual security levels directly associated with the current market and system conditions. In other words, these limits are determined off-line based on system operating conditions that do not necessarily correspond to the actual dispatch scenarios, which are mostly driven by market conditions at the time of dispatch, resulting in some cases in insecure operating conditions and/or inappropriate price signals [Cañizares and Kodsi, 2006]. Therefore, the proper representation of system security in dispatch models typically used by system operators for clearing and dispatching power markets has become quite relevant [Battistelli et al., 2011].

In the context of stressed operative conditions, it is desirable to determine an optimal equilibrium point where the system remains stable after the occurrence of either a credible contingency or a small perturbation on the system parameters. Since the solution of the conventional OPF problem, however, does not guarantee this condition, diverse research has proposed different ways of incorporating stability constraints into the OPF program to obtain an equilibrium point which achieves a combined goal of economic and secure power system operative conditions.

Lastly, the two general approaches to formulate the OPF problem are based on either an AC or a DC formulation. The former is considered the "correct model" with no assumptions regarding the modeling of the electric components making up the power system. Because of its nonlinear approach, however, the optimal solution can take much longer to solve if it even reaches a solution at all. On the other hand, many real-time applications, such as several day-ahead New York, New England, Midwest, and PJM electricity markets, use a form of the DC-based OPF, which neglects resistance, reactive power and voltage magnitudes, but results in a linear optimization problem that is solved more quickly and more reliably than the AC-based OPF. Since the DC-based OPF does not take into account voltage magnitudes, however, there is no direct way of having voltage constraints in the formulation in order to dispatch generating units in the most economical manner while keeping within bounds all the voltage security constraints imposed on the system.

Based on the aforementioned, this work proposes a representation of voltage collapse and voltage oscillatory stability constraints within the DC-OPF formulation based on the concept of security boundary constraints (SBC). In this case, an accurate voltage

stability/security boundary that separates stable and unstable operating points is computed based on an AC continuation power flow and is linearized by a set of hyperplanes that can be readily used as linear constraints in the DC-OPF formulation. In this case, the voltage stability/security boundary is represented in terms of the generators' active power, such that constraining the active power dispatch in the DC-OPF model acts like this model has voltage constraints. This is a novel idea that has not previously been proposed to the best of the author's knowledge.

1.2 State of the art

Several approaches to properly represent the system security in OPF models have been proposed in the literature [Stott et al., 1987], the objective is to obtain an optimal security-constrained dispatch that assures a feasible operation of the power system. In this context, a comprehensive survey of different models and solution techniques used for the SC-OPF problem from the early 1960s to 2009 is reported in [Bhaskar et al., 2011].The simplest formulations extend the conventional OPF approach by adding a set of steady-state security constraints, such as limits on branch currents and voltage magnitudes, properly modified for each credible contingency considered in the study [Alsac and Stott, 1974]. This formulation, referred to as the security-constrained optimal power flow (SC-OPF) problem, can be classified within the context of preventive and/or corrective control actions [Monticelli et al., 1987]. The theoretical difference between these two sets of control actions stems from the fact that the former does not consider the possibility of adjustments in control variables, other than the automatic ones, in the post-contingency states.

Despite the fact that the solution of the SC-OPF problem gives a secure operating condition, it provides no information of an explicit measure of the system security margin with respect to stability problems [Chattopadhyay and Deqiang, 2000], [Gan et al., 2000],[Milano et al., 2005] and [Rosehart et al., 1999], with the voltage stability problem being one of the major security concerns for today's electric power system operation [Besanger et al., 2013]. In order to overcome this drawback, the SC-OPF has been reformulated as a voltage-stability-constrained OPF (VSC-OPF) by adding one stability constraint derived from a selected voltage stability index, which quantifies how close the

current operating point is to voltage instability [Avalos et al., 2008],[Cañizares et al., 2001]and [Rosehart et al., 1999]. This index, however, should be algebraically realizable in order to be included in gradient-based optimization methods used to assess the optimal security-constrained dispatch. In [Cañizares et al., 2001], the authors propose the use of a new index to also account for oscillatory stability. These indices, however, represent only one single stress direction corresponding to the dispatch being computed.

In the present restructured power systems, competition between electricity market participants increases the number of possible energy transactions, resulting in different load and generation patterns which can aggravate stability problems caused by high active power transfers or insufficient reactive power supply, by increasing thermal overload and voltage instability issues in power systems. Hence, an alternative approach to achieve a proper representation of the voltage system security in this operative context consists of characterizing the entire voltage stability region in the dispatch spacethat properly represents multiple load and/or generation patterns [Gu and Cañizares, 2007], [Gutierrez-Martinezet al., 2011] and then representing the stability boundary by means of a differentiable function to be included as a constraint in the OPF approach. This alternative allows the secure power system operation, as proposed in [Gutierrez-Martinezet al., 2011]. In this formulation, a back-propagation neural network (BPNN) is used to represent the system security boundary (SB), and an explicit differentiable function is extracted from the BPNN to be used as the voltage stability constraint, allowing a secure power system operation.

In order to avoid the time-consuming iteration process of solving nonlinear AC OPF models, which may not even yield adequate solutions, a common practice in competitive electricity markets is to adopt DC formulations, which have the advantage of simplicity and robustness in the solution algorithm to obtain the optimal market dispatch [Cañizares and Kodsi, 2006], [Stott and Alsac, 2012]. In this case,system security is introduced via limits on certain optimization variables and iterative procedures to account for the system nonlinearities [Cañizares and Kodsi, 2006]. On the other hand, since each participant in the electricity market has its own interests, no attention is given to the system security. Thus, the independent system operator has the key role of maintaining the system security and must perform the market clearing based on a security-constrained DC-OPF (SC DC-OPF)

based dispatch model.

A typical SC DC-OPF dispatch model only imposes active power transfer constraints on transmission lines, which certainly have the most impact on active power dispatch. Since these limits, however, are determined from off-line studies that do not necessarily correspond to the actual operative system conditions, which may result in unrealistic generation dispatches and thereby jeopardize system security[Cañizares and Kodsi, 2006]. Therefore, how to include additional constraints into the SC DC-OPF dispatch model is an important issue to be investigated. In this context, typical single- and multi-period SC DC-OPF dispatch models were extended in [Battistelli et al., 2011] by including the security boundary constraint (SBC) proposed in [Gutierrez-Martinezet al., 2011]. Since this constraint, however, is a nonlinear function of the system variables, the resulting SBC dispatch model is nonlinear, introducing nonlinearities into the SC DC-OPF. For this reason, the main motivation of this Thesis is to obtain a proper and novel linear representation of the security/stability boundaries, which can be readily introduced as a linear constraint in the SC DC-OPF dispatch model.

1.3 Objectives

The main objective of the present work is to provide a systematic approach to address the fundamental question regarding how to include security boundaries associated with system voltage stability into a security-constrained DC-OPF-based model.

In order to achieve this main objective, the following goals must to be accomplished:

- To establish a procedure to compute the voltage stability/security boundary in the P_G-parameter space for different dispatch directions.

- To obtain a proper and adequate piecewise linear representation of the stability/security boundary based on the use of hyperplanes.

- To derive from the piecewise linear approximation of the stability/security boundary a set of linear inequality security/stability constraints that can directly be included into a proposed voltage security-constrained DC-OPF dispatch model

- To reduce the dimension of the proposed voltage security-constrained DC-OPF dispatch model.

- To prove the effectiveness and feasibility of the proposed voltage security-constrained DC-OPF dispatch model.

1.4 Main Contribution

The main contribution of this thesis is to obtain a proper and novel linear representation of the security/stability boundaries, which can be readily introduced as a linear constraint in a SC DC-OPF dispatch model.

The proposed SBC DC-OPF linear dispatch approach consists of three main stages. The first is aimed at computing the nonlinear feasibility region and its associated boundary considering voltage and small-perturbation angle stability, as previously proposed by several researchers. The second and new contribution of our work corresponds to the linear representation of the nonlinear boundary by an appropriate piecewise approximation based on a set of hyperplanes. Finally, the third consists of adding a set of linear feasibility boundary constraints to the DC-OPF model, thus converting it into the proposed, novel and practical linear SBC DC-OPF model.

1.5 Organization of the Thesis

To the best of the author's knowledge, the proposed idea reported in Chapter 1 had not been explored before this work was developed. The proposed approach is detailed in the rest of this thesis, which is structured as follows.

Chapter 2 presents the mathematical models of the electric power system components to be considered in this work. The formulations to integrate these models in a

single frame of reference as well as the unified solution of the resulting set of differential-algebraic equations are also presented. Lastly, theoretical concepts of bifurcation theory, the application of these concepts to obtain stability/security boundaries and the numerical computation of these boundaries are detailed.

Chapter 3 details the procedure for the linear approximation of the security/stability boundaries, along with two proposed approaches to reduce the number of hyperplanes used in this approximation. The proposed procedure is applied to the analysis of a benchmark IEEE power system.

Chapter 4 discusses two relevant security-constrained OPF dispatch models, and the proposed SBC DC-OPF linear model is also formulated. Furthermore, discussions and comparisons based on the results obtained from the implementation and application of the proposed linear SBC DC-OPF to the IEEE 3-machine 9-bus system and the IEEE 54-machine 118-bus system are presented.

Finally, the main conclusions and contributions of this paper are summarized in Chapter 5.

Chapter 2

Theoretical concepts

2.1 Introduction

This chapter reports the mathematical models of the electric power components to be considered in this thesis. The main concepts of the bifurcation theory are also reviewed in order to establish the existing relation between codimension-1 bifurcations and the occurrence of voltage stability problems in electric power systems. Based on the bifurcation theory, the procedure to compute bifurcation points based on the equilibrium analysis of electric power systems is also detailed. Lastly, the concepts of feasibility region and boundary are reported in detail as well as their numerical computation process based on the continuation method.

2.2 Formulation of the power system DAE model

An electric power system can be represented by a set of time-independent parameterized differential equations constrained by a set of algebraic equations (DAEs), as given by (2.1) [Venkatasubramanian et al., 1995]:

$$\begin{aligned} \dot{\boldsymbol{x}} &= \boldsymbol{f}(\boldsymbol{x}, \boldsymbol{y}, \boldsymbol{\rho}, \boldsymbol{\lambda}) \\ \mathbf{0} &= \boldsymbol{g}(\boldsymbol{x}, \boldsymbol{y}, \boldsymbol{\rho}, \boldsymbol{\lambda}) \end{aligned}, \tag{2.1}$$

where $\boldsymbol{x} \in \Re^{n_x}$ is the vector of dynamic state variables governing the dynamics of generators and controls; $\boldsymbol{y} \in \Re^{n_y}$ is the vector of instantaneous (or algebraic) state variables resulting from neglecting fast dynamics, such as network nodal voltages; $\boldsymbol{\rho} \in \Re^{n_\rho}$ are a set of "controllable" parameters associated with control settings, such as automatic voltage regulator set points; and $\boldsymbol{\lambda} \in \Re^{n_\lambda}$ stands for "uncontrollable parameters" whose quasi-static variation modifies the system's equilibrium point and can lead to an operational scenario where voltage stability is lost. For the purpose of this work, the active and reactive power loads are slowly changed by a loading parameter λ to generate different operating scenarios. Since the transmission network dynamics are much faster than the dynamics of the equipment, it is considered that the variables ***y*** are considered to instantaneously change

with variations of the $\boldsymbol{x}$ states. Hence, only the dynamics of the equipment, e.g. generators and controls, are explicitly modeled by the set of ordinary differential equations in (2.1). Based on the mentioned above, the generator mechanical dynamics, control devices and dynamic loads are represented by the set of ordinary differential equations $\dot{\boldsymbol{x}} = \boldsymbol{f}(\boldsymbol{x}, \boldsymbol{y}, \boldsymbol{\rho}, \boldsymbol{\lambda})$ $\boldsymbol{f} : \Re^{n_x+n_y+n_\rho+n_\lambda} \to \Re^{n_x}; (\boldsymbol{x}, \boldsymbol{y}, \boldsymbol{\rho}, \boldsymbol{\lambda}) \mapsto \boldsymbol{f}(\boldsymbol{x}, \boldsymbol{y}, \boldsymbol{\rho}, \boldsymbol{\lambda})$, while algebraic equations $\boldsymbol{0} = \boldsymbol{g}(\boldsymbol{x}, \boldsymbol{y}, \boldsymbol{\rho}, \boldsymbol{\lambda})$ $\boldsymbol{g} : \Re^{n_x+n_y+n_\rho+n_\lambda} \to \Re^{n_y}; (\boldsymbol{x}, \boldsymbol{y}, \boldsymbol{\rho}, \boldsymbol{\lambda}) \mapsto \boldsymbol{g}(\boldsymbol{x}, \boldsymbol{y}, \boldsymbol{\rho}, \boldsymbol{\lambda})$ represent the machines' stator algebraic equations and mismatch AC power flow equations at each nodein addition to restricting the dynamic trajectory of the system in phase space.

2.2.1 Synchronous generator model

The two-axis model describing the synchronous machine dynamics is adopted in this work, where the stator transients are neglected, and the rotor is represented via a direct (*d*) and quadrature (*q*) magnetic axes. This model considers a field and a damper winding on the *d*-axis as well as a damper winding on the *q*-axis.

Four differential equations are used to represent the generator's rotor dynamic performance. Two equations are related to the rotor angle and angular speed, which are referred to as swing equations; the other two equations, though, are related to the two electrical systems on the *d-q* axes and depend on the two internal voltages [Sauer and Pai, 1988]. The rotor mechanical model is given by

$$\dot{\delta}_i = (\omega_i - \omega_m)\omega_0 \qquad i = 1,...,m-1 \tag{2.2}$$

$$\dot{\omega}_i = M_i^{-1}\left[P_{m_i} - D_i(\omega_i - \omega_m) - \left(E'_{q_i} - X'_{d_i} I_{d_i}\right) I_{q_i} - \left(E'_{d_i} + X'_{q_i} I_{q_i}\right) I_{d_i}\right] \quad i = 1,...,m, \tag{2.3}$$

and the equations of the two electrical systems of the rotor are

$$\dot{E}'_{q_i} = T_{d0_i}^{-1}\left[E_{fd_i} - E'_{q_i} - \left(X_{d_i} - X'_{d_i}\right) I_{d_i}\right] \quad i = 1,...,m, \tag{2.4}$$

$$\dot{E}'_{d_i} = T_{d0_i}^{-1}\left[-E'_{d_i} + \left(X_{q_i} - X'_{q_i}\right) I_{q_i}\right] \quad i = 1,...,m, \tag{2.5}$$

where the rotor angle of the *m-th* generator is chosen as the system reference. Furthermore, *m* is the number of generators. In equations (2.2)-(2.5) all variables are given in per unit,

unless it is specified otherwise. Hence, $\delta_i$is the *i-th* generator's rotor angle in electrical radians (rad), M_i is the machine inertia constant, ω_i is the actual angular speed of the *i-th* generator, $\omega_m$is the system frequency, ω_0 is the system rated frequency, generally the synchronous speed, P_{m_i} is the input mechanical power of the *i*-th generator, and D_i is the machine damping constant. The set of variables associated with the *d*-axis and *q*-axis, respectively, are the transient internal voltage magnitudes E'_{d_i} and E'_{q_i}, the stator currents I_{d_i} and I_{q_i}, open-circuit time constants T_{d0} and T_{q0}, synchronous steady-state reactances X_d and X_q, and synchronous transient reactances X'_d and X'_q.

From a physical generator's design viewpoint, the stator represents the coupling between the generator and the electrical network, with the stator currents I_{d_i} and I_{q_i} being the corresponding stator algebraic variables. Hence, the stator voltage and power expressions depend on generator dynamic variables as well as the stator and electrical network algebraic variables. Based on the information mentioned above, the machines' stator algebraic equations, which are the interface of the machine's internal voltage to the network's nodal voltage at the machine´s terminals, are given by

$$E'_{q_i} = V_i \cos\left(\delta_i - \theta_i\right) + R_{s_i} I_{q_i} + X'_{d_i} I_{d_i} \quad i = 1,...,m \tag{2.6}$$

$$E'_{d_i} = V_i \sin\left(\delta_i - \theta_i\right) + R_{s_i} I_{d_i} - X'_{q_i} I_{q_i} \quad i = 1,...,m, \tag{2.7}$$

where R_{s_i} is the machine's armature resistance. Moreover, V_i and θ_i are the voltage magnitude and angle at the terminals of the *i-th* machine, respectively. Note that V_i and θ_i also correspond to the voltage at the *i-th* node of the electrical network.

2.2.2 Excitation system model

The simplified IEEE type DC-1 excitation system [Kundur, 1994] is used in this work. The corresponding mathematical model is as follows:

$$\dot{E}_{fd_i} = T_{e_i}^{-1}\left[V_{r_i} - \left(K_{e_i} + S_{e_i}\left(E_{fd_i}\right)\right)E_{fd_i}\right] \quad i = 1,...,m \tag{2.8}$$

$$\dot{V}_{r_i} = T_{a_i}^{-1}\left[-V_{r_i} + K_{a_i}\left(V_{ref_i} - V_i - R_{f_i}\right)\right] \quad i = 1,...,m \tag{2.9}$$

$$\dot{R}_{f_i} = T_{f_i}^{-1}\left[-R_{f_i} - \left(K_{e_i} + S_{e_i}\left(E_{fd_i}\right)\right)K_{f_i}E_{fd_i}/T_{e_i} + K_{f_i}V_{r_i}/T_{e_i}\right] \quad i = 1,...,m, \tag{2.10}$$

where V_{ref_i} is the reference voltage of the automatic voltage regulator (AVR); V_{r_i} and R_{f_i} are the outputs of the AVR and exciter soft feedback, respectively, E_{fd_i} is the DC-controlled voltage applied to the generator's field winding, and T_{a_i}, T_{e_i} and T_{f_i} are the AVR, exciter and feedback time constants. In addition, K_{a_i}, K_{e_i} and K_{f_i} are gains associated with the AVR, exciter and feedback, respectively. Lastly, V_i refers to the voltage at the *i-th* generator terminal

2.2.3 Load model

The load dynamic response is an important mechanism when power system voltage stability is assessed. In this context, load modeling is a difficult problem because the accurate composition of load is not only difficult to estimate, but also changes depending on many factors including time and weather conditions among others. In the analysis of an electric power system, load models can be represented as a constant complex power model, a constant current model, or a constant impedance model. Nevertheless, when the analysis is focused on the computation of stability/security regions, the use of a constant complex power model for representing the system load is completely accepted. The mathematical representation of this type of load model is given by [Gutiérrez-Martínez, 2011-1]:

$$\overrightarrow{S_d} = P_d + jQ_d, \tag{2.11}$$

where

$$P_d = \lambda P_{d0} \tag{2.12}$$

$$Q_d = \lambda Q_{d0}, \tag{2.13}$$

and P_{d0} and Q_{d0} are the active and reactive base power demands at each system bus, respectively. Finally, λ is a loading parameter that represents the active and reactive power

demands increases that can drive the system to an unstable operative scenario from the voltage stability viewpoint.

2.2.4 Network power equations

The structure preserving model of the electric network is formulated based on the concept of power flow balance at all network nodes. The active and reactive power flow mismatch equations that represent a steady-state network operation of a system with *n* buses and *m* synchronous machines are

$$\begin{aligned} P_{g_i} - \lambda P_{d0i} - P_{inj_i} &= 0 \quad i = 1,...,m \\ -\lambda P_{d0i} - P_{inj_i} &= 0 \quad i = m+1,...,n \end{aligned} \tag{2.14}$$

$$\begin{aligned} Q_{g_i} - \lambda Q_{d0i} - Q_{inj_i} &= 0 \quad i = 1,...,m \\ -\lambda Q_{d0i} - Q_{inj_i} &= 0 \quad i = m+1,...,n \end{aligned}, \tag{2.15}$$

where

$$P_{inj_i} = \sum_{k=1}^{n} V_i V_k Y_{ik} \cos\left(\theta_i - \theta_k - \alpha_{ik}\right) \quad i = 1,...,m,m+1,...,n \tag{2.16}$$

$$Q_{inj_i} = \sum_{k=1}^{n} V_i V_k Y_{ik} \sin\left(\theta_i - \theta_k - \alpha_{ik}\right) \quad i = 1,...,m,m+1,...,n \tag{2.17}$$

$$P_{g_i} = I_{d_i} V_i \sin\left(\delta_i - \theta_i\right) + I_{q_i} V_i \cos\left(\delta_i - \theta_i\right) \quad i = 1,...,m \tag{2.18}$$

$$Q_{g_i} = I_{d_i} V_i \cos\left(\delta_i - \theta_i\right) - I_{q_i} V_i \sin\left(\delta_i - \theta_i\right) \quad i = 1,...,m \tag{2.19}$$

where Y_{ik} and α_{ik} are the admittance magnitude and phase angle of the transmission element connecting buses *i* and *k,* respectively. Furthermore, P_{g_i} and Q_{g_i} are the generator output powers and P_{inj_i} and Q_{inj_i} are the powers injected into the network at bus *i*. P_{d_i} and Q_{d_i} are the active and reactive load powers at bus *i*; note that (2.14) and (2.15) are generic in the sense that they are used for all of the buses.

2.3 Voltage stability

Generally speaking, voltage stability refers to the ability to control the steady voltages along the transmission network within a narrow band around nominal operating voltages. This control is accomplished by adjusting key network parameters, such as mechanical input power, electrical load and controllers' settings, in order to keep the power system operating at a stable equilibrium point; however, as this point is continuously moving in the parameter space, it may then become unstable for some critical parameter values [Taylor, 1994]. Hence voltage instability occurs in power systems when the system is unable to maintain an acceptable voltage profile under an increasing load demand and/or configuration changes.

Voltage stability problems associated with both voltage collapse and poor damping of voltage magnitude oscillations have been of major concerns to engineers in charge of the planning and operation of power systems. These instability problems have lead to major disruptions in power systems operation, such as the blackouts that occurred in August 1996 in the WSCC system, August 2003 in the Northeast system, September 2003 in the Sweden and Italy systems and November 2006 from Germany to Spain systems [Besanger et al., 2013]. Hence, the identification of both voltage collapse and voltage oscillatory stability is of great interest for power system dispatchers. In this context, bifurcation theory provides a natural framework for studying the mechanisms associated with these phenomena [Van Cutsem and Vournas, 2008]. Bifurcation theory predicts how the system equilibrium points become unstable due to quasi-static changes of system parameters. Depending on the generic model of the power system, three major local bifurcations have been directly related to a monotonic voltage collapse and voltage oscillatory instabilities, namely saddle-node bifurcation (SNB), limit-induced bifurcation (LIB) and Hopf bifurcations, respectively.

Voltage collapse is the process by which the voltage magnitude at some buses falls to a low, unacceptable value as a result of an avalanche of events accompanying voltage instability [Taylor, 1994]. Voltage collapse is classified as a static phenomenon mathematically related to a SNB or a LIB induced by a violation of operational limits, during which the system equilibrium disappears as system parameters, mostly system load,

change slowly [Illic and Zaborsky, 2000], [Taylor, 1994], [Van Cutsem and Vournas, 2008]. Hence, from a physical viewpoint, at voltage collapse the system loses the ability to supply enough power to a heavily loaded network. On the other hand, voltage oscillatory instability refers to the periodic oscillation of the voltage magnitude at some nodes for a given operating condition and is mathematically related to a Hopf bifurcation [Hassard et al., 1981], which connects equilibrium with periodic motions. Voltage oscillatory instability is a dynamic phenomenon where the stability of the system's equilibrium point can be lost before reaching the voltage collapse point (SNB), as shown in Figure 2.1.

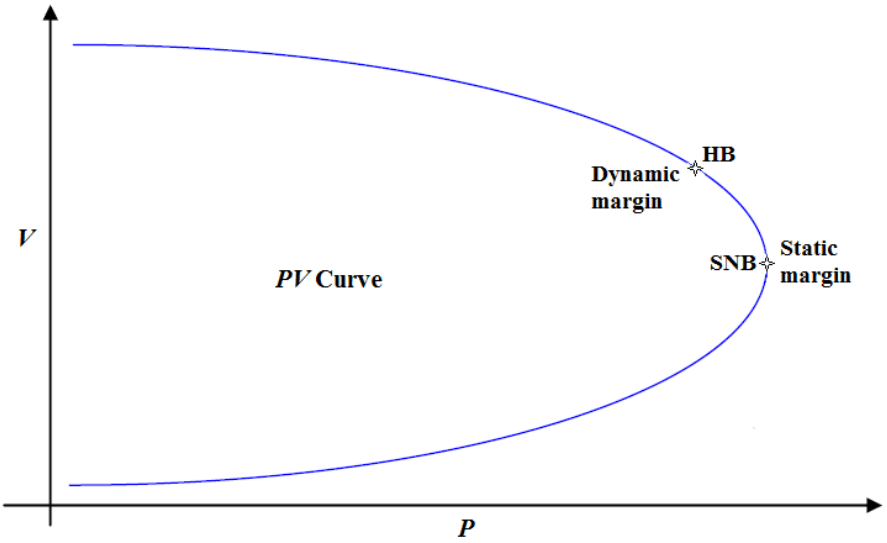

Figure 2.1.Dynamic and static stability margin.

2.4 Feasibility region and bifurcation concepts

In the real-life operation of power systems, the knowledge of the parameter space region where all equilibrium points that can be reached by a continuous slow variation of system parameters are asymptotically stable, referred to as the feasibility region [Venkatasubramanian et al., 1995], is of paramount importance. Similarly, the boundary location of this region in the parameter space must be known in order to avoid an operation condition where an equilibrium point becomes unstable for small changes in system parameters. In this context, bifurcation theory provides a natural framework for studying the mechanisms associated with the loss of stability of equilibrium points in the vicinity of the feasibility region boundary [Venkatasubramanian et al., 1995].

Bifurcation theory is the study of qualitative changes that occur in the system's structural properties because of system parameters' variations [Nayfeh and Balachandran, 1995], and it is an important issue in the theory of nonlinear systems. A qualitative change in the system's structural properties could mean a change in the stability of the original system. In other words, solutions of the system bifurcate at critical values of parameters at which stability may be lost or gained. The parameter values at which bifurcations take place are called bifurcation points. Unlike linear systems, where closed-form solutions can be expressed in terms of the system's eigenvalues and eigenvectors, few nonlinear systems possess closed-form solutions. The bifurcation approach, however, allows the understanding of the qualitative behavior of nonlinear systems and their change of stability properties under quasi-static variations of system's parameters.

In the context of electric power systems, bifurcation analysis is related to the emergence of sudden changes in a power system's response arising from smooth, continuous variations on system parameters. The bifurcation events are classified as local and global bifurcations. The former, which are the purpose of study in this work, are those related to qualitative changes occurring in the neighborhood of an equilibrium point or limit cycle, such that equilibrium points or limit cycles appear, disappear or change their stability. Therefore, qualitative changes in the power system behavior can be obtained by the equilibrium point's stability.

2.4.1 Equilibrium solutions and stability analysis

Equilibrium analysis is the first step in determining local stability and bifurcations of the power system near an equilibrium point. For an arbitrary fixed set of parameters $\{\boldsymbol{\rho}, \boldsymbol{\lambda}\} \in \boldsymbol{\beta}$, the constrained system (2.1) possesses equilibrium in an open connected set $F_{EQ} \subseteq \Re^{n_x} \times \Re^{n_y} \times \Re^{n_\rho} \times \Re^{n_\lambda}$ if $\exists (\boldsymbol{x}^*, \boldsymbol{y}^*, \boldsymbol{\beta}^*) \in X \times Y \times B$, such that $\boldsymbol{f}(\boldsymbol{x}^*, \boldsymbol{y}^*, \boldsymbol{\beta}^*)=0$ and $\boldsymbol{g}(\boldsymbol{x}^*, \boldsymbol{y}^*, \boldsymbol{\beta}^*)=0$ [Hill and Mareels, 1990]. Furthermore, for a safe operation of the power system, it must operate in a feasibility region F, $F \subseteq F_{EQ}$, where equilibrium remains asymptotically stable forsmall changes of parameters [Venkatasubramanian et al., 1995]. This region is bounded by a feasibility boundary Σ at which the system equilibrium points change their stability properties [Venkatasubramanian et al., 1995]. The most essential fact

about this boundary is that it is composed of a set of equilibrium points, referred to as bifurcation points, associated with the appearance of one of the three types of codimension-1 generic local bifurcations, namely SNB, HB or LIB, which cause the loss of voltage stability [Venkatasubramanian et al., 1995]. Based on this characteristic, the concepts of bifurcation theory have been applied for the direct computation of the feasibility boundary.

For slowly varying parameters $\boldsymbol{\beta}$, the DAE system (2.1) can be linearized around an isolated equilibrium point E_p, which results in

$$\begin{bmatrix} \Delta\dot{\boldsymbol{x}} \\ \mathbf{0} \end{bmatrix} = \underbrace{\left[\begin{array}{cc} \dfrac{\partial \boldsymbol{f}(\cdot)}{\partial \boldsymbol{x}} & \dfrac{\partial \boldsymbol{f}(\cdot)}{\partial \boldsymbol{y}} \\ \dfrac{\partial \boldsymbol{g}(\cdot)}{\partial \boldsymbol{x}} & \dfrac{\partial \boldsymbol{g}(\cdot)}{\partial \boldsymbol{y}} \end{array}\right]_{E_p}}_{J_{DAE}} \begin{bmatrix} \Delta\boldsymbol{x} \\ \Delta\boldsymbol{y} \end{bmatrix} = \underbrace{\left[\begin{array}{cc} \boldsymbol{f}_x(\cdot) & \boldsymbol{f}_y(\cdot) \\ \boldsymbol{g}_x(\cdot) & \boldsymbol{g}_y(\cdot) \end{array}\right]_{E_p}}_{J_{DAE}} \begin{bmatrix} \Delta\boldsymbol{x} \\ \Delta\boldsymbol{y} \end{bmatrix}, \tag{2.20}$$

where J_{DAE} is the unreduced Jacobian matrix of the DAEs.

The small-signal stability of an E_p associated with a DAEs system is thoroughly discussed in [Hill and Mareels, 1990], where it is shown that if E_p is away from the singular set $S_s = \left\{(\boldsymbol{x}, y, \boldsymbol{\beta}) \in X \times Y \times B : \det\left(\boldsymbol{g}_y\big|_{E_P}\right) = 0\right\}$, which means that $\boldsymbol{g}_y$ has constant full rank on F_{EQ}, the system (2.20) can be locally reduced to a set of ordinary differential equations (ODEs), with the same dynamic and algebraic properties as the DAEs model. In this case, the ODE system equivalent to (2.20) is derived from the implicit function [Van Cutsem and Vournas, 2008], which results in (2.21); futhermore the well-known stability theory of nonlinear dynamical systems described by nonlinear ODEs can directly be applied to assess the stability properties of a DAE system´s equilibrium point

$$\begin{aligned} \dot{\boldsymbol{x}} &= \boldsymbol{f}_e(\boldsymbol{x}, \boldsymbol{\psi}(\boldsymbol{x}, \boldsymbol{\rho}, \boldsymbol{\lambda}), \boldsymbol{\rho}, \boldsymbol{\lambda}) \\ &= \boldsymbol{f}_e(\boldsymbol{x}, \boldsymbol{\psi}(\boldsymbol{x}, \boldsymbol{\beta}), \boldsymbol{\beta}) \end{aligned} \quad . \tag{2.21}$$

Hence, for an $E_p \notin S_s$, the linearized equivalent ODE model is obtained from Schur's theorem [Van Cutsem and Vournas, 2008] and it is given by

$$\Delta\dot{\boldsymbol{x}} = \left[\boldsymbol{f}_x(\cdot) - \boldsymbol{f}_y(\cdot)\boldsymbol{g}_y^{-1}(\cdot)\boldsymbol{g}_x(\cdot)\right]_{E_p} \Delta\boldsymbol{x} = \boldsymbol{J}_{RS}\big|_{E_p} \Delta\boldsymbol{x} \,. \tag{2.22}$$

According to the Lyapunov stability theory of ODEs, the eigenvalue analysis of the reduced Jacobian $\boldsymbol{J}_{RS}\big|_{E_p}$ will give small-signal stability information about the current equilibrium point E_p under small disturbances. In this case, E_p is stable if all eigenvalues of the reduced Jacobian $\boldsymbol{J}_{RS}\big|_{E_p}$ have negative real parts, $\boldsymbol{\lambda}(\boldsymbol{J}_{RS}\big|_{E_p}) \subset \mathbb{C}^-$, and the set of equilibrium points composing the feasibility region F is then given by $OP = \left\{ (\boldsymbol{x}, y, \boldsymbol{\beta}) \in X \times Y \times B : \quad EQ \notin S_s \ , \ \boldsymbol{\lambda}(\boldsymbol{J}_{RS}\big|_{E_p \in EQ}) \subset \mathbb{C}^- \right\}$. Furthermore, those eigenvalues indicate the appearance of bifurcation points when one of the following conditions are satisfied: (i) $\boldsymbol{g}_y$ is singular or (ii) $\boldsymbol{J}_{RS}\big|_{E_p}$ has eigenvalues crossing the imaginary axis in the complex plane $\mathbb{C}$. The set of bifurcation points where the former condition is satisfied belongs to LIBs which take place when some eigenvalues diverge to infinity. On the other hand, the second condition occurs when the equilibrium has zero eigenvalues which correspond to the set of SNBs or purely imaginary but nonzero eigenvalues for bifurcation points composing the set of HBs. Therefore, the feasibility boundary is composed of the manifolds of SNBs, HBs and LIBs, where the electric power system becomes unstable as follows [Venkatasubramanian et al., 1995]:

$$\Sigma = \left(\Sigma \cap W^{SNB}\right) \cup \left(\Sigma \cap W^{HB}\right) \cup \left(\Sigma \cap W^{LIB}\right). \tag{2.23}$$

2.4.2 Saddle-node bifurcation

The SNB arises when a stable equilibrium point E_{PS} coalesces with a nearby unstable equilibrium point E_{PU} and disappears, causing the system to lose stability. Formally, the system (2.1) undergoes the SNB at the single bifurcation parameter $\boldsymbol{\beta}_B = \boldsymbol{\beta}^*$ and equilibrium point E_p when the following conditions are satisfied.

1. $\boldsymbol{J}_{RS}\big|_{E_p}$ has a single zero eigenvalue with normalized right eigenvector $\boldsymbol{\upsilon}$ and left eigenvector $\boldsymbol{w}$, i.e. $\boldsymbol{J}_{RS}\big|_{E_p} \boldsymbol{\upsilon} = 0$ and $\boldsymbol{w}^t \boldsymbol{J}_{RS}\big|_{E_p} = 0$, and all other eigenvalues have nonzero real parts.

2. $\boldsymbol{w}^t \left.\dfrac{\partial \boldsymbol{f}_e(\cdot)}{\partial \boldsymbol{\beta}_B}\right|_{E_p} \neq 0$.

3. $\boldsymbol{w}^t \left.\dfrac{\partial^2 \boldsymbol{f}_e(\cdot)}{\partial^2 \boldsymbol{\beta}_B}\right|_{E_p} \boldsymbol{v}\boldsymbol{v} \neq 0$.

The first condition implies that the Jacobian matrix is singular; the second and third conditions ensure transversality so that the bifurcations are not degenerate cases. Depending on the sign of the expressions in conditions 2 and 3, there are no equilibria near E_p when the bifurcation parameter is $\boldsymbol{\beta}_B < \boldsymbol{\beta}^* \left(\boldsymbol{\beta}_B > \boldsymbol{\beta}^*\right)$, and there are equilibria near E_p for each bifurcation parameter value $\boldsymbol{\beta}_B > \boldsymbol{\beta}^* \left(\boldsymbol{\beta}_B < \boldsymbol{\beta}^*\right)$ [Kuznetsov, 1998].

2.4.3 Limit induced bifurcation (LIB)

In power systems, control and/or operational limits have shown to yield bifurcations known as limit-induced bifurcations (LIB) [Lerm et al., 2003]. As the load increases, there exists a major demand of reactive power, and a voltage collapse scenario can be precipitated by the hitting of reactive power limits of generators or other voltage regulating controllers. For instance, once one of the AVR's limits is reached, either because of the generator field current limitation or the armature current limitation, the reactive power output can no longer be regulated; therefore, the generator terminal voltage cannot be maintained at the specified value. In this case, there exists a reduction on the voltage stability margin, which leads to two possible operating point scenarios. First, no local equilibria may exist for increasing loading conditions [Dobson and Lu, 1992] resulting in a voltage collapse, which is similar to what happens in the occurrence of a SNB. It is also possible that the system remains stable since the equilibrium point may be on the stable part of the limit-induced model's bifurcation diagram. In other words, the equilibrium points continue to exist after the LIB is reached as the bifurcation parameter changes.

2.4.4 Hopf bifurcation

The Hopf theorem [Kuznetsov, 1998] states that if the linearized system $\boldsymbol{J}_{RS}\big|_{E_P}$ has a pair of complex conjugate eigenvalues that cross the imaginary axis as $\boldsymbol{\beta}$ varies through a critical value $\boldsymbol{\beta}_B^c$, then for a near critical value of $\boldsymbol{\beta}$ there exists a limit cycle close to the equilibrium point. When $\boldsymbol{\beta}$ is varied, the system (2.21) undergoes the Hopf bifurcation at $\boldsymbol{\beta}^* = \boldsymbol{\beta}_B^c$ and at the equilibrium point E_P if the following conditions are satisfied:

1. The Jacobian matrix $\boldsymbol{J}_{RS}\big|_{E_P}$ possesses a pair of complex conjugate, simple eigenvalues $\lambda(\boldsymbol{\beta}_B^c) = \pm j\omega_e$, and there is no other eigenvalue on the imaginary axis.

2. $\left(\dfrac{\partial \mathrm{Re}\left(\lambda(\boldsymbol{\beta})\right)}{\partial \boldsymbol{\beta}}\right)\Bigg|_{\boldsymbol{\beta}_B^c} \neq 0$.

The last condition implies that the simple pair of complex conjugate eigenvalues cross the imaginary axis transversally at $\boldsymbol{\beta}^* = \boldsymbol{\beta}_B^c$. On the other hand, the first condition indicates that the equilibrium point E_P is non-hyperbolic, such that the local stability of the equilibrium cannot readily be determined from (2.22) alone. The system is hyperbolic, however, at values of $\boldsymbol{\beta}$ close enough to $\boldsymbol{\beta}_B^c$, and therefore the linearized system (2.22) permits the disclosure of the local stability of E_P.

At a Hopf bifurcation, limit cycles emerge in a vicinity of E_P with an initial period of $2\pi/\omega_e$ [Seydel, 1988]. Therefore, there exists a unique branch of periodic orbits with increasing amplitudes bifurcating from E_P as $\boldsymbol{\beta}$ is varied in the neighborhood of $\boldsymbol{\beta}_B^c$. In this context, there are two types of Hopf bifurcations: supercritical and subcritical. The former bifurcation occurs when an unstable equilibrium point and a stable limit cycle coalesce. Before the supercritical bifurcation $\boldsymbol{\beta} < \boldsymbol{\beta}_B^c$, the power system is at a stable equilibrium point; at the bifurcation the stable equilibrium gives birth to a stable limit cycle and grows from zero amplitude as $\boldsymbol{\beta}$ is further varied. After the bifurcation $\boldsymbol{\beta} > \boldsymbol{\beta}_B^c$, the equilibrium becomes unstable, and the system has an oscillating behavior according to the stable limit

cycle. On the other hand, the subcritical bifurcation corresponds to the coalescing of a stable equilibrium point and an unstable limit cycle. In this case, an unstable limit cycle exists prior to the subcritical Hopf bifurcation (SHB), $\beta < \beta_B^c$, which is attracted to the stable equilibrium as $\beta \to \beta_B^c$. At the bifurcation point E_P, the unstable limit cycle shrinks to zero amplitude transferring its instability to the equilibrium state. After the bifurcation $\beta > \beta_B^c$, the equilibrium point becomes unstable, and the system oscillates with growing amplitude.

2.5 Numerical computation of bifurcations

In general, there are two classes of traditional numerical methods to locate bifurcation points, namely the continuation method or also called the "indirect" method [Ajjarapu and Christy, 1992] and the "direct" method (DM). The continuation method is the one adopted in this work, and since a full and detailed description of the theoretical concepts associated with this method are well reported in the open access literature [Ajjarapu and Christy, 1992], [Illic and Zaborsky, 2000], [Van Cutsem and Vournas, 2008], only the most relevant principles and procedures associated with this computation are discussed here.

Continuation methods trace a continuous set of equilibrium solutions of (2.24) in the parameter space by small successive increments of a system's parameter called the continuation parameter, from a base case up to the point where a SNB, HB or LIB occurs. When the continuation parameter is the system load, it is called loadability parameter:

$$\begin{aligned} \mathbf{0} &= \boldsymbol{f}(\boldsymbol{x}, \boldsymbol{y}, \boldsymbol{\rho}, \boldsymbol{\lambda}) = \boldsymbol{f}(\boldsymbol{x}, \boldsymbol{y}, \boldsymbol{\beta}) \\ \mathbf{0} &= \boldsymbol{g}(\boldsymbol{x}, \boldsymbol{y}, \boldsymbol{\rho}, \boldsymbol{\lambda}) = \boldsymbol{g}(\boldsymbol{x}, \boldsymbol{y}, \boldsymbol{\beta}) \end{aligned} \tag{2.24}$$

A predictor-corrector scheme is employed to compute this continuum of equilibrium solutions, with a representation in the state-parameter space which is referred to as a bifurcation diagram, in order to overcome the difficulties associated with the computation of equilibrium solutions in the vicinity of the maximum loadability limit. These difficulties are directly linked with the singularity of the Jacobian matrix associated with the

linearization of the set of DAEs (2.24) or the violation of generators' reactive power limits at this loadability limit [Ajjarapu and Christy, 1992], [Besanger et al., 2013].

The continuation method starts from a known solution $\boldsymbol{f}\left(\boldsymbol{x}^{*(k)}, \boldsymbol{y}^{*(k)}, \boldsymbol{\beta}^{*(k)}\right) = \mathbf{0}$ and $\boldsymbol{g}\left(\boldsymbol{x}^{*(k)}, \boldsymbol{y}^{*(k)}, \boldsymbol{\beta}^{*(k)}\right) = \mathbf{0}$, where k denotes the *k-th* solution of the ongoing continuation process, and uses a predictor scheme to estimate a subsequent solution corresponding to a different value of the set of system parameters. The predicted solution, $\boldsymbol{f}\left(\hat{\boldsymbol{x}}^{*(k+1)}, \hat{\boldsymbol{y}}^{*(k+1)}, \hat{\boldsymbol{\beta}}^{*(k+1)}\right) = \mathbf{0}$ and $\boldsymbol{g}\left(\hat{\boldsymbol{x}}^{*(k+1)}, \hat{\boldsymbol{y}}^{*(k+1)}, \hat{\boldsymbol{\beta}}^{*(k+1)}\right) = \mathbf{0}$, is then corrected to the true solution, $\boldsymbol{f}\left(\boldsymbol{x}^{*(k+1)}, \boldsymbol{y}^{*(k+1)}, \boldsymbol{\beta}^{*(k+1)}\right) = \mathbf{0}$ and $\boldsymbol{g}\left(\boldsymbol{x}^{*(k+1)}, \boldsymbol{y}^{*(k+1)}, \boldsymbol{\beta}^{*(k+1)}\right) = \mathbf{0}$, by using a local parameterization based on the Newton-Raphson technique. The local parameterization provides a means of identifying each point along the solution path and of convergence to solutions irrespective of their stability properties. The stability of each equilibrium point composing the solution branch can then be analyzed from the corresponding eigenvalues to locate bifurcation points [Ajjarapu and Christy, 1992], [Besanger et al., 2013].

The prediction is along the tangent direction of the continuum at the current operating point, and this tangent direction is found by solving the following set of equations [Feng et al., 2000]:

$$\begin{bmatrix} \boldsymbol{f}_x(\cdot) & \boldsymbol{f}_y(\cdot) & \boldsymbol{f}_\lambda(\cdot) \\ \boldsymbol{g}_x(\cdot) & \boldsymbol{g}_y(\cdot) & \boldsymbol{g}_\lambda(\cdot) \\ & e_k & \end{bmatrix} \begin{bmatrix} \Delta\hat{\boldsymbol{x}} \\ \Delta\hat{\boldsymbol{y}} \\ \Delta\hat{\lambda} \end{bmatrix} = \begin{bmatrix} \mathbf{0} \\ \mathbf{0} \\ \pm 1 \end{bmatrix}, \tag{2.25}$$

where $\left[\Delta\hat{\boldsymbol{x}} \quad \Delta\hat{\boldsymbol{y}} \quad \Delta\hat{\lambda}\right]^t$ is the tangent vector being sought. $\lambda$is a factor applied to the system's parameter which is varied slowly from a base value, as given by (2.12) and (2.13) to represent load changes, in order to steer the power system to a different operating point. In addition, e_k is an appropriately dimensioned row vector with all elements zero except the *k-th*, which equals one and corresponds to the continuation parameter. Whether +1 or -1 is

used in the independent vector of (2.25) depends on how the continuation parameter is changing as the solution path is being traced. If it is increasing, a +1 should be used; otherwise a -1 is used. Once the tangent direction has been computed by solving (2.25), the prediction can be obtained as follows:

$$\begin{bmatrix} \hat{\boldsymbol{x}}^{*(k+1)} \\ \hat{\boldsymbol{y}}^{*(k+1)} \\ \hat{\lambda}^{*(k+1)} \end{bmatrix}_p = \begin{bmatrix} \boldsymbol{x}^{*(k)} \\ \boldsymbol{y}^{*(k)} \\ \lambda^{*(k)} \end{bmatrix} \pm \sigma \begin{bmatrix} \Delta\hat{\boldsymbol{x}} \\ \Delta\hat{\boldsymbol{y}} \\ \Delta\hat{\lambda} \end{bmatrix}, \tag{2.26}$$

where$p$ denotes the predicted solution, and σ is a positive scalar that defines the step size of the tangent vector to the solution path. The selection of sign is based on the direction of continuum. Note that the step size length has to be controlled to obtain the continuum of equilibrium solutions in lesser time. The step length could be small near to the maximum loading point and larger if not close to maximum loading point. It could be dependent on the number of iterations that the corrector took to converge.

After the predictor has produced an approximate solution for the next equilibrium solution, the corrector stage finds the exact solution with the initial guess provided by (2.26). The local parameterization is used such that the original set of DAEs equations is augmented by one equation associated with the value of the continuation parameter. Hence, the set of equations to be solved is given by

$$-\begin{bmatrix} \boldsymbol{f}_x(\cdot) & \boldsymbol{f}_y(\cdot) & \boldsymbol{f}_\lambda(\cdot) \\ \boldsymbol{g}_x(\cdot) & \boldsymbol{g}_y(\cdot) & \boldsymbol{g}_\lambda(\cdot) \\ & e_k & \end{bmatrix} \begin{bmatrix} \Delta\boldsymbol{x} \\ \Delta\boldsymbol{y} \\ \Delta\lambda \end{bmatrix} = \begin{bmatrix} \boldsymbol{f}(\cdot) \\ \boldsymbol{g}(\cdot) \\ 0 \end{bmatrix}, \tag{2.27}$$

and the exact equilibrium solution is given by

$$\begin{bmatrix} \boldsymbol{x}^{*(k+1)} \\ \boldsymbol{y}^{*(k+1)} \\ \lambda^{*(k+1)} \end{bmatrix}_c = \begin{bmatrix} \boldsymbol{x}^{*(k)} \\ \boldsymbol{y}^{*(k)} \\ \lambda^{*(k)} \end{bmatrix} + \begin{bmatrix} \Delta\boldsymbol{x} \\ \Delta\boldsymbol{y} \\ \Delta\lambda \end{bmatrix}. \tag{2.28}$$

There are several ways of explaining the proper choice of the continuation parameter. Mathematically, it corresponds to the state variable that has the largest tangent vector component [Ajjarapu and Christy, 1992]. In other words, this corresponds to the state variable that has the greatest rate of change near the given solution. In the context of power systems, the load parameter λ has been recognized as the best choice when starting the solution path computation from a base case and during light loading conditions [Ajjarapu and Christy, 1992], where the voltage magnitudes and angles remain fairly constant under load changes. When loads are considered as constant powers, such as the *PQ* load model, they are made to vary in direct proportion to any change of the loading factor λ as given by (2.12) and (2.13). When the solution path approaches the maximum loadability point, the load parameter has a lower rate of change in comparison to other state variables. Hence, the choice of a new continuation parameter must be evaluated near this solution. In general, the continuation parameter changes from load parameter to either the magnitude or phase angle voltage parameter with the largest rate of decrease. Since the voltage magnitude is used in per unit and voltage angle is used in radians, the scaling problem must be compensated for when choosing the new continuation parameter. This can be done by expressing the angles in per unit on an appropriate base.

Since the excitation system model is considered in the set of DAEs, where system limits such as the generator field and armature current limits are explicitly taken into account, all the assumptions for the slack bus and voltage controlled buses are removed from the formulation and computation process. Note that when a generator is assumed to be controlling the voltage magnitude at its terminal, it implies from the dynamic view point that the generator is equipped with an AVR of infinite static gain or has a perfect secondary voltage control. These assumptions are completely unrealistic in practice because as the load increases, the voltage magnitude decreases according to the AVR steady-state voltage-regulating characteristic.

Lastly, a radically different approach to perform bifurcation analysis is proposed in [Flores et al., 20011], which is beyond the scope of this thesis, based on particle swarm optimization (PSO). Opposite to the continuation concept generally used to compute bifurcation diagrams, the proposed approach transforms the problem of finding one equilibrium point for a given system's conditions into a problem of computing several

equilibrium points for the same operating conditions. This approach represents a new and useful technique to automatically compute a feasible operating region of a power system, as well as the boundaries of this region.

2.6 Numerical computation of the feasibility region and its boundary

Power system security operation requires that the system operates inside a feasibility region F, which is composed of the set of all asymptotically stable equilibrium points that can be reached from a specific initial operating point through the change of system parameters [Venkatasubramanian et al., 1995]. In this context, this region is defined as a set of load demands and power generations (in the dispatch parameter space) or magnitudes and phase angles of nodal voltages (in the state space), for which the power flow mismatch equations and all types of constraints representing the power system operation are satisfied [Wu and Kumagai, 1982]. This region is bounded by a feasibility boundary Σ, at which the system equilibrium points change their stability properties [Venkatasubramanian, 1995]. Therefore, this feasibility region, and in particular its boundary, is of great importance in the secure operation of the electric power system. A full and detailed description about the computation of the feasibility region and its associated boundary based on the continuation method can be found in [Gu and Cañizares, 2007], [Gutierrez-Martinez et al., 2011]. Furthermore, the theoretical concepts of the continuation methods have been reported in Section 2.5. Therefore, only the most relevant principles and procedures associated with this computation are discussed here.

The feasibility region and its boundary can be constructed for a specific operating point by identifying equilibrium points in the parameter space that are stable with respect to small and large perturbations for a system associated with the set of differential-algebraic equations (2.1) representing the power system. In this computation process, the feasibility region (boundary) corresponds to a stability region (boundary) for stable equilibrium points corresponding to the full base system; for resulting operating points associated with the system with one less element corresponding to the worst contingency (N-1 contingency criteria), the resulting region (boundary) is called the security region (boundary). In this last case, the system is able to withstand a credible contingency without serious consequences.

In this work, the feasibility region and its corresponding boundary are computed considering a full AC modeling of the network under analysis, which allows the computation of nodal voltage magnitudes and angles as well as the influence of reactive power. For purpose of our research, an AC continuation power flow, and not a DC power flow, is used for computing the equilibrium points composing this region and its boundary, which satisfy the set of equations $0 = f(\cdot)$ and $0 = g(\cdot)$. The stability of these equilibrium points is determined by an eigenvalue analysis of the Jacobian matrix associated with the linearization of the set of DAEs (2.1); thus, the boundary includes a set of equilibrium points associated with codimension-1 generic local bifurcations, i.e. saddle-node, Hopf, or limit-induced bifurcations, which directly reflect voltage and small-signal angle stability limits. Therefore, each one of these equilibrium points, which defines an operating state of the system, defines a loadability limit representing the system's critical active and reactive powers beyond which the system loses its voltage or angle stability. For the purpose of this work, this boundary is only represented in the P_G-parameter space due to the fact that generator active powers are the main control variables in the proposed OPF model, but voltage and angle stability and as well as the influence of reactive powers are implicitly considered in the security boundary.

Despite the fact that end-users may participate in demand response and demand-side management programs or bid on current electricity markets, in practice load patterns still remain reasonably forecastable in a way that the overall load profile is predictable with reasonable accuracy, so that the market clearing price can be determined by matching a highly elastic supply with a forecast of expected load. In this context, the feasibility region and boundary are then constructed by stressing the system progressively in one particular loading direction at a constant power factor, from the base load scenario, until the instability occurs considering an N-1 contingency criterion and a variety of generation dispatch patterns.

Based on the aforementioned, let $\boldsymbol{\Delta S_{G_k}} = \left[\Delta S_{G_{1,k}} \; \Delta S_{G_{2,k}} \cdots \Delta S_{G_{nG,k}} \right]^T$ be a k-th particular set of complex power increase rates for all generators participating in the dispatch, where $\Delta S_{G_{i,k}} = \alpha d_{i,k}$ is the complex power increase rate for the i-th generator from its base generation $S_{G_{i,0}}$ in its corresponding k-th dispatch direction $d_{i,k}$, and $\alpha \geq 0$ is the

generation increasing factor. The complex power output required by the *i*-th generator to supply a specific load increase λ from the base load is then given by $S_{G_{i,k}} = \Delta S_{G_{i,k}} S_{G_{i,0}} = \alpha d_{i,k} \left(P_{G_{i,0}} + jQ_{G_{i,0}} \right)$. In addition, the critical dispatchable generator power output $S^c_{G_{i,k}} = \Delta S^c_{G_{i,k}} S_{G_{i,0}}$, $P^c_{G_{i,k}} + jQ^c_{G_{i,k}} = \alpha^c d_{i,k} \left(P_{G_{i,0}} + jQ_{G_{i,0}} \right)$ corresponds to the active and reactive powers supplied at a loadability limit beyond which the system loses its voltage stability; hence $\Delta S_{G_{i,k}}$ basically represents the sensitivity of generator *i* with respect to a loadability limit in the *k*-th load direction. Note that in order to properly represent multiple generation dispatch patterns, the *k*-th direction at which the *i*-th generator is dispatched must lie in the interval $0 \le d_{ik} \le 1 \quad \forall i = 1,\ldots,n_G$ such that $\sum_{i=1}^{n_G} d_{ik} = 1$. Furthermore, a suitable number of different dispatch directions $\boldsymbol{TN}_{dd} = \left[\boldsymbol{d}_1 \boldsymbol{d}_2 \cdots \boldsymbol{d}_{n_{dd}} \right]$, where $\boldsymbol{d}_k = \left[d_{1,k}\, d_{2,k} \cdots d_{n_G,k} \right]^T$, must be specified in order to assure that a reasonable density is achieved to get a complete boundary. Based on the information mentioned above, the discrete representation of the Σ in the P_G-parameter space is mathematically expressed by the critical active power generation matrix given by (2.29), where n_{dd} is the number of dispatch directions considered in the study and is selected in such a way that a reasonable density to accurately represent Σ is achieved [Gutiérrez-Martínez et al., 2011]. Note that each column of this matrix defines one boundary point on the discrete Σ in the P_G-parameter space of dimension n_G.

Lastly, the flowchart of the Figure 2.2 shows the process followed to obtain the discrete feasibility boundary in the P_G-parameter space. This process is performed using the PSAT software [Milano, 2005] in the present work.

$$M_{CP}=\begin{bmatrix} P^c_{G_{1,1}} & \cdots & P^c_{G_{1,k}} & \cdots & P^c_{G_{1,n_{dd}}} \\ \vdots & \ddots & \vdots & \ddots & \vdots \\ P^c_{G_{i,1}} & \cdots & P^c_{G_{i,k}} & \cdots & P^c_{G_{i,n_{dd}}} \\ \vdots & \ddots & \vdots & \ddots & \vdots \\ P^c_{G_{n_G,1}} & \cdots & P^c_{G_{n_G,k}} & \cdots & P^c_{G_{n_G,n_{dd}}} \end{bmatrix}. \tag{2.29}$$

$\uparrow$ $\uparrow$ $\overbrace{\quad\uparrow\quad}$

$\left[\boldsymbol{P}^c_{G_1}\right]$ $\left[\boldsymbol{P}^c_{G_k}\right]$ $\left[\boldsymbol{P}^c_{G_{n_{dd}}}\right]$

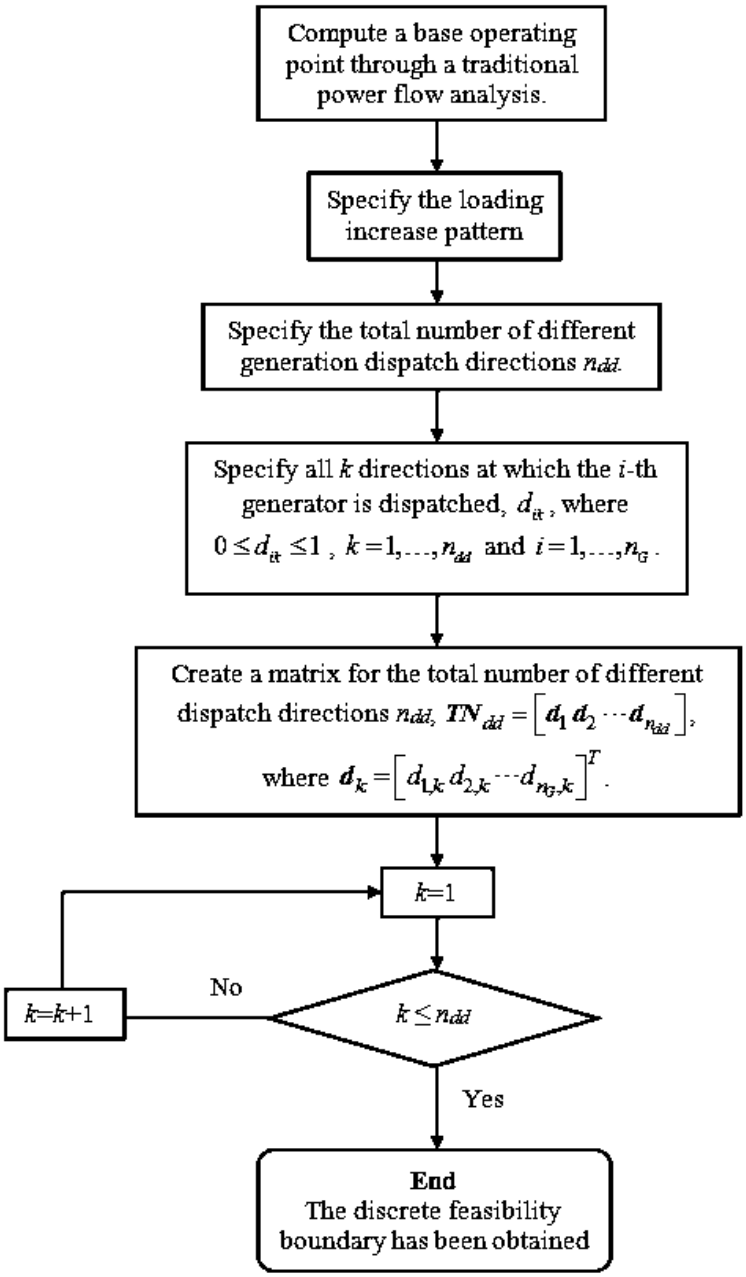

Figure 2.2.Flowchart to obtain the feasibility boundary.

2.6.1 Study case

The simulation results regarding the computation of a feasibility region and its boundary are presented in this section. The power system under consideration corresponds to the IEEE 3-machine 9-bus test system shown in Figure 2.3.

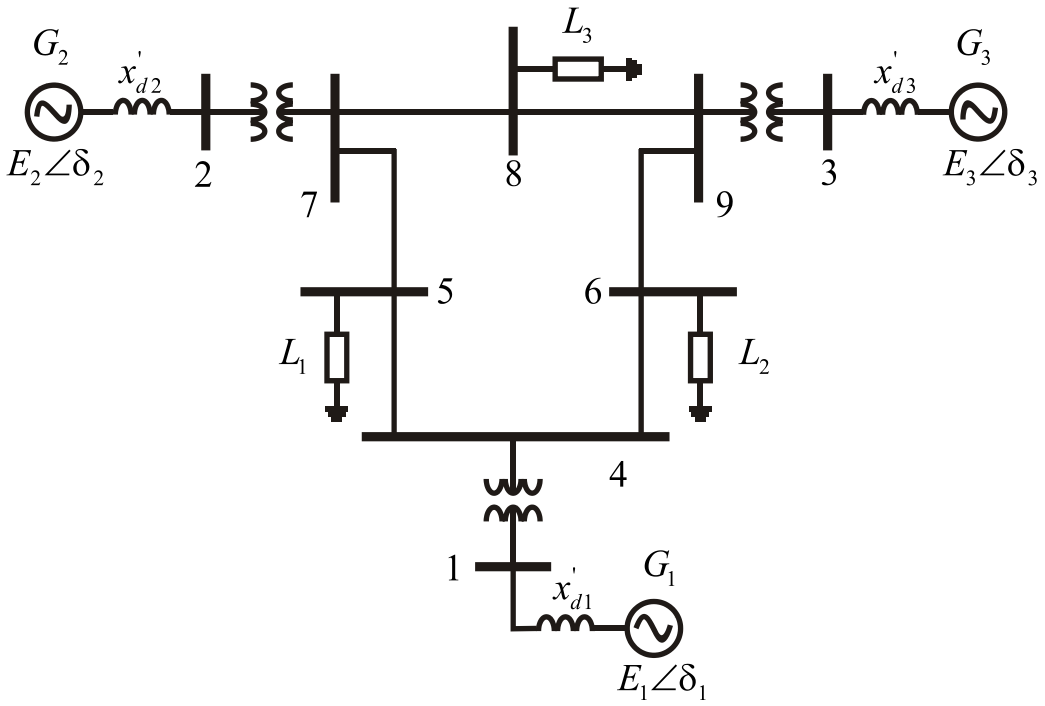

Figure 2.3.On-line diagram of the IEEE 3-machine 9-bus test system.

This system is composed of three generators at buses 1, 2, and 3, with active power output limits of 900 MW, 700 MW and 600 MW, respectively, and three loads at buses 5, 6, and 8. The system is divided into three generation areas directly related to each generator, i.e. areas A, B, and C corresponding to generators G_1, G_2, and G_3, respectively. All data for this system are reported in [Sauer and Pai, 1988]. The system stability boundary was obtained following the procedure discussed in the last section, based on static and dynamic studies (an exciter model Type I was used), assuming that the loading increments are supplied from 631 different generation dispatches at each generation area.

From a geometrical viewpoint, the existing relationship between the critical active and reactive powers, as well as the voltage stability, is illustrated below.

Let one equilibrium point of this boundary be defined by the critical complex powers $P_{GA}+jQ_{GA}$= 1.174+j2.6207 pu, $P_{GB}+jQ_{GB}$= 2.3858+j1.0356 pu and $P_{GC}+jQ_{Gc}$= 1.2442+j0.98434 pu. Since these complex powers define an operation state of the system and the voltage profile along the network, the voltage magnitude at any node, for example node 4, can be directly related to these powers in the complex power parameter space, as illustrated in Figures 2.4, 2.5 and 2.6 for generation areas A, B, and C, respectively.

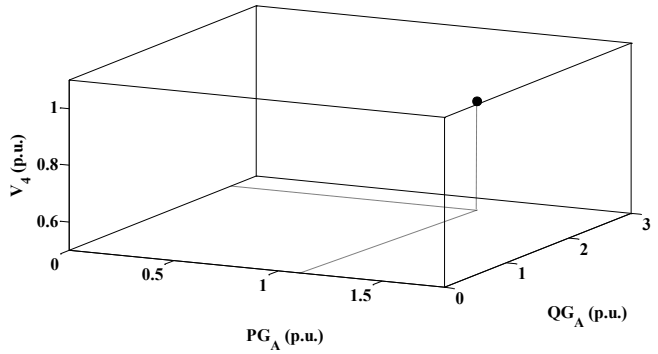

Figure 2.4. Voltage magnitude at node 4 in the (P_G+jQ_G)-parameter space (generation area A).

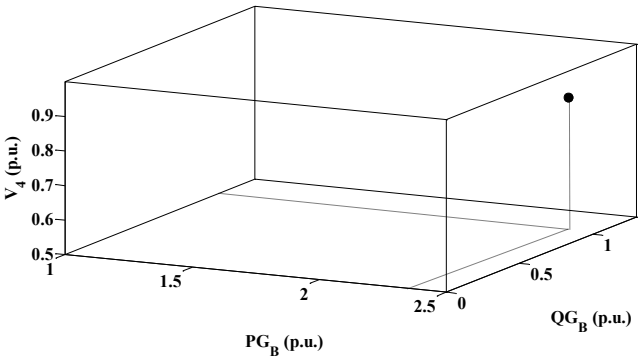

Figure 2.5. Voltage magnitude at node 4 in the (P_G+jQ_G)-parameter space (generation area B).

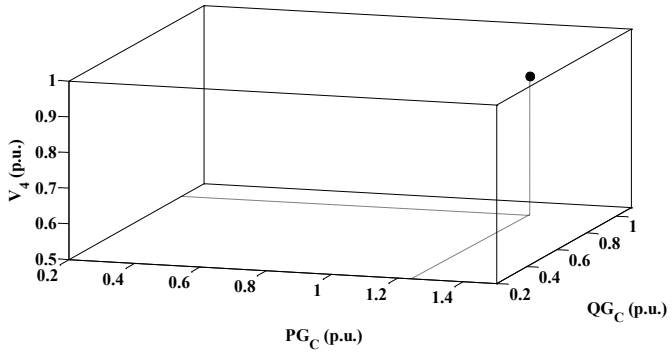

Figure 2.6. Voltage magnitude at node 4 in the (P_G+jQ_G)-parameter space (generation area C).

On the other hand, this equilibrium point of the feasibility boundary can be explicitly represented in the P_G-parameter or Q_G-parameter spaces as shown in Figures 2.7 and 2.8, respectively. Note that the reason for representing this boundary only in the P_G-parameter space is to formulate a true security boundary-constrained DC-OPF, but the voltage stability and the influence of reactive power are implicitly considered in the proposed SBC DC-OPF model using the stability/security boundary constraints.

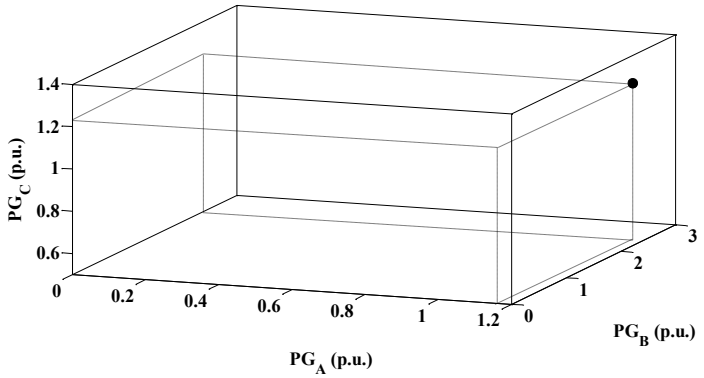

Figure 2.7.Isolated equilibrium point of the feasibility boundary in the P_G-parameter space.

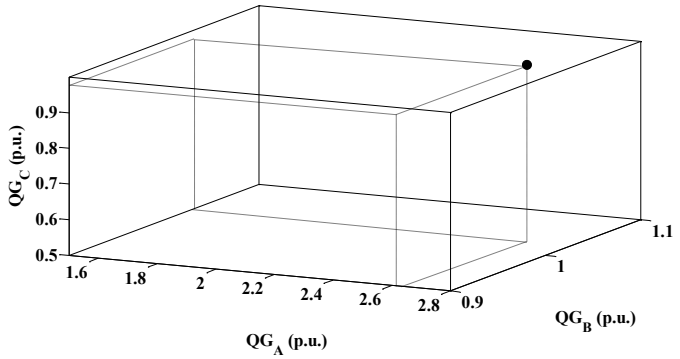

Figure 2.8.Isolated equilibrium point of the feasibility boundary in the Q_G-parameter space.

Lastly, the set of equilibrium points of the feasibility boundary considering all 631 different generation dispatch patterns at each generation area is given in Figure 2.9 in the P_G-parameter space.

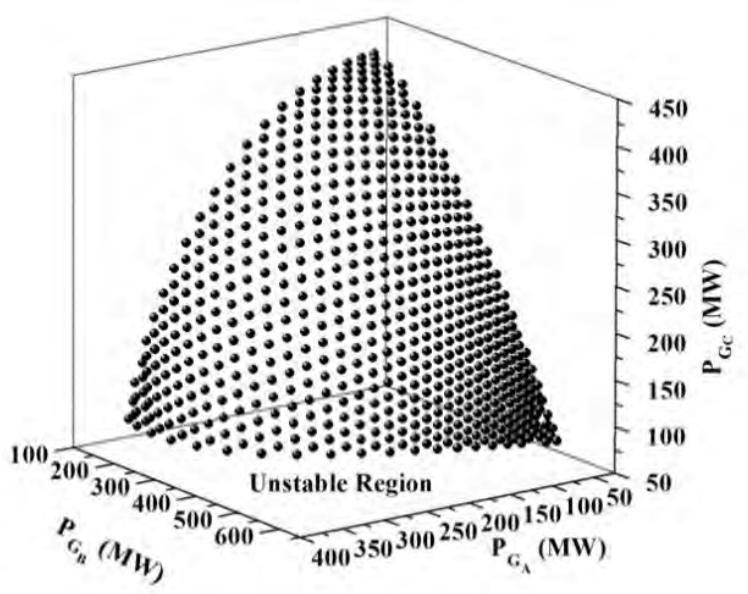

Figure 2.9.Stability boundary for the IEEE 9-bus system.

2.7 Conclusions

The mathematical models of the power system components to be considered in this thesis have been described in this chapter. These models have been developed based on the concept of power injections and have been integrated in a single frame of reference by means of a set of differential-algebraic equations using the concept of nodal power injection balance. Bifurcation theory has been employed to qualitatively explain the mechanisms of voltage stability problems occurring in electric power systems by relating the voltage collapse and voltage oscillatory problems to the appearance of saddle-node, limit-induced and Hopf bifurcations. The numerical computation of voltage stability problems has been formulated based on the equilibrium analysis of the set of differential-algebraic equations representing the electric power system and the application of the continuation method.

The concepts of an electrical power system's feasibility region and its boundary have been explained in terms of the practical importance for utilities in order to guarantee the secure operation of power systems. How to determine the feasible operating region of a power system and the bifurcation boundaries of this region has also been explained by applying the principle of continuation, which has been successfully illustrated by a numerical example.

Chapter 3

Linearization of the Feasibility Boundary

3.1 Introduction

From the context of OPF-based dispatch mechanisms, the knowledge of stability/security boundaries and their proper representation in a security-constrained OPF is of paramount importance to assure the security of electricity markets. Once the nonlinear voltage feasibility region and its associated boundary have been computed, as reported in Chapter 2, the next step corresponds to the linear representation of the nonlinear boundary by an appropriate piecewise approximation based on a set of hyperplanes, which will be used as linear feasibility boundary constraints for the DC-OPF model proposed in Chapter 4.

In this Chapter, the proposed linear approximation of the feasibility boundary based on the use of hyperplanes, under the assumption that the boundaries are convex, is detailed. This approximation results in a set of linear inequalities in the multidimensional dispatch space. In order to decrease the dimension of the problem formulation, two new methods to reduce the number of linear inequalities to be employed in the analytical description of these boundaries are also proposed. Finally, the effectiveness of the proposed approach to obtain an appropriate representation of the feasibility boundary is demonstrated by means of realistic examples.

3.2 Definitions

The Euclidian spaces theory establishes that formulas describing geometric objects and their properties in $\mathbb{R}^2$ and $\mathbb{R}^3$ can be readily generalized to higher dimensions, and the dimension of this space refers to how many are needed to represent one point in the space. Hence, the real line $\mathbb{R}^1$ consists of single numbers, the plane $\mathbb{R}^2$ consists of ordered pairs of numbers, while the Euclidian *n*-space consists of a set of ordered *n*-tuples of numbers. Furthermore, each space will have its origin, indicating the point with respect to which we make our coordinate measurements.

The fundamental objects of Euclidian geometry are points, lines and planes, being a line in $\mathbb{R}^2$ and a plane in $\mathbb{R}^3$ examples of sets described by a one single linear equation in $\mathbb{R}^n$. These spaces are often referred to as hyperplanes, where a line in $\mathbb{R}^2$ can be written as

$$ax + by = C, \tag{3.1}$$

where*a*, *b*, and *C* are some constants (with *a* and *b* not all zero), by representing a line in the *xy*-plane. On the other hand, a plane in $\mathbb{R}^3$ can be written in point-normal form as

$$ax + by + cz = D, \tag{3.2}$$

where*a*, *b*, *c*, and *D* are constants (with *a*, *b* and *c* not all zero), by representing a plane in the three-dimensional space $\mathbb{R}^3$. Generally speaking, a hyperplane in $\mathbb{R}^n$ can be written in point-normal form as

$$a_1x_1 + a_2x_2 + \cdots + a_nx_n = C, \tag{3.3}$$

wherea_1, a_2, …, a_n, and *C* are some constants (with a_1, a_2, …, a_n not all zero), by representing an object called a hyperplane in the *n*-dimensional space $\mathbb{R}^n$. The hyperplane described by Equation (3.3) can be thought of as the set of all vectors with a tail at $(0,\ldots,0,C/a_n)$ which are perpendicular to the vector $\boldsymbol{\eta} = (a_1,\ldots,a_n)$. We say that a point $\boldsymbol{p} = (p_1, p_2, \ldots, p_n)$ in $\mathbb{R}^n$ is on the hyperplane*H* represented by (3.3) if the coordinates of $\boldsymbol{p}$ satisfy Equation (3.3), that is:

$$a_1p_1 + a_2p_2 + \cdots + a_np_n = C. \tag{3.4}$$

Certainly when $a_1p_1 + a_2p_2 + \cdots + a_np_n \neq C$, we say that $\boldsymbol{p}$ is not on *H* (or *H* does not contain $\boldsymbol{p}$).

3.3 Hyperplanedefinition

A plane in $\mathbb{R}^3$ is completely described by giving its inclination and a point on it. We usually express its inclination by specifying a vector $\boldsymbol{\eta}$, called a normal vector, which is perpendicular to the plane [Simon andBlume, 1994]. If we want to obtain the equation for

the plane through the point $\boldsymbol{p}=(p_1,p_2,p_3)$ with the normal vector $\boldsymbol{\eta}=(\eta_1,\eta_2,\eta_3)$to the plane, and $\boldsymbol{x}=(x,y,z)$ is an arbitrary point in the plane, then $\boldsymbol{x}-\boldsymbol{p}$ will be a vector in the plane. Consequently, the vector will be perpendicular to $\boldsymbol{\eta}$, as shown in Figure 3.1.

Recalling that two vectors are perpendicular if and only if their dot product is zero, we obtain

$$\boldsymbol{\eta}\bullet(\boldsymbol{x}-\boldsymbol{p})=(\eta_1,\eta_2,\eta_3)\bullet(x-p_1,y-p_2,z-p_3)=0 \tag{3.5}$$

or

$$\eta_1(x-p_1)+\eta_2(y-p_2)+\eta_3(z-p_3)=0\,. \tag{3.6}$$

Equation (3.6) is called the point-normal equation of the plane. This equation can be expressed as (3.2), i.e. $D=\eta_1x+\eta_2y+\eta_3z$ with $D=\eta_1p_1+\eta_2p_2+\eta_3p_3$. Conversely, Equation (3.2) can be interpreted as the equation of the plane which has a normal vector (a,b,c) and which contains each of the points $(0,0,D/c)$, $(0,D/b,0)$, and $(D/a,0,0)$.

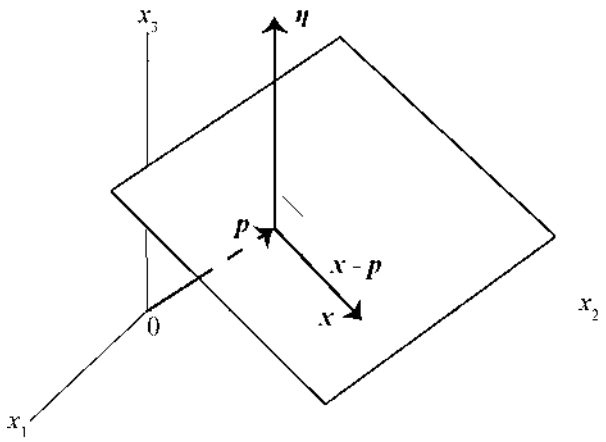

Figure 3.1.Plane through $\boldsymbol{p}$ with normal vector $\boldsymbol{\eta}$.

3.4 Linear representation of the feasibilities' boundary

The linear representation of the feasibilities boundaries in the multidimensional active power dispatch space (analyzed in Section 2.7.2) is obtained by its piecewise approximation based on a set of hyperplanes. Each hyperplanein R^{n_G} is completely described by its inclination, which is obtained by specifying a normal vector $\boldsymbol{\eta}$ to the

hyperplane and one boundary point $\boldsymbol{P}_{\boldsymbol{G}_k}^{c}$ on it [Simon andBlume, 1994]. Furthermore, if in Equation (2.31) $\boldsymbol{P}_{\boldsymbol{G}_j}^{c}$ is an arbitrary boundary point on the hyperplane, $\boldsymbol{P}_{\boldsymbol{G}_j}^{c} - \boldsymbol{P}_{\boldsymbol{G}_k}^{c}$ will be a vector in the hyperplane and, consequently, will be perpendicular to $\boldsymbol{\eta}$, as shown in Figure3.2 for n_G=3. Hence, the single linear point-normal equation representing the hyperplane is derived from the dot product given by $\boldsymbol{\eta} \bullet \left(\boldsymbol{P}_{\boldsymbol{G}_j}^{c} - \boldsymbol{P}_{\boldsymbol{G}_k}^{c} \right) = \boldsymbol{\eta} \bullet \boldsymbol{P}_{\boldsymbol{G}_j}^{c} - C = 0$, where $C = \boldsymbol{\eta} \bullet \boldsymbol{P}_{\boldsymbol{G}_k}^{c}$ [Simon andBlume, 1994].

In order to obtain the point-normal equation representing each *i*-thhyperplane, first finding its corresponding normal vector $\boldsymbol{\eta}_i$ is necessary. This is achieved by selecting the hyperplane's vertices given by a set ofn_G neighboring points of the feasibility boundary Σ, which have the shortest Euclidean norm with respect to one selected point of this set, referred to as reference point, $\boldsymbol{P}_{\boldsymbol{G}_j}^{c,i}$ $\forall j \in$ {n_G boundary points}. These hyperplane's vertices are then used to find a set of (n_G-1) vectors that spans the hyperplane containing them. Based on these vectors, an underdetermined set of (n_G-1) linear equations is formulated and solved for n_G-1 elements of $\boldsymbol{\eta}_i$, as well as for the constant term C^i, under the assumption that the first element of $\boldsymbol{\eta}_i$ is set to a specified value [Simon andBlume, 1994], [Makarov et al., 2010]. A unit value $\eta_{i,1} = 1$ has been selected here as proposed in [Makarov et al., 2010].

By considering that the hyperplane's vertices are the n_G boundary points corresponding to the first n_G dispatch directions, $\left[\boldsymbol{P}_{\boldsymbol{G}_1}^{c,i} \cdots \boldsymbol{P}_{\boldsymbol{G}_{n_G}}^{c,i} \right]$, and that the boundary point $\boldsymbol{P}_{\boldsymbol{G}_1}^{c,i}$ is the reference hyperplane's vertex from which the (n_G-1) vectors are obtained, as illustrated in Figure 3.2 for n_G=3, the set of equations to be solved is given, for $j \neq 1$, by

$$\begin{gathered} \boldsymbol{\eta}_i \bullet \left(\boldsymbol{P}_{\boldsymbol{G}_j}^{c,i} - \boldsymbol{P}_{\boldsymbol{G}_1}^{c,i} \right) = \boldsymbol{\eta}_i \bullet \boldsymbol{P}_{\boldsymbol{G}_j}^{c} - C^i = 0 \quad \forall\, j = 2, \ldots, n_G \\ \eta_{i,1} = 1 \end{gathered} \tag{3.7}$$

or in matrix form

$$\begin{bmatrix} P_{G_{1,2}}^{c,i} & \cdots & P_{G_{n_G,2}}^{c,i} & -1 \\ \vdots & \ddots & \vdots & \vdots \\ P_{G_{1,n_G}}^{c,i} & \cdots & P_{G_{n_G,n_G}}^{c,i} & -1 \\ 1 & \cdots & 0 & 0 \end{bmatrix} \begin{bmatrix} \eta_{i,1} \\ \vdots \\ \eta_{i,n_G} \\ C_i \end{bmatrix} = \begin{bmatrix} 0 \\ \vdots \\ 0 \\ 1 \end{bmatrix}. \tag{3.8}$$

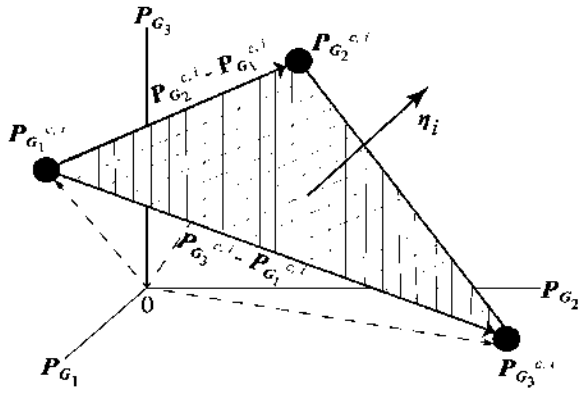

Figure 3.2.Hyperplane with vertices $\boldsymbol{P}_{\boldsymbol{G}_1}^{c,i}$, $\boldsymbol{P}_{\boldsymbol{G}_2}^{c,i}$ and $\boldsymbol{P}_{\boldsymbol{G}_3}^{c,i}$.

Once Equation (3.8) is solved for n_G-1 elements of $\boldsymbol{\eta}_i$ and the constant term C^i, an i-thhyperplane is completely described by

$$\eta_{i,1} P_{G_{1,n}}^{c,i} + \ldots + \eta_{i,n_G} P_{G_{n_G,n}}^{c,i} = C^i \quad \forall i = 1,\ldots n_{hy} \tag{3.9}$$

for any arbitrary boundary point $\boldsymbol{P}_{\boldsymbol{G}_n}^{c,i}$ on the hyperplane, with the set of n_{hy}hyperplanes piecewiselinearly approximating the feasibility boundary Σ.

The set of equations (3.8) or (3.9) is always linearly independent because the set of vectors in the hyperplane is not equal to nor multiples of each other. This is because we are selecting the hyperplane's vertices given by n_G different neighboring points of the feasibility boundary to find the set of (n_G-1) vectors that span the hyperplane containing them. Hence, the set of (n_G-1) linear equations (3.8) or (3.9) directly derived from these vectors is linearly independent under the assumption that one coordinate of the normal vector to the hyperplane is set at a specified value. This statement can be mathematically illustrated detailing the derivation of (3.8) or (3.9) as given below.

Let the vertices of the i-thhyperplane be the n_G boundary points corresponding to the first n_G dispatch directions, $\left[\boldsymbol{P}_{\boldsymbol{G}_1}^{c,i} ,\cdots, \boldsymbol{P}_{\boldsymbol{G}_{n_G}}^{c,i} \right]$, where

$$\boldsymbol{P}_{\boldsymbol{G}_k}^{c,i} = \begin{bmatrix} P_{G_{1,k}}^{c,i} & P_{G_{2,k}}^{c,i} & \cdots & P_{G_{nG,k}}^{c,i} \end{bmatrix}^T \ \forall k = 1,\ldots,n_G . \tag{3.10}$$

By considering that the boundary point $\boldsymbol{P}_{\boldsymbol{G}_1}^{c,i}$ is the reference hyperplane's vertex, the set of (n_G-1) vectors spanning the hyperplane is

$$\begin{matrix} \boldsymbol{P}_{\boldsymbol{G}_2}^{c,i} - \boldsymbol{P}_{\boldsymbol{G}_1}^{c,i} \\ \boldsymbol{P}_{\boldsymbol{G}_3}^{c,i} - \boldsymbol{P}_{\boldsymbol{G}_1}^{c,i} \\ \vdots \\ \boldsymbol{P}_{\boldsymbol{G}_{n_G}}^{c,i} - \boldsymbol{P}_{\boldsymbol{G}_1}^{c,i} \end{matrix} \tag{3.11}$$

or $\boldsymbol{P}_{\boldsymbol{G}_j}^{c,i} - \boldsymbol{P}_{\boldsymbol{G}_1}^{c,i} \ \ \forall \ j = 2,\ldots,n_G ; j \neq 1.$ Since the boundary points $\boldsymbol{P}_{\boldsymbol{G}_j}^{c,i}$ correspond to the hyperplane's vertices which are all different, the (n_G-1) vectors (3.11) spanning the hyperplane are linearly independent. Based on these vectors, a set of underdetermined (n_G-1) linear equations is formulated as follows:

$$\begin{matrix} \boldsymbol{\eta}_i \bullet \left(\boldsymbol{P}_{\boldsymbol{G}_2}^{c,i} - \boldsymbol{P}_{\boldsymbol{G}_1}^{c,i} \right) = \boldsymbol{\eta}_i \bullet \boldsymbol{P}_{\boldsymbol{G}_2}^{c,i} - C_i = 0 \\ \boldsymbol{\eta}_i \bullet \left(\boldsymbol{P}_{\boldsymbol{G}_3}^{c,i} - \boldsymbol{P}_{\boldsymbol{G}_1}^{c,i} \right) = \boldsymbol{\eta}_i \bullet \boldsymbol{P}_{\boldsymbol{G}_3}^{c,i} - C_i = 0 \\ \vdots \\ \boldsymbol{\eta}_i \bullet \left(\boldsymbol{P}_{\boldsymbol{G}_{n_G}}^{c,i} - \boldsymbol{P}_{\boldsymbol{G}_1}^{c,i} \right) = \boldsymbol{\eta}_i \bullet \boldsymbol{P}_{\boldsymbol{G}_{n_G}}^{c,i} - C_i = 0 \end{matrix} , \tag{3.12}$$

where $\boldsymbol{\eta}_i = \begin{bmatrix} \eta_{i,1} & \eta_{i,2} & \cdots & \eta_{i,n_G} \end{bmatrix}^T$. Under the assumption that the first element of $\boldsymbol{\eta}_i$ is set to a unit value $\eta_{i,1} = 1$, the set of equations to be solved for the normal vector to the hyperplane is given by (3.13), which corresponds to Equations (3.8) or (3.9), which are also linearly independent:

$$
\begin{aligned}
\eta_{i,1}P_{G_{1,2}}^{c,i} + \eta_{i,2}P_{G_{2,2}}^{c,i} + \cdots + \eta_{i,n_G}P_{G_{n_G,2}}^{c,i} - C_i &= 0 \\
\eta_{i,1}P_{G_{1,3}}^{c,i} + \eta_{i,2}P_{G_{2,3}}^{c,i} + \cdots + \eta_{i,n_G}P_{G_{n_G,3}}^{c,i} - C_i &= 0 \\
\vdots \qquad\qquad & \\
\eta_{i,1}P_{G_{1,n_G}}^{c,i} + \eta_{i,2}P_{G_{2,n_G}}^{c,i} + \cdots + \eta_{i,n_G}P_{G_{n_G,n_G}}^{c,i} - C_i &= 0 \\
\eta_{i,1} &= 1
\end{aligned} \quad . \tag{3.13}
$$

In order to clarify the process to obtain the piecewise approximation of the feasibility boundary, the flowchart of the Figure 3.3 is presented.

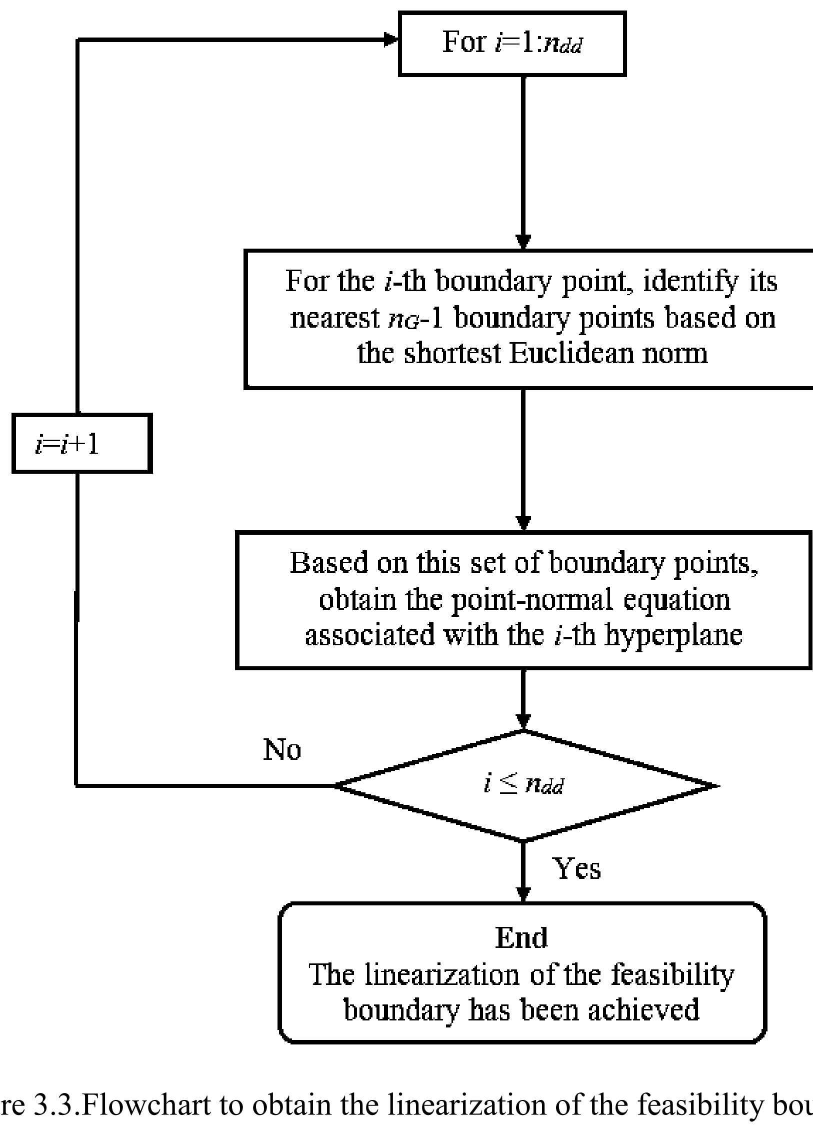

Figure 3.3.Flowchart to obtain the linearization of the feasibility boundary.

3.5 Linear inequalities

The goal of the piecewise linear approximation of the feasibility boundary by hyperplanes, presented in the previous Section, is to obtain a set of linear inequalities that properly represent this boundary in the multidimensional dispatch space. Hence, the active power dispatched by all generators must satisfy the following set of linear inequality constraints, which are directly derived from the set of point-normal equations (3.9):

$$\eta_{i,1} P_{G_1} + \ldots + \eta_{i,n_G} P_{G_{n_G}} \leq \pm C^i \quad \forall\, i = 1, \ldots n_{hy} \quad . \tag{3.14}$$

The sign on the right side of this inequality constraint will depend on the direction at which the normal vector is pointing to from the feasibility boundary in the P_G-parameter space. If the normal vector points outward (inward) from the feasibility region, the sign is positive (negative). The direction of the normal vector is determined by evaluating (3.14) while considering the generation of active powers that define the base operating point for which the feasibility boundary is computed: $\boldsymbol{P_{G,0}} = \begin{bmatrix} P_{G_{1,0}} & P_{G_{2,0}} & \cdots & P_{G_{n_G,0}} \end{bmatrix}^T$. Since $\left\| \boldsymbol{P_{G,0}} \right\| < \left\| \boldsymbol{P}_{\boldsymbol{G}_k}^{c,i} \right\|$, the normal vector $\boldsymbol{\eta}_i$ is pointing outward from the feasibility region if $\boldsymbol{\eta}_i \bullet \boldsymbol{P}_{\boldsymbol{G}}^{\boldsymbol{b}} < C^i$; otherwise, the direction of $\boldsymbol{\eta}_i$ is inward from the feasibility region.

3.6 Reduction of the number of approximant hyperplanes

In order to diminish the number of inequality constraints directly associated with the original set of hyperplanes used to approximate the feasibility boundary, the following two reduction algorithms are proposed.

- ***Algorithm 1: Boundary points' approximation***

1. Each point-normal equation (3.9) is evaluated at all boundary points composing the discrete SB Σ, i.e. evaluate $\boldsymbol{\eta}_i \bullet \boldsymbol{P}_{\boldsymbol{G}_k}^{\boldsymbol{c}} \;\; \forall\, k \in n_{dd}$, $i \in n_{hy}$.

2. An approximation error criterion is then defined such that $-0.001 \leq \boldsymbol{\eta}_i \bullet \boldsymbol{P}_{\boldsymbol{G}_k}^{\boldsymbol{c}} - C^i \leq 0$, which defines how far the boundary point is from the *i*-thhyperplane. Note that the maximum limit cannot be bigger than zero; otherwise, the boundary point may be located in the P_G-parameter space below the hyperplane, which implies that an infeasible region is below the hyperplane; thus it will be considered as a secure region during the optimization process.
3. The hyperplanes are sorted in descending order according to the number of boundary points that satisfy the error criterion.
4. The following criteria are then used to reduce the number of hyperplanes:
   a. The first approximant hyperplane is the one at which the largest number of boundary points satisfies the error criterion. These boundary points are excluded for the subsequent selection of hyperplanes.
   b. For the rest of the boundary points, Step 4a is repeated until all boundary points composing the discrete Σ have been considered.

- ***Algorithm 2: Inner product***

1. The inner product of the normal vectors associated with the original set of hyperplanes is calculated.
2. Two normal vectors to their corresponding hyperplanes are considered "parallel" to each other if the angle between them does not exceed five degrees. These normal vectors are then sorted in descending order according to the number of so defined parallel vectors.
3. The following criteria are then used to reduce the number of hyperplanes:
   a. The first approximant hyperplane is the one with the largest number of "parallel" vectors. All hyperplanes associated with this set of normal vectors are excluded for the subsequent selection of hyperplanes.
   b. For the rest of the hyperplanes, Step 3a is repeated until all hyperplanes of the original set have been considered.

Note that the proposed algorithms to linearly approximate the feasibility boundary assure that the boundary points are located on or above the approximant hyperplanesin the P_G-parameter space. From a practical viewpoint, this means that the feasibility region

bounded by the hyperplanes $\sum^{hy}$ is always contained within the original feasibility region $\sum$, i.e. $\sum^{hy} \subseteq \sum$. On the other hand, the selection of an angle of five degrees between two normal vectors was done heuristically considering that two hyperplanes strictly have the same inclination if the existing angle between their corresponding normal vectors is null. This implies that the boundary points contained in one hyperplane can be considered as an extension of the other hyperplane. Based on this reasoning, we assumed that the existing inclination between two hyperplanes with an angle of five degrees between their corresponding normal vectors is reasonable for merging all boundary points into one single hyperplane. The validity of this conjecture was numerically demonstrated in the numerical examples by plotting the absolute error between the boundary points composing the security or stability boundary and their corresponding approximant hyperplanes obtained under this assumption.

The accuracy of the proposed reduction algorithms is quantified by calculating the absolute errors between the boundary points composing Σ and their corresponding approximating hyperplanes by

$$\frac{\left|\boldsymbol{\eta}_i \bullet \boldsymbol{P}_{\boldsymbol{G}}^{\boldsymbol{c,i}} - C^i\right|}{C^i} \quad \forall i = 1,\ldots n_{hy} . \tag{3.15}$$

Lastly, detailed numerical examples to highlight step-by step how implementation of the proposed two algorithms mentioned above works is reported in Appendix D.

3.7 Study cases

The results of the proposed approaches to approximate the stability/security boundary by a set of linear equations are presented in this section. Two systems are considered in the numerical examples, namely the IEEE 3-machine 9-bus test system [Sauer and Pai, 1988], and the IEEE 54-machine 118-bus test system [University of Washington].

3.7.1 IEEE 3-machine 9-bus system

This system is composed of three generators at buses 1, 2, and 3, with active power output limits of 900 MW, 400 MW, and 300 MW, respectively, and three loads at buses 5, 6, and 8, as shown in Figure 3.4. The system generators were modeled using detailed sub-transient models including excitation systems' model Type I. All data for this system can be found in [Sauer and Pai, 1988].

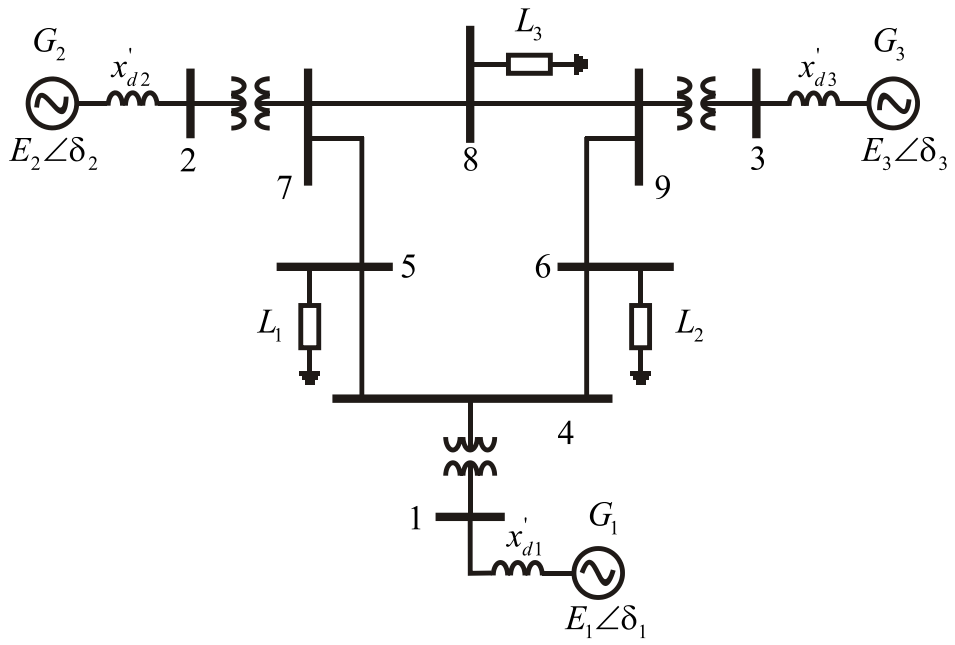

Figure 3.4.On-line diagram of the IEEE 3-machine 9-bus test system.

A. Two areas' study case: stability boundary

In this study case, the generators are grouped in two areas: G_1 in area A, and G_2 and G_3 in area B. The system stability boundary was obtained following the procedure discussed in Section 2.7.1 for 21 feasible and different generation directions for each generationarea and aprespecified loading pattern, based on static and dynamic studies using the continuation method described in [Milano, 2005]. Hence, the resulting stability boundary is composed of pairs $\left[P^c_{G_A}, P^c_{G_B}\right]$ associated with the dispatch directions of each control area, as shown in Figure 3.5.

Once the boundary points of the feasibility boundary are obtained, and the process described in Section 3.4 is applied, we obtain the piecewise linear approximation of the boundary with a total number of 20 hyperplanes, as shown in Figure 3.6.

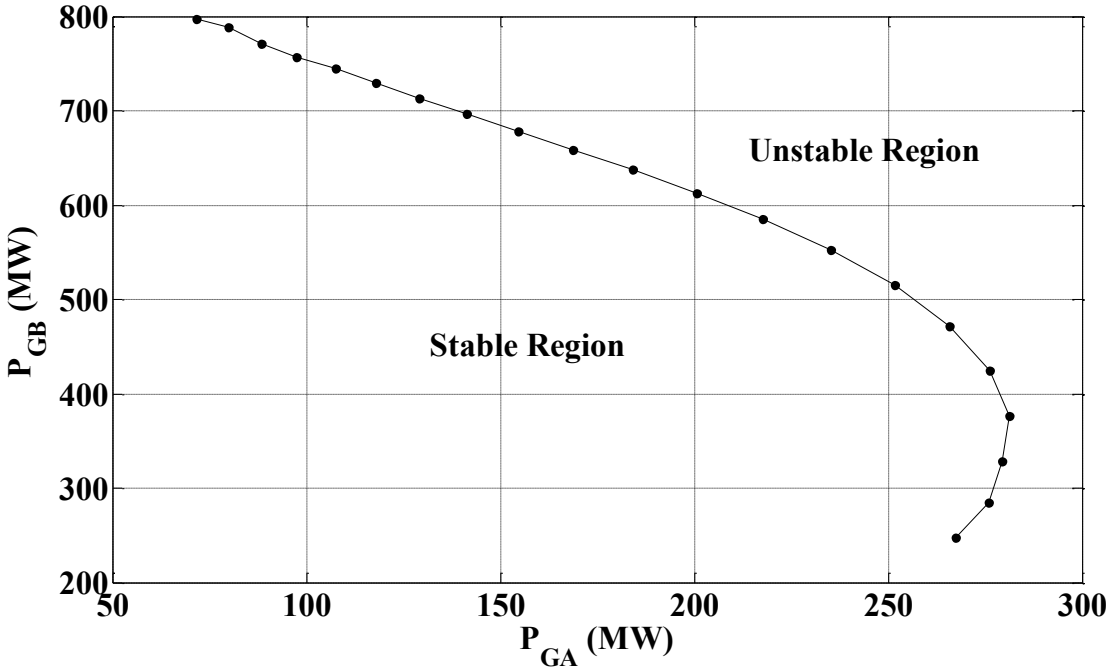

Figure 3.5. Stability boundary of the IEEE 9-bus test system: two areas.

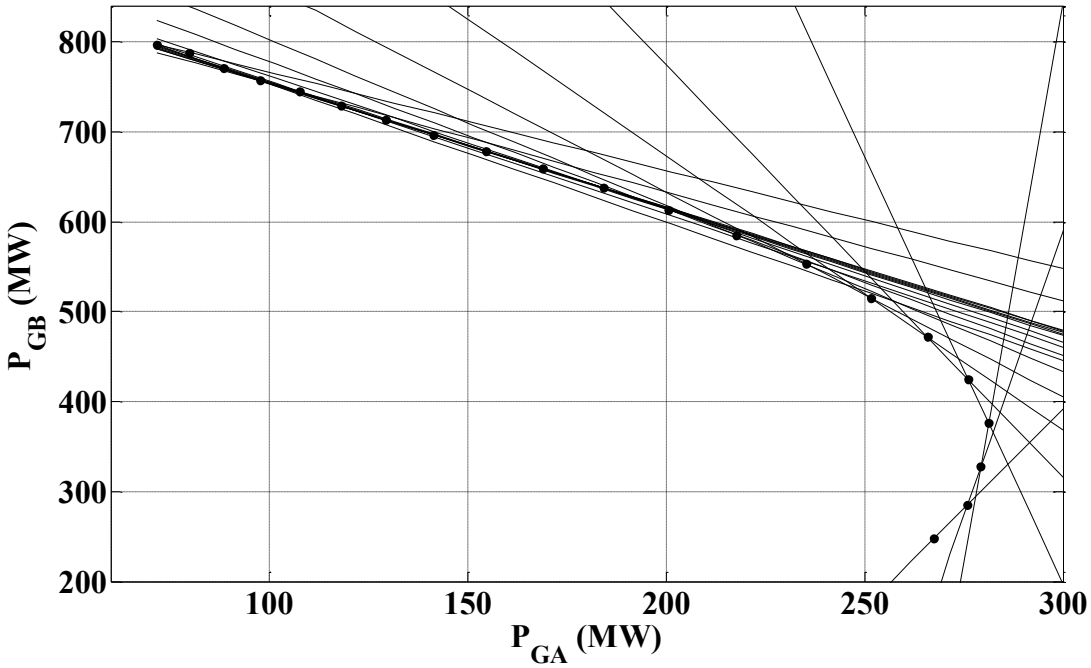

Figure 3.6. Approximation of stability boundary of the IEEE 9-bus test system: two areas.

B.1 Three areas' study case: stability boundary

In the next two cases the IEEE 9-bus test system is divided into three generation control areas directly related to each generator, i.e. areas A, B, and C correspond to generators G_1, G_2, and G_3, respectively. Similarly to the previous case, the system feasibility boundary was obtained for a given loading direction supplied from 631 different generation directions for each generation area, using static and dynamic analysis.

The resulting stability boundary is composed of points $\left[P^c_{G_A}, P^c_{G_B}, P^c_{G_C}\right]$ associated with the generation directions of the generators located at A, B and C control areas. The stability boundary for this system is shown in Figure 3.7, while the total number of hyperplanes required to approximate this boundary by brute force, boundary points' approximation, and inner product approaches, respectively, is illustrated in Table 3.1. Note that a reduction of 79% and 91% in the number of approximant hyperplanes is achieved by the boundary points' approximation and inner product approaches with respect to the brute force approach, respectively.

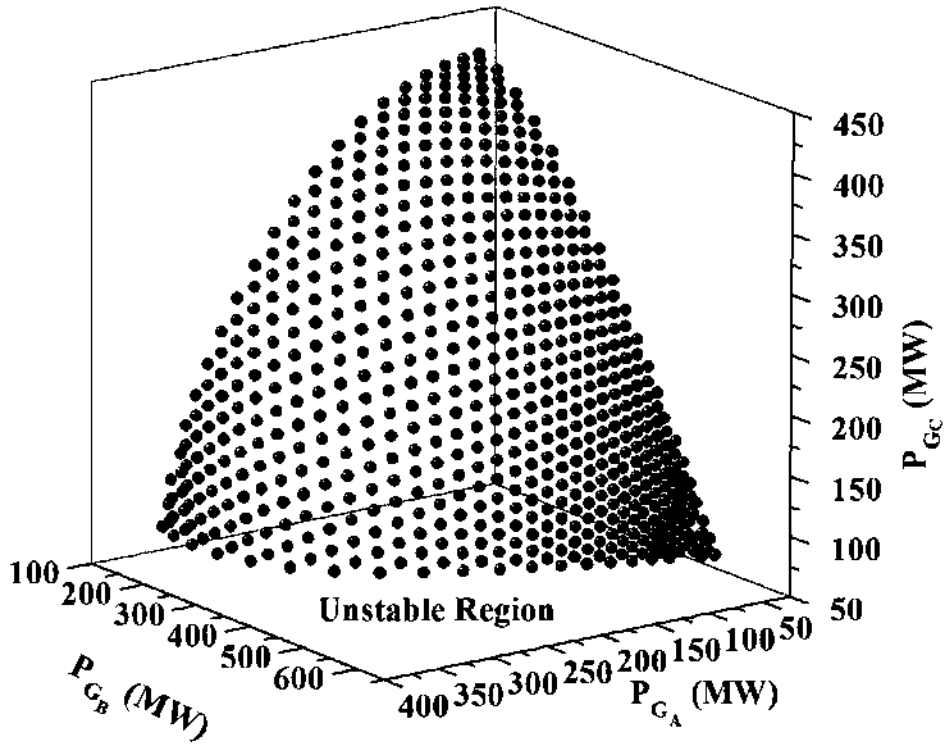

Figure 3.7. Stability boundary of the IEEE 3-machine 9-bus test system: areas.

Table 3.1: Number of Σ^{hy} for the IEEE 3-machine 9-bus system: stability boundary.

Approximationapproach	***Number of planes***
Brute force	630
Boundary points' approximation	132
Inner product	52

The absolute errors between the boundary points composing Σ and their corresponding approximants hyperplanes is obtained by Equation (3.15), and these are reported in Figures. 3.8and3.9 for the boundary points' approximation and inner product approaches, respectively. Note that the maximum absolute error of the boundary points' approximation does not exceed 0.25%, proving that the approximation is fairly accurate. Moreover, the maximum absolute error related to the application of the inner product approach is below 0.9%; this increment with respect to the boundary points' approximation is due to the minimum number of hyperplanes employed to perform the linear approximation of Σ, so that each hyperplane approximates a greater number of boundary points.

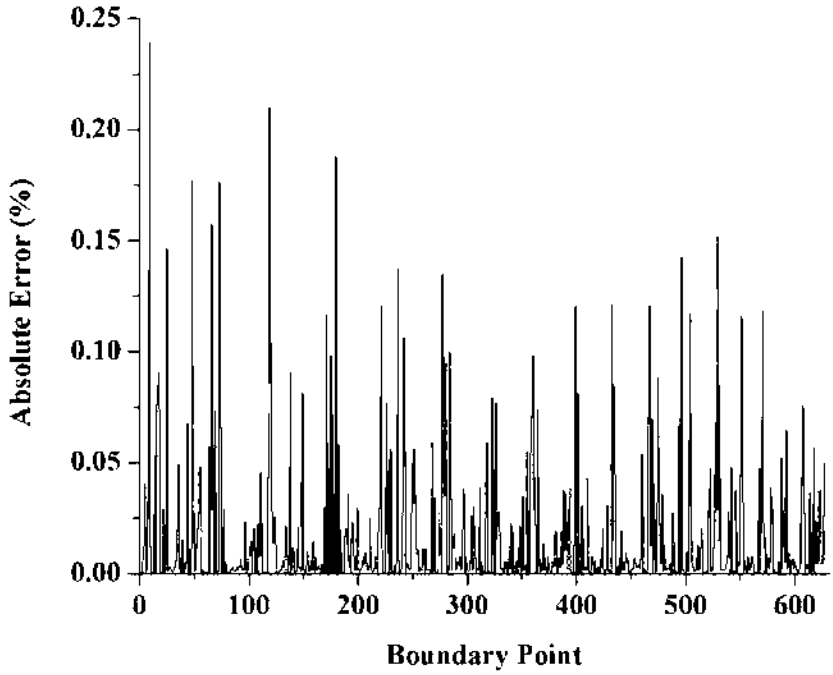

Figure 3.8 Absolute error with the boundary points' approximation of the IEEE 9-bus stability boundary.

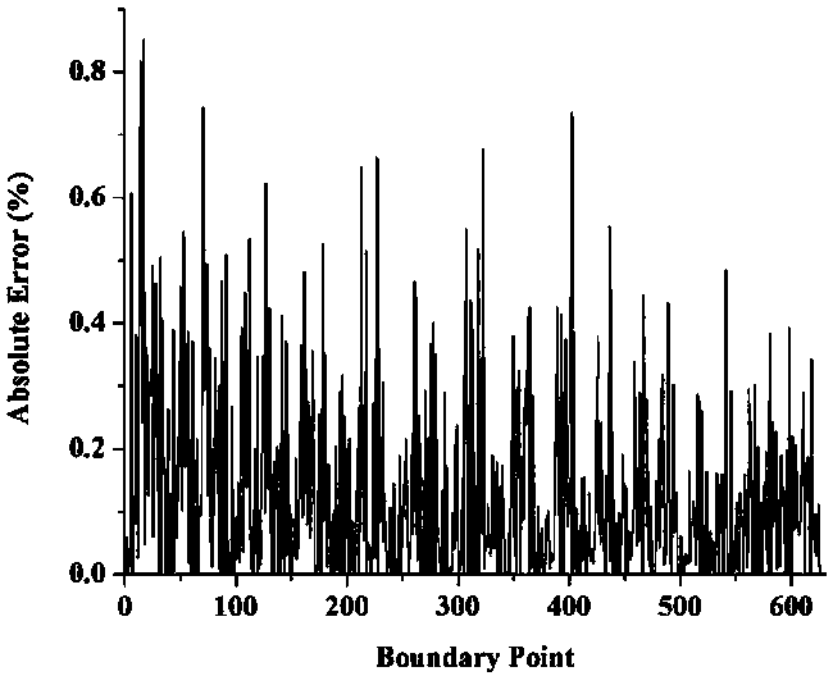

Figure 3.9.Absolute error with the inner product approach approximation of the IEEE 9-bus stability boundary.

B.2 Three areas' study case: security boundary

The study previously reported in **B.1** has been repeated considering a contingency corresponding to the tripping of the line connecting nodes 5-7. Hence, the system's stability boundary in Figure 3.7 becomes the security boundary shown in Figure 3.10, which required 630, 80, and 20 hyperplanes to approximate it using the brute force, boundary points' approximation, and inner product approaches, respectively, as shown in Table 3.2. In this case, the maximum absolute errors between the security boundary points and their corresponding approximant hyperplanes were 0.23247% and 0.7304% for the boundary points' approximation and inner product approaches, respectively, as shown in Figures 3.11 and 3.12, respectively.

Table 3.2: Number of Σ^{hy} for the IEEE 3-machine 9-bus system: security boundary.

Approximationapproach	***Number of planes***
Brute force	630
Boundary points' approximation	80
Inner product	20

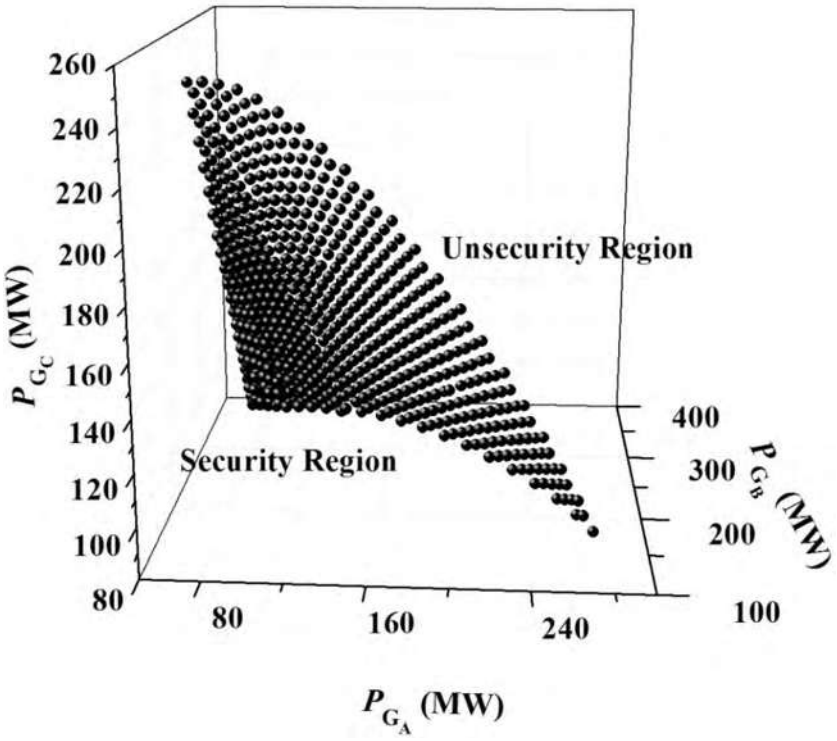

Figure 3.10. Security boundary of the IEEE 3-machine 9-bus test system: three areas.

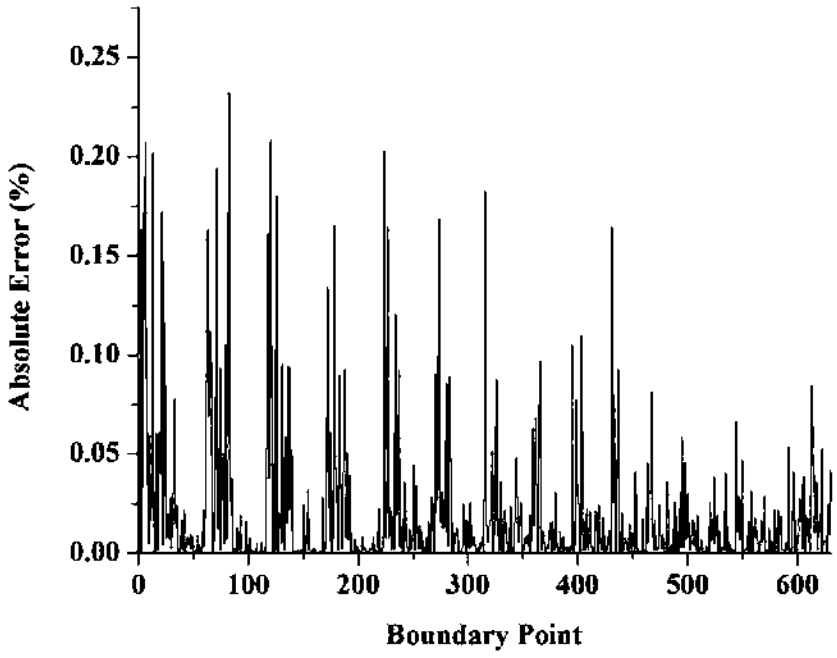

Figure. 3.11. Absolute error with the boundary points' approximation.

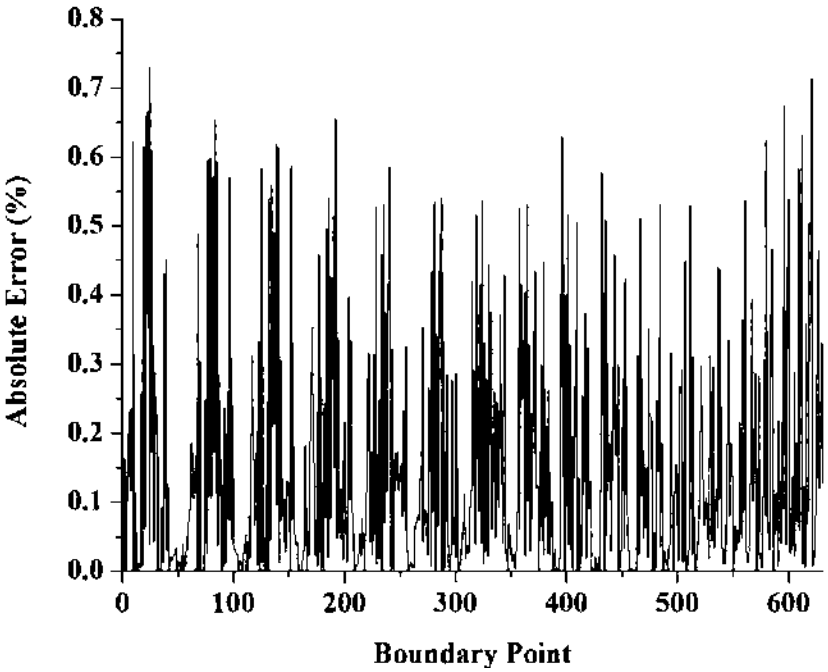

Figure 3.12.Absolute error with the inner product approach.

3.7.2 IEEE 54-machine 118-bus test system

Once it has been proved that the proposed approach accurately represents the security boundaries, the IEEE 118-bus test system [University of Washington]was used to prove its effectiveness and efficiency when dealing with a more realistic and larger power system. For this system,a static voltage security boundary was obtained for the worst single contingency, corresponding to a line 39-40 trip.

A. Two areas study case

For this case, the system has been divided into two operating areas: area A with 26 generators and area B with 28 generators. The security boundary shown in Figure 3.13 has been obtained by considering 21 different generation directions for each control area. A total of 20 hyperplanes were necessary to linearly approximate the resulting security boundary, as shown in Figure 3.14.

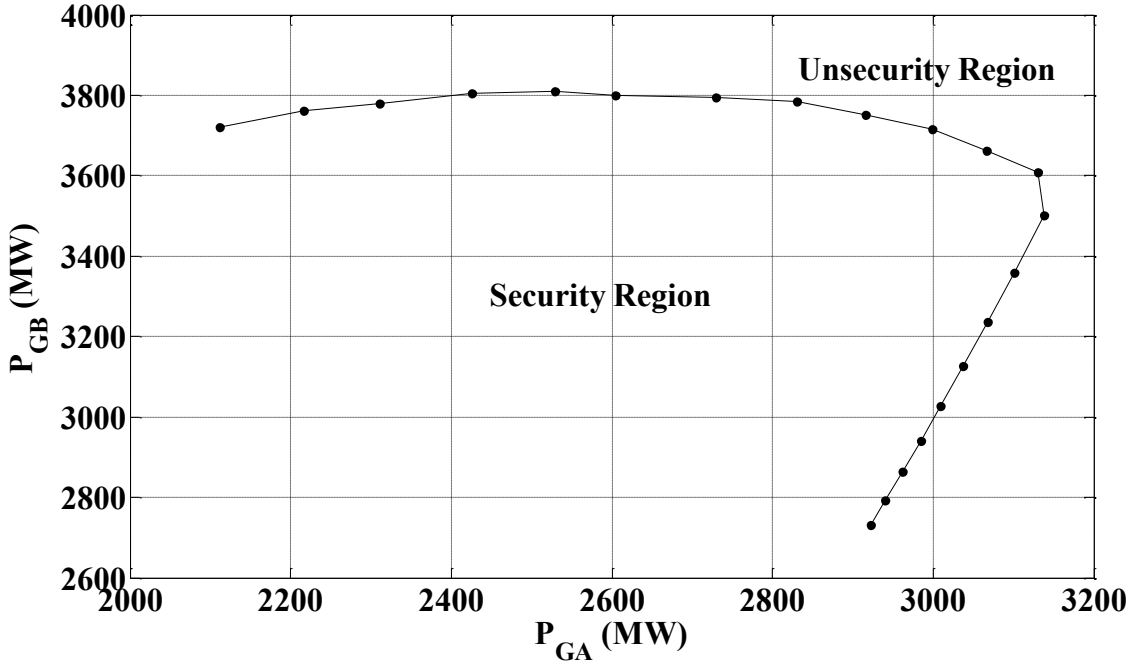

Figure 3.13. Security boundary of the IEEE 118-bus test system: two control areas.

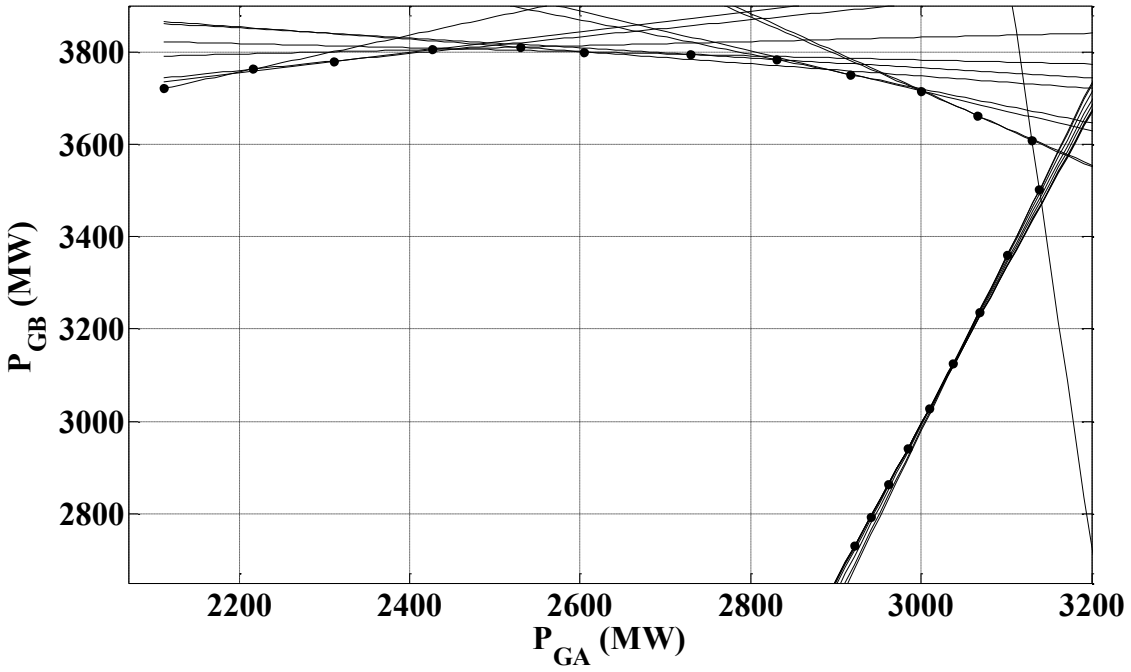

Figure 3.14. Linear approximation of the security boundary of the IEEE 118-bus test system: two control areas.

B. Threeareas study case

The 118-bus system was divided into three operating areas: area A, area B, and area C, with 18 generation units each. The resulting security boundary was obtained for 631 generation directions for each dispatch area, which is depicted in Figure 3.15, while the number of hyperplanes required for its linear approximation is shown in Table 3.3. Note that the boundary points' approximation and inner product approaches reduce the number of hyperplanes by 76% and 96%, respectively, in regards to the brute force methodology. As expected, the boundary points' approximation is the one with the smallest errors, which do not exceed 2.4%, as shown in Figure 3.16, whereas the errors do not exceed 9.8% when the inner product approach is applied, as shown in Figure3.17; the errors for the latter approach are due to the larger reduction in the total number of hyperplanes used to represent Σ.Please note that these errors could be reduced if the approximation error criterion and the angle between two normal vectors to their corresponding hyperplanes were made smaller in the boundary points and inner product approximations, respectively; this would, however, increase the number of approximant hyperplanes required to approximate the security boundary.Thus,computational costs would increase when the hyperplanes are introduced as linear constraints in the SC DC-OPF dispatch model.

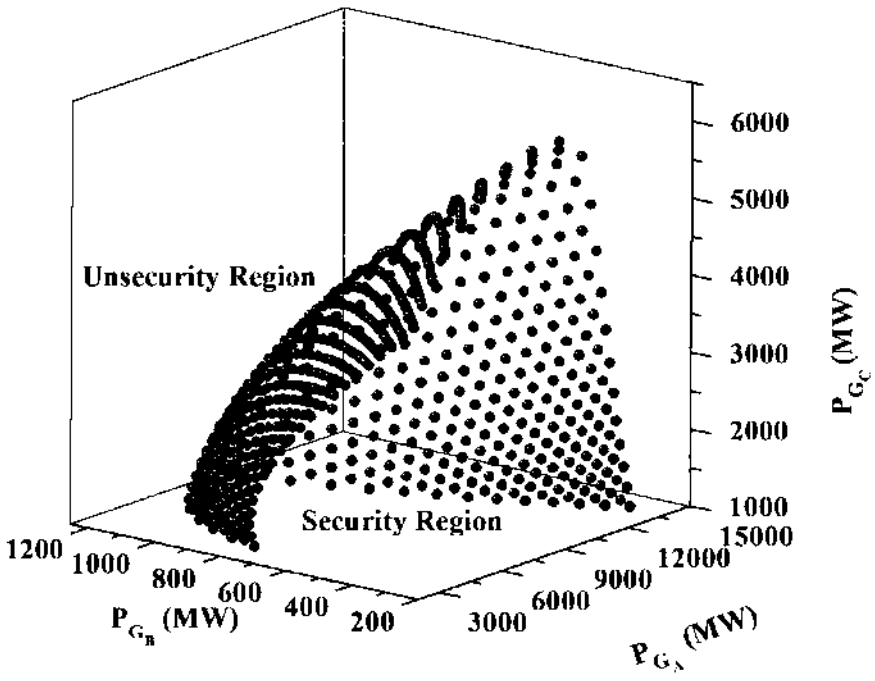

Figure 3.15.Security boundary of the IEEE 118-bus test system, three areas.

Table 3.3: Number of $\sum^{hy}$ for the IEEE 54-machine 118-bus system $\sum$ security boundary.

Approximation approach	*Number of planes*
Brute force	630
Boundary points' approximation	153
Inner product	25

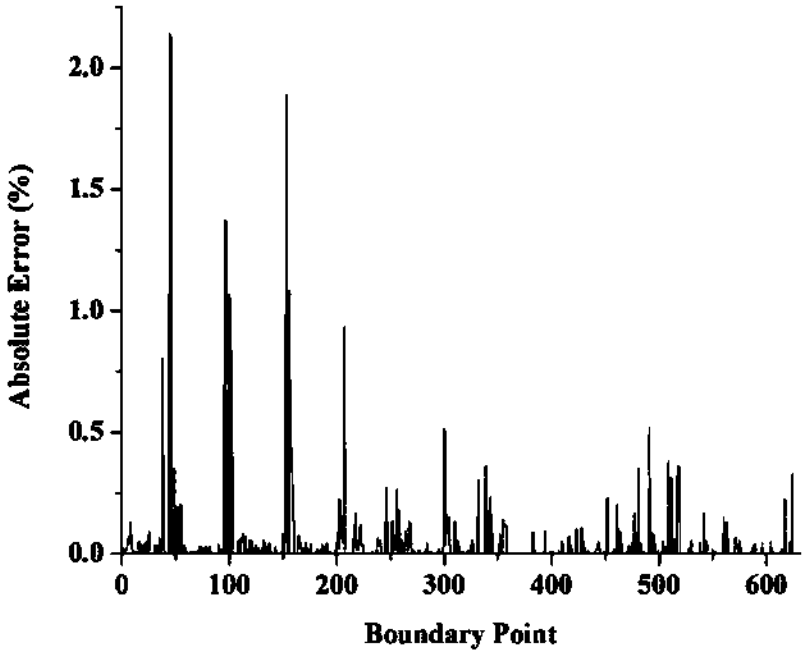

Figure 3.16.Absolute error with the boundary points' approximation of the IEEE 118-bus test system.

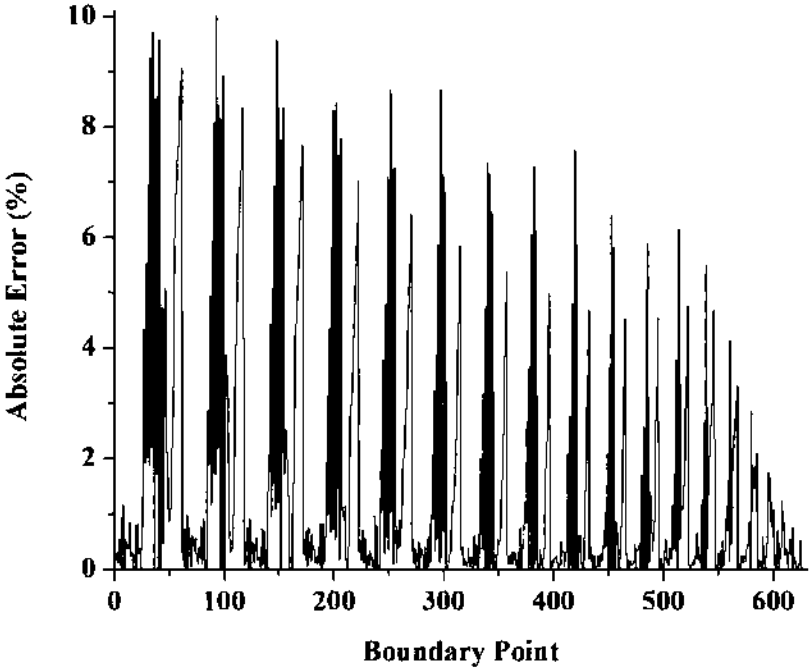

Figure 3.17.Absolute error with the inner product approach of the IEEE 118-bus test system.

3.8 Conclusions

A proposed approach to linearly approximate a voltage feasibility boundary using a set of hyperplanes has been detailed in this Chapter. Furthermore, two new methods to reduce the number of linear hyperplanes to be used in the analytical description of this boundary have also been proposed. The application of these algorithms allowed a significant reduction in the number of hyperplanes required to achieve the approximation, which was of the order of 87% and 96% for the boundary points' approximation and inner product, respectively.

The accuracy of the proposed reduction algorithms was obtained by calculating the existing absolute error between the bifurcation points composing the feasibility boundary and the corresponding approximant hyperplanes. In these cases, higher errors were obtained when the inner product algorithm, with respect to boundary points' approximation, was employed.

Chapter 4

Stability/security boundary-constrained DC optimal power flow

4.1 Introduction

The proposed stability/security boundary-constrained DC optimal power flow, in which the feasibility boundary is represented by a set of linear inequality constraints directly derived from the boundary's piecewise linearization based on approximant hyperplanes, is detailed in this chapter. Additionally, the formulations of the typical security-constrained (SC) DC-OPF linear model and the nonlinear security boundary-constrained (SBC) DC-OPF model are presented in order to discuss and compare the results obtained from the application of the proposed approach.

4.2 Security constrained DC-OPF

The typical single-period SC DC-OPF based dispatch model represents the system security based on constraints of power flow transfer limits. Furthermore, it is formulated as a linear programming problem, consisting of a scalar objective function to be minimized subject to a set of linear equality and inequality constraints, as follows [Battistelli et al., 2011]:

$$\min_{P_{G_i},\delta_k} \sum_{i=1}^{n_G} C_{G_i} P_{G_i} \tag{4.1}$$

s.t.

$$P_{G_k} - P_{L_k} - \sum_{\substack{m=1 \\ m\neq k}}^{n_b} \left(P_{km}^{loss} + P_{km} \right) = 0 \quad \forall k \in n_b \tag{4.2}$$

$$P_{km} - b_{km}\left(\delta_k - \delta_m\right) = 0 \qquad \forall k,m,k \neq m \in n_b \tag{4.3}$$

$$P_{km}^{\min} \leq P_{km} \leq P_{km}^{\max} \qquad \forall k,m,k \neq m \in n_b \tag{4.4}$$

$$P_{G_i}^{\min} \leq P_{G_i} \leq P_{G_i}^{\max} \qquad \forall i \in n_G \tag{4.5}$$

where C_{G_i} is the cost of the *i*-th generator's bid power in \$/MWh, n_b is the number of buses, and n_G is the number of generators, with their individual active power generation represented by P_{G_i} in MW, which cannot exceed its minimum and maximum limits $P_{G_i}^{\min}$ and $P_{G_i}^{\max}$, respectively. Furthermore, P_{G_k} and P_{L_k} are the active power generation and demand at the *k*-th bus, respectively; P_{km} represents the power flowing through the transmission element connecting buses k and m, with its susceptance given by b_{km}. In addition, δ is the bus voltage phasorangle. The system losses cause significant impact on generation dispatch; thus, transmission system losses P_{km}^{loss} are incorporated in the dispatch model by means of a piecewise linear approximation, as detailed in [Motto et al., 2002]. The system losses P_{km}^{loss} are given by [Motto et al., 2002]

$$P_{km}^{loss} = g_{km} \sum_{\ell=1}^{L} \alpha_{km}(\ell)\left(\delta_k(\ell) - \delta_m(\ell)\right), \tag{4.6}$$

where $\alpha_{km}(\ell)$ is the slope of the ℓ-th segment of the piecewise linear (PWL) approximation, while g_{km} is the conductance of the transmission element connecting buses *k* and *m*. Finally, system security is represented in this model by minimum and maximum power flow limits, $P_{km}^{\min}$ and $P_{km}^{\max}$, respectively, which are calculated off-line by means of loadability and contingency studies.

Participants in the electricity market demand correct market signals for their operational and investment decisions; however, as mentioned before, improper market signals and/or insecure operating conditions may result from this dispatch model, because its resulting generation dispatch depends on power transfer limits obtained from off-line studies, which do not properly reflect system security for the obtained dispatch. Hence, we explain in the next Sections more proper representations of system security by characterizing security/stability boundaries, from which security constraints are derived, and by considering a variety of generation dispatch patterns.

4.3 SBC DC-OPF nonlinear model

In this Section, an alternative approach for including security constraints into the DC-OPF formulation for electricity markets [Battistelli et al., 2011] is presented. A proper representation of the voltage system security in an operative context consists of characterizing the entire voltage stability region in the parameter space and then representing the stability boundary by means of a differentiable function to be included as a constraint in the OPF approach, which allows the secure power system operation, as proposed in [Gutierrez-Martinez et al., 2011]. In this formulation, a back-propagation neural network (BPNN) is used to represent the system security boundary (SB), and an explicit differentiable function is extracted from the BPNN to be used as the voltage stability constraint [Gutierrez-Martinez et al., 2011]:

$$\min_{P_{G_i},\delta_k} \sum_{i=1}^{n_G} C_{G_i} P_{G_i} = \sum_{i=1}^{n_G} C_{G_i} P_{G_{i_0}} \left(1 + K_{G_i}\right) \tag{4.7}$$

s.t.

$$P_{G_k} - P_{L_k} - \sum_{\substack{m=1 \\ m \neq k}}^{n_b} \left(P_{km}^{loss} + b_{km} \left(\delta_k - \delta_m \right) \right) = 0 \quad \forall k \in n_b \tag{4.8}$$

$$K_{G_\ell}^{C} - f\left(\hat{K}_G\right) \leq 0 \tag{4.9}$$

$$P_{G_i}^{\min} \leq P_{G_i} \leq P_{G_i}^{\max} \qquad \forall i \in n_G \tag{4.10}$$

where K_{G_i} and $P_{G_{i_0}}$ are the factor of generation active power increase in a given direction and the base active power generation of the *i*-th generator unit, respectively. $K_{G_\ell}^{C}$ are the critical values, which define the SB for the power system model (2.1) along different dispatch directions for a given loading condition, which is used as training and testing sets of the BPNN to determine the SB mapping function. Therefore, as explained in detail in [Gutierrez-Martinez et al., 2011], the SB can be approximated with the following highly nonlinear function, closed-form, differentiable function [Battistelli et al., 2011]:

$$K_{G_\ell}^{C} = \sum_{h=1}^{H} f_h \left[\left(\hat{K}_G^T w^{in} + b_{in} \right) w_{21}^h + b_h \right] w_{32}^h + b_{out} = f\left(\hat{K}_G \right), \tag{4.11}$$

where w, b and $f_h(\cdot)$ correspond to the input (*in*), output (*out*) and hidden layer neuron h weights, biases, and activation functions, respectively, of the BPNN; in addition $\hat{K}_G^T = \begin{bmatrix} K_{G_1} & \cdots & K_{G_{\ell-1}} & K_{G_{\ell+1}} \cdots & K_{G_{n_G}} \end{bmatrix}$ defines the $n_G - 1$ set of generation increases for a given base value of $P_{G_i} = P_{G_{i_0}} \left(1 + K_{G_i}\right)$ [Gutiérrez-Martínez, 2011-1].

4.4 Proposed SBC DC-OPF linear model

Based on the results reported in Section 3.5, where the stability/security boundary of a power system model (2.1) is linearly represented by a set of linear constraints (3.14) directly derived from the set of point-normal equations representing the hyperplanes, we propose a true SBC DC-OPF linear dispatch model to improve existing DC-OPF results. This proposed linear dispatch model is formulated as follows:

$$\min_{P_{G_i}, \delta_k} \sum_{i=1}^{n_G} C_{G_i} P_{G_i} \tag{4.12}$$

s.t.

$$P_{G_k} - P_{L_k} - \sum_{\substack{m=1 \\ m \neq k}}^{n_b} \left(P_{km}^{loss} + b_{km} \left(\delta_k - \delta_m \right) \right) = 0 \quad \forall k \in n_b \tag{4.13}$$

$$\sum_{j=1}^{n_G} \eta_{i,j} P_{G_j} \mp C^i \leq 0 \qquad \forall i = 1, \ldots n_{hy} \tag{4.14}$$

$$P_{G_i}^{\min} \leq P_{G_i} \leq P_{G_i}^{\max} \qquad \forall i \in n_G, \tag{4.15}$$

where Equation (4.14) represents the voltage feasibility boundary constraints which guarantee that the resulting operating point remains within the feasibility region, as illustrated in the next Section. Note that this constraint replaces Equation (4.4) in the typical dispatch model (4.1)-(4.5) to better represent system security in terms of both system voltage and small-perturbation angle stability limits and different operating conditions. As

described before, the set of active power transfer constraints (4.4) are determined from off-line studies that do not necessarily correspond to the actual operating conditions, which may result in unrealistic generation dispatches or jeopardize system security, and demonstrated in the results presented in the next section. Therefore, the main point of the work and proposed linear security constraints is to bring voltage and some angle stability limits for a variety of realistic dispatch patterns into a linear DC-OPF dispatch to improve existing SC DC-OPF techniques used in practice, which is a topic that has not been addressed in previous proposals of SC DC-OPF approaches. If generators are grouped in generation control areas, (4.14) is given by

$$\sum_{k=1}^{n_{G_A}} \left(\eta_{i,k} \sum_{j \in k} P_{Gj}^{A_k} \right) \mp C^i \leq 0 \qquad \forall\, i = 1, \ldots n_{hy}\,, \tag{4.16}$$

where n_{G_A} is the total number of generation control areas, and $P_{Gj}^{A_k}$ corresponds to the active power produced by the *j*-th generator embedded at the *k*-th generation control area.

Lastly, the proposed optimization problem described by (4.12)-(4.15) can be solved via any linear optimization technique. In this thesis, this model was solved using AMPL [Fourer et al., 2003] with the KNITRO solver [KNITRO]. Finally, the flowchart process to solve the proposed linear SBC DC-OPF model is presented in Figure 4.1.

4.5 Study cases

In order to demonstrate the feasibility and benefits of the proposed SBC DC-OPF linear model, the IEEE 3-machine 9-bus test system and the IEEE 54-machine 118-bus test system are used here as examples. Additionally, the typical SC DC-OPF and nonlinear SBC DC-OPF models are used to compare and to validate the proposed model and its results. For both test systems, the stability/security boundaries were obtained by specifying one single direction of loading increase in (2.31), and their corresponding linear stability/security constraints are derived from the piecewise linear approximation by hyperplanes. The parameters associated with the set of point-normal equations representing the hyperplanes are reported in Appendix A.

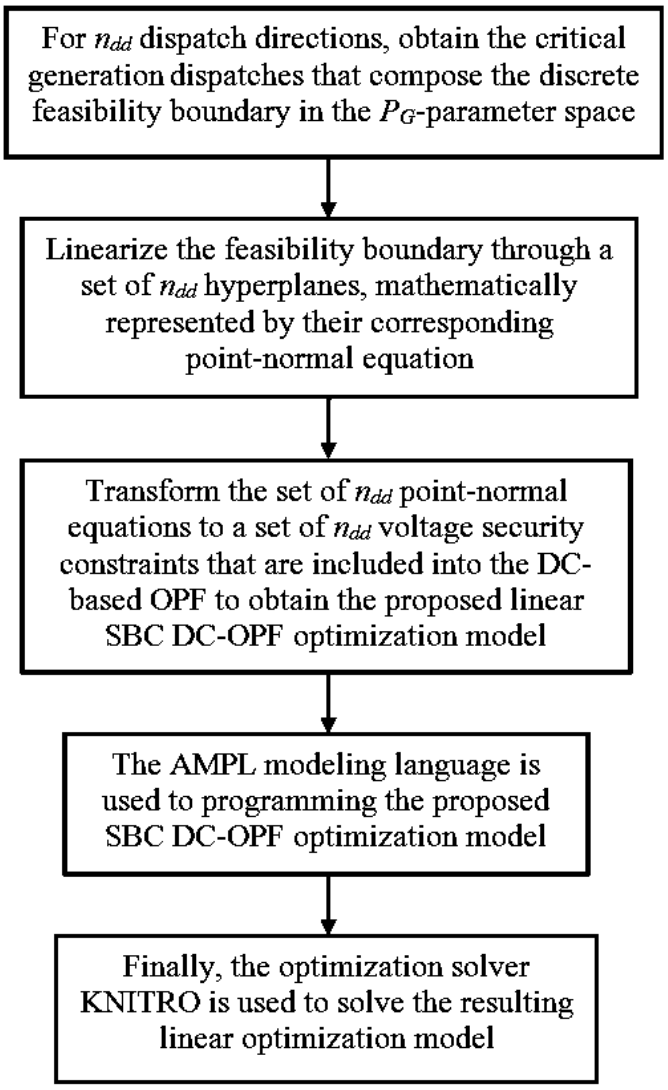

Figure 4.1.Flowchart of the process to solve the proposed linear SBC DC-OPF model.

4.5.1 IEEE 3-machine 9-bus test system

The IEEE 3-machine 9-bus test system shown in Figure 3.4 is used to test the prowess of the proposed linear SBC DC-OPF model for electricity markets. The three cases presented in Subsection 3.7.1 are considered in order to show how the proposed approach can be readily applied to systems containing several control areas.

4.5.1.1 Two control areas: stability boundary

Based on the procedure to obtain the stability boundary in the P_G-parameter space, described in Chapter 2, the resulting boundary was presented in Figure 3.5, and a total of 20 hyperplanes were required to obtain its piecewise linear approximation. The resulting set of linear inequalities associated with these hyperplanes were considered as constraints in Equation (4.14) of the proposed approach in order to achieve the most economic power dispatch when the system load is increased by 10% and 20%, referred to as Case 1 and Case 2 respectively, from the base load scenario. The resulting power dispatches from the optimization solution process are reported in Tables 4.1 and 4.2 for each case, and these are also compared with those results obtained by the application of the classical SC DC-OPF and nonlinear SBC DC-OPF models.

Table 4.1: DC-OPF dispatch results for the IEEE 9-bus system: Case 1.

OPF model	P_{G_A} ***(MW)***	P_{G_B} ***(MW)***	***Losses (MW)***	***Generation Cost ($/h)***
SC DC-OPF	250.598	276.390	7.238	754.083
Nonlinear SBC DC-OPF	250.639	276.349	7.238	754.083
Linear SBC DC-OPF	250.593	276.395	7.238	754.084

Table 4.2: DC-OPF dispatch results for the IEEE 9-bus system: Case 2.

OPF model	P_{G_A} ***(MW)***	P_{G_B} ***(MW)***	***Losses (MW)***	***Generation Cost ($/h)***
SC DC-OPF	306.566	317.760	10.076	890.366
Nonlinear SBC DC-OPF	279.247	345.490	10.486	897.338
Linear SBC DC-OPF	279.964	344.680	10.394	890.802

The dispatch results obtained for Case 1 by the three optimization models provide similar stable dispatch solutions, which all are located within the feasibility region as shown in Figure 4.2.

Regarding the dispatch solutions associated with Case 2, the power dispatches resulting from the optimization solution process associated with the nonlinear SBC DC-OPF and linear SBC DC-OPF models are within the desired feasible and secure region, as shown in Figure 4.3, contrary to the solution provided by the typical security-constrained DC-OPF dispatch model which fails to meet this condition.

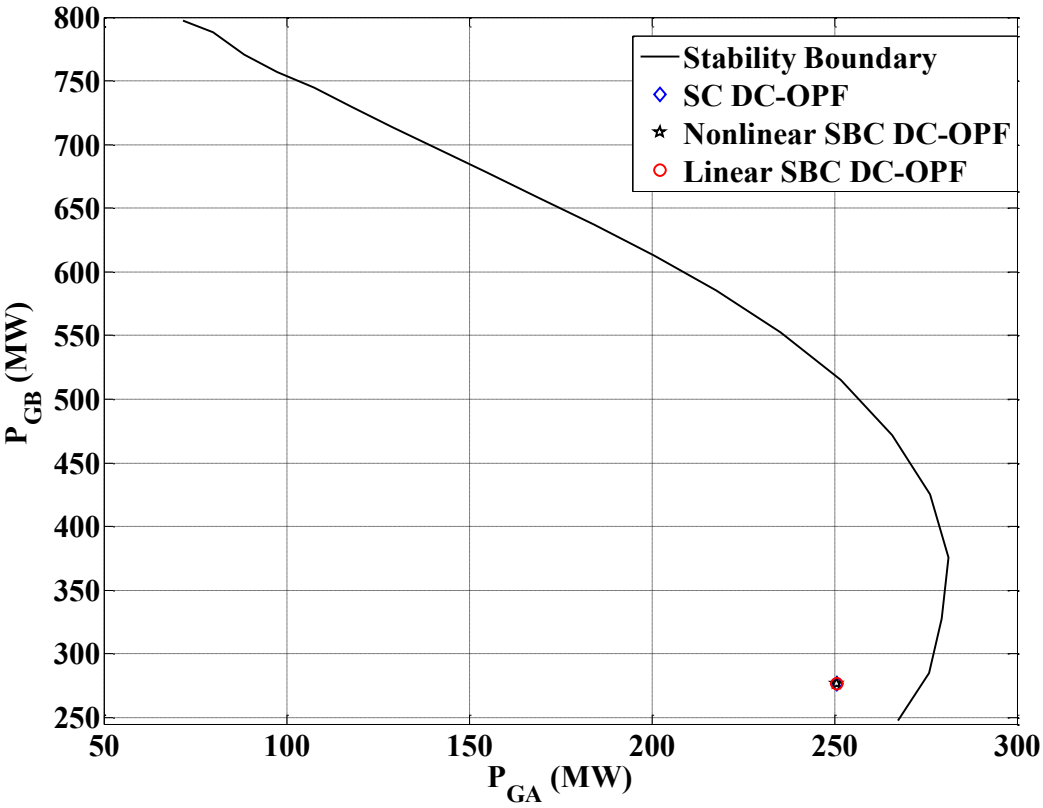

Figure 4.2. Dispatch solutions for the IEEE 9-bus system: loading Case 1.

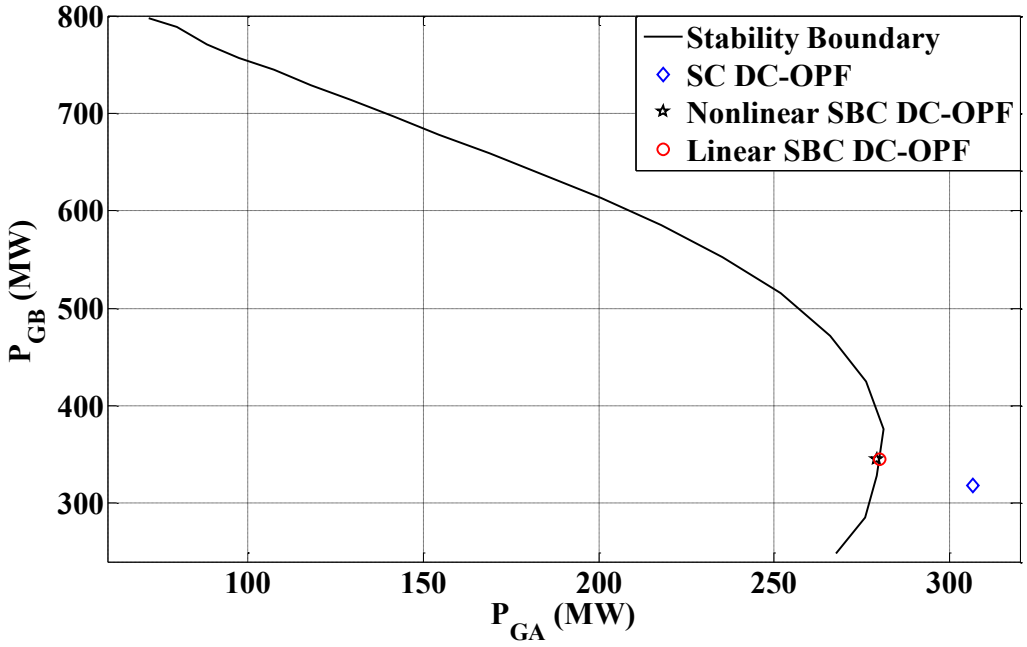

Figure 4.3. Dispatch solutions for the IEEE 9-bus system: loading Case 2.

4.5.1.2 Three control areas

A. Stability analysis

In order to assess if the proposed approach can be applied to systems containing more than two control areas, the IEEE 9-bus test system is divided into three generation areas directly related to each generator, i.e. Areas A, B, and C correspond to generators G_1, G_2, and G_3, respectively. The system stability boundary obtained in the Section 3.7 and shown in Figure 3.7 is used for the following study cases, and the for sake of completeness is newly shown in Figure 4.4. This boundary is linearly approximated by 630 hyperplanes, as we mentioned in Section 3.7.1, such that the security constraint equation (4.14) is composed of 630 linear inequality constraints.

Two loading scenarios with increments of 40% and 60% in the base load were analyzed and are referred to here as Case 3 and 4, respectively. The solutions obtained by the SC DC-OPF, nonlinear SBC DC-OPF and linear SBC DC-OPF optimization models are reported in Tables 4.3 and 4.4 for both scenarios, respectively.

Table 4.3: DC-OPF dispatch results for the IEEE 9-bus system: Case 3.

OPF model	P_{G_A} ***(MW)***	P_{G_B} ***(MW)***	P_{G_C} ***(MW)***	***Losses (MW)***	***Generation Cost ($/h)***
SC DC-OPF	306.042	163.000	135.801	10.192	863.079
Nonlinear SBC DC-OPF	306.036	163.000	135.806	10.192	863.079
Linear SBC DC-OPF	306.034	163.000	135.808	10.192	863.079

The location in the P_G-parameter space of solutions obtained by the three optimization models when a load increment of 40% is considered is shown in Figure 4.4. Note that all solutions lie inside the feasibility region, with very similar generation dispatches and equal production cost, as reported in Table 4.3.

A more stressed scenario is represented in Case 4 with its results shown in Table 4.4 and Figure 4.5.The solution obtained by the SC DC-OPF model is the most economical, but as shown in Figure 4.5, is infeasible since it lies outside of the stability region. Solutions obtained by nonlinear SBC DC-OPF and linear SBC DC-OPF models are a little more expensive, but both are feasible from the point of view of voltage stability.

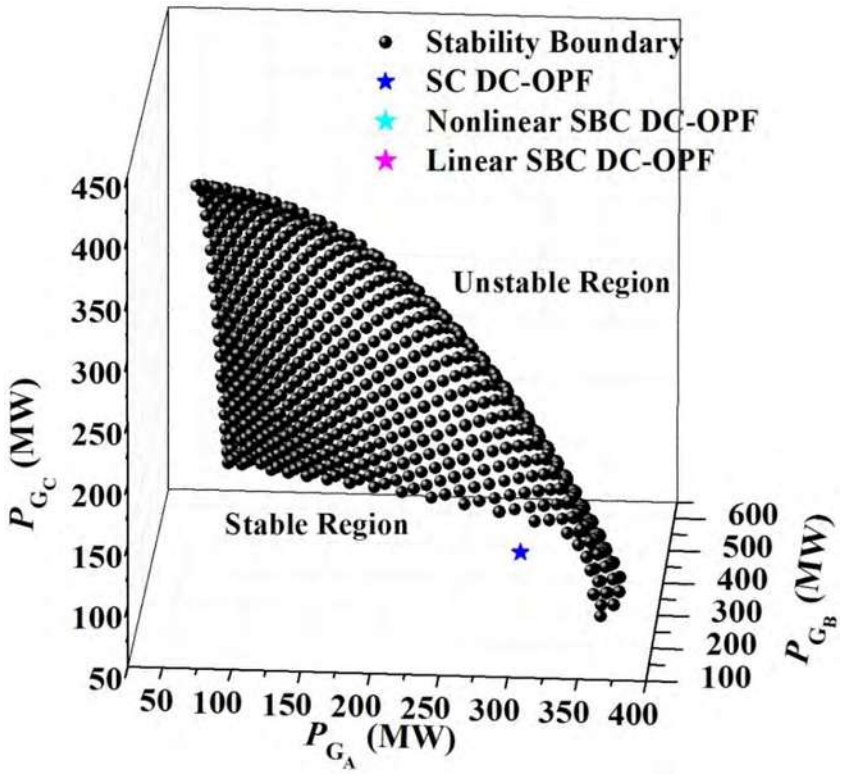

Figure 4.4. Stability boundary and DC-OPF dispatch solutions for the IEEE 9-bus system: Case 3.

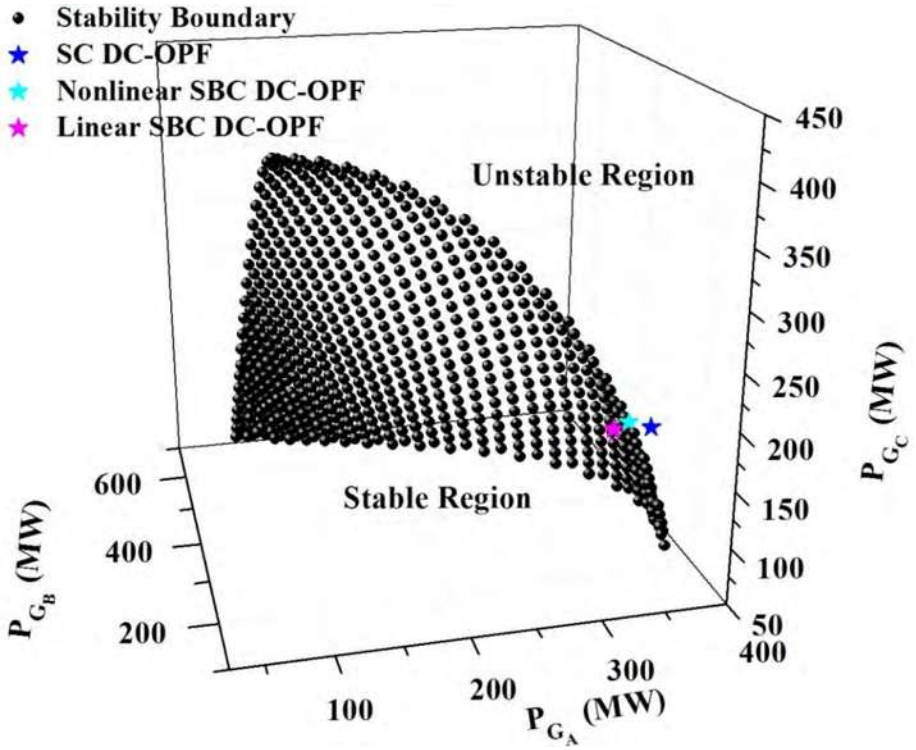

Figure 4.5. Stability boundary and DC-OPF dispatch solutions for the IEEE 9-bus system: Case 4.

Table 4.4: DC-OPF dispatch results for the IEEE 9-bus system: Case 4.

OPF model	P_{G_A} (MW)	P_{G_B} (MW)	P_{G_C} (MW)	Losses (MW)	Generation Cost ($/h)
SC DC-OPF	340.930	163.000	189.096	13.426	986.536
Nonlinear SBC DC-OPF	330.113	164.423	198.628	13.564	986.872
Linear SBC DC-OPF	322.638	182.319	188.221	13.578	988.680

These results reflect the impact of considering the constraints related to the voltage stability problem in the optimization model and confirm that feasible solutions not only depend on the active power demanded from the system and its associated dispatch, but also on the system stability. Note that the solution obtained with the nonlinear SBC DC-OPF model is located at the boundary of the security region where any variation on a system parameter may lead to a system's instability.

The proposed optimization model (4.12)-(4.15) is now solved considering, independently, each set of linear inequality constraints related to each of the three piecewise linear approximation approaches, which required 630, 132 and 52 approximant hyperplanes, respectively . The generation dispatches of each area, system losses and optimal generation cost obtained are reported in Table 4.5. Note that the most economical generation dispatch corresponds to the inner product approach, by presenting the lowest transmission losses and lowest cost of the most expensive generator with respect to the results obtained with the brute force and boundary points' approximation approaches.

Table 4.5: Linear SBC DC-OPF dispatch results for the IEEE 3-machine 9-bus system.

Approximation approach	P_{G_A} (MW)	P_{G_B} (MW)	P_{G_C} (MW)	Losses (MW)	Generation Cost ($/h)
Brute force	322.638	182.319	188.221	13.578	988.680
Boundary points' approximation	323.081	181.254	188.837	13.572	988.567
Inner product	333.381	163.000	196.750	13.531	986.683

B. Security analysis

Table 4.6 shows the optimal generation dispatch obtained with the proposed linear SBC DC-OPF while considering the security constraints associated with each linear representation of the security boundary computed in Section 3.7.1 and shown in Figure 3.10, for a base load increment of 27%. This security boundary is associated with a

contingency corresponding to the tripping of the line connecting nodes 5-7. The numerical comparisons of the results obtained with the proposed linear SBC DC-OPF using the brute force approximation with the results obtained with the SC DC-OPF and the SBC DC-OPF nonlinear model are also reported in Table 4.6; observe in Figure 4.6 that the SC DC-OPF yields an insecure dispatch, i.e. the corresponding solution is located outside the security region. In this case, the optimal generation costs are cheaper than the ones obtained when the stability boundary is considered because of the loadability limit of the system. These results show that the SC DC-OPF linear model provides the cheapest generation dispatch; however, this solution is located outside the security region, which is the opposite of the other two generation dispatches, such that the system is unstable from a voltage stability viewpoint, as shown in Figure 4.6.

Table 4.6: Security DC-OPF dispatch solutions for the IEEE 9-bus system.

OPF model	P_{G_A} *(MW)*	P_{G_B} *(MW)*	P_{G_C} *(MW)*	*Losses (MW)*	*Generation Cost ($/h)*
SC DC-OPF	277.829	163.000	107.055	8.452	783.338
Nonlinear SBC DC-OPF	227.089	196.883	124.610	9.149	787.702
Linear SBC DC-OPF	227.532	224.329	97.119	9.547	791.005

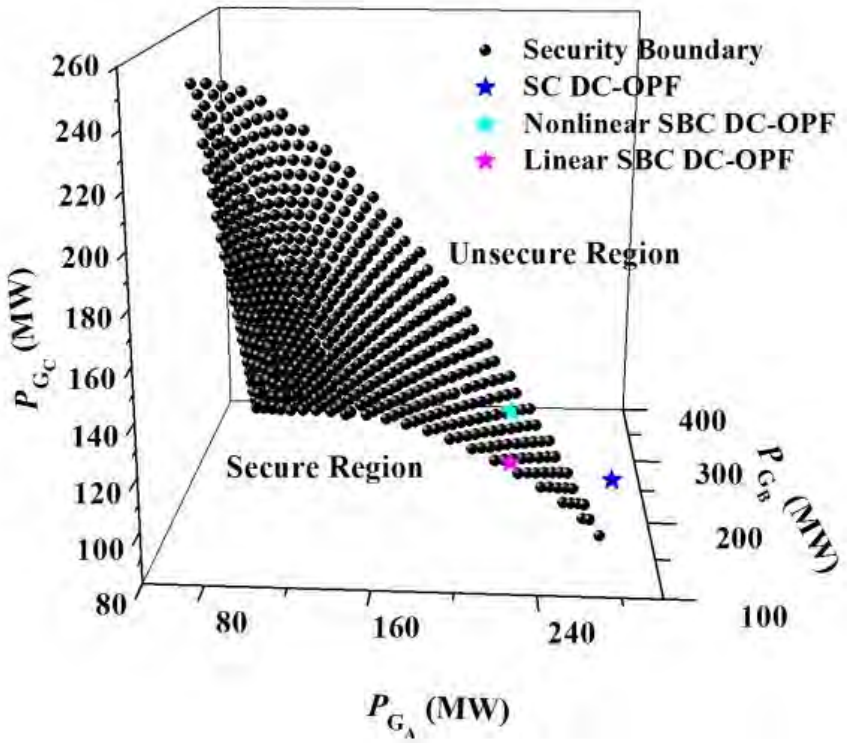

Figure 4.6. Security boundary and DC-OPF dispatch solutions for the IEEE 9-bus system.

Table 4.7 shows the optimal generation dispatch obtained by the proposed linear SBC DC-OPF while considering 630, 80 and 20 linear security constraints associated with each linear representation of the security boundary, respectively. Note that the most economical dispatches correspond to the cases where the security constraints are derived from the linear approximations associated with the use of approximants hyperplanes. Furthermore, the optimal generation costs are cheaper than the ones obtained when the stability boundary is considered because of the loadability limit of the system.

Table 4.7: Secure linear SBC DC-OPF dispatch results for the IEEE 3-machine 9-bus system.

Approximation approach	P_{G_A} ***(MW)***	P_{G_B} ***(MW)***	P_{G_C} ***(MW)***	***Losses (MW)***	***Generation Cost ($/h)***
Brute force	227.532	224.329	97.119	9.547	791.005
Boundary points' approximation	226.796	194.329	127.442	9.134	787.427
Inner product	230.654	196.508	121.364	9.094	787.587

Lastly, Tables 4.8 and 4.9 provide the CPU times required by the security-based DC-OPF models and the proposed linear SBC DC-OPF approaches, respectively. All OPF models were solved using AMPL [Fourer et al., 2003] with the KNITRO solver [KNITRO] in a computer with a 2.93GHz CPU and 16 GB of RAM.

Table 4.8: CPU times for the security-based DC-OPF models.

Model	**Time *(Seconds)***
SC DC-OPF	8.86e-3
Nonlinear SBC DC-OPF	7.95e-3
Linear SBC DC-OPF	32.08e-3

Table 4.9: CPU times for the linear SBC DC-OPF approaches.

Approximation approach	**Time *(Seconds)***
Brute force	32.08e-3
Boundary Points´ approximation	15.98e-3
Inner product	13.69e-3

4.5.2 IEEE 54-machine 118-bus test system

Once it had been proved that the proposed approach accurately considers feasibility boundaries as constraints in the optimization model, the IEEE 54-machine 118-bus test system was used to prove the effectiveness of the proposed approach when dealing with a larger power system. This system was divided into three operational areas with 18 generators each. The static voltage security boundary obtained in Chapter 3 for the worst single contingency, corresponding to a line 39-40 trip, is shown in Figure 4.7. The dispatch solutions regarding the three approximation approaches, considering a 15% increment in the system's base load, are shown in Table 4.10. In these cases, all generators have been assumed to have different production costs in the range of 0.3 to 0.8 $/MWh, while 630, 153 and 25 linear inequality constraints were required by the proposed approach when the brute force, boundary points' approximation and inner product approaches are used to approximate the security boundary, respectively.

Table 4.10: Linear SBC DC-OPF dispatch results for the IEEE 118-bus system.

Approximation approach	P_{G_A} ***(MW)***	P_{G_B} ***(MW)***	P_{G_C} ***(MW)***	***Losses (MW)***	***Generation Cost ($/h)***
Brute force	3096.140	848.939	1816.800	139.025	1775.755
Boundary points' approximation	3156.700	861.471	1766.500	161.815	1783.309
Inner product	3141.140	859.914	1765.340	143.535	1777.921

For comparison purposes, the SC DC-OPF and linear SBC DC-OPF models were used to obtain the optimal generation dispatches for this loading scenario, with the corresponding solutions being shown in Table 4.11; the "location" of the corresponding dispatches in the P_G-parameter space are depicted in Figure 4.7. Note that the SC DC-OPF model provides the most expensive and insecure solution, while the solution obtained with the linear SBC DC-OPF model is the most economical and secure.

Table 4.11: DC-OPF solutions for the IEEE 118-bus system.

OPF model	P_{G_A} ***(MW)***	P_{G_B} ***(MW)***	P_{G_C} ***(MW)***	***Losses (MW)***	***Generation Cost ($/h)***
SC DC-OPF	2694.120	1217.990	1844.460	133.714	1778.863
Linear SBC DC-OPF	3096.140	848.939	1816.800	139.025	1775.755

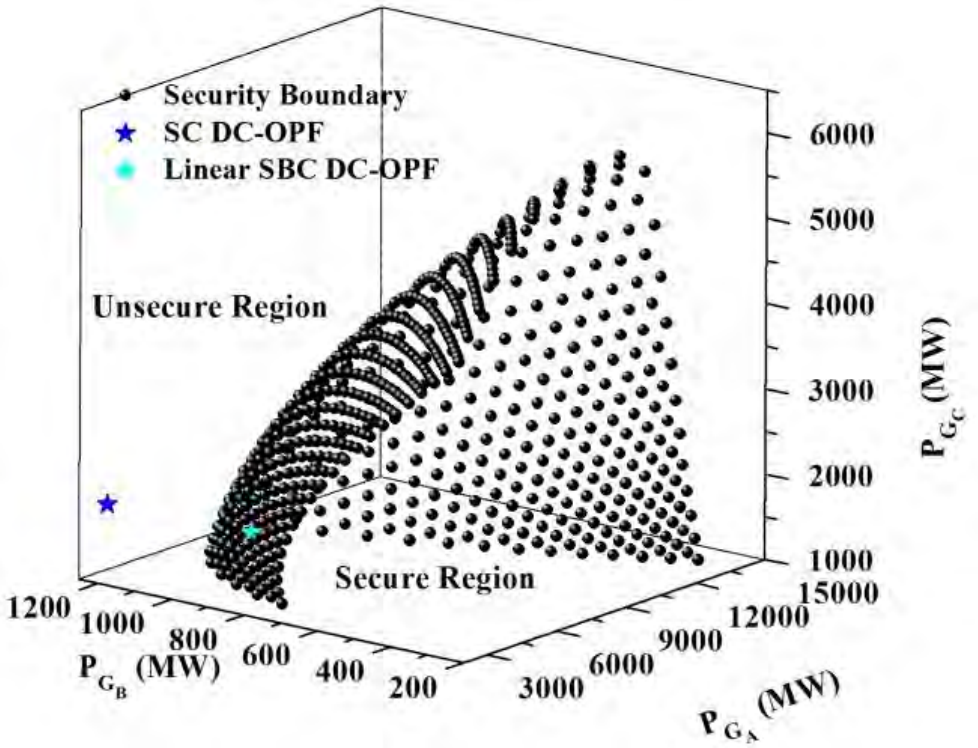

Figure 4.7. Security boundary and DC-OPF dispatch solutions for the IEEE 118-bus system.

CPU times required by the SC DC-OPF and linear SBC DC-OPF models are reported in Tables 4.12 and 4.13, respectively, for the aforementioned computer system.

Table 4.12: CPU times for the security-based DC-OPF models for the 118-bus system.

Model	**Time** ***(Seconds)***
SC DC-OPF	0.33139
Linear SBC DC-OPF	1.85205

Table 4.13: CPU times for the linear SBC DC-OPF approaches for the 118-bus system.

Approximation approach	**Time** ***(Seconds)***
Brute force	1.85205
Boundary Points' approximation	1.25721
Inner product	0.65581

Even though the operator would intuitively expect that one can sacrifice economic gain for security, the reason for the non-intuitive behavior in the results summarized in Table 4.11 and Figure 4.7 is that the proposed approach reduced the amount of generation in area B in order to maintain the operation within the secure operating region; this does not occur when the SC DC-OPF is employed to obtain the optimal operation state. The impact of this security control action on the generation cost of each area is reported in Table 4.14, where one can infer that the generation cost in areas B and C is reduced to 114.31 *$/h* and 12.71*$/h*, respectively. In order to supply the demand, however, generation in area A is increased resulting in a cost increment of 123.9 *$/h*. Since the reduction in the generation cost of areas B and C is higher than the increment in area A, the system security is preserved at the minimum operation cost.

Table 4.14: Generation costs of control areas for the IEEE 118-bus system.

OPF model	**Generation costs**			
	Area A ($/h)	***Area B ($/h)***	***Area C ($/h)***	***Total Cost ($/h)***
SC DC-OPF	809.57	411.54	557.74	1778.86
Linear SBC DC-OPF	933.47	297.23	545.03	1775.74

Independently of the cost of generation in area B, the proposed approach will tend to reduce the generation of active power in this area to give priority to the system security rather than its economic operation. In order to validate this statement, the previous study case has been repeated but by considering a production cost of 0.1 *$/MWh* for all generators embedded in the generation area B and of 0.3 *$/MWh* for all generators located in areas A and C. The results are reported in Table 4.15; the proposed approach sacrifices an economic operation for security gain, and its optimal operating point is more expensive than the one obtained by the SC DC-OPF, which is the intuitive and expected result. The latter, however, obtains an optimal operating point outside the voltage feasibility region as shown in Figure 4.8.

Table 4.15: DC-OPF solutions for the IEEE 54-machine 118-bus system.

OPF model	P_{G_A} ***(MW)***	P_{G_B} ***(MW)***	P_{G_C} ***(MW)***	***Losses (MW)***	***Generation Cost ($/h)***
SC DC-OPF	2397.77	1472.85	1880.04	127.81	1430.63
Linear SBC DC-OPF	3383.02	919.52	1476.80	156.48	1549.90

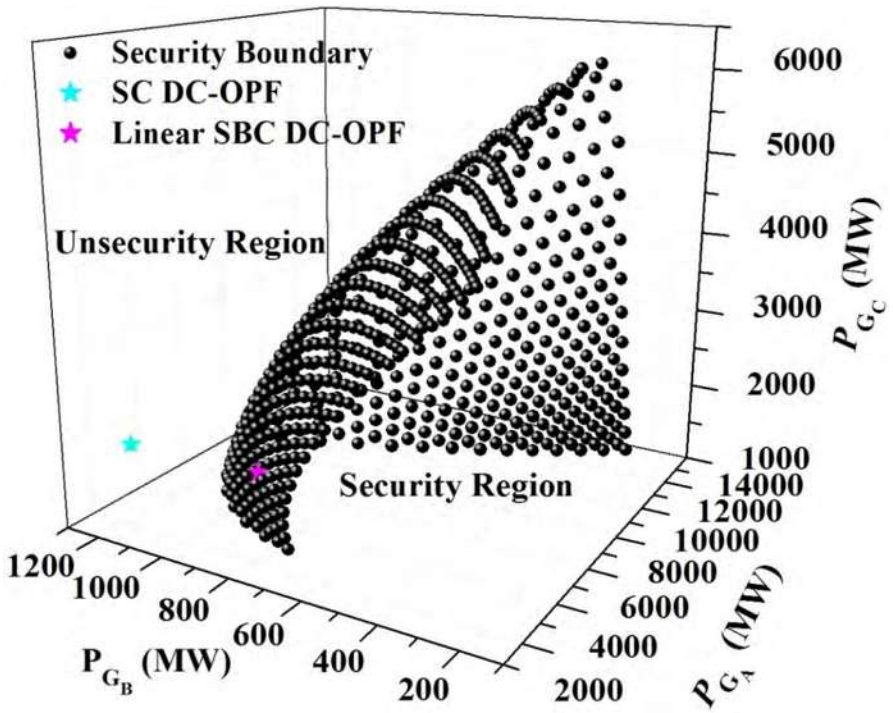

Figure 4.8. Security boundary and DC-OPF dispatch solutions for the IEEE 118-bus system with modified generation costs.

4.6 Conclusions

Before to present the proposed SBC DC-OPF linear model, a typical SC DC-OPF and a nonlinear SBC DC-OPF dispatch models was reported. The SC DC-OPF model includes active power transfer equations as part of the optimization dispatch constraints. On the other hand, the nonlinear SBC DC-OPF model uses a technique that yields a better representation of the feasibility boundary in form of an explicit function, which accounts for system dynamics; this function, however, is highly nonlinear introducing nonlinearities to the DC-OPF, which is undesirable. On the contrary, the proposed model uses an accurate and proper technique to approximate the feasibility boundary by a piecewise linear representation derived from a set of hyperplanes. This technique represents a novel and advanced approach in terms of efficiently characterizing the feasibility boundary with respect to previously proposed security-based DC-OPF models.

Based on the proposed approach, the set of hyperplanes equations that compose the piecewise linear approximation were included as constraints into a SC DC-OPF dispatch model, resulting in the proposed SBC DC-OPF. Furthermore, the dimension of the proposed SBC DC-OPF linear model was considerably reduced applying the boundary points' approximation and the inner product algorithms.

All the aforementioned models were solved using AMPL with the KNITRO solver. Numerical results of the proposed approach were presented by using the IEEE 3-machine 9-bus and IEEE 54-machine 118-bus test systems. Results obtained with the proposed approach were validated using the SC DC-OPF and nonlinear SBC DC-OPF models, where in some cases the three models yield the same feasible dispatch solution. In more stressed cases, the SC DC-OPF provides unsecured dispatch solutions that compromise system security, while the nonlinear SBC DC-OPF and the proposed approach provide similar and feasible dispatch solutions. Finally, the computational burden of the proposed approach was presented and compared with respect to the other security-based DC-OPF models.

Chapter 5

Conclusions and contributions

5.1 Conclusions

The set of active power transfer constraints used in the classical SC DC-OPF model formulationis determined from off-line studies that do not necessarily correspond to the actual operating conditions. The result may bein unrealistic generation dispatches or jeopardize system security, as demonstrated in the results presented in this thesis. Therefore, the main point of this work and proposed linear security constraints is to bring voltage and some angle stability limits for a variety of realistic dispatch patterns into a linear DC-OPF dispatch to improve existing SC DC-OPF techniques used in practice, which is a topic that has not been addressed in previous proposals of SC DC-OPF approaches. In this context, this thesis proposes a DC OPF-based approach that properly considers system security/stability boundaries. The original nonlinear stability/security boundaries have been linearized based on point-normal equations representing hyperplanes. These equations have been transformed in a set of linear inequality security/stability constraints that has been included into the proposed voltage security-constrained DC-OPF dispatch model. Practical methodologies and procedures have also been proposed to reduce the number of hyperplanes required to linearly approximate the power system security/stability boundaries, which substantially reduce the dimension of the proposed linear optimization model.

On the other hand, the voltage and the influence of reactive power are implicitly considered in the proposed SBC DC-OPF model through the stability/security boundary constraints. This is because the feasibility boundary, from which the stability constraints are derived, is computed considering a full AC model of the network under analysis, including relevant system dynamics. This boundary includes a set of equilibrium points associated with codimension-1 generic local bifurcations, i.e. saddle-node, Hopf, or limit-induced bifurcations, which directly reflect voltage and small-signal angle stability limits.

Therefore, each one of these equilibrium points which defines an operating state of the system defines a loadability limit representing the system's critical active and reactive powers beyond which the system loses its voltage or angle stability. This boundary is only represented in the P_G-parameter space in the Thesissince generator active powers are the main control variables in an OPF model; however,voltage and angle stability and the influence of reactive powers are implicitly considered in the security boundary.

Since the proposed technique better represents system security, by considering the worst contingencies than simple limits on transmission corridors used in SC DC-OPF based dispatch approaches, the linear SBC DC-OPF is expected to generate optimal generator dispatches that are in principle closer to the dispatch required to reduce/avoid congestions and load shedding. Despite that the proposed approach determines appropriate dispatches for the given set of stability/security constraints, the possibility exists that no feasible solution might be obtained by the proposed approach, which can be associated with an inability of the system to supply its demand in a stable and/or secure way.

The discussed numerical examples illustrate the effectiveness of the proposed piecewise linear SBC DC-OPF dispatch model demonstrating its merits with respect to a DC OPF-based dispatch models used in practice. The presented case studies and their results show that the proposed dispatch algorithm ensures that the resulting operating points are optimal from both the economical and security points of view. Therefore, this dispatch model should provide system operators with a more complete and reliable support tool for market clearing and power dispatch.

Lastly, the proposed approach can provide a measure of the capability of the system to handle different kinds of generation dispatches without losing its voltage stability and can also provide a means to develop preventive and corrective control schemes in order to maintain the system operation inside the feasibility region.

5.2 Contributions

The main contributions of the Thesis can be summarized as follows:

- The linear representation of the nonlinear boundary by an appropriate piecewise approximation based on a set of hyperplanes.

- The proposed stability/security representation can be applied to DC OPF-based dispatch models, which in practice is used in most energy dispatch and market clearing mechanisms.

- From the complete piecewise linear representation of the stability/security boundaries, two reduction algorithms were proposed and tested in order to reduce the dimensions of the SBC DC-OPF linear dispatch model.

- The proposed SBC DC-OPF linear dispatch model should provide the power system operators with a more complete and reliable support tool for market clearing and power dispatch.

5.3 Future Work

The work reported in this Thesis can be extended in the following areas:

- An essential feature of smart grids is to enable demand response and demand side management, with loads varying following both prices and end-user preferences; hence, these can no longer be considered constant. Therefore, proper load models for OPF applications such as the one described here are needed to adequately reflect the interaction between markets and end-users.

- Although no trouble occurred in the system losses modeling in the numerical results, the piecewise load approximation used here suffers from one short coming: it is not necessarily a tight approximation when nodal prices are negative. Therefore, a better linear representation of the power system transmission losses is needed.

Appendix A

Hyperplanes' coefficients

The hyperplanes' coefficients which have been found in the piecewise linearization process of the feasibility boundaries in the P_G-parameter space are presented in this Appendix. These linear functions were used as stability/security constraints for the proposed linear SBC DC-OPF dispatch model.

A.1 IEEE 3-machine 9-bus test system

A.1.1 Two control areas

For the case when two dispatch areas were considered, the following hyperplanes' parameters, shown in Table A.1, was found to approximate the stability boundary of Figure. 3.6:

Table A.1:Brute force approximation for the IEEE 9-bus, stability boundary: Two control areas.

Hyperplane i	η_{i,d_1}	η_{i,d_2}	C^i	Hyperplane i	η_{i,d_1}	η_{i,d_2}	C^i
1	1	-0.22595	2.1148	11	1	0.71197	6.3791
2	1	-0.078781	2.5346	12	1	0.73026	6.4996
3	1	-0.040282	2.6608	13	1	0.72662	6.4749
4	1	0.10532	3.2083	14	1	0.72064	6.4333
5	1	0.2177	3.6859	15	1	0.71059	6.3616
6	1	0.32784	4.2058	16	1	0.67767	6.1215
7	1	0.43858	4.7762	17	1	0.82748	7.2371
8	1	0.54218	5.349	18	1	0.651	5.9017
9	1	0.61206	5.7578	19	1	0.4923	4.6785
10	1	0.676	6.1498	20	1	0.91448	8.0059

A.1.2 Three control areas, stability boundary

When three generation areas are considered, the tridimensional stability boundary shown in Figure. 3.7, is linearly approximated by brute force methodology with the hyperplanes of Table A.2.

Table A.2:Brute force approximation for the IEEE 9-bus, stability boundary, three control areas.

Hyperplane i	η_{i,d_1}	η_{i,d_2}	$\eta_{i,d3}$	C^i	Hyperplane i	η_{i,d_1}	η_{i,d_2}	$\eta_{i,d3}$	C^i
1	1	-0.13204	0.27991	3.6676	316	1	2.2299	2.1605	16.144
2	1	0.10504	0.49217	4.3506	317	1	2.3211	2.3041	16.877
3	1	-0.30568	0.11356	3.2133	318	1	2.3143	2.415	17.106

4	1	-0.011816	0.29614	3.9699	319	1	2.3152	2.5586	17.483
5	1	0.014797	0.43092	4.1236	320	1	2.2822	2.7813	18.005
6	1	0.12912	0.42545	4.4615	321	1	2.242	2.9939	18.546
7	1	-0.24452	0.18902	3.3543	322	1	2.1259	3.13	18.647
8	1	0.27431	0.50232	4.9839	323	1	1.9971	3.3901	19.233
9	1	-0.052704	0.39384	4.0037	324	1	0.10793	0.43315	4.4099
10	1	0.46393	0.63405	5.7842	325	1	0.24357	0.5235	4.9066
11	1	-0.013952	0.44452	4.1608	326	1	0.15324	0.49756	4.6147
12	1	0.68402	0.7586	6.7753	327	1	0.42964	0.64167	5.6677
13	1	0.027509	0.5033	4.3511	328	1	0.20585	0.56348	4.8579
14	1	0.93223	0.8901	7.9729	329	1	0.75682	0.85102	7.1846
15	1	0.067185	0.56147	4.5514	330	1	0.26243	0.62351	5.1173
16	1	1.1729	0.99037	9.1763	331	1	1.0078	0.99494	8.4316
17	1	0.10945	0.63637	4.8126	332	1	0.32486	0.70003	5.4415
18	1	1.3927	1.0886	10.334	333	1	1.227	1.0998	9.5493
19	1	0.16446	0.71025	5.1123	334	1	0.47671	0.86587	6.25
20	1	1.5238	1.1539	11.054	335	1	1.5098	1.2624	11.096
21	1	0.21638	0.80804	5.4959	336	1	0.56415	1.018	6.9059
22	1	1.6015	1.2853	11.572	337	1	1.7008	1.3664	12.174
23	1	0.27976	0.91457	5.9507	338	1	0.65535	1.122	7.4619
24	1	1.6893	1.3009	12.052	339	1	1.6122	1.3854	11.746
25	1	0.34338	1.061	6.5663	340	1	0.76403	1.304	8.3309
26	1	1.7097	1.3465	12.204	341	1	1.7981	1.4812	12.823
27	1	0.41837	1.2657	7.4418	342	1	0.89594	1.5041	9.3506
28	1	1.7035	1.3647	12.186	343	1	1.8193	1.525	12.991
29	1	0.52244	1.5409	8.6708	344	1	1.0607	1.8163	10.879
30	1	1.6873	1.3999	12.127	345	1	1.7541	1.5115	12.619
31	1	0.63767	1.9324	10.415	346	1	1.2599	2.2154	12.856
32	1	1.8564	1.7298	13.389	347	1	5.2996	3.8075	34.822
33	1	0.75785	2.4544	12.737	348	1	1.5131	2.7641	15.576
34	1	1.3849	1.097	10.092	349	1	2.5385	2.2965	17.952
35	1	0.90495	3.2062	16.097	350	1	1.7718	3.3063	18.323
36	1	1.092	4.0291	19.869	351	1	1.751	1.5702	12.67
37	1	2.1148	2.9169	15.982	352	1	2.0027	1.8554	14.442
38	1	1.3858	6.2911	29.947	353	1	2.0681	1.9263	14.899
39	1	1.9136	2.8052	14.68	354	1	2.1314	2.0316	15.409
40	1	1.6514	9.7684	45.204	355	1	2.149	2.1367	15.711
41	1	1.3347	1.4825	10.085	356	1	2.2232	2.2631	16.335
42	1	2.2344	1.4571	15.342	357	1	2.2583	2.417	16.868
43	1	1.4114	1.2627	10.338	358	1	2.2308	2.5369	17.08
44	1	2.6558	2.622	19.15	359	1	2.1403	2.7214	17.303
45	1	1.8861	1.8073	13.751	360	1	2.093	2.9087	17.765
46	1	2.1167	2.0961	15.466	361	1	1.8952	3.0075	17.519
47	1	2.229	2.2509	16.338	362	1	0.16687	0.48171	4.6296
48	1	2.0853	2.1857	15.513	363	1	0.32289	0.58369	5.2329
49	1	2.4329	2.5902	18.074	364	1	0.21972	0.54285	4.8619
50	1	2.4329	2.7419	18.476	365	1	0.6147	0.78487	6.538
51	1	2.5677	3.0386	19.873	366	1	0.27547	0.60845	5.125
52	1	2.5368	3.2011	20.261	367	1	0.84773	0.91717	7.6473
53	1	2.5333	3.4503	21.074	368	1	0.34462	0.68243	5.459
54	1	2.4061	3.6702	21.447	369	1	1.0997	1.064	8.9296
55	1	2.3218	4.0611	22.677	370	1	0.49859	0.85732	6.2913
56	1	2.1045	4.5144	23.927	371	1	1.3864	1.2158	10.445
57	1	2.3542	7.0462	34.911	372	1	0.59876	0.96404	6.8538
58	1	-0.02119	0.31748	3.9656	373	1	1.541	1.3014	11.299
59	1	0.097679	0.4979	4.4337	374	1	0.67059	1.1223	7.5034
60	1	0.27228	0.50688	4.9811	375	1	1.6814	1.3914	12.111
61	1	-0.058207	0.40155	4.0075	376	1	0.79939	1.2871	8.3706
62	1	0.46807	0.62574	5.7926	377	1	1.8645	1.5096	13.201

63	1	-0.02175	0.455	4.1679	378	1	0.91456	1.495	9.3687
64	1	0.81268	0.83242	7.3924	379	1	1.8305	1.5466	13.076
65	1	0.019403	0.51396	4.3606	380	1	1.0634	1.7274	10.572
66	1	1.0581	0.96767	8.6198	381	1	1.8517	1.5545	13.201
67	1	0.053473	0.57939	4.5716	382	1	1.2507	2.0387	12.185
68	1	1.28	1.0547	9.7511	383	1	2.6464	1.4457	17.409
69	1	0.10232	0.64585	4.8258	384	1	1.4486	2.4231	14.124
70	1	1.4459	1.154	10.66	385	1	1.7428	3.0503	17.261
71	1	0.14747	0.73389	5.1525	386	1	1.8349	1.6245	13.202
72	1	1.671	1.3057	11.954	387	1	1.8935	1.7298	13.668
73	1	0.20266	0.8286	5.5375	388	1	2.0612	1.9747	14.953
74	1	1.6965	1.3051	12.095	389	1	2.187	2.0685	15.744
75	1	0.34995	1.0688	6.6046	390	1	2.1472	2.1662	15.769
76	1	1.703	1.3358	12.158	391	1	2.1899	2.2585	16.172
77	1	0.42146	1.2697	7.4618	392	1	2.174	2.3965	16.461
78	1	1.7209	1.3916	12.307	393	1	2.0759	2.5457	16.518
79	1	0.52278	1.5414	8.6732	394	1	2.022	2.7218	16.899
80	1	2.0203	1.9094	14.459	395	1	1.8929	2.8625	16.983
81	1	0.63802	1.933	10.418	396	1	0.23423	0.54354	4.9055
82	1	1.618	1.3667	11.701	397	1	0.41371	0.65203	5.6259
83	1	0.78665	2.5085	13.007	398	1	0.29454	0.60794	5.1804
84	1	1.7389	1.1565	12.196	399	1	0.72231	0.85945	7.0607
85	1	0.97416	3.361	16.858	400	1	0.35978	0.68642	5.512
86	1	1.5398	5.1626	25.397	401	1	0.99543	1.0039	8.391
87	1	1.279	1.4124	9.6898	402	1	0.53555	0.84344	6.3699
88	1	1.6805	7.2885	34.679	403	1	1.2692	1.1407	9.7952
89	1	5.9469	5.0447	40.775	404	1	0.62696	0.94713	6.8956
90	1	1.6514	9.7684	45.204	405	1	1.4443	1.2762	10.803
91	1	1.9813	2.5871	14.998	406	1	0.70819	1.0475	7.4035
92	1	1.7792	1.4231	12.596	407	1	1.6978	1.4191	12.227
93	1	2.4037	2.3149	17.312	408	1	0.8249	1.2613	8.363
94	1	1.9543	1.8937	14.258	409	1	1.8477	1.4487	13.024
95	1	2.1625	2.1413	15.784	410	1	0.91946	1.3815	9.0143
96	1	1.61	1.7646	12.326	411	1	1.8221	1.5506	13.038
97	1	2.4173	2.4484	17.651	412	1	1.0802	1.6587	10.384
98	1	2.3348	2.5696	17.595	413	1	1.8531	1.5955	13.26
99	1	2.4585	2.8239	18.811	414	1	1.2388	1.9326	11.776
100	1	2.5062	3.168	20.043	415	1	1.8753	1.6429	13.443
101	1	2.5068	3.4192	20.878	416	1	1.447	2.2823	13.603
102	1	2.467	3.7498	21.923	417	1	1.6943	1.5465	12.327
103	1	2.342	4.0912	22.848	418	1	1.7316	2.8191	16.361
104	1	2.1859	4.6609	24.711	419	1	1.8932	1.6859	13.602
105	1	2.0523	6.2775	31.092	420	1	2.4094	1.546	15.909
106	1	0.20913	0.44568	4.7207	421	1	2.0415	1.9547	14.82
107	1	-0.035154	0.38147	4.0157	422	1	2.2058	2.1115	15.915
108	1	0.36607	0.55301	5.3486	423	1	2.0758	2.1568	15.429
109	1	-0.0062067	0.4444	4.1742	424	1	2.1167	2.2481	15.83
110	1	0.6662	0.74483	6.6898	425	1	2.0344	2.337	15.739
111	1	0.029273	0.50328	4.3541	426	1	1.9726	2.5284	16.096
112	1	0.92231	0.883	7.9224	427	1	1.8723	2.6616	16.211
113	1	0.075917	0.56137	4.5666	428	1	0.30485	0.59332	5.1887
114	1	1.1676	0.98696	9.1487	429	1	0.60029	0.79807	6.5044
115	1	0.11577	0.63632	4.8236	430	1	0.37289	0.65947	5.5029
116	1	1.4385	1.1167	10.585	431	1	0.86741	0.9497	7.7738
117	1	0.16227	0.71027	5.1084	432	1	0.5277	0.82902	6.3153
118	1	1.6251	1.2135	11.625	433	1	1.0972	1.0744	8.9335
119	1	0.22415	0.80803	5.5096	434	1	0.6121	0.92649	6.8014
120	1	1.5422	1.2488	11.229	435	1	1.3428	1.2302	10.264
121	1	0.37853	1.0358	6.5421	436	1	0.71549	1.0503	7.4335

122	1	1.7112	1.3357	12.203	437	1	1.5951	1.3579	11.637
123	1	0.45877	1.1867	7.2266	438	1	0.86376	1.1832	8.259
124	1	1.7439	1.3856	12.429	439	1	1.6825	1.429	12.166
125	1	0.56554	1.4529	8.4131	440	1	0.93908	1.3587	9.0009
126	1	1.6985	1.3891	12.18	441	1	1.8628	1.5494	13.244
127	1	0.66616	1.7488	9.7429	442	1	1.081	1.564	10.077
128	1	1.6697	0.87154	11.504	443	1	1.8277	1.5583	13.077
129	1	0.80978	2.2162	11.866	444	1	1.2734	1.8604	11.628
130	1	1.8821	1.3376	13.188	445	1	1.8444	1.6104	13.234
131	1	0.98826	2.827	14.68	446	1	1.4467	2.185	13.257
132	1	1.5991	1.1765	11.403	447	1	1.8495	1.5817	13.222
133	1	1.2344	3.7797	19.075	448	1	1.6368	2.5041	14.944
134	1	1.147	3.4796	17.641	449	1	2.1168	1.9686	15.213
135	1	2.1681	1.3036	14.866	450	1	2.0362	1.9685	14.824
136	1	3.2603	11.581	55.719	451	1	2.1588	2.1181	15.708
137	1	2.8133	2.6267	20.015	452	1	2.0254	2.146	15.188
138	1	2.0673	1.7258	14.577	453	1	2.0136	2.2403	15.388
139	1	2.1167	2.0961	15.466	454	1	1.9329	2.3844	15.501
140	1	2.229	2.2509	16.338	455	1	1.8124	2.4649	15.35
141	1	2.1661	2.0314	15.514	456	1	0.39435	0.65475	5.5646
142	1	2.4362	2.5761	18.052	457	1	0.69245	0.86773	6.96
143	1	2.4341	2.7046	18.376	458	1	0.56059	0.81629	6.3979
144	1	2.5784	3.1194	20.159	459	1	0.91899	1.0181	8.0953
145	1	2.58	3.3942	21.045	460	1	0.66135	0.92264	6.9536
146	1	2.6215	3.7617	22.447	461	1	1.2498	1.1878	9.7788
147	1	2.5204	4.0619	23.233	462	1	0.75075	1.0085	7.4482
148	1	2.5145	4.7409	25.832	463	1	1.461	1.2985	10.912
149	1	2.3883	5.7163	29.466	464	1	0.83272	1.1439	8.0563
150	1	-0.0029243	0.33449	4.0278	465	1	1.6663	1.4473	12.114
151	1	0.2224	0.4257	4.7147	466	1	0.94157	1.2927	8.8158
152	1	-0.023914	0.37325	4.0264	467	1	1.8225	1.5369	13.019
153	1	0.27631	0.51034	4.9982	468	1	1.075	1.4805	9.797
154	1	0.014577	0.42283	4.1768	469	1	1.8584	1.5798	13.266
155	1	0.4598	0.61905	5.7542	470	1	1.2521	1.7516	11.206
156	1	0.054601	0.47522	4.347	471	1	1.9198	1.6514	13.689
157	1	0.7923	0.81723	7.2915	472	1	1.4107	1.9833	12.459
158	1	0.089695	0.55407	4.5759	473	1	1.8825	1.6333	13.469
159	1	1.0503	0.96219	8.5789	474	1	1.6436	2.4098	14.63
160	1	0.14045	0.61559	4.8173	475	1	2.4078	1.5452	15.9
161	1	1.3101	1.074	9.9138	476	1	2.1211	1.9582	15.208
162	1	0.18887	0.69469	5.1154	477	1	2.0739	1.9301	14.91
163	1	1.4661	1.1665	10.773	478	1	2.1178	2.1328	15.553
164	1	0.24062	0.78844	5.4811	479	1	2.009	2.1418	15.106
165	1	1.5924	1.2576	11.504	480	1	1.9093	2.2031	14.874
166	1	0.40571	0.99866	6.4717	481	1	1.7394	2.2478	14.394
167	1	1.7498	1.3374	12.407	482	1	0.58261	0.8079	6.4578
168	1	0.48215	1.141	7.1116	483	1	0.82068	0.95072	7.5922
169	1	1.9523	1.7077	13.872	484	1	0.66883	0.89316	6.92
170	1	0.57225	1.3203	7.9369	485	1	1.1004	1.1124	9.0065
171	1	1.7769	1.437	12.661	486	1	0.75556	1.011	7.4702
172	1	0.68261	1.5867	9.1521	487	1	1.3181	1.2454	10.176
173	1	2.0449	1.322	14.043	488	1	0.87641	1.1126	8.1275
174	1	0.84233	2.0193	11.148	489	1	1.5959	1.4067	11.713
175	1	1.6797	1.4441	12.127	490	1	0.98009	1.2529	8.8395
176	1	1.0284	2.5877	13.785	491	1	1.709	1.4771	12.367
177	1	2.2834	2.0925	16.236	492	1	1.097	1.4195	9.6918
178	1	1.2564	3.3158	17.202	493	1	1.862	1.5898	13.297
179	1	1.6434	5.11	25.371	494	1	1.2484	1.6684	10.932
180	1	3.3464	3.0877	23.519	495	1	1.8923	1.647	13.54

181	1	1.9628	5.753	28.73	496	1	1.4184	1.9485	12.368
182	1	1.367	1.4654	10.34	497	1	1.6066	2.2217	13.872
183	1	1.5115	1.2525	10.913	498	1	2.0156	1.8255	14.45
184	1	1.718	1.4503	12.297	499	1	1.8601	1.8451	13.744
185	1	1.9831	1.8796	14.384	500	1	2.003	1.9842	14.706
186	1	2.0605	1.9824	14.964	501	1	1.9928	2.0838	14.892
187	1	2.1726	2.132	15.814	502	1	1.8878	2.1035	14.513
188	1	2.4102	2.4675	17.667	503	1	1.7488	2.2049	14.29
189	1	2.3362	2.56	17.575	504	1	0.67774	0.87673	6.9212
190	1	2.462	2.8957	19.035	505	1	0.95515	1.0224	8.248
191	1	2.5038	3.154	19.99	506	1	0.77936	0.98622	7.5029
192	1	2.5031	3.4041	20.815	507	1	1.2286	1.2253	9.7474
193	1	2.4799	3.7962	22.129	508	1	0.8677	1.0989	8.0655
194	1	2.3473	4.1108	22.937	509	1	1.4636	1.3435	10.996
195	1	2.2126	4.7748	25.23	510	1	1.0079	1.2378	8.8991
196	1	0.060182	0.38867	4.2381	511	1	1.6893	1.4891	12.288
197	1	-0.013724	0.36294	4.0347	512	1	1.1313	1.3712	9.6807
198	1	0.025604	0.4142	4.1873	513	1	1.8338	1.5876	13.151
199	1	0.35051	0.56219	5.3014	514	1	1.2687	1.5647	10.696
200	1	0.066675	0.46518	4.3554	515	1	1.8901	1.6561	13.543
201	1	0.66286	0.75009	6.6815	516	1	1.4191	1.8483	12.054
202	1	0.11413	0.52437	4.5649	517	1	1.9393	1.699	13.861
203	1	0.91277	0.88137	7.8791	518	1	1.6531	2.1896	13.915
204	1	0.15113	0.60849	4.822	519	1	1.9766	1.8122	14.234
205	1	1.1615	1.0308	9.1634	520	1	1.9382	1.8211	14.066
206	1	0.2006	0.67609	5.0896	521	1	2.0134	1.9236	14.621
207	1	1.371	1.1365	10.275	522	1	1.9439	1.9648	14.398
208	1	0.26235	0.76348	5.4529	523	1	1.8608	1.9896	14.103
209	1	1.5691	1.2439	11.371	524	1	1.7279	2.0115	13.637
210	1	0.41547	0.94657	6.3272	525	1	0.79871	0.96843	7.5398
211	1	1.723	1.2889	12.208	526	1	1.0911	1.1539	9.0396
212	1	0.50236	1.0953	6.9992	527	1	0.92449	1.0997	8.2746
213	1	1.7452	1.4014	12.451	528	1	1.2819	1.2679	10.054
214	1	0.58895	1.2594	7.7544	529	1	1.0131	1.1808	8.7846
215	1	1.7185	1.0754	11.944	530	1	1.5746	1.4395	11.668
216	1	0.71808	1.5426	9.0608	531	1	1.1473	1.3725	9.7418
217	1	1.7371	1.446	12.452	532	1	1.7226	1.534	12.522
218	1	0.86854	1.8593	10.583	533	1	1.2987	1.5069	10.645
219	1	1.7307	1.4697	12.442	534	1	1.8816	1.641	13.474
220	1	1.04	2.2976	12.656	535	1	1.4269	1.7005	11.644
221	1	1.9594	1.8889	14.174	536	1	1.9378	1.7231	13.891
222	1	1.2587	2.9177	15.592	537	1	1.6196	2.053	13.37
223	1	1.5813	3.8423	20.026	538	1	1.9768	1.7862	14.188
224	1	2.7437	2.3742	19.244	539	1	2.1222	1.9811	15.24
225	1	1.9122	4.9082	25.11	540	1	1.9067	1.8955	14.078
226	1	2.1427	2.0856	15.51	541	1	1.8216	1.9304	13.794
227	1	2.0169	1.5609	14.095	542	1	1.6974	1.935	13.309
228	1	1.7121	1.661	12.59	543	1	0.92698	1.0634	8.2124
229	1	2.0451	1.956	14.837	544	1	1.1881	1.2389	9.601
230	1	2.0879	2.0368	15.205	545	1	1.0052	1.1782	8.749
231	1	2.1701	2.1598	15.859	546	1	1.4558	1.3869	11.035
232	1	2.4941	2.5215	18.176	547	1	1.1562	1.3055	9.6154
233	1	2.323	2.4661	17.276	548	1	1.7324	1.5549	12.6
234	1	2.403	2.6684	18.147	549	1	1.2423	1.4673	10.336
235	1	2.4305	2.948	19.072	550	1	1.8487	1.6461	13.319
236	1	2.3901	3.1494	19.572	551	1	1.4058	1.6435	11.411
237	1	2.3735	3.4465	20.542	552	1	1.9898	1.7381	14.171
238	1	2.3146	3.8189	21.732	553	1	1.6204	1.8987	12.914
239	1	1.937	3.7583	20.503	554	1	2.0051	1.8154	14.372

240	1	-0.0052111	0.34979	4.0385	555	1	1.9163	1.8234	13.967
241	1	0.15262	0.36513	4.45	556	1	1.8372	1.8446	13.655
242	1	0.037305	0.40335	4.1989	557	1	1.7231	1.8599	13.212
243	1	0.26106	0.51594	4.9534	558	1	1.0712	1.1754	8.9999
244	1	0.079575	0.45486	4.3684	559	1	1.2788	1.2918	10.085
245	1	0.44486	0.63453	5.7145	560	1	1.1593	1.2632	9.5328
246	1	0.12841	0.51332	4.5775	561	1	1.5694	1.4813	11.719
247	1	0.77225	0.83336	7.2254	562	1	1.2966	1.4321	10.458
248	1	0.17907	0.57764	4.8171	563	1	1.7443	1.5981	12.735
249	1	1.0309	0.95713	8.4869	564	1	1.456	1.6292	11.563
250	1	0.22332	0.66409	5.1095	565	1	1.9034	1.7075	13.691
251	1	1.2214	1.0889	9.5102	566	1	1.6139	1.8022	12.624
252	1	0.2807	0.74749	5.4491	567	1	1.8819	1.7582	13.678
253	1	1.5186	1.2109	11.079	568	1	1.7768	1.7843	13.258
254	1	0.43837	0.94506	6.3736	569	1	1.7108	1.819	13.06
255	1	1.6688	1.3008	11.938	570	1	1.1726	1.2512	9.561
256	1	0.51679	1.0714	6.9538	571	1	1.4508	1.4287	11.092
257	1	1.7593	1.3843	12.505	572	1	1.3039	1.3745	10.356
258	1	0.61296	1.2164	7.6598	573	1	1.7145	1.599	12.598
259	1	1.9469	1.3793	13.495	574	1	1.4248	1.5491	11.245
260	1	0.74176	1.4417	8.7487	575	1	1.818	1.6782	13.229
261	1	1.8024	1.4736	12.84	576	1	1.5233	1.7194	12.058
262	1	0.89329	1.733	10.163	577	1	1.7995	1.7146	13.211
263	1	1.7558	1.4841	12.596	578	1	1.7106	1.7199	12.825
264	1	1.0645	2.1166	12.007	579	1	1.3054	1.3508	10.312
265	1	1.7291	1.5026	12.468	580	1	1.5787	1.5362	11.864
266	1	1.2895	2.6643	14.651	581	1	1.4681	1.5107	11.33
267	1	1.6738	1.3506	11.974	582	1	1.7834	1.6564	13.023
268	1	1.5326	3.3361	17.873	583	1	1.6031	1.6835	12.286
269	1	1.8358	1.3095	12.876	584	1	1.6698	1.6851	12.573
270	1	1.8187	4.1301	21.719	585	1	1.4132	1.4675	11.01
271	1	2.5006	2.2896	17.768	586	1	1.6705	1.6252	12.451
272	1	2.0054	1.7799	14.329	587	1	1.5384	1.6039	11.836
273	1	2.0867	1.9931	15.116	588	1	1.591	1.6013	12.051
274	1	2.182	2.1032	15.8	589	1	1.456	1.6292	11.563
275	1	3.6447	3.3571	25.387	590	1	2.1472	2.1662	15.769
276	1	2.3206	2.3809	17.055	591	1	0.24357	0.5235	4.9066
277	1	2.3937	2.576	17.86	592	1	2.3937	2.576	17.86
278	1	2.3591	2.6873	18.02	593	1	2.5031	3.4041	20.815
279	1	2.3358	2.963	18.772	594	1	1.9439	1.9648	14.398
280	1	2.2401	3.0702	18.799	595	1	2.0451	1.956	14.837
281	1	2.2135	3.4435	20.045	596	1	1.8861	1.8073	13.751
282	1	2.0884	3.8654	21.299	597	1	0.18887	0.69469	5.1154
283	1	0.050117	0.39222	4.2161	598	1	2.3146	3.8189	21.732
284	1	0.17439	0.47639	4.6445	599	1	-2.7678	0.88567	-6.8238
285	1	0.093132	0.44762	4.391	600	1	2603.6	-2603.4	4.0877
286	1	0.3371	0.57403	5.2681	601	1	-42.552	-15.04	-112.8
287	1	0.14198	0.50674	4.5997	602	1	-6.6839	-2.2021	-16.74
288	1	0.63695	0.76978	6.6027	603	1	21.348	-19.314	-0.065775
289	1	0.1948	0.56518	4.8317	604	1	11.059	-9.0504	-0.022084
290	1	0.88566	0.91054	7.7965	605	1	7.5892	-5.6097	0.038778
291	1	0.24863	0.6381	5.111	606	1	-6.488	3.8372	-16.379
292	1	1.1874	1.0503	9.3034	607	1	-6.8073	-0.21939	-17.082
293	1	0.3003	0.73005	5.4497	608	1	960.59	-960.85	4.0615
294	1	1.3883	1.1636	10.389	609	1	21.215	-19.191	-0.039052
295	1	0.45352	0.90115	6.2834	610	1	11.175	-9.1436	-0.062652
296	1	1.5417	1.2656	11.259	611	1	-1.727	0.90304	-3.9743
297	1	0.55267	1.0395	6.9404	612	1	-6.8073	-0.21939	-17.082
298	1	1.8024	1.4274	12.767	613	1	-0.673	2.667	-0.015298

299	1	0.64469	1.2043	7.6949	614	1	-2.3132	4.3389	0.049183
300	1	1.7894	1.463	12.755	615	1	784.45	-784.51	4.0967
301	1	0.7724	1.3835	8.618	616	1	21.02	-19.017	-0.0027718
302	1	1.7674	1.4675	12.644	617	1	-1.2374	3.2261	-0.031546
303	1	0.90923	1.6391	9.8583	618	1	899.93	-899.92	4.118
304	1	1.8229	1.5443	13.032	619	1	-0.34618	2.3346	-0.032313
305	1	1.0487	1.9188	11.225	620	1	-0.41184	2.4248	0.040423
306	1	1.2293	2.319	13.173	621	1	-0.53786	2.5398	0.0020644
307	1	1.915	1.4106	13.408	622	1	-1.2415	3.228	-0.039333
308	1	1.4984	2.9195	16.142	623	1	-0.68022	2.6684	-0.031777
309	1	2.1325	1.7947	15.081	624	1	-1.253	3.2269	-0.066262
310	1	1.9975	4.0896	21.956	625	1	-0.66402	2.6634	0.0048609
311	1	2.3195	1.7631	16.077	626	1	-2.3187	4.3301	0.027741
312	1	1.8658	1.718	13.502	627	1	-10.98	-3.4799	-25.977
313	1	2.6659	1.8034	17.853	628	1	-2.3105	4.3254	0.04017
314	1	1.99	1.8578	14.38	629	1	-1.4917	3.5019	0.01972
315	1	2.0928	2.0296	15.215	630	1	-2.2933	4.326	0.076818

Applying the hyperplane reduction methodologies: boundary points' approximation and inner product to the hyperplanes of Table A.2, Tables A.4 and A.5 are obtained, respectively.

Table A.3:Boundary points' approximation for the IEEE 9-bus, stability boundary, three control areas.

Hyperplane i	η_{i,d_1}	η_{i,d_2}	$\eta_{i,d3}$	C^i	Hyperplane i	η_{i,d_1}	η_{i,d_2}	$\eta_{i,d3}$	C^i
1	1	1.7558	1.4841	12.596	67	1	0.39435	0.65475	5.5646
2	1	2.0879	2.0368	15.205	68	1	1.2498	1.1878	9.7788
3	1	2.3362	2.56	17.575	69	1	0.26106	0.51594	4.9534
4	1	0.097679	0.4979	4.4337	70	1	0.44486	0.63453	5.7145
5	1	0.079575	0.45486	4.3684	71	1	1.7279	2.0115	13.637
6	1	1.1874	1.0503	9.3034	72	1	0.75075	1.0085	7.4482
7	1	1.4681	1.5107	11.33	73	1	0.77936	0.98622	7.5029
8	1	0.10504	0.49217	4.3506	74	1	0.21972	0.54285	4.8619
9	1	0.95515	1.0224	8.248	75	1	2.0136	2.2403	15.388
10	1	1.8608	1.9896	14.103	76	1	1.4558	1.3869	11.035
11	1	0.81268	0.83242	7.3924	77	1	1.279	1.4124	9.6898
12	1	1.147	3.4796	17.641	78	1	0.26235	0.76348	5.4529
13	1	0.17907	0.57764	4.8171	79	1	0.67059	1.1223	7.5034
14	1	2.242	2.9939	18.546	80	1	1.6974	1.935	13.309
15	1	0.32486	0.70003	5.4415	81	1	0.79871	0.96843	7.5398
16	1	0.49859	0.85732	6.2913	82	1	2.3591	2.6873	18.02
17	1	0.60029	0.79807	6.5044	83	1	1.456	1.6292	11.563
18	1	0.86376	1.1832	8.259	84	1	0.17439	0.47639	4.6445
19	1	0.40571	0.99866	6.4717	85	1	2.4078	1.5452	15.9
20	1	2.4305	2.948	19.072	86	1	-0.013952	0.44452	4.1608
21	1	1.1593	1.2632	9.5328	87	1	0.2006	0.67609	5.0896
22	1	1.5238	1.1539	11.054	88	1	0.59876	0.96404	6.8538
23	1	0.61296	1.2164	7.6598	89	1	0.8677	1.0989	8.0655
24	1	1.7394	2.2478	14.394	90	1	1.371	1.1365	10.275
25	1	1.2687	1.5647	10.696	91	1	0.6662	0.74483	6.6898
26	1	0.019403	0.51396	4.3606	92	1	-0.0029243	0.33449	4.0278
27	1	1.9975	4.0896	21.956	93	1	0.45352	0.90115	6.2834
28	1	0.89594	1.5041	9.3506	94	1	0.79939	1.2871	8.3706
29	1	2.4061	3.6702	21.447	95	1	0.27976	0.91457	5.9507
30	1	1.2734	1.8604	11.628	96	1	1.9329	2.3844	15.501
31	1	0.41837	1.2657	7.4418	97	1	2.6659	1.8034	17.853
32	1	0.63767	1.9324	10.415	98	1	1.6066	2.2217	13.872
33	1	0.68261	1.5867	9.1521	99	1	0.089695	0.55407	4.5759
34	1	1.04	2.2976	12.656	100	1	2.3358	2.963	18.772
35	1	1.0487	1.9188	11.225	101	1	1.2423	1.4673	10.336
36	1	1.9971	3.3901	19.233	102	1	2.0884	3.8654	21.299
37	1	1.5131	2.7641	15.576	103	1	1.081	1.564	10.077
38	1	1.6368	2.5041	14.944	104	1	1.4467	2.185	13.257
39	1	2.3542	7.0462	34.911	105	1	1.4191	1.8483	12.054
40	1	1.6514	9.7684	45.204	106	1	2.1045	4.5144	23.927
41	1	1.2344	3.7797	19.075	107	1	2.342	4.0912	22.848
42	1	1.8349	1.6245	13.202	108	1	1.8723	2.6616	16.211
43	1	1.8935	1.7298	13.668	109	1	0.58261	0.8079	6.4578
44	1	1.9766	1.8122	14.234	110	1	2.3735	3.4465	20.542
45	1	1.9768	1.7862	14.188	111	1	0.80978	2.2162	11.866
46	1	1.8923	1.647	13.54	112	1	0.89329	1.733	10.163
47	1	1.9831	1.8796	14.384	113	1	1.2895	2.6643	14.651
48	1	1.8517	1.5545	13.201	114	1	1.2599	2.2154	12.856
49	1	1.6943	1.5465	12.327	115	1	1.0634	1.7274	10.572
50	1	2.187	2.0685	15.744	116	1	-0.13204	0.27991	3.6676
51	1	1.8861	1.8073	13.751	117	1	0.10504	0.49217	4.3506
52	1	2.0051	1.8154	14.372	118	1	-0.30568	0.11356	3.2133
53	1	1.7981	1.4812	12.823	119	1	0.16446	0.71025	5.1123
54	1	1.7035	1.3647	12.186	120	1	0.21638	0.80804	5.4959
55	1	1.9594	1.8889	14.174	121	1	0.27976	0.91457	5.9507

56	1	1.6251	1.2135	11.625	122	1	0.52244	1.5409	8.6708
57	1	2.2058	2.1115	15.915	123	1	0.75785	2.4544	12.737
58	1	1.4443	1.2762	10.803	124	1	1.3347	1.4825	10.085
59	1	2.1899	2.2585	16.172	125	1	2.0853	2.1857	15.513
60	1	2.0853	2.1857	15.513	126	1	0.81268	0.83242	7.3924
61	1	1.5991	1.1765	11.403	127	1	0.20266	0.8286	5.5375
62	1	1.8564	1.7298	13.389	128	1	1.6251	1.2135	11.625
63	1	1.6705	1.6252	12.451	129	1	3.3464	3.0877	23.519
64	1	1.3428	1.2302	10.264	130	1	0.67774	0.87673	6.9212
65	1	0.32289	0.58369	5.2329	131	1	1.0131	1.1808	8.7846
66	1	2.0203	1.9094	14.459	132	1	1.1726	1.2512	9.561

Table A.4:Inner product reduction for the IEEE 9-bus, stability boundary, three control areas.

Hyperplane i	η_{i,d_1}	η_{i,d_2}	$\eta_{i,d3}$	C^i	Hyperplane i	η_{i,d_1}	η_{i,d_2}	$\eta_{i,d3}$	C^i
1	1	1.7558	1.4841	12.596	67	1	0.39435	0.65475	5.5646
2	1	2.0879	2.0368	15.205	68	1	1.2498	1.1878	9.7788
3	1	2.3362	2.56	17.575	69	1	0.26106	0.51594	4.9534
4	1	0.097679	0.4979	4.4337	70	1	0.44486	0.63453	5.7145
5	1	0.079575	0.45486	4.3684	71	1	1.7279	2.0115	13.637
6	1	1.1874	1.0503	9.3034	72	1	0.75075	1.0085	7.4482
7	1	1.4681	1.5107	11.33	73	1	0.77936	0.98622	7.5029
8	1	0.10504	0.49217	4.3506	74	1	0.21972	0.54285	4.8619
9	1	0.95515	1.0224	8.248	75	1	2.0136	2.2403	15.388
10	1	1.8608	1.9896	14.103	76	1	1.4558	1.3869	11.035
11	1	0.81268	0.83242	7.3924	77	1	1.279	1.4124	9.6898
12	1	1.147	3.4796	17.641	78	1	0.26235	0.76348	5.4529
13	1	0.17907	0.57764	4.8171	79	1	0.67059	1.1223	7.5034
14	1	2.242	2.9939	18.546	80	1	1.6974	1.935	13.309
15	1	0.32486	0.70003	5.4415	81	1	0.79871	0.96843	7.5398
16	1	0.49859	0.85732	6.2913	82	1	2.3591	2.6873	18.02
17	1	0.60029	0.79807	6.5044	83	1	1.456	1.6292	11.563
18	1	0.86376	1.1832	8.259	84	1	0.17439	0.47639	4.6445
19	1	0.40571	0.99866	6.4717	85	1	2.4078	1.5452	15.9
20	1	2.4305	2.948	19.072	86	1	-0.013952	0.44452	4.1608
21	1	1.1593	1.2632	9.5328	87	1	0.2006	0.67609	5.0896
22	1	1.5238	1.1539	11.054	88	1	0.59876	0.96404	6.8538
23	1	0.61296	1.2164	7.6598	89	1	0.8677	1.0989	8.0655
24	1	1.7394	2.2478	14.394	90	1	1.371	1.1365	10.275
25	1	1.2687	1.5647	10.696	91	1	0.6662	0.74483	6.6898
26	1	2.0203	1.9094	14.459					

A.1.3 Three control areas, security boundary

Security boundary of the IEEE 9-bus system, shown in Figure 3.10, is approximated by brute force methodology by the hyperplanes of Table A.5.

Table A.5:Brute force approximation for the IEEE 9-bus, security boundary, three control areas.

Hyperplane i	η_{i,d_1}	η_{i,d_2}	$\eta_{i,d3}$	C^i	Hyperplane i	η_{i,d_1}	η_{i,d_2}	$\eta_{i,d3}$	C^i
1	1	0.38751	0.77295	4.0312	316	1	1.2595	1.1483	6.4907
2	1	0.37455	0.68427	3.9193	317	1	0.70284	1.1063	5.0762
3	1	0.46924	0.8467	4.2607	318	1	0.82498	1.246	5.5617
4	1	0.41091	0.73783	4.0306	319	1	0.75128	1.1745	5.2832
5	1	0.50786	0.88939	4.3822	320	1	0.99711	1.4211	6.2562

6	1	0.437	0.7835	4.123	321	1	0.81006	1.2199	5.488
7	1	0.59019	0.96033	4.6429	322	1	1.238	1.6808	7.2795
8	1	0.48227	0.81699	4.2375	323	1	0.9306	1.3807	6.0217
9	1	0.65977	1.0562	4.91	324	1	1.4313	1.9899	8.2267
10	1	0.55802	0.85891	4.417	325	1	0.99775	1.4526	6.2944
11	1	0.74194	1.1959	5.2653	326	1	2.4196	3.0649	12.61
12	1	0.52317	0.93231	4.4677	327	1	1.1712	1.6686	7.0719
13	1	0.86337	1.3386	5.7559	328	1	1.395	1.9642	8.1235
14	1	0.62181	1.0271	4.7889	329	1	5.6288	6.7739	27.276
15	1	0.99427	1.4868	6.3004	330	1	1.7482	2.4383	9.8255
16	1	0.66915	1.0793	4.9603	331	1	19.956	20.99	90.727
17	1	1.2002	1.756	7.2167	332	1	2.3912	3.1815	12.72
18	1	0.65763	1.105	4.9906	333	1	3.5787	4.6075	18.203
19	1	1.6292	2.2563	9.1192	334	1	3.4621	4.249	17.006
20	1	0.7651	1.2408	5.4389	335	1	4.5892	5.6632	22.54
21	1	0.81619	1.2767	5.5977	336	1	0.69246	1.0963	5.0391
22	1	0.94434	1.4859	6.2651	337	1	0.44389	0.87172	4.1177
23	1	3.6987	4.2756	18.13	338	1	0.76216	1.1814	5.3181
24	1	1.0202	1.5533	6.5414	339	1	0.91833	1.3231	5.9131
25	1	11.851	13.372	55.302	340	1	0.79122	1.1994	5.4137
26	1	1.2825	1.9064	7.7933	341	1	1.1131	1.5593	6.7606
27	1	1.5493	2.196	8.9198	342	1	0.90824	1.3491	5.9195
28	1	4.9465	3.3234	21.587	343	1	1.8692	2.3429	9.9896
29	1	2.3544	3.0068	12.205	344	1	1.0209	1.5092	6.444
30	1	5.1872	7.1615	25.72	345	1	2.0382	2.5962	10.85
31	1	3.6407	4.6882	18.446	346	1	1.1352	1.6138	6.8922
32	1	8.1286	9.5537	38.424	347	1	3.2088	3.9438	16.17
33	1	6.7721	8.7767	33.704	348	1	1.3882	1.9305	8.0449
34	1	14.048	17.136	66.383	349	1	1.6649	2.2556	9.2858
35	1	0.29459	0.68427	3.789	350	1	15.127	17.814	71.07
36	1	14.622	17.17	68.483	351	1	2.226	2.956	11.907
37	1	19.241	22.779	90.042	352	1	3.389	4.4208	17.411
38	1	31.723	39.121	149.55	353	1	21.489	25.729	100.99
39	1	42.524	52.209	200.05	354	1	2.8543	3.6345	14.577
40	1	23.048	29.65	110.33	355	1	0.82664	1.2295	5.5454
41	1	13.352	16.804	63.838	356	1	0.7827	1.1896	5.3793
42	1	9.5244	11.914	45.67	357	1	1.0161	1.4501	6.3456
43	1	7.7806	9.817	37.558	358	1	0.89269	1.3075	5.8192
44	1	7.0654	8.9454	34.22	359	1	1.2649	1.7334	7.4225
45	1	6.8256	8.5621	32.968	360	1	1.0258	1.4943	6.4308
46	1	7.1926	9.0474	34.737	361	1	1.4115	1.6748	7.7796
47	1	0.38751	0.77295	4.0312	362	1	1.0954	1.5525	6.6937
48	1	0.34733	0.73556	3.9247	363	1	2.5653	3.2253	13.265
49	1	0.46924	0.8467	4.2607	364	1	1.3198	1.8412	7.7259
50	1	0.38845	0.78009	4.0401	365	1	1.6067	2.1676	8.9878
51	1	0.50786	0.88939	4.3822	366	1	6.8403	8.1415	32.817
52	1	0.4206	0.81454	4.134	367	1	2.0873	2.7697	11.233
53	1	0.65497	1.0365	4.88	368	1	3.0622	3.9879	15.821
54	1	0.46133	0.85771	4.2578	369	1	5.3477	6.8035	26.558
55	1	0.71773	1.1069	5.1181	370	1	238.97	286.47	1115
56	1	0.52358	0.92835	4.4621	371	1	8.3872	10.081	40.058
57	1	0.83507	1.2359	5.5799	372	1	0.79424	1.2137	5.4413
58	1	0.52317	0.93231	4.4677	373	1	0.93137	1.357	5.9912
59	1	0.95279	1.3497	6.048	374	1	0.86871	1.2841	5.7265
60	1	0.64761	1.0519	4.8758	375	1	1.1307	1.5904	6.8504
61	1	1.149	1.5587	6.8736	376	1	0.99945	1.4541	6.3043
62	1	0.6498	1.0606	4.8931	377	1	1.4457	1.9561	8.2408
63	1	1.4995	1.9566	8.4129	378	1	1.0834	1.5525	6.6651
64	1	0.75935	1.2052	5.358	379	1	2.0925	2.6751	11.114

65	1	0.85688	1.3174	5.7509	380	1	1.273	1.7762	7.5017
66	1	3.6987	4.2756	18.13	381	1	2.7369	3.1819	13.757
67	1	1.0601	1.5704	6.6477	382	1	1.5602	2.1562	8.8584
68	1	11.851	13.372	55.302	383	1	2.849	3.6144	14.566
69	1	1.2151	1.7247	7.2612	384	1	1.9463	2.5733	10.536
70	1	1.4658	2.081	8.5105	385	1	33.527	39.406	156.2
71	1	1.7687	2.3817	9.7294	386	1	2.8263	3.6726	14.67
72	1	3.4997	3.9279	16.856	387	1	4.929	6.2878	24.59
73	1	2.774	3.6984	14.594	388	1	30.142	36.099	141.43
74	1	7.9105	9.2714	37.393	389	1	4.9907	6.0653	24.339
75	1	6.7721	8.7767	33.704	390	1	0.84858	1.2508	5.6299
76	1	10.288	12.307	48.612	391	1	1.0381	1.483	6.449
77	1	14.048	16.472	65.819	392	1	0.96957	1.4103	6.1643
78	1	14.622	17.17	68.483	393	1	1.0985	1.5853	6.7546
79	1	19.241	22.779	90.042	394	1	1.9071	2.1237	9.8409
80	1	23.307	27.718	109.03	395	1	1.2348	1.7153	7.3066
81	1	20.501	24.605	96.226	396	1	2.6899	3.3792	13.846
82	1	7.9147	9.7085	37.845	397	1	2.3145	2.9143	12.006
83	1	7.3039	8.9996	35.025	398	1	1.9478	2.0952	9.6981
84	1	6.2183	7.7339	30.018	399	1	8.5294	10.186	40.702
85	1	5.8077	7.2589	28.13	400	1	2.6382	3.4202	13.752
86	1	5.7109	7.3103	27.919	401	1	14.664	17.819	69.684
87	1	5.9387	7.5092	28.871	402	1	3.4301	4.2445	17.16
88	1	6.5443	8.2738	31.74	403	1	14.174	16.777	66.599
89	1	18.969	27.886	100.48	404	1	0.94758	1.3813	6.0668
90	1	0.34735	0.73395	3.9233	405	1	1.1507	1.6222	6.9484
91	1	0.42464	0.80482	4.1316	406	1	1.0782	1.5551	6.6573
92	1	0.38828	0.77691	4.0365	407	1	1.481	2.0018	8.4039
93	1	0.49783	0.88923	4.3588	408	1	1.2052	1.6743	7.1664
94	1	0.42267	0.81355	4.1365	409	1	2.1541	2.7715	11.425
95	1	0.58028	0.96947	4.6255	410	1	1.6312	2.1631	9.0432
96	1	0.46227	0.85491	4.2558	411	1	1.2896	1.5154	7.0662
97	1	0.67729	1.0459	4.9484	412	1	3.4468	4.3091	17.32
98	1	0.52067	0.91832	4.4421	413	1	2.4681	3.1962	12.933
99	1	0.77886	1.1692	5.3514	414	1	18.575	22.212	87.487
100	1	0.52352	0.92847	4.4622	415	1	1.0595	1.5187	6.5557
101	1	0.88915	1.2951	5.7993	416	1	1.3361	1.8332	7.7581
102	1	0.63046	1.0333	4.8144	417	1	1.1967	1.6988	7.1825
103	1	1.0507	1.4562	6.4589	418	1	1.7888	2.3644	9.7934
104	1	0.65484	1.0899	4.9553	419	1	1.4207	1.9237	8.1184
105	1	1.2831	1.7255	7.4717	420	1	2.8662	3.5868	14.655
106	1	0.74781	1.1796	5.2887	421	1	1.4629	2.3504	8.9169
107	1	1.8028	2.29	9.7539	422	1	2.3456	3.0797	12.423
108	1	5.0434	5.93	24.39	423	1	12.764	15.253	60.417
109	1	1.457	2.0438	8.4107	424	1	3.4177	4.3411	17.335
110	1	1.8244	2.4721	10.047	425	1	1.1698	1.654	7.0452
111	1	15.159	12.369	65.82	426	1	1.5438	2.0411	8.6368
112	1	2.7091	3.6109	14.276	427	1	1.3336	1.8391	7.759
113	1	9.7557	11.578	46.057	428	1	2.2302	2.8726	11.787
114	1	14.81	17.779	69.706	429	1	1.6019	2.2772	9.155
115	1	26.717	32.068	125.17	430	1	2.2275	2.9195	11.849
116	1	14.687	16.901	68.426	431	1	4.4884	5.6036	22.227
117	1	62.883	75.962	294.14	432	1	4.1505	5.1847	20.683
118	1	47.7	58.112	223.87	433	1	1.3222	1.8404	7.7303
119	1	13.352	16.804	63.838	434	1	1.8512	2.416	10.045
120	1	9.5244	11.914	45.67	435	1	1.6308	2.2225	9.145
121	1	7.7806	9.817	37.558	436	1	3.054	3.8294	15.545
122	1	7.0654	8.9454	34.22	437	1	2.1114	2.7613	11.286
123	1	6.8256	8.5621	32.968	438	1	2.9882	3.8295	15.357

124	1	7.1926	9.0474	34.737	439	1	3.7198	4.6409	18.644
125	1	2.6838	3.5496	13.696	440	1	1.6074	2.1439	8.9625
126	1	0.3879	0.77332	4.0323	441	1	2.3433	2.9892	12.279
127	1	0.4688	0.84627	4.2593	442	1	2.0132	2.6255	10.808
128	1	0.42327	0.81091	4.1347	443	1	2.8099	3.5968	14.503
129	1	0.50114	0.883	4.3605	444	1	3.3397	4.1705	16.862
130	1	0.46354	0.85147	4.254	445	1	1.9249	2.5058	10.383
131	1	0.64593	1.0279	4.8487	446	1	3.1866	4.0018	16.176
132	1	0.52157	0.91235	4.4358	447	1	2.6513	3.3794	13.728
133	1	0.72548	1.1143	5.1466	448	1	2.5153	3.1974	13.073
134	1	0.51819	0.92335	4.4448	449	1	0.48227	0.81699	4.2375
135	1	0.84746	1.2479	5.6277	450	1	0.62181	1.0271	4.7889
136	1	0.6163	1.0141	4.758	451	1	1.6292	2.2563	9.1192
137	1	0.96394	1.3605	6.0927	452	1	0.94434	1.4859	6.2651
138	1	0.66686	1.0923	4.9809	453	1	0.65497	1.0365	4.88
139	1	1.1883	1.5972	7.0369	454	1	0.95279	1.3497	6.048
140	1	0.7333	1.1506	5.2089	455	1	0.64761	1.0519	4.8758
141	1	1.5679	2.0169	8.6988	456	1	11.851	13.372	55.302
142	1	0.81825	1.2678	5.5851	457	1	23.307	27.718	109.03
143	1	2.2459	2.7694	11.722	458	1	0.46227	0.85491	4.2558
144	1	1.0215	1.5096	6.4497	459	1	0.65484	1.0899	4.9553
145	1	4.0235	4.693	19.658	460	1	7.0654	8.9454	34.22
146	1	1.1186	1.6192	6.8585	461	1	3.4301	4.2445	17.16
147	1	14.483	16.517	67.504	462	1	14.174	16.777	66.599
148	1	1.4111	1.995	8.2193	463	1	0.52352	0.92847	4.4622
149	1	3.9651	5.218	20.297	464	1	0.93606	1.3703	6.0078
150	1	9.4662	11.182	44.668	465	1	14.687	16.901	68.426
151	1	12.981	15.458	61.079	466	1	5.411	6.7053	26.192
152	1	47.006	55.559	215.9	467	1	1.9249	2.5058	10.383
153	1	18.439	22.43	86.929	468	1	15.159	12.369	65.82
154	1	19.346	23.374	91.018	469	1	0.96394	1.3605	6.0927
155	1	7.831	9.6393	37.491	470	1	1.2831	1.7255	7.4717
156	1	7.0051	8.7875	33.814	471	1	0.50786	0.88939	4.3822
157	1	6.0952	7.6764	29.563	472	1	238.97	286.47	1115
158	1	5.7298	7.2518	27.886	473	1	0.55802	0.85891	4.417
159	1	5.7508	7.2812	27.993	474	1	0.95279	1.3497	6.048
160	1	5.9469	7.4527	28.808	475	1	2.0132	2.6255	10.808
161	1	7.103	10.589	36.977	476	1	1.0161	1.4501	6.3456
162	1	0.42379	0.8088	4.1336	477	1	2.3912	3.1815	12.72
163	1	0.50053	0.88031	4.3559	478	1	1.4962	2.0462	8.4992
164	1	0.4651	0.85078	4.2563	479	1	5.3477	6.8035	26.558
165	1	0.57849	0.9669	4.6183	480	1	1.457	2.0438	8.4107
166	1	0.51762	0.90557	4.4197	481	1	1.5679	2.0169	8.6988
167	1	0.69932	1.0667	5.0268	482	1	0.68074	1.1026	5.0239
168	1	0.51859	0.9183	4.4382	483	1	1.8484	2.4036	9.9098
169	1	0.78664	1.1827	5.3862	484	1	4.3159	5.4304	21.151
170	1	0.60333	1.0017	4.7144	485	1	0.437	0.7835	4.123
171	1	0.87701	1.2952	5.7628	486	1	1.4115	1.6748	7.7796
172	1	0.68074	1.1026	5.0239	487	1	3.1451	3.8463	15.853
173	1	1.0716	1.4766	6.5443	488	1	0.70667	1.1218	5.1058
174	1	0.72259	1.1341	5.1596	489	1	1.0215	1.5096	6.4497
175	1	1.3245	1.7603	7.6405	490	1	1.1026	1.5258	6.6906
176	1	0.8037	1.2426	5.5107	491	1	1.273	1.7762	7.5017
177	1	1.8075	2.3174	9.7958	492	1	0.58987	0.98252	4.662
178	1	0.907	1.3849	5.9781	493	1	0.99775	1.4526	6.2944
179	1	0.97976	1.4478	6.2456	494	1	2.5759	3.4111	13.584
180	1	1.6806	2.1984	9.1295	495	1	1.1698	1.654	7.0452
181	1	1.1555	1.7034	7.1058	496	1	1.5179	2.3728	9.2017
182	1	1.3243	1.8683	7.7814	497	1	1.4111	1.995	8.2193

183	1	1.6983	2.3456	9.5319	498	1	1.0209	1.5092	6.444
184	1	2.2404	3.0109	12.043	499	1	2.0382	2.5962	10.85
185	1	3.8243	4.3396	18.37	500	1	5.3477	6.8035	26.558
186	1	11.102	13.15	52.285	501	1	8.3872	10.081	40.058
187	1	2.937	3.8474	15.114	502	1	1.4457	1.9561	8.2408
188	1	12.291	14.823	58.071	503	1	0.9306	1.3807	6.0217
189	1	6.5247	8.1296	31.473	504	1	1.1507	1.6222	6.9484
190	1	5.5821	6.9772	27.068	505	1	2.7369	3.1819	13.757
191	1	5.0322	6.3388	24.54	506	1	0.73217	1.1262	5.1764
192	1	4.8503	6.131	23.711	507	1	0.51762	0.90557	4.4197
193	1	4.8831	6.1753	23.873	508	1	0.42327	0.81091	4.1347
194	1	5.1194	6.4038	24.889	509	1	73.766	87.357	341.79
195	1	0.46647	0.84834	4.2565	510	1	2.6382	3.4202	13.752
196	1	0.4982	0.88474	4.3553	511	1	3.8605	4.8691	19.017
197	1	0.51363	0.89665	4.4012	512	1	0.46354	0.85147	4.254
198	1	0.65429	1.0401	4.8817	513	1	3.3082	4.1217	16.351
199	1	0.51486	0.911	4.4211	514	1	0.42379	0.8088	4.1336
200	1	0.73217	1.1262	5.1764	515	1	0.50053	0.88031	4.3559
201	1	0.59795	0.99853	4.6998	516	1	1.7687	2.3817	9.7294
202	1	0.85642	1.2624	5.6679	517	1	0.8037	1.2426	5.5107
203	1	0.69109	1.104	5.0462	518	1	1.4658	2.081	8.5105
204	1	0.97329	1.3769	6.1373	519	1	1.2896	1.5154	7.0662
205	1	0.71654	1.1203	5.1245	520	1	0.85642	1.2624	5.6679
206	1	1.197	1.6197	7.0866	521	1	5.8077	7.2589	28.13
207	1	0.78781	1.2132	5.4271	522	1	0.93606	1.3703	6.0078
208	1	1.5851	2.061	8.7982	523	1	2.0442	2.7863	11.168
209	1	0.89522	1.3543	5.8973	524	1	3.1866	4.0018	16.176
210	1	2.2849	2.8417	11.926	525	1	47.006	55.559	215.9
211	1	0.93606	1.3703	6.0078	526	1	7.3039	8.9996	35.025
212	1	1.1366	1.6568	6.9736	527	1	2.0535	2.7576	11.123
213	1	2.2883	2.1051	11.132	528	1	0.99775	1.4526	6.2944
214	1	1.2628	1.7754	7.4659	529	1	0.42464	0.80482	4.1316
215	1	32.483	37.143	150.19	530	1	1.6983	2.3456	9.5319
216	1	1.6273	2.2693	9.2303	531	1	1.4629	2.3504	8.9169
217	1	2.0535	2.7576	11.123	532	1	0.46647	0.84834	4.2565
218	1	3.3188	4.3787	17.174	533	1	-20.898	-23.43	-94.415
219	1	3.5707	4.4018	17.533	534	1	-32.86	-41.248	-155.5
220	1	6.4377	8.2893	31.977	535	1	-5.4293	-6.9535	-25.153
221	1	1.9943	2.7034	10.733	536	1	-1.9775	-2.1536	-8.0079
222	1	8.929	10.746	42.372	537	1	-2.6566	-3.027	-11.254
223	1	5.411	6.7053	26.192	538	1	-3.5771	-4.2029	-15.651
224	1	4.7672	5.9535	23.222	539	1	-4.5801	-5.6444	-20.79
225	1	4.4319	5.5718	21.691	540	1	-3.8473	-4.6662	-17.183
226	1	4.3159	5.4304	21.151	541	1	-7.9383	-10.802	-38.98
227	1	4.3776	5.5188	21.458	542	1	-20.898	-23.43	-94.415
228	1	14.93	18.107	70.488	543	1	-5.5636	-6.2139	-24.401
229	1	0.50819	0.8876	4.3799	544	1	-32.694	-40.287	-152.87
230	1	0.58085	0.96915	4.6263	545	1	-32.86	-41.248	-155.5
231	1	0.51034	0.90303	4.402	546	1	-3.0835	-3.0848	-12.474
232	1	0.6895	1.0868	5.0214	547	1	-2.1169	-2.4696	-8.9238
233	1	0.59339	0.9909	4.6801	548	1	-2.8669	-3.4277	-12.514
234	1	0.79111	1.1982	5.4147	549	1	-3.9346	-4.8133	-17.676
235	1	0.69212	1.1023	5.0457	550	1	-4.9242	-6.0802	-22.436
236	1	0.8801	1.2774	5.7526	551	1	-16.653	-18.499	-74.878
237	1	0.71396	1.116	5.1124	552	1	-8.3948	-9.436	-37.359
238	1	1.081	1.5046	6.6021	553	1	-229.19	-278.02	-1065.3
239	1	0.76858	1.1811	5.333	554	1	-5.1451	-6.7602	-24.095
240	1	1.4117	1.8471	8.0095	555	1	-1.9371	-2.1433	-7.8911
241	1	0.87114	1.3188	5.7844	556	1	-2.5978	-2.9947	-11.056

242	1	1.8457	2.3866	9.9935	557	1	-3.466	-4.1177	-15.234
243	1	0.93433	1.4112	6.0827	558	1	-4.7892	-5.84	-21.64
244	1	3.0249	3.6967	15.292	559	1	-14.867	-16.865	-67.06
245	1	1.0917	1.5809	6.733	560	1	-5.5757	-6.0151	-24.267
246	1	1.8484	2.4036	9.9098	561	1	-2.2307	-2.4966	-9.2543
247	1	1.27	1.8164	7.5651	562	1	-3.0191	-3.5128	-13.035
248	1	5.0688	5.5745	24.131	563	1	-4.1922	-5.0186	-18.663
249	1	1.9237	2.5299	10.366	564	1	-4.852	-6.0129	-22.142
250	1	2.0442	2.7863	11.168	565	1	-9.3444	-10.404	-41.592
251	1	2.9455	3.8721	15.324	566	1	-6.6989	-7.5863	-29.674
252	1	3.0655	3.8015	15.195	567	1	-21.93	-29.802	-106.34
253	1	5.6729	7.3162	28.314	568	1	-1.8873	-2.036	-7.5861
254	1	4.5458	5.6279	22.124	569	1	-2.625	-2.9725	-11.09
255	1	4.2068	5.2682	20.601	570	1	-3.6349	-4.2485	-15.89
256	1	3.9322	4.9351	19.324	571	1	-5.1719	-6.2156	-23.257
257	1	3.8605	4.8691	19.017	572	1	-4.9049	-6.0577	-22.348
258	1	5.6888	4.9129	24.648	573	1	-8.2901	-10.517	-38.898
259	1	40.211	46.667	184.98	574	1	-11.578	-13.307	-52.174
260	1	4.3591	5.4806	21.587	575	1	-14.064	-14.67	-62.102
261	1	0.50444	0.89479	4.3799	576	1	-5.2317	-5.6152	-22.452
262	1	0.66986	1.0574	4.9382	577	1	-2.1804	-2.3863	-8.945
263	1	0.58987	0.98252	4.662	578	1	-3.057	-3.4915	-13.099
264	1	0.74048	1.1375	5.2103	579	1	-4.3915	-5.1715	-19.436
265	1	0.68546	1.0905	5.0148	580	1	-6.4762	-7.8314	-29.42
266	1	0.83793	1.2602	5.6136	581	1	-6.7784	-8.159	-30.749
267	1	0.71571	1.1249	5.1297	582	1	-6.6958	-7.3913	-29.46
268	1	0.98595	1.3955	6.1946	583	1	-5.6122	-6.4034	-24.757
269	1	0.7527	1.1574	5.2608	584	1	-3.0327	-2.9876	-12.284
270	1	1.21	1.6529	7.1625	585	1	-2.5444	-2.812	-10.619
271	1	0.85212	1.2908	5.696	586	1	-3.6807	-4.2251	-15.976
272	1	1.5451	2.0511	8.6572	587	1	-5.5299	-6.5363	-24.732
273	1	0.95042	1.4289	6.1486	588	1	-8.8501	-10.69	-40.484
274	1	2.3344	2.937	12.19	589	1	-11.031	-13.193	-50.387
275	1	1.0489	1.5199	6.5277	590	1	-8.6006	-9.899	-38.528
276	1	1.2449	1.7882	7.4575	591	1	-43.435	-52.499	-201.42
277	1	4.8346	5.6383	23.391	592	1	-6.2702	-6.6564	-27.062
278	1	1.4962	2.0462	8.4992	593	1	-2.0283	-2.2588	-8.3227
279	1	1.5179	2.3728	9.2017	594	1	-2.9565	-3.413	-12.7
280	1	2.6666	3.4993	13.958	595	1	-4.507	-5.2141	-19.82
281	1	48.385	45.02	211.88	596	1	-7.2068	-8.5711	-32.583
282	1	4.8236	6.2156	24.205	597	1	-11.558	-14.068	-53.335
283	1	4.0028	4.948	19.569	598	1	-5.3335	-5.9131	-23.294
284	1	3.6314	4.5264	17.87	599	1	-4.6957	-5.368	-20.577
285	1	3.538	4.4457	17.473	600	1	-30.036	-33.195	-134.86
286	1	5.0848	4.8179	22.857	601	1	-3.1822	-3.4777	-13.457
287	1	14.35	12.221	60.94	602	1	-3.5203	-4.0981	-15.333
288	1	73.766	87.357	341.79	603	1	-5.6966	-6.6194	-25.328
289	1	2.6665	3.4666	13.778	604	1	-9.8142	-11.699	-44.733
290	1	0.58571	0.97456	4.6434	605	1	-15.446	-18.799	-71.567
291	1	0.66225	1.0715	4.9359	606	1	-28.059	-28.486	-122.78
292	1	0.68011	1.0767	4.9848	607	1	-6.9882	-8.1107	-31.201
293	1	0.80509	1.2118	5.4673	608	1	-78.588	-79.617	-346.93
294	1	0.70667	1.1218	5.1058	609	1	-2.892	-3.2304	-12.242
295	1	0.90255	1.2991	5.8409	610	1	-4.4111	-5.1434	-19.442
296	1	0.7462	1.1494	5.2343	611	1	-7.5248	-8.7867	-33.81
297	1	1.1026	1.5258	6.6906	612	1	-15.626	-18.65	-71.789
298	1	0.83354	1.2586	5.6021	613	1	-64.514	-77.479	-299.9
299	1	1.549	2.0189	8.629	614	1	-4.4111	-4.8771	-19.086
300	1	0.96162	1.4248	6.165	615	1	-4.3615	-4.6187	-18.624

301	1	1.9474	2.5157	10.466	616	1	-3.101	-3.4433	-13.164
302	1	1.018	1.4789	6.3859	617	1	-3.3905	-3.8571	-14.595
303	1	3.1451	3.8463	15.853	618	1	-5.6005	-6.575	-24.984
304	1	1.2064	1.7281	7.2599	619	1	-11.069	-13.257	-50.661
305	1	2.0763	2.6886	10.978	620	1	-35.691	-42.647	-165.23
306	1	1.3998	1.9753	8.1556	621	1	-6.0846	-6.1351	-25.988
307	1	1.7557	2.6567	10.28	622	1	-4.2294	-4.8374	-18.461
308	1	2.5759	3.4111	13.584	623	1	-7.8147	-9.1727	-35.215
309	1	4.0717	5.2386	20.566	624	1	-19.298	-23.149	-89.051
310	1	3.3082	4.1217	16.351	625	1	-11.612	-13.65	-52.801
311	1	4.8506	4.6547	22.063	626	1	-77.304	-92.712	-359.48
312	1	9.2267	8.469	40.586	627	1	-14.551	-16.626	-65.092
313	1	9.888	11.955	47.055	628	1	-7.4555	-8.5749	-33.306
314	1	1.9244	2.5835	10.357	629	1	-187.3	-220.2	-866.18
315	1	0.67576	1.0678	4.964	630	1	-23.787	-26.625	-106.51

Hyperplane reduction techniques: boundary points' approximation and inner product are applied to the set of hyperplanes of Table A.5 to obtain the hyperplanes reduction of Tables A.6 and A.7, respectively.

Table A.6:Boundary points' approximation for the IEEE 9-bus, security boundary, three control areas.

Hyperplane i	η_{i,d_1}	η_{i,d_2}	$\eta_{i,d3}$	C^i	Hyperplane i	η_{i,d_1}	η_{i,d_2}	$\eta_{i,d3}$	C^i
1	1	0.93606	1.3703	6.0078	41	1	0.87114	1.3188	5.7844
2	1	0.64761	1.0519	4.8758	42	1	1.9943	2.7034	10.733
3	1	5.1194	6.4038	24.889	43	1	2.849	3.6144	14.566
4	1	2.0535	2.7576	11.123	44	1	-5.6005	-6.575	-24.984
5	1	0.46227	0.85491	4.2558	45	1	-3.101	-3.4433	-13.164
6	1	2.6665	3.4666	13.778	46	1	-1.9775	-2.1536	-8.0079
7	1	2.3344	2.937	12.19	47	1	-3.5771	-4.2029	-15.651
8	1	4.8236	6.2156	24.205	48	1	3.8243	4.3396	18.37
9	1	14.174	16.777	66.599	49	1	2.937	3.8474	15.114
10	1	-4.9242	-6.0802	-22.436	50	1	3.4997	3.9279	16.856
11	1	-6.6958	-7.3913	-29.46	51	1	-6.9882	-8.1107	-31.201
12	1	23.307	27.718	109.03	52	1	1.4658	2.081	8.5105
13	1	-3.0835	-3.0848	-12.474	53	1	-4.2294	-4.8374	-18.461
14	1	0.29459	0.68427	3.789	54	1	6.8256	8.5621	32.968
15	1	14.483	16.517	67.504	55	1	7.1926	9.0474	34.737
16	1	-64.514	-77.479	-299.9	56	1	5.7298	7.2518	27.886
17	1	-187.3	-220.2	-866.18	57	1	5.9387	7.5092	28.871
18	1	-78.588	-79.617	-346.93	58	1	1.2896	1.5154	7.0662
19	1	238.97	286.47	1115	59	1	7.9105	9.2714	37.393
20	1	1.2628	1.7754	7.4659	60	1	1.9478	2.0952	9.6981
21	1	1.2151	1.7247	7.2612	61	1	5.9469	7.4527	28.808
22	1	1.1186	1.6192	6.8585	62	1	3.4301	4.2445	17.16
23	1	1.4962	2.0462	8.4992	63	1	7.7806	9.817	37.558
24	1	1.2052	1.6743	7.1664	64	1	7.0654	8.9454	34.22
25	1	1.3243	1.8683	7.7814	65	1	4.4884	5.6036	22.227
26	1	-2.625	-2.9725	-11.09	66	1	2.9882	3.8295	15.357
27	1	1.0985	1.5853	6.7546	67	1	14.048	17.136	66.383
28	1	-2.0283	-2.2588	-8.3227	68	1	14.622	17.17	68.483
29	1	-2.892	-3.2304	-12.242	69	1	4.1505	5.1847	20.683
30	1	-2.9565	-3.413	-12.7	70	1	-11.558	-14.068	-53.335
31	1	1.0209	1.5092	6.444	71	1	8.3872	10.081	40.058

32	1	3.0655	3.8015	15.195	72	1	1.9071	2.1237	9.8409
33	1	1.549	2.0189	8.629	73	1	2.7091	3.6109	14.276
34	1	1.395	1.9642	8.1235	74	1	5.0434	5.93	24.39
35	1	-3.057	-3.4915	-13.099	75	1	-7.4555	-8.5749	-33.306
36	1	1.0258	1.4943	6.4308	76	1	3.1451	3.8463	15.853
37	1	1.6312	2.1631	9.0432	77	1	18.439	22.43	86.929
38	1	0.83793	1.2602	5.6136	78	1	19.346	23.374	91.018
39	1	-3.466	-4.1177	-15.234	79	1	12.291	14.823	58.071
40	1	0.81006	1.2199	5.488	80	1	8.5294	10.186	40.702

Table A.7:Inner product reduction for the IEEE 9-bus, security boundary, three control areas.

Hyperplane i	η_{i,d_1}	η_{i,d_2}	$\eta_{i,d3}$	C^i	Hyperplane i	η_{i,d_1}	η_{i,d_2}	$\eta_{i,d3}$	C^i
1	1	5.411	6.7053	26.192	11	1	4.9465	3.3234	21.587
2	1	0.83507	1.2359	5.5799	12	1	2.0763	2.6886	10.978
3	1	1.3882	1.9305	8.0449	13	1	1.0716	1.4766	6.5443
4	1	-11.069	-13.257	-50.661	14	1	9.5244	11.914	45.67
5	1	0.52358	0.92835	4.4621	15	1	-64.514	-77.479	-299.9
6	1	-2.892	-3.2304	-12.242	16	1	-2.1169	-2.4696	-8.9238
7	1	0.29459	0.68427	3.789	17	1	-7.5248	-8.7867	-33.81
8	1	9.2267	8.469	40.586	18	1	0.46133	0.85771	4.2578
9	1	2.2883	2.1051	11.132	19	1	4.9465	3.3234	21.587
10	1	1.2595	1.1483	6.4907	20	1	0.5236	0.9284	4.4618

A.2 IEEE 54-machine 118-bus test system

A.2.1 Two control areas

Regarding to the security boundary of Figure 3.14 associated to the IEEE 118-bus system, the piecewise linear approximation by brute force is composed by the hyperplanes of Table A.8.

Table A.8:Brute force approximation for the IEEE 118-bus, two control areas.

Hyperplane i	η_{i,d_1}	η_{i,d_2}	C^i	Hyperplane i	η_{i,d_1}	η_{i,d_2}	C^i
1	1	1.5063	82.682	11	1	-0.28509	21.463
2	1	9.2701	379.04	12	1	-0.29056	21.297
3	1	2.6831	129.82	13	1	-0.29505	21.165
4	1	2.3158	116.04	14	1	-0.29578	21.144
5	1	1.2506	76.46	15	1	-0.29656	21.122
6	1	1.2042	74.76	16	1	-2.5086	-72.225
7	1	0.078989	34.153	17	1	-55.619	-2070.5
8	1	-0.26458	22.122	18	1	-2.8118	-82.733
9	1	-0.26818	22.001	19	1	-21.949	-810.95
10	1	-0.27697	21.716	20	1	-3.6074	-109.59

A.2.2 Three control areas

For the security boundary shown in Figure 3.15, the piecewise approximation obtained by brute force is composed by the set of hyperplanes of Table A.9.

Table A.9:Brute force approximation for the IEEE 118-bus, three control areas.

Hyperplane i	η_{i,d_1}	η_{i,d_2}	$\eta_{i,d3}$	C^i	Hyperplane i	η_{i,d_1}	η_{i,d_2}	$\eta_{i,d3}$	C^i
1	1	6.8246	0.63025	151.27	316	1	-20.556	-5.5974	-321.73
2	1	6.3885	0.45096	147.9	317	1	-17.924	-1.2456	-158.79
3	1	6.2775	0.47381	147.9	318	1	-13.703	-3.7183	-193.54
4	1	6.6561	0.62699	150.99	319	1	-11.969	-0.83599	-90.204
5	1	6.2397	0.50431	148.03	320	1	-10.66	-2.8481	-137.07
6	1	6.2432	0.44325	147.16	321	1	-9.1634	-0.39542	-56.416
7	1	5.461	0.50474	145.92	322	1	-8.8013	-2.2876	-102.61
8	1	5.9487	0.34118	144.64	323	1	-6.2484	-0.19343	-26.647
9	1	5.0009	0.61073	146.99	324	1	-7.4649	-1.8723	-78.409
10	1	5.5378	0.10987	139.72	325	1	-4.5318	0.10059	-8.3876
11	1	5.4275	0.45982	145.05	326	1	-6.3978	-1.5353	-59.76
12	1	5.1575	0.079619	137.24	327	1	-4.8146	-0.1322	-13.706
13	1	5.1247	0.44702	143.89	328	1	-5.2706	-0.45824	-22.66
14	1	5.2105	0.1522	138.49	329	1	-5.4409	-0.62029	-27.137
15	1	4.8292	0.43116	142.6	330	1	-5.4888	-0.74168	-30.119
16	1	5.023	0.45724	144.11	331	1	-5.571	-0.86681	-33.665
17	1	4.4751	-0.25894	128	332	1	-5.721	-1.0488	-39.504
18	1	4.2885	0.42817	141.17	333	1	-5.6488	-1.123	-41.212
19	1	4.2647	0.51649	145.66	334	1	-5.6215	-1.1761	-42.709
20	1	3.9532	-0.1087	125.19	335	1	-5.7049	-1.2319	-45.028
21	1	7.2508	1.2124	193.43	336	1	-5.7318	-1.2806	-46.88
22	1	9.8621	-0.31483	188.65	337	1	-5.787	-1.3243	-48.759
23	1	26.897	6.8716	585.15	338	1	-5.8719	-1.3673	-50.795
24	1	7.1576	0.56171	151.27	339	1	-5.9768	-1.4088	-52.89
25	1	6.1782	0.43064	147.05	340	1	-6.1046	-1.4501	-55.088
26	1	5.9031	0.56976	148.15	341	1	-6.2371	-1.4913	-57.313
27	1	6.255	0.46219	147.44	342	1	-46.629	-3.8494	-517.33
28	1	5.8876	0.48671	146.77	343	1	-31.803	-8.6706	-536.9
29	1	6.3706	0.38977	147.05	344	1	-23.915	-1.9073	-233.79
30	1	5.4823	0.50669	146.02	345	1	-15.084	-4.0861	-218.35
31	1	5.0836	0.24002	138.85	346	1	-15.438	-1.1023	-130.08
32	1	5.2242	0.43232	143.73	347	1	-11.51	-3.089	-152.47
33	1	4.9156	0.41941	142.44	348	1	-10.462	-0.59252	-71.717
34	1	4.6182	0.40919	141.23	349	1	-9.3206	-2.4438	-112.04
35	1	4.3428	0.40484	140.27	350	1	-7.8316	-1.9873	-84.974
36	1	4.5959	0.45046	143.08	351	1	-5.2907	-0.026984	-16.241
37	1	4.0727	-0.05456	127.06	352	1	-5.6753	-0.4769	-26.209
38	1	4.7413	0.74138	159.45	353	1	-5.8694	-0.61962	-30.425
39	1	3.9707	-0.10097	125.48	354	1	-6.1007	-0.77737	-35.498
40	1	17.644	3.8386	376.99	355	1	-6.0137	-0.90359	-37.751
41	1	5.8411	0.55229	147.28	356	1	-6.3149	-1.1143	-45.325
42	1	5.7869	0.4052	144.87	357	1	-6.1838	-1.2031	-46.995
43	1	5.56	0.54657	147	358	1	-6.0967	-1.2714	-48.553
44	1	5.9487	0.34118	144.64	359	1	-6.1043	-1.3204	-50.215
45	1	4.5754	0.42282	141.56	360	1	-6.1391	-1.3745	-52.299
46	1	5.456	0.47205	145.45	361	1	-6.1579	-1.4189	-54.033

47	1	4.9204	0.21805	137.68	362	1	-6.2128	-1.4608	-55.911
48	1	5.1247	0.44702	143.89	363	1	-6.2924	-1.5013	-57.892
49	1	4.8292	0.43116	142.6	364	1	-6.3998	-1.5422	-60.028
50	1	4.318	0.54723	145.63	365	1	-6.5368	-1.5852	-62.38
51	1	4.2625	0.414	140.45	366	1	-108.41	-9.6332	-1307.2
52	1	4.0391	-0.05443	126.75	367	1	-38.217	-10.162	-645.08
53	1	4.1485	0.44634	141.68	368	1	-30.911	-2.697	-323.03
54	1	4.0026	-0.1099	125.68	369	1	-17.66	-4.762	-264.71
55	1	7.2508	1.2124	193.43	370	1	-14.303	-1.2339	-119.68
56	1	109.6	27.73	2085.6	371	1	-12.616	-3.394	-172.36
57	1	5.8729	0.56139	147.73	372	1	-9.9898	-0.75507	-69.096
58	1	5.8777	0.42936	145.64	373	1	-9.9376	-2.6239	-123.14
59	1	5.1378	0.36042	142.01	374	1	-8.3135	-0.56201	-50.528
60	1	4.8692	0.19555	137.54	375	1	-8.2264	-2.1113	-92.16
61	1	5.2176	0.31516	140.94	376	1	-6.988	-1.7171	-69.741
62	1	4.8861	0.22794	137.61	377	1	-6.4247	-0.63178	-35.138
63	1	5.2534	0.44508	144.17	378	1	-6.4914	-0.79234	-38.879
64	1	4.9364	0.42889	142.81	379	1	-6.8121	-0.94856	-44.843
65	1	4.6182	0.40919	141.23	380	1	-6.7474	-1.1822	-50.226
66	1	4.2003	0.33061	136.7	381	1	-6.8709	-1.2848	-54.005
67	1	4.079	-0.013054	127.72	382	1	-6.6656	-1.3645	-55.055
68	1	3.8905	0.53257	144.74	383	1	-6.5631	-1.4237	-56.346
69	1	4.0418	-0.068094	126.59	384	1	-6.6182	-1.4764	-58.5
70	1	5.2339	1.0418	177.48	385	1	-6.5893	-1.5222	-60.032
71	1	3.9707	-0.10097	125.48	386	1	-6.7586	-1.6282	-65.024
72	1	6.2843	0.47667	147.73	387	1	-6.862	-1.6729	-67.335
73	1	5.6732	0.44084	145.18	388	1	-206.35	-54.477	-3811.4
74	1	4.954	0.23118	138.46	389	1	-37.297	-3.4984	-406.78
75	1	5.3318	0.5055	145.54	390	1	-21.332	-5.7215	-331.38
76	1	5.6591	0.29942	142.8	391	1	-20.9	-1.8837	-200.43
77	1	5.3489	0.43967	144.3	392	1	-14.003	-3.7608	-196.84
78	1	4.8056	0.22738	137.17	393	1	-11.824	-1.0234	-91.37
79	1	5.0463	0.41787	142.79	394	1	-10.666	-2.8301	-136.12
80	1	4.8165	0.15802	135.99	395	1	-9.173	-0.72877	-61.129
81	1	4.7205	0.40418	141.35	396	1	-8.7195	-2.2569	-100.82
82	1	4.5269	0.10101	133.07	397	1	-6.4988	-0.44963	-32.573
83	1	4.1103	0.43663	140.65	398	1	-7.3376	-1.8333	-76.172
84	1	4.2389	0.096164	130.78	399	1	-6.9361	-0.59958	-38.819
85	1	3.5105	0.43522	138.42	400	1	-7.2453	-0.80417	-45.288
86	1	3.44	-0.019128	121.79	401	1	-7.1286	-0.97638	-47.99
87	1	3.6602	0.48755	141.75	402	1	-7.2915	-1.0794	-51.664
88	1	13.964	3.3702	338.78	403	1	-7.3534	-1.3516	-59.338
89	1	298.55	78.671	5715.7	404	1	-7.3874	-1.4618	-62.879
90	1	5.4883	0.41055	143.72	405	1	-7.1654	-1.5321	-63.671
91	1	5.3559	0.35842	142.5	406	1	-7.0508	-1.6245	-66.258
92	1	4.954	0.23118	138.46	407	1	-7.0834	-1.6833	-68.706
93	1	5.1622	0.41875	143.17	408	1	-7.1465	-1.7339	-71.062
94	1	4.9145	0.19937	137.28	409	1	-62.341	-6.287	-733.56
95	1	4.826	0.40926	141.81	410	1	-37.229	-9.9422	-628.88
96	1	4.6173	0.13878	134.32	411	1	-26.706	-2.6227	-275.65
97	1	4.4981	0.3959	140.33	412	1	-15.568	-4.1583	-223.99
98	1	3.2891	0.07162	123.1	413	1	-14.467	-1.4243	-124.85
99	1	4.1892	0.40233	139.59	414	1	-11.593	-3.0842	-152.47
100	1	3.5556	0.32011	133.48	415	1	-10.01	-0.90056	-71.832
101	1	3.4096	-0.021303	121.22	416	1	-9.2725	-2.4163	-110.49
102	1	4.8268	0.63724	154.04	417	1	-7.3962	-0.61185	-43.05
103	1	4.0322	-0.011146	127.5	418	1	-7.7075	-1.9478	-82.693
104	1	43.146	11.085	885.44	419	1	-7.7131	-0.78888	-48.966
105	1	4.7716	0.27424	138.33	420	1	-8.1465	-0.99493	-56.814

106	1	5.3618	0.35729	142.5	421	1	-7.9459	-1.1695	-59.104
107	1	5.096	0.22672	138.85	422	1	-8.3039	-1.4612	-69.513
108	1	5.2637	0.39145	142.81	423	1	-8.0882	-1.5499	-70.49
109	1	5.0029	0.23861	138.47	424	1	-7.9242	-1.6471	-72.421
110	1	4.8766	0.34973	140.24	425	1	-7.6118	-1.6912	-71.887
111	1	4.6914	0.17835	135.51	426	1	-7.5605	-1.7309	-73.022
112	1	3.6391	0.27848	132.72	427	1	-7.5728	-1.8756	-78.902
113	1	4.3343	0.36363	138.59	428	1	-7.6234	-1.9114	-80.705
114	1	4.0504	0.054465	128.57	429	1	-257.37	-27.682	-3290.2
115	1	3.5105	0.43522	138.42	430	1	-42.96	-11.163	-719.91
116	1	3.6386	0.089305	125.39	431	1	-32.819	-3.46	-357.03
117	1	3.6602	0.48755	141.75	432	1	-18.415	-4.8759	-273.77
118	1	3.7475	-0.0065562	124.68	433	1	-17.915	-1.8014	-167.2
119	1	134.43	12.466	1799.9	434	1	-12.832	-3.4119	-174.07
120	1	5.1172	0.23562	139.11	435	1	-10.805	-1.0743	-82.33
121	1	5.3942	0.39752	143.45	436	1	-9.9338	-2.6014	-121.98
122	1	5.2977	0.28375	140.84	437	1	-7.861	-0.64917	-47.627
123	1	5.0547	0.39204	142.05	438	1	-8.1545	-2.0778	-90.298
124	1	4.884	0.25002	138.01	439	1	-8.1355	-0.87744	-54.194
125	1	4.7443	0.37187	140.37	440	1	-8.852	-1.1498	-66.159
126	1	4.4675	0.15183	133.53	441	1	-9.1896	-1.5187	-78.07
127	1	4.114	0.36211	137.66	442	1	-8.9352	-1.6766	-80.54
128	1	3.9432	0.084482	128.26	443	1	-8.1189	-1.9747	-85.595
129	1	3.314	0.45909	138.15	444	1	-8.0737	-2.0092	-86.85
130	1	3.1203	0.14867	121.8	445	1	-8.0979	-2.0449	-88.552
131	1	6.4296	0.96942	178.07	446	1	-44.251	-4.9819	-510.48
132	1	4.8974	0.38505	143.99	447	1	-22.804	-5.9667	-350.71
133	1	99.48	25.471	1918.5	448	1	-22.825	-2.4999	-231.9
134	1	5.427	0.24953	140.65	449	1	-14.505	-3.8301	-202.43
135	1	5.2403	0.341	141.62	450	1	-11.636	-1.2515	-93.352
136	1	4.8602	0.30494	138.98	451	1	-10.733	-2.8168	-135.68
137	1	4.6427	0.22287	136.07	452	1	-9.0222	-0.86203	-61.861
138	1	3.9725	0.45068	139.6	453	1	-8.6661	-2.2239	-99.023
139	1	4.3092	0.17154	132.85	454	1	-8.9272	-1.0497	-64.52
140	1	4.2459	0.34197	137.42	455	1	-9.4122	-1.3083	-74.528
141	1	4.0258	0.11748	129.63	456	1	-10.241	-1.7741	-93.633
142	1	4.0218	0.35182	136.86	457	1	-9.2129	-1.7998	-86.34
143	1	3.9383	0.30627	133.87	458	1	-8.9171	-2.0846	-94.325
144	1	3.9312	0.067392	127.97	459	1	-8.8108	-2.1326	-95.666
145	1	5.3297	0.38093	142.84	460	1	-8.7024	-2.1663	-96.554
146	1	4.5349	0.28424	136.92	461	1	-8.6556	-2.1952	-97.637
147	1	4.7239	0.26234	137.38	462	1	-86.396	-10.323	-1076.5
148	1	4.4345	0.20574	134.42	463	1	-43.763	-11.339	-733.09
149	1	4.3334	0.3239	137.16	464	1	-28.303	-3.3101	-305.91
150	1	4.1097	0.15413	131.07	465	1	-16.187	-4.2342	-230.55
151	1	4.0715	0.33205	136.28	466	1	-14.543	-1.6781	-130.28
152	1	3.314	0.45909	138.15	467	1	-11.767	-3.0849	-153.18
153	1	10.175	1.8134	239.04	468	1	-10.433	-1.1256	-79.843
154	1	29.335	3.7109	476.53	469	1	-9.2557	-2.3874	-109.02
155	1	667.96	170.56	12361	470	1	-10.044	-1.2656	-79.003
156	1	4.0426	0.3293	135.67	471	1	-11.037	-1.8492	-102.31
157	1	4.7651	0.26565	137.68	472	1	-9.9149	-1.8283	-92.417
158	1	3.9294	0.37008	136.27	473	1	-9.7568	-2.2676	-106.48
159	1	4.5158	0.24038	135.71	474	1	-9.6696	-2.3119	-107.74
160	1	4.436	0.32488	137.64	475	1	-9.4324	-2.3384	-107.59
161	1	4.0212	0.22762	132.18	476	1	-9.3072	-2.3627	-108.07
162	1	4.1688	0.31686	136.16	477	1	-93.623	-23.609	-1622.4
163	1	3.8829	0.14339	129.13	478	1	-19.201	-4.9549	-281.39
164	1	3.8396	0.38705	137.31	479	1	-15.379	-1.9109	-143.23

165	1	3.7779	0.10969	127.45	480	1	-13.152	-3.4327	-176.45
166	1	4.6682	0.54811	149.14	481	1	-12.048	-1.4399	-101.36
167	1	4.7438	0.4582	144.98	482	1	-9.9846	-2.5808	-121.16
168	1	55.693	13.701	1081.7	483	1	-11.376	-1.5293	-96.902
169	1	4.6018	0.27069	136.93	484	1	-12.17	-2.1295	-119.84
170	1	4.4793	0.26476	136.1	485	1	-10.967	-2.4877	-122.72
171	1	3.89	0.16483	129.79	486	1	-10.521	-2.4942	-120.14
172	1	4.1688	0.36731	137.64	487	1	-10.366	-2.5452	-121.4
173	1	4.0229	0.16961	130.83	488	1	-10.122	-2.5622	-120.91
174	1	2.9901	0.25886	127.24	489	1	-136.92	-20.296	-1844
175	1	3.7537	0.1347	127.89	490	1	-24.943	-6.3108	-378.82
176	1	3.8947	0.33204	135.32	491	1	-18.335	-2.4239	-183.95
177	1	3.9148	0.12953	129.18	492	1	-15.141	-3.9113	-209.4
178	1	69.91	10.041	1052.2	493	1	-12.445	-1.5837	-108.03
179	1	4.5424	0.3363	138.26	494	1	-10.888	-2.8085	-135.92
180	1	4.3904	0.24841	135.2	495	1	-14.588	-2.3958	-148.32
181	1	4.3534	0.29003	136.17	496	1	-12.79	-2.116	-124.5
182	1	3.9694	0.14582	129.84	497	1	-12.55	-2.7401	-143.12
183	1	3.8685	0.35561	135.71	498	1	-11.83	-2.7672	-139.29
184	1	3.3077	0.28272	128.36	499	1	-11.526	-2.787	-138.26
185	1	3.4843	0.17888	126.87	500	1	-11.143	-2.7994	-136.72
186	1	3.7403	0.14974	128.17	501	1	-55.045	-13.714	-912.86
187	1	5.9717	0.81721	168.97	502	1	-27.144	-4.2526	-317.62
188	1	23.867	3.5565	418.02	503	1	-17.116	-4.3464	-240.68
189	1	126.68	30.96	2338.3	504	1	-13.829	-1.8439	-126.76
190	1	4.4669	0.28048	136.47	505	1	-12.04	-3.0881	-154.56
191	1	4.156	0.23205	133.38	506	1	-14.487	-3.0227	-167.71
192	1	4.0368	0.30043	134.79	507	1	-13.654	-3.1098	-165.03
193	1	3.0737	0.15195	122.98	508	1	-12.917	-3.0595	-158.15
194	1	3.1363	0.35234	131.55	509	1	-12.396	-3.0809	-156.05
195	1	3.7177	0.16799	128.51	510	1	-176.72	-42.376	-3021.9
196	1	4.0358	0.36914	137.74	511	1	-32.569	-5.3384	-400.88
197	1	11.849	2.6218	277.17	512	1	-21.373	-5.3362	-311.69
198	1	37.817	8.7982	736.75	513	1	-18.545	-2.9907	-201.09
199	1	280.05	43.801	4074.8	514	1	-13.559	-3.4483	-179.17
200	1	4.2822	0.26278	134.99	515	1	-16.966	-3.3549	-198.88
201	1	3.9734	0.22121	131.92	516	1	-15.981	-3.5025	-196.83
202	1	3.7712	0.30307	133.36	517	1	-14.778	-3.4144	-184.91
203	1	3.0445	0.15898	122.96	518	1	-14.115	-3.453	-182.45
204	1	3.8802	0.30166	134.1	519	1	-177.31	-30.114	-2526.3
205	1	4.6207	0.32845	141.09	520	1	-27.721	-6.701	-413.41
206	1	60.197	9.8877	954.7	521	1	-15.848	-3.9781	-216.28
207	1	4.0661	0.24609	133.25	522	1	-20.089	-3.7577	-238.49
208	1	3.1087	0.19654	124.6	523	1	-19.235	-4.0144	-240.8
209	1	3.8296	0.26245	132.36	524	1	-17.512	-3.9243	-224.5
210	1	3.7955	0.2156	130.55	525	1	-16.628	-3.9898	-221.42
211	1	4.4487	0.45114	143.82	526	1	-80.975	-14.639	-1145.7
212	1	24.199	4.1151	439.13	527	1	-76.031	-17.946	-1241.3
213	1	68.233	15.74	1252.2	528	1	-18.765	-4.5682	-260.44
214	1	3.8923	0.23865	131.94	529	1	-23.964	-4.7236	-304.65
215	1	3.5236	0.10409	124.71	530	1	-21.857	-4.7308	-288.39
216	1	3.8007	0.29465	133.32	531	1	-20.593	-4.7848	-281.68
217	1	20.718	4.04	408.75	532	1	-1635.8	-371.33	-27648
218	1	3.7699	0.2417	131.23	533	1	-31.595	-5.8407	-408.51
219	1	4.1795	0.38843	139.31	534	1	-22.953	-5.4513	-326.48
220	1	32.244	5.7705	567.73	535	1	-29.399	-6.0933	-399.52
221	1	52.78	11.256	946.15	536	1	-26.398	-5.8365	-366.57
222	1	9.9833	1.974	243.87	537	1	-42.992	-8.3401	-594.56
223	1	169.49	34.399	2771.2	538	1	-33.494	-7.732	-497.5

224	1	55.496	11.613	978.32	539	1	-35.636	-7.589	-506.77
225	1	-389.44	-32.29	-4849	540	1	-56.371	-12.289	-855.35
226	1	-87.561	-23.696	-1605	541	1	26.897	6.8716	585.15
227	1	-33.345	-2.5471	-348.25	542	1	5.1247	0.44702	143.89
228	1	-22.716	-6.2231	-364.86	543	1	-29.399	-6.0933	-399.52
229	1	-17.704	-1.2784	-156.76	544	1	-26.398	-5.8365	-366.57
230	1	-14.759	-4.0271	-214.06	545	1	-6.1046	-1.4501	-55.088
231	1	-12.383	-0.91615	-95.442	546	1	3.9532	-0.1087	125.19
232	1	-10.66	-2.8481	-137.07	547	1	-22.953	-5.4513	-326.48
233	1	-9.0951	-0.4174	-56.012	548	1	-29.399	-6.0933	-399.52
234	1	-8.8013	-2.2876	-102.61	549	1	4.4751	-0.25894	128
235	1	-6.282	-0.26933	-27.909	550	1	-10.967	-2.4877	-122.72
236	1	-7.8554	-1.9733	-84.369	551	1	-10.521	-2.4942	-120.14
237	1	-6.8403	-1.6661	-66.974	552	1	4.1795	0.38843	139.31
238	1	-2.8283	0.064758	4.2941	553	1	32.244	5.7705	567.73
239	1	-5.9073	-1.3671	-50.936	554	1	6.3885	0.45096	147.9
240	1	-3.7286	-0.070183	-4.4576	555	1	5.2339	1.0418	177.48
241	1	-4.1355	-0.17314	-9.0699	556	1	3.9707	-0.10097	125.48
242	1	-4.2262	-0.33824	-12.625	557	1	3.7699	0.2417	131.23
243	1	-4.4705	-0.43939	-16.313	558	1	4.1795	0.38843	139.31
244	1	-4.488	-0.57487	-19.292	559	1	-17.924	-1.2456	-158.79
245	1	-4.6783	-0.66476	-22.626	560	1	-15.084	-4.0861	-218.35
246	1	-4.6822	-0.75879	-24.978	561	1	4.114	0.36211	137.66
247	1	-4.7247	-0.83987	-27.392	562	1	3.9432	0.084482	128.26
248	1	-4.7903	-0.91015	-29.764	563	1	5.4275	0.45982	145.05
249	1	-4.8985	-0.96573	-32.031	564	1	-5.3194	-1.146	-40.107
250	1	-4.9741	-1.02	-34.145	565	1	-5.3776	-1.1932	-42.056
251	1	-5.067	-1.071	-36.299	566	1	-5.2701	-1.0945	-38.127
252	1	-5.1793	-1.1196	-38.509	567	1	-46.662	-12.483	-809.02
253	1	-5.3075	-1.1667	-40.765	568	1	-7.041	-0.38966	-36.353
254	1	-5.4527	-1.2126	-43.072	569	1	-5.9768	-1.4088	-52.89
255	1	-5.6026	-1.2587	-45.422	570	1	-6.1046	-1.4501	-55.088
256	1	-5.7686	-1.3041	-47.816	571	1	-8.8264	-2.2723	-101.91
257	1	-73.727	-19.02	-1280.8	572	1	-5.3743	-0.061933	-17.411
258	1	-33.036	-2.5605	-344.87	573	1	-5.9768	-1.4088	-52.89
259	1	-22.581	-6.0516	-354.14	574	1	20.718	4.04	408.75
260	1	-17.924	-1.2456	-158.79	575	1	43.146	11.085	885.44
261	1	-15.084	-4.0861	-218.35	576	1	-17.503	-1.4068	-156.34
262	1	-12.645	-0.85897	-97.49	577	1	24.199	4.1151	439.13
263	1	-12.5	-3.3742	-170.93	578	1	68.233	15.74	1252.2
264	1	-9.1634	-0.39542	-56.416	579	1	9.9833	1.974	243.87
265	1	-10.01	-2.6351	-123.94	580	1	-8.6661	-2.2239	-99.023
266	1	-7.041	-0.38966	-36.353	581	1	-8.9272	-1.0497	-64.52
267	1	-8.3911	-2.1347	-93.785	582	1	3.9312	0.067392	127.97
268	1	-3.0211	0.20928	4.5885	583	1	5.3297	0.38093	142.84
269	1	-5.9073	-1.3671	-50.936	584	1	4.6427	0.22287	136.07
270	1	-4.015	0.029281	-5.1363	585	1	3.9725	0.45068	139.6
271	1	-4.2262	-0.33824	-12.625	586	1	169.49	34.399	2771.2
272	1	-4.4705	-0.43939	-16.313	587	1	-5.787	-1.3243	-48.759
273	1	-4.488	-0.57487	-19.292	588	1	-5.2706	-0.45824	-22.66
274	1	-4.6783	-0.66476	-22.626	589	1	5.3559	0.35842	142.5
275	1	-4.6822	-0.75879	-24.978	590	1	-4.7247	-0.83987	-27.392
276	1	-4.7892	-0.91012	-29.758	591	1	-4.9791	-1.0648	-35.668
277	1	-4.8243	-0.96248	-31.525	592	1	-5.0593	-1.1098	-37.629
278	1	-4.9191	-1.0168	-33.76	593	1	-389.44	-32.29	-4849
279	1	-4.9791	-1.0648	-35.668	594	1	4.0661	0.24609	133.25
280	1	-5.0593	-1.1098	-37.629	595	1	5.9487	0.34118	144.64
281	1	-5.1615	-1.1533	-39.674	596	1	4.5754	0.42282	141.56
282	1	-5.2818	-1.1956	-41.776	597	1	-5.067	-1.071	-36.299

283	1	-5.4185	-1.2389	-44.005	598	1	-5.1793	-1.1196	-38.509
284	1	-5.5635	-1.2808	-46.216	599	1	-17.924	-1.2456	-158.79
285	1	-5.7221	-1.3241	-48.547	600	1	-13.703	-3.7183	-193.54
286	1	-740.04	-62.199	-9290.7	601	1	-6.0967	-1.2714	-48.553
287	1	-46.662	-12.483	-809.02	602	1	169.49	34.399	2771.2
288	1	-41.793	-3.4578	-455.42	603	1	4.156	0.23205	133.38
289	1	-17.725	-4.7805	-265.97	604	1	3.4843	0.17888	126.87
290	1	-17.503	-1.4068	-156.34	605	1	3.7403	0.14974	128.17
291	1	-13.706	-3.7091	-193.04	606	1	-12.616	-3.394	-172.36
292	1	-11.818	-0.82446	-88.51	607	1	-9.9898	-0.75507	-69.096
293	1	-10.678	-2.8321	-136.27	608	1	5.023	0.45724	144.11
294	1	-7.8484	-0.20275	-41.464	609	1	4.4751	-0.25894	128
295	1	-8.8264	-2.2723	-101.91	610	1	-3.7286	-0.070183	-4.4576
296	1	-5.3743	-0.061933	-17.411	611	1	5.0836	0.24002	138.85
297	1	-6.1419	-1.4452	-55.023	612	1	3.44	-0.019128	121.79
298	1	-4.6858	-0.096234	-12.126	613	1	3.6602	0.48755	141.75
299	1	-4.8132	-0.47376	-19.499	614	1	4.6914	0.17835	135.51
300	1	-4.975	-0.58633	-22.971	615	1	3.9148	0.12953	129.18
301	1	-5.0121	-0.71808	-26.176	616	1	-4.7903	-0.91015	-29.764
302	1	-5.1268	-0.80449	-29.046	617	1	-4.8985	-0.96573	-32.031
303	1	-5.2052	-0.97822	-34.219	618	1	3.314	0.45909	138.15
304	1	-5.1968	-1.0437	-36.107	619	1	4.8268	0.63724	154.04
305	1	-5.2701	-1.0945	-38.127	620	1	4.0322	-0.011146	127.5
306	1	-5.3194	-1.146	-40.107	621	1	-10.044	-1.2656	-79.003
307	1	-5.3776	-1.1932	-42.056	622	1	6.2775	0.47381	147.9
308	1	-5.4631	-1.2369	-44.056	623	1	6.6561	0.62699	150.99
309	1	-5.5624	-1.2788	-46.089	624	1	55.496	11.613	978.32
310	1	-5.6874	-1.3212	-48.27	625	1	2.9901	0.25886	127.24
311	1	-5.8219	-1.363	-50.478	626	1	55.496	11.613	978.32
312	1	-5.9749	-1.4056	-52.795	627	1	4.8974	0.38505	143.99
313	1	-1915.4	-143.64	-23961	628	1	3.8685	0.35561	135.71
314	1	-87.561	-23.696	-1605	629	1	4.0715	0.33205	136.28
315	1	-33.036	-2.5605	-344.87	630	1	-10.01	-2.6351	-123.94

Finally, boundary points' approximation and inner product algorithms are applied to the set of hyperplanes of Table A.9, we obtain the reduced sets of Tables A.10 and A.11, respectively.

Table A.10:Boundary points' approximation for the IEEE 118-bus, three control areas.

Hyperplane i	η_{i,d_1}	η_{i,d_2}	$\eta_{i,d3}$	C^i	Hyperplane i	η_{i,d_1}	η_{i,d_2}	$\eta_{i,d3}$	C^i
1	1	5.3942	0.39752	143.45	78	1	-11.376	-1.5293	-96.902
2	1	4.3334	0.3239	137.16	79	1	-18.335	-2.4239	-183.95
3	1	4.0391	-0.05443	126.75	80	1	-9.0951	-0.4174	-56.012
4	1	3.9383	0.30627	133.87	81	1	-73.727	-19.02	-1280.8
5	1	7.1576	0.56171	151.27	82	1	-33.036	-2.5605	-344.87
6	1	17.644	3.8386	376.99	83	1	-22.581	-6.0516	-354.14
7	1	4.4487	0.45114	143.82	84	1	-5.6753	-0.4769	-26.209
8	1	4.7413	0.74138	159.45	85	1	-6.1007	-0.77737	-35.498
9	1	134.43	12.466	1799.9	86	1	-6.3149	-1.1143	-45.325
10	1	29.335	3.7109	476.53	87	1	-6.6656	-1.3645	-55.055
11	1	55.693	13.701	1081.7	88	1	-21.332	-5.7215	-331.38
12	1	280.05	43.801	4074.8	89	1	-32.819	-3.46	-357.03
13	1	24.199	4.1151	439.13	90	1	-8.9171	-2.0846	-94.325

14	1	68.233	15.74	1252.2	91	1	-93.623	-23.609	-1622.4
15	1	20.718	4.04	408.75	92	1	-10.521	-2.4942	-120.14
16	1	169.49	34.399	2771.2	93	1	-14.588	-2.3958	-148.32
17	1	667.96	170.56	12361	94	1	-11.143	-2.7994	-136.72
18	1	4.5158	0.24038	135.71	95	1	-17.116	-4.3464	-240.68
19	1	4.4345	0.20574	134.42	96	1	-12.917	-3.0595	-158.15
20	1	4.8056	0.22738	137.17	97	1	-389.44	-32.29	-4849
21	1	4.6914	0.17835	135.51	98	1	-17.924	-1.2456	-158.79
22	1	5.096	0.22672	138.85	99	1	-62.341	-6.287	-733.56
23	1	4.6018	0.27069	136.93	100	1	-136.92	-20.296	-1844
24	1	4.3904	0.24841	135.2	101	1	-27.144	-4.2526	-317.62
25	1	3.9734	0.22121	131.92	102	1	-14.487	-3.0227	-167.71
26	1	4.8292	0.43116	142.6	103	1	-13.559	-3.4483	-179.17
27	1	3.7699	0.2417	131.23	104	1	-27.721	-6.701	-413.41
28	1	4.826	0.40926	141.81	105	1	-20.089	-3.7577	-238.49
29	1	4.0661	0.24609	133.25	106	1	-17.512	-3.9243	-224.5
30	1	4.6182	0.40919	141.23	107	1	-76.031	-17.946	-1241.3
31	1	4.1097	0.15413	131.07	108	1	-31.595	-5.8407	-408.51
32	1	4.0258	0.11748	129.63	109	1	-35.636	-7.589	-506.77
33	1	5.2534	0.44508	144.17	110	1	-1915.4	-143.64	-23961
34	1	4.5269	0.10101	133.07	111	1	-5.9073	-1.3671	-50.936
35	1	5.1247	0.44702	143.89	112	1	-5.3075	-1.1667	-40.765
36	1	3.9432	0.084482	128.26	113	1	-7.861	-0.64917	-47.627
37	1	4.0229	0.16961	130.83	114	1	-9.9149	-1.8283	-92.417
38	1	5.8876	0.48671	146.77	115	1	-7.0508	-1.6245	-66.258
39	1	4.4675	0.15183	133.53	116	1	-10.044	-1.2656	-79.003
40	1	5.4275	0.45982	145.05	117	1	-46.662	-12.483	-809.02
41	1	5.0836	0.24002	138.85	118	1	-7.3534	-1.3516	-59.338
42	1	5.0547	0.39204	142.05	119	1	-9.4122	-1.3083	-74.528
43	1	4.3534	0.29003	136.17	120	1	-9.9898	-0.75507	-69.096
44	1	6.2775	0.47381	147.9	121	1	-9.2129	-1.7998	-86.34
45	1	4.5424	0.3363	138.26	122	1	-4.6822	-0.75879	-24.978
46	1	4.0368	0.30043	134.79	123	1	-5.571	-0.86681	-33.665
47	1	4.1892	0.40233	139.59	124	1	-17.66	-4.762	-264.71
48	1	3.4843	0.17888	126.87	125	1	-15.568	-4.1583	-223.99
49	1	5.2403	0.341	141.62	126	1	-7.7131	-0.78888	-48.966
50	1	5.3618	0.35729	142.5	127	1	-14.505	-3.8301	-202.43
51	1	5.456	0.47205	145.45	128	1	-9.0222	-0.86203	-61.861
52	1	4.1485	0.44634	141.68	129	1	-3.0211	0.20928	4.5885
53	1	4.436	0.32488	137.64	130	1	-7.3874	-1.4618	-62.879
54	1	4.954	0.23118	138.46	131	1	-7.9242	-1.6471	-72.421
55	1	3.5105	0.43522	138.42	132	1	-42.96	-11.163	-719.91
56	1	3.1203	0.14867	121.8	133	1	-9.1896	-1.5187	-78.07
57	1	43.146	11.085	885.44	134	1	-21.373	-5.3362	-311.69
58	1	10.175	1.8134	239.04	135	1	-21.857	-4.7308	-288.39
59	1	5.9717	0.81721	168.97	136	1	-20.593	-4.7848	-281.68
60	1	-5.7686	-1.3041	-47.816	137	1	-8.0737	-2.0092	-86.85
61	1	-6.862	-1.6729	-67.335	138	1	-8.6556	-2.1952	-97.637
62	1	-8.0979	-2.0449	-88.552	139	1	-9.9338	-2.6014	-121.98
63	1	-4.8985	-0.96573	-32.031	140	1	-5.2052	-0.97822	-34.219
64	1	-9.2557	-2.3874	-109.02	141	1	-11.767	-3.0849	-153.18
65	1	-4.015	0.029281	-5.1363	142	1	-5.6488	-1.123	-41.212
66	1	-6.282	-0.26933	-27.909	143	1	-4.2262	-0.33824	-12.625
67	1	-10.678	-2.8321	-136.27	144	1	-17.503	-1.4068	-156.34
68	1	-8.1355	-0.87744	-54.194	145	1	-7.9459	-1.1695	-59.104
69	1	-5.0121	-0.71808	-26.176	146	1	-44.251	-4.9819	-510.48
70	1	-4.4705	-0.43939	-16.313	147	1	-22.825	-2.4999	-231.9
71	1	-15.084	-4.0861	-218.35	148	1	-86.396	-10.323	-1076.5
72	1	-12.5	-3.3742	-170.93	149	1	-32.569	-5.3384	-400.88

73	1	-11.818	-0.82446	-88.51	150	1	-18.545	-2.9907	-201.09
74	1	-14.303	-1.2339	-119.68	151	1	-16.966	-3.3549	-198.88
75	1	-7.2915	-1.0794	-51.664	152	1	-14.115	-3.453	-182.45
76	1	-7.5605	-1.7309	-73.022	153	1	-177.31	-30.114	-2526.3
77	1	-8.9352	-1.6766	-80.54					

Table A.11:Inner product reduction for the IEEE 118-bus, three control areas.

Hyperplane i	η_{i,d_1}	η_{i,d_2}	$\eta_{i,d3}$	C^i	Hyperplane i	η_{i,d_1}	η_{i,d_2}	$\eta_{i,d3}$	C^i
1	1	1	4.0661	0.24609	14	1	-18.335	-2.4239	-183.95
2	2	1	13.964	3.3702	15	1	-22.825	-2.4999	-231.9
3	3	1	9.8621	-0.31483	16	1	-28.303	-3.3101	-305.91
4	4	1	3.7475	-0.0065562	17	1	-11.636	-1.2515	-93.352
5	5	1	55.496	11.613	18	1	-10.433	-1.1256	-79.843
6	6	1	4.4487	0.45114	19	1	-9.0222	-0.86203	-61.861
7	7	1	5.56	0.54657	20	1	-8.1355	-0.87744	-54.194
8	8	1	5.0009	0.61073	21	1	-136.92	-20.296	-1844
9	9	1	4.0504	0.054465	22	1	-6.9361	-0.59958	-38.819
10	10	1	-9.2129	-1.7998	23	1	-7.9459	-1.1695	-59.104
11	11	1	-5.3743	-0.061933	24	1	-5.571	-0.86681	-33.665
12	12	1	-2.8283	0.064758	25	1	-35.636	-7.589	-506.77
13	13	1	-14.543	-1.6781					

Appendix B

Critical dispatches

The critical dispatches that compose the feasibility boundaries presented in this work are reported in this Appendix.

Table B.1:Critical dispatches for the Figure 3.5.

Dispatch direction	P_{G_A} (MW)	P_{G_B} (MW)	Dispatch direction	P_{G_A} (MW)	P_{G_B} (MW)
1	267.52	248	12	168.77	658.93
2	275.93	285.22	13	154.53	678.43
3	279.29	327.87	14	141.4	696.5
4	281.23	376.03	15	129.25	713.36
5	276.08	424.93	16	117.98	729.22
6	265.82	472.06	17	107.51	744.67
7	251.7	515.13	18	97.572	756.68
8	235.17	552.82	19	88.419	770.74
9	217.69	585.06	20	79.853	788.14
10	200.54	613.08	21	71.641	797.12
11	184.12	637.37			

Table B.2:Critical dispatches for the Figure 3.7.

Dispatch direction	P_{G_A} (MW)	P_{G_B} (MW)	P_{G_C} (MW)	Dispatch direction	P_{G_A} (MW)	P_{G_B} (MW)	P_{G_C} (MW)	Dispatch direction	P_{G_A} (MW)	P_{G_B} (MW)	P_{G_C} (MW)
1	364.49	163	85	212	84.126	503.87	188.69	423	105.15	525.12	154.57
2	372.32	199.01	85	213	84.528	485.54	207.32	424	106.32	508.19	172.43
3	359.46	163	102.97	214	84.896	464.59	226.54	425	107.55	489.79	191.51
4	374.65	239.6	85	215	85.361	443.94	247.78	426	108.83	469.76	211.87
5	357.1	163	122.63	216	85.776	420.28	269.48	427	110.13	447.61	233.42
6	373.3	284.12	85	217	86.184	394.62	292.06	428	111.45	423.38	256.2
7	348.27	163	142.92	218	86.567	366.76	315.22	429	112.73	396.7	279.99
8	365.18	329.97	85	219	86.899	336.57	338.44	430	113.92	367.43	304.48
9	343.7	163	165.7	220	87.161	304.25	361.22	431	114.99	335.6	329.31
10	350.71	374.65	85	221	87.316	269.99	382.56	432	115.82	301.22	353.65
11	334.38	163	188.91	222	87.332	234.4	401.5	433	338.75	293.23	152.91
12	329.54	414.48	85	223	365.84	214.49	111.85	434	322.36	338.52	153.65
13	323.41	163	213.02	224	364.22	258.1	113.34	435	323.5	295.24	176.95
14	304.14	447.84	85	225	357.97	216.18	133.53	436	300.36	379.83	152.84
15	310.71	163	237.73	226	356.91	304.1	114.43	437	306.47	296.57	201.09
16	276.98	474.46	85	227	348.38	217.75	156.38	438	274.7	415	150.71
17	296.26	163	262.67	228	342.97	349.63	114.95	439	288	297.26	225.02
18	250.41	495.79	85	229	337.09	219.18	180.22	440	247.87	443.68	147.73
19	280.23	163	287.49	230	322.61	391.41	114.78	441	268.17	297.14	248.22
20	225.51	513.1	85	231	323.97	220.41	204.75	442	221.83	466.74	144.4
21	262.58	163	311.54	232	297.64	427.05	113.99	443	247.37	296.28	270.33
22	202.81	527.75	85	233	309.02	221.39	229.62	444	197.74	485.76	141.1
23	243.63	163	334.41	234	270.58	455.89	112.77	445	226.03	294.73	291.08

24	182.15	540.17	85	235	292.37	222.08	254.46	446	175.8	501.56	137.97
25	223.57	163	355.39	236	243.97	479.2	111.38	447	204.36	292.41	309.95
26	163.52	551.24	85	237	274.12	222.44	278.74	448	156.02	514.96	135.06
27	202.75	163	373.88	238	218.89	498.03	109.96	449	182.95	289.63	327.12
28	146.65	561.19	85	239	254.49	222.43	301.95	450	138.29	526.92	132.44
29	181.65	163	389.55	240	195.92	513.62	108.59	451	161.92	286.24	342.06
30	131.32	570.36	85	241	233.86	222.05	323.66	452	122.31	537.66	130.09
31	160.7	163	402.01	242	175.14	526.93	107.33	453	141.64	282.44	354.91
32	117.33	578.85	85	243	212.58	221.31	343.44	454	107.82	547.19	127.93
33	140.42	163	411.42	244	156.21	537.72	106.12	455	122.38	278.44	365.92
34	104.45	586	85	245	191.09	220.21	360.98	456	109.1	532.36	144.27
35	121.21	163	418.26	246	139.5	549	105.13	457	110.43	516.03	161.71
36	92.086	581.66	85	247	169.67	218.76	375.76	458	111.82	498.17	180.33
37	103.32	163	423.31	248	124.21	558.62	104.19	459	113.27	478.72	200.25
38	81.745	599.81	85	249	148.81	217.02	387.85	460	114.78	457.47	221.5
39	86.782	163	426.32	250	110.29	567.49	103.34	461	116.28	433.86	243.9
40	71.641	605.09	85	251	128.89	215.1	397.43	462	117.8	408.07	267.56
41	71.641	163	427.87	252	97.475	574.44	102.51	463	119.23	379.57	292.05
42	364.33	174.48	90.987	253	110.15	213.07	404.84	464	120.54	348.45	317.09
43	71.641	594.39	96.84	254	85.808	582.03	101.81	465	121.63	314.65	342.02
44	71.641	583.26	109.35	255	92.743	211.01	410.49	466	328.87	309.31	161.3
45	71.641	569.71	122.43	256	86.233	569.71	115.3	467	309.64	353.26	161.32
46	71.641	559.44	136.68	257	86.705	557.16	129.68	468	312.17	310.91	185.27
47	71.641	544.66	151.34	258	87.195	543.42	144.98	469	285.62	392.11	159.67
48	71.641	530.87	167.21	259	87.676	527.82	161.1	470	293.78	311.65	209.03
49	71.641	509.74	182.36	260	88.212	511.75	178.39	471	259.16	424.5	156.77
50	71.641	497.48	201.28	261	88.75	493.89	196.65	472	274.17	311.65	232.28
51	71.641	478.9	219.78	262	89.313	474.61	216.04	473	232.62	450.77	153.21
52	71.641	458.79	239.25	263	89.886	453.58	236.53	474	253.56	310.82	254.59
53	71.641	437.02	259.65	264	90.468	430.72	258.12	475	207.52	472.15	149.49
54	71.641	413.42	280.88	265	91.036	405.71	280.6	476	232.43	309.33	275.77
55	71.641	387.82	302.73	266	91.581	378.5	303.84	477	184.44	489.64	145.83
56	71.641	360.29	325.05	267	92.072	348.94	327.41	478	210.82	306.93	295.16
57	71.641	330.64	347.25	268	92.482	317.11	350.82	479	163.66	504.61	142.46
58	71.641	299.05	368.78	269	92.761	283.13	373.17	480	189.43	304.05	313.01
59	71.641	265.8	388.79	270	92.853	247.46	393.3	481	144.94	517.39	139.35
60	71.641	231.45	406.25	271	363.21	229.34	119.59	482	168.35	300.52	328.83
61	71.641	196.77	419.55	272	358.87	274.23	121.25	483	128.14	528.85	136.56
62	367.81	212.01	91.389	273	353.98	231.34	142.02	484	147.95	296.55	342.68
63	362.33	175.03	110.08	274	348.55	320.51	122.33	485	112.97	539.18	134.04
64	372.8	255.24	91.871	275	343.01	233.16	165.49	486	128.43	292.2	354.51
65	353.72	175.34	130.05	276	331.38	364.8	122.58	487	113.79	517.85	150.02
66	368.11	300.66	92.179	277	330.2	234.74	189.75	488	115.72	504.02	168.69
67	349.65	175.91	152.32	278	308.67	404.27	122	489	117.66	487.59	188.74
68	356.96	346.46	92.359	279	315.56	236.02	214.47	490	119.34	466.88	209.51
69	340.66	176.31	175.2	280	282.49	437.13	120.74	491	121.09	444.25	231.67
70	339.15	389.48	92.381	281	299.15	236.95	239.25	492	122.8	419.09	254.96
71	330.05	176.67	199.08	282	255.35	463.42	119.06	493	124.5	391.5	279.41
72	315.67	426.73	92.238	283	281.16	237.49	263.67	494	126.06	361.1	304.52
73	317.67	176.99	223.66	284	229.45	484.9	117.28	495	127.42	327.98	329.87
74	289.15	457.26	91.975	285	261.76	237.58	287.23	496	317.42	324.88	169.41
75	303.62	177.27	248.65	286	205.33	502.28	115.5	497	295.69	366.9	168.54
76	262.06	481.57	91.645	287	241.25	237.21	309.45	498	299.45	325.9	193.12
77	287.76	177.46	273.54	288	183.45	516.93	113.84	499	270.19	402.99	165.98
78	236.16	501.1	91.297	289	219.94	236.35	329.81	500	280.09	326.03	216.39
79	270.38	177.59	297.98	290	163.69	529.5	112.3	501	243.72	433.02	162.44
80	212.28	517.27	90.959	291	198.42	235.11	348.23	502	259.7	325.3	238.88
81	251.53	177.62	321.3	292	145.91	540.71	110.92	503	217.77	457.12	158.35
82	190.53	530.89	90.642	293	176.86	233.41	364.06	504	238.53	323.65	260.16

83	231.6	177.56	343.11	294	129.84	550.79	109.66	505	193.65	476.81	154.23
84	170.88	542.72	90.352	295	155.78	231.37	377.34	506	217.07	321.25	280.05
85	210.83	177.39	362.74	296	115.27	560.1	108.53	507	171.77	493.34	150.34
86	153.13	553.31	90.088	297	135.52	229.07	388.18	508	195.71	318.26	298.45
87	189.59	177.12	379.61	298	101.92	567.79	107.46	509	152.03	507.31	146.72
88	137.05	562.94	89.85	299	116.37	226.6	396.76	510	174.67	314.68	315.1
89	168.39	176.76	393.49	300	89.813	576.46	106.56	511	134.35	519.68	143.46
90	122.42	571.79	89.634	301	98.474	224.05	403.36	512	154.13	310.46	329.67
91	147.71	176.31	404.34	302	90.325	562.6	120.47	513	118.42	530.68	140.5
92	108.98	579.22	89.43	303	90.977	550.15	135.47	514	134.49	305.99	342.59
93	127.98	175.82	412.53	304	91.488	533.27	150.93	515	120.15	514.16	158.25
94	96.795	588.15	89.264	305	92.247	519.31	168.12	516	121.94	495.95	177.24
95	109.47	175.3	418.45	306	92.936	502.16	186.06	517	123.85	476.16	197.62
96	85.369	592.48	89.072	307	93.65	483.48	205.12	518	125.79	454.19	219.32
97	92.35	174.78	422.84	308	94.383	463.12	225.31	519	127.76	429.97	242.38
98	74.935	597.64	88.908	309	95.13	440.9	246.64	520	129.7	403.17	266.6
99	76.588	174.26	425.46	310	95.871	416.59	268.99	521	131.52	373.56	291.68
100	75.03	587.13	101.09	311	96.589	390.05	292.2	522	133.14	341.09	317.18
101	75.093	571.41	113.67	312	97.26	361.18	316.01	523	304.7	339.76	177.17
102	75.258	566.2	127.91	313	97.83	329.84	339.79	524	281.03	379.55	175.34
103	75.356	551.78	142.3	314	98.275	296.32	363.09	525	285.6	340.02	200.39
104	75.464	537.06	157.58	315	98.507	260.8	384.63	526	254.84	413.09	171.94
105	75.589	522.28	173.99	316	359.27	244.8	127.66	527	265.33	339.28	222.89
106	75.71	505.53	191.21	317	352.14	290.64	129.37	528	228.37	440.35	167.65
107	75.836	487.48	209.42	318	348.62	247.03	150.73	529	244.55	337.85	244.56
108	75.964	467.88	228.6	319	338.6	336.54	130.25	530	203.37	462.71	163.15
109	76.095	446.73	248.81	320	336.12	248.96	174.66	531	223.26	335.49	264.89
110	76.226	423.82	269.98	321	318.64	379.14	130.09	532	180.33	480.93	158.69
111	76.353	398.86	291.85	322	321.8	250.56	199.16	533	201.9	332.35	283.7
112	76.473	371.9	314.34	323	293.92	415.87	128.95	534	159.58	496.47	154.56
113	76.579	342.76	336.92	324	305.67	251.75	223.84	535	180.85	328.64	300.95
114	76.665	311.59	359.19	325	267.14	446.05	127.17	536	140.93	509.84	150.77
115	76.719	278.55	380.25	326	287.9	252.46	248.28	537	160.29	324.36	316.39
116	76.734	244.11	399.22	327	240.45	470.27	125.06	538	124.18	521.64	147.34
117	76.694	208.99	414.75	328	268.65	252.65	272	539	140.48	319.63	330.03
118	367.41	187.03	97.533	329	215.27	489.78	122.87	540	126.18	504.22	165.88
119	370.54	227.16	98.382	330	248.31	252.33	294.62	541	128.26	485.03	185.76
120	359.06	187.68	117.17	331	192.25	506.01	120.77	542	130.35	463.55	206.9
121	368.96	271.24	99.11	332	227.19	251.48	315.69	543	132.61	440.46	229.69
122	355.33	188.82	138.85	333	171.44	519.83	118.83	544	134.8	414.48	253.61
123	361.32	317.26	99.625	334	205.57	250.07	334.71	545	136.92	385.79	278.63
124	346.68	189.63	161.37	335	152.68	531.79	117.05	546	138.84	354.12	304.26
125	347	362.35	99.851	336	183.96	248.19	351.53	547	290.77	353.63	184.41
126	336.41	190.38	184.96	337	135.81	542.61	115.45	548	265.75	390.94	181.58
127	326.15	403.1	99.73	338	162.68	245.85	365.83	549	270.91	353.13	207.02
128	324.45	191.06	209.37	339	120.54	552.41	114.01	550	239.26	421.79	177.34
129	300.95	437.59	99.319	340	142.15	243.22	377.82	551	250.15	351.57	228.72
130	310.62	191.62	234.24	341	106.67	561.45	112.7	552	213.5	447.03	172.52
131	273.94	465.47	98.716	342	122.64	240.36	387.55	553	229.11	349.31	249.41
132	295.15	192.06	259.27	343	93.963	569.3	111.48	554	189.43	467.54	167.58
133	247.34	487.81	98.029	344	104.34	237.41	395.4	555	207.92	346.22	268.74
134	277.98	192.34	283.91	345	94.7	556.48	126.04	556	167.6	484.74	162.9
135	222.33	505.85	97.33	346	95.45	542.2	141.5	557	186.89	342.41	286.5
136	259.27	192.44	307.61	347	96.236	526.74	157.95	558	147.93	499.32	158.55
137	199.33	520.57	96.654	348	97.061	510.02	175.48	559	166.32	338.02	302.64
138	239.48	192.37	330.09	349	97.926	491.93	194.15	560	130.31	512.11	154.61
139	178.71	533.7	96.046	350	98.829	472.29	214.03	561	146.43	333.17	317.09
140	218.67	192.09	350.45	351	99.749	450.78	235.07	562	132.57	493.57	173.97
141	160.02	545.07	95.486	352	100.67	427.23	257.24	563	134.93	473.14	194.75

142	197.43	191.62	368.57	353	101.58	401.41	280.37	564	137.38	450.65	217
143	143.11	555.18	94.976	354	102.44	373.23	304.26	565	139.83	425.57	240.59
144	176.03	190.94	383.72	355	103.21	342.57	328.46	566	142.23	397.73	265.39
145	127.61	563.23	94.487	356	103.83	309.49	352.37	567	144.45	366.88	290.99
146	155.04	190.11	395.99	357	104.23	274.23	375.03	568	276.12	366.54	191.14
147	113.85	573.31	94.105	358	353.95	260.74	135.97	569	250.19	401.14	187.27
148	134.85	189.15	405.44	359	343.85	307.03	137.58	570	255.67	365.13	212.99
149	101.03	580.94	93.718	360	341.78	263.06	159.54	571	223.87	429.42	182.25
150	115.82	188.13	412.58	361	327.03	351.85	138.03	572	234.74	362.82	233.86
151	89.11	584.3	93.29	362	327.71	264.96	183.74	573	199.02	452.82	176.99
152	98.052	187.04	417.16	363	304.7	392.3	137.31	574	213.64	359.66	253.48
153	78.4	593.57	93.019	364	311.94	266.44	208.29	575	176.05	471.82	171.71
154	81.776	186.06	421.69	365	278.69	426.25	135.58	576	192.76	355.9	271.81
155	78.339	566.86	104.87	366	294.4	267.35	232.7	577	155.38	488.01	166.82
156	78.837	572.32	119.15	367	251.68	453.71	133.23	578	172.21	351.44	288.56
157	79.017	557.39	133.13	368	275.32	267.64	256.5	579	136.81	501.9	162.32
158	79.268	544.75	148.34	369	225.77	476.1	130.72	580	152.29	346.5	303.72
159	79.499	529.54	164.25	370	255.22	267.42	279.47	581	139.38	482.26	182.6
160	79.744	513.27	181.13	371	201.63	494.26	128.19	582	142.04	460.45	204.32
161	79.998	495.76	199.03	372	234.05	266.47	300.82	583	144.75	436.27	227.5
162	80.262	476.85	217.98	373	179.59	509.09	125.75	584	147.42	409.29	251.97
163	80.523	456.04	237.81	374	212.56	265.02	320.59	585	149.97	379.39	277.5
164	80.803	434.01	258.94	375	159.91	522.39	123.58	586	260.85	378.25	197.25
165	81.069	409.68	280.76	376	190.87	262.94	338.15	587	234.54	410.09	192.37
166	81.326	383.35	303.32	377	142.15	533.97	121.6	588	240.03	375.85	218.2
167	81.561	354.84	326.27	378	169.52	260.43	353.55	589	209	436.46	186.86
168	81.759	324.14	349.09	379	126.1	544.26	119.79	590	219.28	372.94	238.27
169	81.899	291.37	371.02	380	148.8	257.53	366.68	591	185.06	457.91	181.12
170	81.967	256.98	391.29	381	111.33	551.31	117.96	592	198.37	368.95	256.84
171	81.933	221.54	408.59	382	128.99	254.34	377.6	593	163.28	475.76	175.61
172	362.67	199.79	104.18	383	98.381	562.81	116.73	594	177.94	364.55	274.19
173	368.14	242.37	105.69	384	110.29	250.94	386.35	595	143.72	490.98	170.52
174	360.74	201.69	125.35	385	99.24	548.74	131.78	596	158.05	359.6	290.04
175	362.29	286.99	106.55	386	100.17	533.88	147.86	597	146.61	470.04	191.74
176	352.45	202.93	147.47	387	101.14	517.76	165	598	149.58	446.71	214.45
177	352.9	333.65	107.25	388	102.16	500.28	183.29	599	152.54	420.68	238.57
178	342.52	204.09	170.71	389	103.22	481.23	202.77	600	155.41	391.7	263.89
179	335.45	377.36	107.36	390	104.31	460.35	223.45	601	245.28	388.76	202.73
180	330.9	205.13	194.86	391	105.43	437.57	245.36	602	219.19	418.14	197.04
181	312.33	415.75	106.97	392	106.54	412.54	268.36	603	224.58	385.7	222.91
182	317.44	206.02	219.6	393	107.6	385.08	292.23	604	194.48	442.49	191
183	285.89	447.35	106.18	394	108.58	355.09	316.64	605	203.97	381.97	242
184	302.16	206.71	244.54	395	109.41	322.57	341.04	606	171.61	462.29	184.89
185	258.9	472.87	105.2	396	110.01	287.7	364.62	607	183.57	377.45	259.73
186	285.29	207.19	269.35	397	347.16	276.98	144.44	608	151.05	479.17	179.21
187	232.86	493.14	104.13	398	333.91	323.1	145.72	609	163.69	372.43	276.12
188	266.84	207.41	293.44	399	333.45	279.23	168.34	610	154.25	456.69	201.4
189	208.84	509.85	103.09	400	314.29	366.4	145.61	611	157.49	431.56	225.05
190	247.13	207.36	316.34	401	317.89	280.95	192.64	612	160.68	403.57	250.06
191	187.06	524.1	102.12	402	289.87	404.17	144.18	613	229.64	398.05	207.57
192	226.36	207	337.41	403	300.63	282.09	216.96	614	204.3	425.45	201.33
193	167.35	536.3	101.22	404	263.22	435.43	141.83	615	209.27	394.45	227
194	205.07	206.37	356.39	405	281.79	282.53	240.83	616	180.5	447.83	194.78
195	149.57	547.15	100.41	406	236.66	460.77	139.01	617	189.02	390.01	245.16
196	183.57	205.44	372.73	407	261.83	282.37	263.97	618	158.82	466.37	188.44
197	133.49	557	99.676	408	211.46	481.13	136.04	619	169.15	384.87	261.95
198	162.38	204.29	386.44	409	240.87	281.47	285.78	620	162.37	442.28	211.64
199	118.89	566.09	99.013	410	188.42	498.01	133.19	621	165.87	415.22	236.25
200	141.83	202.92	397.27	411	219.39	279.92	306.03	622	214.31	406.45	211.95

201	105.56	574.65	98.417	412	167.62	512.39	130.55	623	189.76	431.74	205.12
202	122.3	201.42	405.59	413	197.77	277.79	324.45	624	194.3	402.21	230.53
203	93.342	582.69	97.874	414	148.87	524.79	128.12	625	167.06	452.47	198.21
204	104.05	199.87	411.86	415	176.29	275.05	340.63	626	174.58	397.22	247.85
205	82.031	588.51	97.327	416	132.02	535.9	125.94	627	170.84	426.32	222.32
206	87.167	198.32	416.57	417	155.37	271.87	354.66	628	199.33	413.9	215.84
207	82.364	577.75	110.44	418	116.8	545.96	123.97	629	175.76	437.29	208.53
208	82.666	564.34	124.24	419	135.32	268.37	366.6	630	179.77	409.01	233.54
209	82.988	550.25	138.85	420	102.99	555.28	122.19	631	184.84	420.55	219.31
210	83.371	536.65	154.59	421	116.32	264.65	376.54				
211	83.741	520.88	171.13	422	104.04	540.75	137.85				

Table B.3:Critical dispatches for the Figure 3.10.

Dispatch direction	P_{G_A} (MW)	P_{G_B} (MW)	P_{G_C} (MW)	Dispatch direction	P_{G_A} (MW)	P_{G_B} (MW)	P_{G_C} (MW)	Dispatch direction	P_{G_A} (MW)	P_{G_B} (MW)	P_{G_C} (MW)
1	272.72	163	85	212	76.999	309.29	129.5	423	86.544	324.07	115.95
2	265.27	186.19	85	213	77.112	299.93	136.93	424	86.943	315.32	123.58
3	264.48	163	97.042	214	77.23	290.16	144.68	425	87.396	306.39	131.73
4	255.77	209.55	85	215	77.353	279.96	152.77	426	87.883	296.96	140.4
5	255.48	163	109.24	216	77.482	269.32	161.23	427	88.362	286.64	149.48
6	244.58	232.44	85	217	77.663	258.91	170.74	428	88.838	275.49	158.97
7	245.89	163	121.48	218	77.84	247.62	180.61	429	89.319	263.56	168.9
8	232.47	254.48	85	219	78.014	235.51	190.87	430	89.816	250.87	179.34
9	235.89	163	133.72	220	78.189	222.59	201.53	431	90.257	237.12	189.92
10	219.63	275.24	85	221	78.368	208.91	212.7	432	90.593	222.29	200.23
11	225.48	163	145.84	222	78.557	194.47	224.49	433	211.46	231.17	120.55
12	206.43	294.44	85	223	249.25	194.09	101.21	434	196.64	250.51	119.22
13	214.51	163	157.65	224	237.94	217.05	101.11	435	199.89	230.34	131.82
14	192.86	311.51	85	225	238.93	194.07	113.35	436	185.11	270.57	118.66
15	203.63	163	169.32	226	225.85	239.27	100.91	437	188.37	229.4	142.71
16	179.27	326.26	85	227	228.06	193.95	125.35	438	171.98	287.53	117.47
17	192.25	163	180.4	228	213.23	260.4	100.63	439	176.97	228.36	153.17
18	165.99	338.63	85	229	217.28	193.82	137.24	440	158.94	302.03	116.07
19	180.82	163	190.99	230	199.98	279.8	100.23	441	165.63	227.16	163.07
20	153	348.1	85	231	205.77	193.52	148.66	442	146.09	313.58	114.45
21	169.56	163	201.18	232	186.48	297.17	99.73	443	154.26	225.66	172.13
22	140.53	354.56	85	233	194.56	193.23	159.89	444	134.1	322.88	112.79
23	158.12	163	210.4	234	173.16	312.46	99.17	445	143.29	224.13	180.63
24	127.97	355.26	85	235	183.14	192.85	170.6	446	122.79	329.24	111.01
25	147	163	219.11	236	160	325.12	98.526	447	132.52	222.36	188.19
26	118.25	359.94	85	237	171.77	192.4	180.81	448	112.44	333.19	109.2
27	135.9	163	226.58	238	147.27	335.06	97.818	449	122.13	220.44	194.83
28	109.04	361.53	85	239	160.35	191.83	190.25	450	103.37	336.29	107.59
29	125.26	163	233.43	240	135.12	342.1	97.051	451	112.18	218.34	200.44
30	100.7	361.32	85	241	149.12	191.21	198.99	452	95.189	337.13	105.95
31	114.87	163	238.88	242	123.17	344.21	96.117	453	102.75	216.08	204.95
32	93.334	360.43	85	243	138.1	190.49	206.87	454	88.077	337.51	104.5
33	105.01	163	243.37	244	113.61	348.97	95.484	455	93.949	213.75	208.51
34	87.052	361.7	85	245	127.4	189.71	213.83	456	88.521	329.42	111.7
35	95.659	163	246.48	246	104.65	350.76	94.791	457	88.975	320.75	119.28
36	81.398	362.79	85	247	117.07	188.84	219.74	458	89.498	311.97	127.37
37	86.939	163	248.34	248	96.596	350.81	94.11	459	90.043	302.57	135.95
38	76.277	363.42	85	249	107.21	187.9	224.57	460	90.583	292.29	144.93
39	78.919	163	249.07	250	89.548	350.42	93.498	461	91.122	281.2	154.34
40	71.641	363.75	85	251	97.882	186.88	228.22	462	91.667	269.32	164.2
41	71.641	163	248.87	252	83.563	352.88	93.083	463	92.225	256.66	174.55

42	267.71	170.69	89.011	253	89.184	185.81	230.7	464	92.687	242.81	184.88
43	71.641	357.39	90.335	254	78.104	354.15	92.668	465	93.368	228.91	196.71
44	71.641	350.74	95.878	255	81.099	184.52	230.89	466	203.23	237.85	124.03
45	71.641	343.83	101.64	256	78.243	346.99	98.707	467	190.14	257.73	123
46	71.641	336.61	107.63	257	78.384	339.45	105	468	191.73	236.85	135.06
47	71.641	329.1	113.87	258	78.525	331.36	111.54	469	176.97	275.77	121.75
48	71.641	321.25	120.37	259	78.668	322.88	118.35	470	180.23	235.67	145.63
49	71.641	312.98	127.11	260	78.816	313.99	125.43	471	163.88	291.62	120.3
50	71.641	304.28	134.12	261	78.968	304.7	132.81	472	168.93	234.4	155.75
51	71.641	295.18	141.39	262	79.127	294.99	140.51	473	151.03	304.93	118.64
52	71.641	285.66	148.96	263	79.292	284.86	148.55	474	157.56	232.82	165.1
53	71.641	275.71	156.84	264	79.501	274.78	157.28	475	138.66	315.49	116.81
54	71.641	265.34	165.05	265	79.742	264.37	166.7	476	146.46	231.09	173.77
55	71.641	254.33	173.45	266	79.978	253.1	176.49	477	126.97	323.23	114.84
56	71.641	242.83	182.13	267	80.211	241	186.69	478	135.65	229.2	181.65
57	71.641	231.55	192.24	268	80.446	228.11	197.3	479	115.91	327.34	112.64
58	71.641	219.42	202.67	269	80.696	214.51	208.55	480	125.15	227.08	188.59
59	71.641	206.48	213.48	270	80.925	199.97	219.93	481	106.62	332.13	110.94
60	71.641	192.76	224.66	271	242.23	201.81	105.24	482	115.1	224.81	194.58
61	71.641	178.29	236.46	272	230.68	224.59	105.07	483	98.087	334.26	109.14
62	259.11	194.02	89.044	273	231.39	201.67	117.26	484	105.55	222.35	199.51
63	258.77	170.74	101.15	274	218.08	246.3	104.74	485	90.516	334.79	107.39
64	248.74	217.24	89.041	275	220.65	201.53	129.2	486	96.594	219.77	203.42
65	249.24	170.77	113.37	276	204.99	266.6	104.29	487	91.028	326.21	114.9
66	237.23	239.89	89.01	277	209.18	201.16	140.72	488	91.62	317.55	122.93
67	239.27	170.78	125.59	278	191.64	285.14	103.73	489	92.226	308.19	131.4
68	224.62	261.36	88.946	279	197.97	200.82	152.05	490	92.826	297.96	140.3
69	228.87	170.78	137.72	280	178.26	301.61	103.07	491	93.428	286.93	149.62
70	211.49	281.4	88.859	281	186.47	200.32	162.85	492	94.04	275.11	159.41
71	217.94	170.74	149.59	282	165.03	315.72	102.31	493	94.647	262.45	169.62
72	198.08	299.65	88.75	283	175.12	199.79	173.25	494	95.127	248.5	179.74
73	207.06	170.7	161.32	284	152.12	327.17	101.46	495	95.945	234.89	191.69
74	184.46	315.63	88.618	285	163.71	199.12	182.95	496	195.08	244.3	127.39
75	195.64	170.63	172.48	286	139.72	335.76	100.53	497	181.85	263.3	126.09
76	171.06	329.33	88.469	287	152.34	198.31	191.79	498	183.49	242.98	138.08
77	184.2	170.53	183.19	288	128.04	341.55	99.548	499	168.83	280.47	124.64
78	157.99	340.46	88.305	289	141.36	197.49	200.1	500	172.2	241.65	148.38
79	173.01	170.44	193.63	290	117.25	344.58	98.527	501	155.87	295.16	122.91
80	145.29	348.51	88.121	291	130.52	196.49	207.25	502	160.84	239.98	157.99
81	161.56	170.31	203.12	292	107.89	347.39	97.651	503	142.96	306.54	120.8
82	131.26	347.48	87.829	293	120.14	195.46	213.64	504	149.61	238.05	166.83
83	150.31	170.16	211.94	294	99.407	348	96.766	505	131.32	316.48	118.86
84	122.02	355.78	87.717	295	110.13	194.28	218.76	506	138.78	236.05	175.04
85	139.24	169.99	219.89	296	91.971	348.02	95.964	507	120.17	323.1	116.67
86	112.43	358.37	87.547	297	100.7	193.05	222.9	508	128.17	233.74	182.26
87	128.45	169.8	226.91	298	85.595	349.52	95.347	509	110.03	327.43	114.47
88	103.66	358.8	87.374	299	91.838	191.72	225.79	510	118.04	231.31	188.62
89	117.99	169.59	232.81	300	79.923	351.43	94.826	511	101.12	330.68	112.48
90	95.915	358.42	87.215	301	83.519	190.03	225.93	512	108.37	228.67	193.95
91	107.95	169.35	237.42	302	80.102	343.95	101.06	513	93.1	331.67	110.46
92	89.17	358.42	87.08	303	80.278	335.94	107.55	514	99.269	225.86	198.24
93	98.496	169.11	241.13	304	80.459	327.52	114.29	515	93.76	323.13	118.4
94	83.31	360.23	86.978	305	80.645	318.7	121.32	516	94.426	313.81	126.78
95	89.626	168.85	243.52	306	80.838	309.47	128.65	517	95.089	303.65	135.58
96	77.97	361.01	86.877	307	81.038	299.84	136.29	518	95.756	292.69	144.82
97	81.429	168.57	244.67	308	81.245	289.74	144.25	519	96.435	280.95	154.53
98	73.146	361.55	86.785	309	81.554	280.28	153.22	520	97.079	268.23	164.57
99	73.962	168.28	244.72	310	81.853	269.88	162.55	521	97.575	254.19	174.51
100	73.175	355	92.281	311	82.149	258.63	172.27	522	98.549	240.92	186.58

101	73.206	348.15	97.997	312	82.442	246.56	182.4	523	186.83	250.36	130.55
102	73.238	341.03	103.95	313	82.738	233.7	192.97	524	173.78	268.63	129.07
103	73.271	333.61	110.14	314	83.054	220.13	204.17	525	175.43	248.87	140.98
104	73.306	325.87	116.6	315	83.318	205.51	215.23	526	160.75	284.64	127.29
105	73.34	317.58	123.29	316	234.68	209.37	109.18	527	164.1	247.15	150.82
106	73.375	308.94	130.25	317	222.55	231.67	108.87	528	148.01	298.14	125.27
107	73.41	299.88	137.48	318	224.01	209.23	121.16	529	152.79	245.06	159.89
108	73.447	290.4	145.01	319	209.92	252.89	108.44	530	135.79	308.95	123.05
109	73.486	280.51	152.85	320	212.55	208.8	132.77	531	141.9	242.92	168.36
110	73.526	270.19	161.02	321	196.72	272.45	107.83	532	124.27	316.94	120.68
111	73.56	259.07	169.25	322	201.37	208.41	144.2	533	131.25	240.5	175.94
112	73.61	248.13	178.46	323	183.27	289.99	107.07	534	113.47	321.63	118.09
113	73.669	236.84	188.49	324	189.79	207.8	155.09	535	120.97	237.83	182.55
114	73.727	224.71	198.87	325	170.08	305.53	106.24	536	104.29	326.46	115.99
115	73.785	211.77	209.63	326	178.44	207.18	165.63	537	111.21	235.02	188.29
116	73.842	198.05	220.77	327	157.02	318.42	105.26	538	95.917	328.71	113.8
117	73.905	183.61	232.76	328	167.07	206.42	175.58	539	101.98	232.02	192.98
118	262.03	178.47	93.068	329	144.39	328.51	104.18	540	96.644	319.45	122.08
119	252.53	201.83	93.099	330	155.66	205.48	184.69	541	97.37	309.35	130.79
120	252.56	178.53	105.25	331	132.41	335.85	103.03	542	98.102	298.46	139.94
121	241.25	224.75	93.05	332	144.6	204.5	193.21	543	98.85	286.81	149.57
122	242.62	178.56	117.46	333	120.76	338.62	101.65	544	99.519	274	159.42
123	229.17	246.88	92.953	334	133.7	203.34	200.71	545	100.03	259.88	169.2
124	232.25	178.55	129.6	335	111.28	343.39	100.68	546	101.19	247.02	181.4
125	216.4	267.8	92.807	336	123.21	202.11	207.37	547	178.65	256.09	133.54
126	221.33	178.48	141.51	337	102.46	345.3	99.625	548	165.66	273.4	131.78
127	203.22	287.13	92.615	338	113.12	200.75	212.94	549	167.34	254.31	143.6
128	210.48	178.41	153.3	339	94.557	345.48	98.594	550	152.79	288.29	129.7
129	189.68	304.35	92.371	340	103.53	199.28	217.43	551	156.03	252.14	152.94
130	199.03	178.25	164.55	341	87.717	345.89	97.716	552	140.35	300.57	127.39
131	176.22	319.36	92.09	342	94.528	197.72	220.77	553	145	249.8	161.6
132	187.67	178.08	175.47	343	81.828	348.43	97.087	554	128.53	310.08	124.88
133	162.99	331.87	91.774	344	86.188	196.1	223.07	555	134.32	247.27	169.51
134	176.42	177.9	186.01	345	82.042	340.49	103.51	556	116.67	313.99	121.56
135	150.15	341.62	91.423	346	82.261	332.15	110.2	557	123.96	244.44	176.47
136	164.98	177.65	195.75	347	82.486	323.39	117.17	558	107.63	321.65	119.69
137	137.82	348.31	91.04	348	82.72	314.24	124.43	559	114.06	241.42	182.52
138	153.56	177.34	204.62	349	82.963	304.68	132.02	560	98.877	325.07	117.31
139	125.58	349.75	90.565	350	83.268	295.27	140.18	561	104.7	238.22	187.6
140	142.55	177.03	213.03	351	83.637	285.81	149.04	562	99.666	315.05	125.92
141	115.94	354.49	90.255	352	83.995	275.43	158.29	563	100.47	304.26	134.98
142	131.63	176.65	220.24	353	84.35	264.21	167.93	564	101.28	292.69	144.51
143	106.85	356.17	89.914	354	84.705	252.17	178	565	101.96	279.76	154.19
144	121.13	176.25	226.61	355	85.064	239.35	188.51	566	102.98	267.21	165.08
145	98.643	356.09	89.577	356	85.44	225.8	199.61	567	103.84	253.16	176.09
146	111.01	175.8	231.79	357	85.728	211.08	210.36	568	170.57	261.47	136.35
147	91.425	355.32	89.268	358	227.36	216.91	113.11	569	157.6	277.65	134.24
148	101.38	175.3	235.76	359	214.78	238.74	112.65	570	159.26	259.24	145.94
149	85.305	357.31	89.053	360	215.91	216.43	124.81	571	144.97	291.34	131.85
150	92.346	174.78	238.54	361	201.71	259.17	112.01	572	148.11	256.68	154.79
151	79.746	358.49	88.847	362	204.75	216	136.33	573	132.91	302.4	129.25
152	83.977	174.23	240.14	363	188.39	277.86	111.21	574	137.38	254.04	162.99
153	74.721	359.2	88.654	364	193.14	215.3	147.34	575	121.57	310.67	126.47
154	76.316	173.64	240.31	365	175.13	294.58	110.28	576	126.54	250.43	169.67
155	74.784	352.49	94.322	366	181.72	214.57	157.99	577	111.04	315.91	123.49
156	74.849	345.48	100.22	367	161.99	308.88	109.21	578	116.92	247.85	176.66
157	74.915	338.08	106.37	368	170.41	213.74	168.16	579	101.98	320.76	120.99
158	74.985	330.37	112.77	369	149.14	320.43	107.99	580	107.45	244.47	182.1
159	75.054	322.19	119.42	370	159.01	212.69	177.55	581	102.84	310.06	129.95

160	75.124	313.59	126.33	371	136.91	329.33	106.68	582	103.72	298.54	139.37
161	75.197	304.58	133.52	372	147.82	211.53	186.24	583	104.41	285.5	148.88
162	75.271	295.16	141	373	125.41	335.39	105.3	584	105.58	273.3	159.78
163	75.349	285.33	148.79	374	136.9	210.25	194.11	585	106.51	259.34	170.7
164	75.43	275.07	156.93	375	114.84	338.91	103.89	586	162.47	266.33	138.88
165	75.497	263.89	165.06	376	126.27	208.79	200.99	587	149.7	281.4	136.45
166	75.618	253.5	174.67	377	105.63	341.84	102.64	588	151.28	263.67	148
167	75.736	242.2	184.61	378	115.92	207.07	206.48	589	137.39	293.89	133.75
168	75.852	230.07	194.93	379	97.293	342.58	101.39	590	140.42	260.81	156.41
169	75.968	217.14	205.64	380	106.38	205.56	211.83	591	125.74	303.67	130.85
170	76.083	203.42	216.75	381	90.016	342.77	100.26	592	129.8	257.52	163.87
171	76.213	189	228.74	382	97.245	203.78	215.63	593	114.22	308.33	127.1
172	255.85	186.28	97.142	383	83.815	345.02	99.444	594	119.82	254.36	170.76
173	245.5	209.54	97.135	384	88.74	201.9	218.32	595	105.24	315.88	124.86
174	245.95	186.33	109.33	385	84.072	336.74	106.07	596	110.21	250.75	176.52
175	233.97	232.25	97.038	386	84.337	328.07	112.98	597	106.16	304.36	134.14
176	235.6	186.32	121.48	387	84.612	319	120.18	598	106.87	291.23	143.51
177	221.36	253.84	96.843	388	84.933	309.9	127.81	599	108.21	279.47	154.41
178	224.72	186.22	133.43	389	85.319	300.82	136.01	600	109.22	265.59	165.25
179	208.25	274.01	96.578	390	85.746	291.38	144.77	601	154.45	270.66	141.14
180	213.89	186.12	145.28	391	86.165	281.02	153.93	602	141.94	284.56	138.38
181	194.87	292.4	96.246	392	86.581	269.83	163.5	603	143.5	267.63	149.79
182	202.41	185.89	156.61	393	86.998	257.84	173.5	604	130.03	295.85	135.38
183	181.37	308.63	95.849	394	87.423	245.08	183.97	605	132.9	264.37	157.69
184	191.12	185.65	167.69	395	87.839	231.44	194.82	606	118.87	304.39	132.19
185	168.06	322.54	95.399	396	88.155	216.67	205.36	607	122.74	260.9	164.77
186	179.79	185.37	178.32	397	219.24	224.06	116.84	608	108.6	310.15	128.85
187	155.07	333.84	94.899	398	206.56	245.36	116.23	609	113	257.11	170.88
188	168.39	185.01	188.31	399	208.12	223.59	128.44	610	109.32	296.95	138.09
189	142.51	342.15	94.342	400	193.44	265.1	115.42	611	110.85	285.67	148.97
190	156.95	184.57	197.46	401	196.52	222.82	139.59	612	111.93	271.87	159.7
191	130.67	347.66	93.754	402	180.13	282.89	114.42	613	146.61	274.52	143.15
192	145.85	184.1	206.06	403	185.01	221.96	150.33	614	134.42	287.21	140.06
193	119.64	350.21	93.136	404	166.99	298.59	113.28	615	135.95	271.14	151.35
194	134.82	183.54	213.51	405	173.71	221.06	160.69	616	122.95	297.26	136.75
195	110.16	352.86	92.616	406	154.04	311.68	111.97	617	125.65	267.46	158.7
196	124.27	182.96	220.29	407	162.33	219.92	170.34	618	111.77	302.65	132.61
197	101.53	353.43	92.093	408	141.53	322.01	110.51	619	115.81	263.5	165.16
198	114.02	182.28	225.79	409	151.04	218.58	179.21	620	113.51	291.87	143.44
199	93.939	353.24	91.614	410	129.7	329.55	108.96	621	114.67	278.17	154.06
200	104.29	181.57	230.25	411	140.1	217.18	187.42	622	138.96	277.87	144.9
201	87.381	353.99	91.225	412	118.34	332.99	107.16	623	127.15	289.31	141.46
202	95.092	180.78	233.39	413	129.39	215.55	194.62	624	128.57	274.03	152.55
203	81.613	355.85	90.915	414	108.97	337.85	105.84	625	116.18	298.11	137.84
204	86.565	179.98	235.51	415	119.07	213.78	200.86	626	118.64	269.93	159.35
205	76.372	356.74	90.613	416	100.27	339.79	104.41	627	117.41	284.48	148.35
206	78.697	179.05	235.69	417	109.27	211.92	206.18	628	131.49	280.61	146.33
207	76.47	349.8	96.46	418	92.529	340.15	103.02	629	120.17	290.86	142.58
208	76.573	342.54	102.56	419	99.986	209.9	210.35	630	121.47	276.37	153.46
209	76.678	334.92	108.91	420	85.891	341.32	101.91	631	124.31	282.83	147.49
210	76.783	326.78	115.5	421	91.328	207.79	213.47				
211	76.889	318.24	122.36	422	86.197	332.73	108.75				

Table B.4:Critical dispatches for the Figure 3.13.

Dispatch direction	P_{G_A} (MW)	P_{G_B} (MW)	Dispatch direction	P_{G_A} (MW)	P_{G_B} (MW)
1	2111.4	3720.7	12	3130.2	3608.9
2	2216.5	3762.6	13	3138.7	3501.7
3	2311.2	3779.9	14	3101	3359.3
4	2426.3	3805.3	15	3067.8	3235.4
5	2529.4	3810	16	3037.4	3125.7
6	2604.8	3799.9	17	3009.6	3028.4
7	2729.3	3794.4	18	2984.3	2941.2
8	2829.8	3783.6	19	2961.4	2863.4
9	2916.4	3751.3	20	2940.7	2793.5
10	2999.4	3715.5	21	2921.9	2730.1
11	3066.3	3662			

Table B.5:Critical dispatches for the Figure 3.15.

Dispatch direction	P_{G_A} (MW)	P_{G_B} (MW)	P_{G_C} (MW)	Dispatch direction	P_{G_A} (MW)	P_{G_B} (MW)	P_{G_C} (MW)	Dispatch direction	P_{G_A} (MW)	P_{G_B} (MW)	P_{G_C} (MW)
1	12754	240	1166	212	2788.8	714.32	2510.2	423	3716.6	869.46	2292.7
2	12394	292.75	1166	213	2793.6	680.03	2720.8	424	3747.5	833.29	2566
3	12607	240	1427.7	214	2796.3	642.72	2926.9	425	3767.7	790.57	2837.8
4	12054	347.57	1166	215	2797.1	603.18	3126.5	426	3776.6	742.18	3101
5	12443	240	1709.7	216	2796.7	562.52	3320.5	427	3780	691.33	3358.7
6	11676	404.17	1166	217	2795.6	521.43	3509.9	428	3774.9	637.78	3602.7
7	12265	240	2014.2	218	2793.7	480.1	3693.4	429	3764.9	583.39	3835.3
8	11310	463.39	1166	219	2791.4	438.9	3871.7	430	3752.4	529.21	4058.9
9	12067	240	2343.6	220	2788.7	398.04	4045.2	431	3737.2	475.53	4271.9
10	10935	525.34	1166	221	2785.8	357.65	4214.5	432	3720.7	422.77	4475.7
11	11953	240	2717.6	222	2782.7	317.83	4380	433	11202	429.17	2085
12	10580	591.61	1166	223	12068	314.58	1528.3	434	10824	499.97	2113.3
13	11764	240	3121.4	224	11710	373.39	1536.3	435	11020	439.51	2458.4
14	10220	662.37	1166	225	11909	317.85	1827.9	436	10452	576.49	2146.9
15	11562	240	3569.7	226	11335	434.8	1544.6	437	10827	451.29	2876.8
16	9842.8	737.7	1166	227	11750	321.54	2156.4	438	10068	659.54	2185.1
17	11344	240	4071.3	228	10983	500.24	1555	439	10617	464.76	3349.9
18	9441.8	817.93	1166	229	11581	325.66	2518.5	440	9677.4	750.98	2229.9
19	11103	240	4635.4	230	10622	569.87	1566.7	441	10382	480.17	3888.6
20	9067.8	908.87	1166	231	11393	330.19	2918.7	442	9273	852.83	2282.5
21	10821	240	5269.2	232	10247	644.16	1579.4	443	10100	497.44	4501.3
22	8662.1	1007.8	1166	233	11192	335.33	3365.8	444	8838.7	966.65	2342.8
23	10407	240	5934.8	234	9865.8	724.55	1594	445	9530.1	508.2	5075.1
24	8223.2	1116.3	1166	235	10973	341.16	3869	446	8066.7	1052.2	2349.8
25	9314.5	240	6220.6	236	9478.3	812.59	1611.1	447	8289.5	493.23	5266.9
26	7376.9	1167.4	1166	237	10696	347.36	4425.9	448	6830.5	1055.1	2246.1
27	7987.2	240	6223.7	238	9079.9	910.09	1631.1	449	6971.6	469.38	5252.2
28	6255.3	1142.9	1166	239	10406	354.71	5067.1	450	5687.4	1032.1	2128.1
29	6705.7	240	6064.5	240	8660.7	1018.8	1654.2	451	5772.7	443.16	5114.1
30	5246.6	1097.6	1166	241	9821	359.1	5650.3	452	4697.1	990.09	2007
31	5581.5	240	5821.8	242	8099.1	1123.7	1671.1	453	4763.2	418.06	4914.8
32	4386.6	1038.7	1166	243	8576	352.65	5818	454	3880.8	935.23	1889.8
33	4642.2	240	5544.2	244	6920.1	1123.3	1630	455	3943.4	395.24	4685.7
34	3673.1	966.19	1166	245	7252	342.5	5772.3	456	3934.3	908.78	2165.7
35	3877	240	5257	246	5803.5	1094.2	1581	457	3975.3	873.77	2448.9
36	3115.2	890.17	1166	247	6035.1	331.23	5598	458	4004.4	831.68	2733.9

37	3263.4	240	4973.9	248	4825.4	1045.9	1530.2	459	4024.1	784.46	3017.6
38	2691.6	805.79	1166	249	4998.7	320.31	5360.5	460	4030.3	731.88	3290.2
39	2776.6	240	4700.9	250	4010.2	984.96	1480.7	461	4028.7	676.79	3553.3
40	2394.5	721.49	1166	251	4150.4	310.4	5099.3	462	4018.1	619.71	3801.4
41	2394.5	240	4440.3	252	3354.2	913.37	1433.1	463	4003.5	562.55	4038.9
42	12580	257.6	1251.5	253	3470.4	301.62	4833.5	464	3985.5	505.78	4265
43	2394.5	730.17	1291.3	254	2854.5	839.41	1390	465	3965.1	449.89	4480.1
44	2394.5	734.77	1433.1	255	2932.7	293.95	4573.1	466	10997	455.56	2213.2
45	2394.5	731.86	1587.7	256	2877.9	833.55	1578	467	10642	530.46	2251.5
46	2394.5	724.86	1754.9	257	2900.4	823.13	1781.9	468	10822	468.3	2607.9
47	2394.5	710.95	1928.7	258	2918.8	804.96	1995.8	469	10261	611.03	2292.6
48	2394.5	693.17	2109.6	259	2933.6	780.35	2216.1	470	10630	482.78	3053.2
49	2394.5	669.96	2290.8	260	2945.5	750.85	2440.5	471	9872.4	699.38	2340.6
50	2394.5	643.9	2474.2	261	2952.9	715.72	2661.5	472	10408	499.1	3557.7
51	2394.5	614.6	2655	262	2958	677.76	2881.2	473	9473	797.45	2397
52	2394.5	583.03	2832.6	263	2960	636.76	3093.6	474	10145	517.43	4131.3
53	2394.5	549.97	3006.6	264	2959.5	593.97	3298.4	475	9048.8	906.96	2462.1
54	2394.5	516.12	3178.3	265	2957.8	550.56	3497.8	476	9794.5	536.68	4769.5
55	2394.5	481.65	3346.4	266	2955	506.87	3690.9	477	8506.4	1019.7	2518.8
56	2394.5	446.86	3511	267	2951.3	463.25	3877.6	478	8748.3	529.47	5103.8
57	2394.5	411.97	3672.4	268	2947	420	4058.6	479	7293.1	1041.1	2421.5
58	2394.5	377.13	3830.9	269	2942.4	377.3	4234.5	480	7432.2	505.76	5168.5
59	2394.5	342.46	3986.8	270	2937.6	335.27	4405.8	481	6094.8	1028.1	2292.2
60	2394.5	308.02	4140.1	271	11898	335.26	1628.8	482	6177.3	476.97	5080.4
61	2394.5	273.86	4291.2	272	11527	395.8	1639.1	483	5035.4	993.38	2155.2
62	12239	311.76	1253.2	273	11736	339.61	1940.3	484	5093.9	448.13	4907.3
63	12424	258.28	1521.2	274	11184	460.25	1652.4	485	4153.5	945.23	2022.6
64	11864	367.76	1254.7	275	11578	344.6	2284	486	4205.5	421.52	4693.6
65	12269	259.03	1813.3	276	10813	528.13	1665.9	487	4212	914.02	2316.5
66	11500	426.26	1256.5	277	11395	350.01	2662.5	488	4255.4	874.19	2615.9
67	12098	259.85	2130.3	278	10440	600.74	1681.5	489	4283.2	826.85	2913.5
68	11134	487.57	1258.5	279	11200	356.13	3084.4	490	4298.9	774.46	3206.2
69	11951	260.82	2481.2	280	10061	679.08	1699.3	491	4301.5	717.85	3487.6
70	10774	552.53	1260.9	281	10991	363.09	3558.1	492	4293.3	658.7	3755
71	11767	261.85	2864.2	282	9672.5	764.31	1719.8	493	4276.5	598.41	4007
72	10416	621.9	1263.7	283	10758	370.97	4093	494	4256.3	538.58	4248.5
73	11572	263	3288.9	284	9263.7	857.28	1742.7	495	4232	479.43	4476.7
74	10040	695.66	1266.6	285	10492	379.94	4701.3	496	10832	484.8	2355.3
75	11363	264.3	3762.8	286	8872.1	964.17	1772.6	497	10452	563.06	2399.2
76	9659.1	775.39	1270	287	10113	388.77	5358.2	498	10638	499.69	2771.8
77	11134	265.76	4295.3	288	8416.4	1079.8	1803.5	499	10055	647.88	2448.2
78	9270.4	862.48	1274	289	9047.4	384.96	5673.3	500	10420	516.51	3242.1
79	10874	267.42	4895.6	290	7390.3	1116.3	1774.2	501	9668.9	742.84	2509.6
80	8871	958.7	1278.6	291	7719.1	373.42	5703.5	502	10149	534.82	3770.2
81	10546	269.18	5560.7	292	6218.3	1096.7	1713.7	503	9256.9	848.46	2579.8
82	8448	1065.2	1283.9	293	6449.4	359.54	5579.7	504	9897.7	558.18	4398.1
83	9755.6	269.51	6040.9	294	5175.4	1056.3	1649.6	505	8795.4	965.25	2656.7
84	7844	1158.6	1286.6	295	5340.9	345.47	5367.8	506	9179.5	565.25	4901
85	8470.2	267.68	6141.8	296	4294	1001.6	1586.4	507	7762.3	1020.1	2603.6
86	6696.3	1147.7	1276.3	297	4424.5	332.49	5120.1	508	7897.4	543.36	5051.5
87	7153.5	265.11	6044.8	298	3574.1	934.6	1525	509	6522.9	1018.9	2466.8
88	5632.9	1112.3	1264.6	299	3685.8	320.9	4860.4	510	6603.4	512.97	5023.9
89	5961.7	262.35	5834.3	300	3016.8	863.79	1469.1	511	5406.7	994.78	2318.5
90	4699.8	1057.6	1252.4	301	3100.1	310.73	4602.3	512	5450.6	480.68	4886.5
91	4950.8	259.71	5570.8	302	3046.3	854.16	1673.9	513	4449.8	951.65	2166.8
92	3921.8	990.12	1240.4	303	3073.7	839.11	1893.7	514	4491.4	450.18	4693.5
93	4123	257.33	5290.5	304	3096.3	816.79	2122.9	515	4511.7	915.23	2478.2
94	3304.5	917.59	1229.3	305	3112.9	787.26	2355.5	516	4556.5	870.39	2793
95	3457.1	255.21	5009.7	306	3126.6	753.64	2592	517	4582.8	818.24	3103.4

96	2826.9	835.92	1218.6	307	3134	714.37	2822.4	518	4591.2	760.42	3402.7
97	2927.8	253.36	4736.8	308	3138.4	672.49	3049.8	519	4589.2	699.95	3692.1
98	2482.9	753.73	1209	309	3138.7	627.89	3267.9	520	4573.2	637.04	3963
99	2511.7	251.74	4475.3	310	3136.2	582	3477.7	521	4550.4	573.95	4220
100	2488.6	758.96	1349.4	311	3132.5	535.91	3681.8	522	4522.7	511.49	4463.5
101	2494.3	760.16	1506.2	312	3127.3	489.75	3878.2	523	10642	515.56	2504.8
102	2499	753.47	1675.1	313	3121.2	443.94	4067.7	524	10258	598.24	2558.4
103	2503.5	742.56	1856	314	3114.4	398.75	4251.1	525	10441	533.27	2947
104	2507	724.92	2042.6	315	3107.3	354.32	4429.1	526	9865.4	689.29	2621.2
105	2509.9	702.91	2234.3	316	11718	356.81	1733.5	527	10205	553.15	3448.1
106	2512	675.95	2425.4	317	11352	419.57	1747.6	528	9458.3	790.68	2694.8
107	2513.7	646.2	2617.1	318	11570	362.62	2059.6	529	9956.1	576.85	4029.9
108	2514.7	613.43	2804.7	319	11005	486.58	1765	530	9019.3	904.01	2779
109	2515.2	578.72	2987.9	320	11393	368.85	2418	531	9533.5	597.78	4642.4
110	2515.4	542.93	3167.5	321	10632	557.55	1783.1	532	8224.8	991.34	2788.3
111	2515.3	506.51	3343.6	322	11206	375.88	2816.3	533	8362.1	581.79	4902.2
112	2515.1	469.71	3515.5	323	10255	633.92	1803.9	534	6971.7	1004.6	2651.9
113	2514.7	432.8	3683.4	324	10971	383.27	3254.2	535	7047.1	550.89	4942
114	2514.2	395.99	3847.7	325	9829.7	714.24	1824.3	536	5795.9	990.03	2491.1
115	2513.6	359.41	4008.8	326	10786	392.92	3766.3	537	5832.1	515.64	4848.7
116	2513	323.15	4166.9	327	9482.2	808.33	1856.3	538	4775.2	955.86	2325.3
117	2512.3	287.25	4322.3	328	10538	403.24	4338.2	539	4802.2	481.33	4683.4
118	12423	275.9	1340.4	329	9064.3	908.52	1887.8	540	4835.1	912.71	2651.6
119	12051	331.31	1343.4	330	10229	414.51	4981.2	541	4876	861.81	2978.6
120	12256	277.3	1619	331	8646	1023.2	1927.1	542	4900.3	805.11	3301.4
121	11690	389.07	1347.1	332	9483.6	417.64	5481.1	543	4903.7	743	3609.7
122	12099	278.91	1922.1	333	7865.3	1101.7	1927.1	544	4892.3	678.12	3902.7
123	11329	449.58	1351.1	334	8199.6	406.24	5608.1	545	4867.9	611.87	4177.1
124	11920	280.63	2251.6	335	6659.2	1094.9	1858.2	546	4838.1	546.15	4438.2
125	10968	513.43	1355.8	336	6886.7	390.09	5541	547	10449	548.67	2665.6
126	11767	282.7	2618.1	337	5557.4	1064.3	1782.1	548	10059	636.48	2731.1
127	10610	581.42	1361.1	338	5710	372.93	5363.7	549	10237	569.65	3137.2
128	11579	284.91	3020.4	339	4602.6	1014.6	1703.6	550	9623.6	731.68	2800.4
129	10235	653.62	1367	340	4722.8	356.69	5134.3	551	9996.6	593.77	3678
130	11377	287.38	3468.1	341	3817.7	953.25	1628	552	9230.1	842.93	2896.9
131	9856.6	731.5	1373.6	342	3921.1	342.01	4883.1	553	9687.3	620.1	4291.1
132	11141	290.1	3964.9	343	3199.9	885.8	1558.2	554	8651.6	952.68	2966.5
133	9471	816.29	1381.4	344	3283.4	329.09	4628.8	555	8801	619.44	4711.1
134	10916	293.38	4537.5	345	3235.5	872.24	1780.3	556	7429.7	983.75	2843.6
135	9076.5	909.74	1390.4	346	3267.1	852.24	2015.9	557	7505.4	590.5	4833.7
136	10627	296.91	5174.9	347	3293.4	825.62	2260.3	558	6204.3	979.86	2673.4
137	8665.1	1013.5	1400.9	348	3311.9	791.74	2506.3	559	6240.6	553.22	4794.7
138	10133	299.66	5804	349	3325.4	753.21	2752.7	560	5119.8	954.43	2493.1
139	8204	1126.1	1412	350	3332.4	710.03	2992.8	561	5138.7	515.05	4660.9
140	8950.2	297.14	6023.9	351	3334.8	664.11	3226.5	562	5182.2	906.3	2836.8
141	7160.5	1147.6	1398.1	352	3332.4	616.05	3449.7	563	5220.7	850.12	3177.4
142	7617.5	292.35	5998.4	353	3327.5	567.31	3664.8	564	5234.4	787.4	3506.3
143	6036.6	1120.4	1374.7	354	3320.8	518.53	3872.4	565	5231.4	721.2	3822.6
144	6367.6	286.85	5832.1	355	3312.5	470.02	4071.6	566	5209	652.3	4117.9
145	5037.2	1072.5	1349.8	356	3303.2	422.16	4263.5	567	5178.4	583.42	4398.7
146	5284.9	281.39	5589.5	357	3293.4	375.15	4449	568	10250	584.47	2839.5
147	4195.9	1011.5	1325.5	358	11545	379.57	1844.1	569	9851.8	678.16	2919.1
148	4390.9	276.38	5319.8	359	11194	445.11	1863.5	570	10025	609.23	3344.2
149	3516.2	942.67	1302.6	360	11390	386.77	2184.7	571	9434.4	782.78	3011.9
150	3668.4	271.92	5043	361	10823	514.55	1884.2	572	9754.2	637.21	3922.8
151	2981.8	864.03	1280.4	362	11207	394.58	2560.7	573	8945.5	896.61	3107.8
152	3092.9	268	4771.2	363	10447	589.04	1907.9	574	9200.4	655.23	4480.2
153	2588.4	784.22	1260.4	364	11014	403.44	2981	575	7888.1	955.82	3038.6
154	2639.7	264.58	4509.3	365	10067	669.72	1935.2	576	7960.4	630.52	4689.5

155	2600	785.83	1416.2	366	10805	413.55	3454.6	577	6633.3	964.77	2865.9
156	2611.4	783.46	1588.5	367	9679.3	758.18	1967	578	6668.5	592.79	4716.4
157	2620.8	773.1	1772.2	368	10572	425.08	3991.9	579	5490.3	949.25	2673.5
158	2629.3	757.82	1966.5	369	9280.7	856.26	2004.3	580	5500.5	551.32	4623.2
159	2636	736.33	2165.8	370	10261	437.11	4586.1	581	5548.1	894.76	3030.7
160	2641.3	710	2367.8	371	8861.3	965.96	2047.7	582	5577.7	832.53	3380.4
161	2645	679.39	2568.8	372	9847.9	449.18	5231	583	5587.9	765.84	3720.7
162	2647.5	645.84	2768	373	8321.5	1077.1	2084.3	584	5571.9	694.97	4039.5
163	2648.8	609.65	2961.9	374	8670.6	440.16	5472.5	585	5542.8	623.18	4341.7
164	2649.2	571.87	3150.4	375	7121.2	1087.8	2014	586	10045	623.43	3028.8
165	2649.1	533.43	3335.4	376	7346.2	422.85	5480.9	587	9603.7	721.72	3116.3
166	2648.4	494.52	3515.4	377	5959	1066.2	1925.4	588	9800.4	652.39	3570.2
167	2647.4	455.46	3690.6	378	6107.7	402.83	5347.4	589	9186.1	835.64	3233
168	2646.1	416.53	3861.5	379	4936.1	1023.8	1832.4	590	9460.6	682.65	4176.8
169	2644.6	377.89	4028.4	380	5046.7	383.14	5139.9	591	8335.4	920.53	3232.4
170	2643	339.65	4191.8	381	4085.9	968.97	1742.5	592	8410.2	670.68	4513.8
171	2641.4	301.87	4352	382	4178.1	365.14	4900.7	593	7076.8	943.97	3066.1
172	12238	294.81	1432.3	383	3404.4	905.21	1657.8	594	7107.5	633.66	4608.6
173	11879	351.84	1437.7	384	3483.9	349.19	4652.2	595	5877.7	938.25	2862.2
174	12085	297.13	1721.1	385	3446.2	887.56	1897.6	596	5885.8	589.94	4566.2
175	11521	411.51	1443.7	386	3481	862.29	2148.6	597	5929.9	877.84	3231.9
176	11927	299.72	2036.4	387	3510.4	831.19	2408	598	5957.1	811.33	3594.7
177	11161	474.31	1450.6	388	3530.3	792.93	2667.2	599	5953.1	739.35	3938.6
178	11764	302.61	2382.7	389	3542.2	749.44	2922.5	600	5928.7	665.08	4263.8
179	10788	540.47	1458	390	3547.8	702.38	3171.7	601	9830.5	665.89	3235.1
180	11581	305.77	2763.7	391	3547	652.56	3410.9	602	9397.3	773.44	3348.4
181	10429	611.68	1467	392	3541	601.18	3638.6	603	9551	699.07	3814.5
182	11387	309.33	3187	393	3532.9	549.72	3858.7	604	8754.5	877.47	3418.4
183	10052	687.72	1476.7	394	3522.4	498.4	4069.1	605	8826.2	708.84	4297.9
184	11178	313.37	3661.1	395	3510.3	447.7	4270.8	606	7525.6	916.7	3270.1
185	9669.4	770.3	1488	396	3497.3	397.91	4464.9	607	7558.8	675.89	4474.9
186	10948	317.93	4195.1	397	11384	403.82	1961.9	608	6284	922.23	3060
187	9279.2	861.05	1501.3	398	11013	471.75	1984.9	609	6292.5	630.7	4487.8
188	10666	322.91	4791.2	399	11145	411.13	2309.2	610	6333	856.82	3443.5
189	8875	961.72	1516.6	400	10639	544.44	2011.2	611	6346.8	784.7	3812.3
190	10337	328.46	5463.5	401	10972	421	2704.8	612	6330.7	708.51	4160.9
191	8441.1	1073.3	1534.1	402	10260	622.91	2041.4	613	9601.1	712.29	3460.5
192	9409.2	327.89	5862.8	403	10817	432.95	3158	614	9096.3	824.11	3578.1
193	7633.7	1140.2	1530.5	404	9875.1	708.62	2076.7	615	9177.6	742.52	4038.2
194	8097.4	321.66	5926.6	405	10598	445.55	3662.6	616	7971.6	882.85	3474.4
195	6463.2	1123.6	1496.2	406	9480.1	803.26	2117.8	617	8001.2	717.67	4305.7
196	6796.8	313.54	5810.7	407	10346	459.85	4236.8	618	6708.8	901.36	3266.9
197	5409.9	1086.3	1459.7	408	9033.4	905.42	2160.7	619	6718.3	673.38	4386.2
198	5645.7	305.17	5598.9	409	10021	475.21	4879.8	620	6745.9	830.07	3658.9
199	4496.4	1030	1421.9	410	8613.7	1026	2219.4	621	6743.4	752.82	4031.2
200	4682.3	297.33	5343.7	411	9125.8	474.67	5299	622	9317.4	760.41	3694.3
201	3751.1	965.2	1386.2	412	7592.5	1073.6	2178.5	623	8405	842.44	3674.7
202	3898.9	290.26	5073.2	413	7814.9	457.32	5389.2	624	8425	758.09	4102.6
203	3157.3	889.91	1351.7	414	6383	1063.1	2080	625	7141.8	874.43	3477.7
204	3273.3	284.04	4803.6	415	6529	435.01	5311	626	7151.1	716.75	4254.3
205	2712	812.83	1320.6	416	5300.6	1030.6	1974.7	627	7164.1	797.74	3875.7
206	2779.6	278.6	4542	417	5396.6	411.95	5134.1	628	8813.3	795.63	3865.5
207	2729.4	810.62	1492.2	418	4379	981.39	1868.8	629	7577.1	841.48	3689.7
208	2746.5	804.55	1680.3	419	4458.3	390.44	4911.8	630	7582.4	759.98	4091.1
209	2760.5	790.32	1879	420	3631.2	921.78	1768.2	631	8007.6	802.6	3899.3
210	2772.5	770.47	2086.4	421	3703.4	371.19	4671.5				
211	2782.1	745.03	2298.4	422	3679	899.84	2026.1				

Appendix C

C IEEE 3-machine 9-bus System Data

Table C.1: Transmission line parameters IEEE 9-bus system.

Nodes	R (pu)	X (pu)	B/2 (pu)
1 4	0	0.0576	0
4 5	0.01	0.085	0.176
2 7	0	0.0625	0
7 5	0.032	0.161	0.306
7 8	0.0085	0.072	0.149
3 9	0	0.0586	0
8 9	0.0119	0.1008	0.209
9 6	0.39	0.17	0.358
6 4	0.017	0.092	0.158

Table C.2: Load parameters IEEE 9-bus system.

Node	P (MW)	Q (Mvar)
5	125	50
6	90	30
8	100	35

Table C.3: Generator parameters.

Parameter	G_1	G_2	G_3
X_d (pu)	0.146	0.8963	1.3125
$X_d^{'}$ (pu)	0.0608	0.1198	0.1813
$T_{d0}^{'}$ (pu)	8.96	6	5.89
X_q (pu)	0.0969	0.8645	1.2578
$X_q^{'}$ (pu)	0.0969	0.1969	0.25
$T_{q0}^{'}$ (pu)	0.31	0.535	0.6
H (s)	23.64	6.4	3.01
D (pu)	0	0	0

Table C.4: Exciter parameters.

Parameter	Value
K_a	20
T_a (s)	0.2
K_e	1
T_e (s)	0.314
K_f	0.063
T_f (s)	0.35
A_e	0.0039
B_e	1.555

Table C.5: Power generation bids for the IEEE 9-bus.

Gen.	C_{G_i} ($/MWh)	$P_{G_i}^{\max}$ (MW)
G_1	1.4	900
G_2	1.5	700
G_3	1.4	600

Appendix D

D Numerical examples illustrating the proposed linearization algorithms:

For the set of bidimensionalhyperplane parameters in Table D.1 obtained from the set of boundary points given in Table D.2, the coefficients can be written in normal-point equation form as follows:

$$H1:\ P_{G_1} + 0.73026P_{G2} = 6.4996$$

$$H2:\ P_{G_1} + 0.72662P_{G_2} = 6.4749$$

$$H3:\ P_{G_1} + 0.72064P_{G_2} = 6.4333$$

$$H4:\ P_{G_1} + 0.6510P_{G_2} = 5.9017$$

$$H5:\ P_{G_1} + 0.4923P_{G_2} = 4.6785$$

$$H6:\ P_{G_1} + 0.91448P_{G_2} = 8.0059$$

In order to reduce the number of hyperplanes that linearly approximate the security/stability boundary, the reduction algorithms described next are used.

Table D.1. Hyperplane Parameters.

	Parameters		$C = \eta \bullet \boldsymbol{P}^{C}_{G_k}$
Hyperplane	$n_{i,1}$	$n_{i,2}$	C_i
H1	1	0.73026	6.4996
H2	1	0.72662	6.4749
H3	1	0.72064	6.4333
H4	1	0.6510	5.9017
H5	1	0.4923	4.6785
H6	1	0.91448	8.0059

Table D.2. Boundary points.

Boundary Point	$P_{G_1}^{c,i}$ (p.u.)	$P_{G2}^{c,i}$ (p.u.)
BP_1	1.5453	6.7843
BP_2	1.414	6.965
BP_3	1.2925	7.1336
BP_4	0.88419	7.7074
BP_5	0.79853	7.8814
BP_6	0.71641	7.9712

Algorithm 1: Boundary Points' Approximation

Step 1. Each left-hand side of all point-normal equations representing the hyperplanesare evaluated for all boundary points. Thus, the boundary points' evaluation in H1 to H6 yields:

$$\text{Eval\_H1} = \underbrace{\begin{bmatrix} 1.5453 \\ 1.414 \\ 1.2925 \\ 0.88419 \\ 0.79853 \\ 0.71641 \end{bmatrix}}_{\substack{\text{Second Column} \\ \text{Table 2}}} + 0.73026 \underbrace{\begin{bmatrix} 6.7843 \\ 6.965 \\ 7.1336 \\ 7.7074 \\ 7.8814 \\ 7.9712 \end{bmatrix}}_{\substack{\text{Third Column} \\ \text{Table 2}}} = \begin{bmatrix} 6.4996 \\ 6.5003 \\ 6.5019 \\ 6.5126 \\ 6.554 \\ 6.5375 \end{bmatrix}$$

$$\text{Eval\_H2} = \begin{bmatrix} 1.5453 \\ 1.414 \\ 1.2925 \\ 0.88419 \\ 0.79853 \\ 0.71641 \end{bmatrix} + 0.72662 \begin{bmatrix} 6.7843 \\ 6.965 \\ 7.1336 \\ 7.7074 \\ 7.8814 \\ 7.9712 \end{bmatrix} = \begin{bmatrix} 6.4749 \\ 6.4749 \\ 6.4759 \\ 6.4845 \\ 6.5253 \\ 6.5084 \end{bmatrix}$$

$$\text{Eval\_H3} = \begin{bmatrix} 1.5453 \\ 1.414 \\ 1.2925 \\ 0.88419 \\ 0.79853 \\ 0.71641 \end{bmatrix} + 0.72064 \begin{bmatrix} 6.7843 \\ 6.965 \\ 7.1336 \\ 7.7074 \\ 7.8814 \\ 7.9712 \end{bmatrix} = \begin{bmatrix} 6.4343 \\ 6.4343 \\ 6.4343 \\ 6.4385 \\ 6.4782 \\ 6.4608 \end{bmatrix}$$

$$\text{Eval\_H4} = \begin{bmatrix} 1.5453 \\ 1.414 \\ 1.2925 \\ 0.88419 \\ 0.79853 \\ 0.71641 \end{bmatrix} + 0.651 \begin{bmatrix} 6.7843 \\ 6.965 \\ 7.1336 \\ 7.7074 \\ 7.8814 \\ 7.9712 \end{bmatrix} = \begin{bmatrix} 5.9619 \\ 5.9482 \\ 5.9365 \\ 5.9017 \\ 5.9293 \\ 5.9057 \end{bmatrix}$$

$$\text{Eval\_H5} = \begin{bmatrix} 1.5453 \\ 1.414 \\ 1.2925 \\ 0.88419 \\ 0.79853 \\ 0.71641 \end{bmatrix} + 0.4923 \begin{bmatrix} 6.7843 \\ 6.965 \\ 7.1336 \\ 7.7074 \\ 7.8814 \\ 7.9712 \end{bmatrix} = \begin{bmatrix} 4.8852 \\ 4.8429 \\ 4.8044 \\ 4.6785 \\ 4.6785 \\ 4.6406 \end{bmatrix}$$

$$\text{Eval\_H6} = \begin{bmatrix} 1.5453 \\ 1.414 \\ 1.2925 \\ 0.88419 \\ 0.79853 \\ 0.71641 \end{bmatrix} + 0.91448 \begin{bmatrix} 6.7843 \\ 6.965 \\ 7.1336 \\ 7.7074 \\ 7.8814 \\ 7.9712 \end{bmatrix} = \begin{bmatrix} 7.7494 \\ 7.834 \\ 7.816 \\ 7.9325 \\ 8.0059 \\ 8.0059 \end{bmatrix}$$

Step 2.Evaluate the point-normal equation of each hyperplane based on the boundary points, in order to assess how far the boundary points are with respect to each hyperplane using the following error criteria $-0.001 \le \boldsymbol{n}_i \bullet \boldsymbol{P}_{G_K}^{C} - C_i \le 0$:

$$\text{Err\_H1} = \begin{bmatrix} 6.4996 \\ 6.5003 \\ 6.5019 \\ 6.5126 \\ 6.554 \\ 6.5375 \end{bmatrix} - 6.4996 \begin{bmatrix} 1 \\ 1 \\ 1 \\ 1 \\ 1 \\ 1 \end{bmatrix} = \begin{bmatrix} 0 \\ 0.0007 \\ 0.0023 \\ 0.013 \\ 0.0544 \\ 0.0379 \end{bmatrix}$$

$$\text{Err\_H2} = \begin{bmatrix} 6.4749 \\ 6.4749 \\ 6.4759 \\ 6.4845 \\ 6.5253 \\ 6.5084 \end{bmatrix} - 6.4749 \begin{bmatrix} 1 \\ 1 \\ 1 \\ 1 \\ 1 \\ 1 \end{bmatrix} = \begin{bmatrix} 0 \\ 0 \\ 0 \\ 0.0096 \\ 0.0504 \\ 0.0335 \end{bmatrix}$$

$$\text{Err\_H3} = \begin{bmatrix} 6.4343 \\ 6.4343 \\ 6.4343 \\ 6.4385 \\ 6.4782 \\ 6.4608 \end{bmatrix} - 6.4333 \begin{bmatrix} 1 \\ 1 \\ 1 \\ 1 \\ 1 \\ 1 \end{bmatrix} = \begin{bmatrix} 0 \\ 0 \\ 0 \\ 0.0052 \\ 0.0449 \\ 0.0275 \end{bmatrix}$$

$$\text{Err\_H4} = \begin{bmatrix} 5.9619 \\ 5.9482 \\ 5.9365 \\ 5.9017 \\ 5.9293 \\ 5.9057 \end{bmatrix} - 5.9017 \begin{bmatrix} 1 \\ 1 \\ 1 \\ 1 \\ 1 \\ 1 \end{bmatrix} = \begin{bmatrix} 0.0599 \\ 0.0465 \\ 0.0348 \\ 0 \\ 0.0276 \\ 0.004 \end{bmatrix}$$

$$\text{Err\_H5} = \begin{bmatrix} 4.8852 \\ 4.8429 \\ 4.8044 \\ 4.6785 \\ 4.6785 \\ 4.6406 \end{bmatrix} - 4.6785 \begin{bmatrix} 1 \\ 1 \\ 1 \\ 1 \\ 1 \\ 1 \end{bmatrix} = \begin{bmatrix} 0.2067 \\ 0.1644 \\ 0.1259 \\ 0 \\ 0 \\ -0.0379 \end{bmatrix}$$

$$\text{Err\_H6} = \begin{bmatrix} 7.7494 \\ 7.834 \\ 7.816 \\ 7.9325 \\ 8.0059 \\ 8.0059 \end{bmatrix} - 8.0059 \begin{bmatrix} 1 \\ 1 \\ 1 \\ 1 \\ 1 \\ 1 \end{bmatrix} = \begin{bmatrix} -0.2565 \\ -0.1719 \\ -0.1899 \\ -0.0734 \\ 0 \\ 0 \end{bmatrix}$$

The difference errors Err_H1, Err_H2, Err_H3, Err_H4, Err_H5, and Err_H6 are then analyzed to determine how many boundary points can be adjusted by the new approximant hyperplanes according to the specified error criterion.

Step 3. The hyperplanes are sorted in descending order based on the number of points that approximate the boundary, as shown in Table D.3.

Table D.3. Arrangement of hyperplanes.

Hyperplane	**BPn**
H2	BP_1, BP_2, BP_3
H3	BP_1, BP_2, BP_3
H5	BP_4, BP_5
H6	BP_5, BP_6
H1	BP_1
H4	BP_4

Step 4.

a) The set of boundary points that must be adjusted by the approximant hyperplanes is $S_{BP}=\{BP_1, BP_2, BP_3, BP_4, BP_5, BP_6\}$. Given that H2 and H3 have the same number of points, H2 is arbitrarily selected as the first approximant plane containing the three boundary points H2= $\{BP_1, BP_2, BP_3\}$; furthermore, the new set of boundary points to be adjusted by a new approximant hyperplane is $S_{BP}=\{BP_4, BP_5, BP_6\}$.

b) By repeating Step 4a, one has the following: The hyperplane H5 is selected as the second approximant hyperplane for the boundary points $\{BP_4, BP_5\}$, because it includes a greater number of boundary points that do not belong to the approximant

hyperplane H2. In this case, the new set of boundary points to be adjusted by a new approximant hyperplane is $S_{BP}=\{BP_6\}$. Finally, H6 is selected as the last approximant hyperplane to include the boundary point BP_6. Hence, the original number of hyperplanes has been reduced to only three approximant hyperplanes, and the set of boundary points to be adjusted is null, $S_{BP}=\{\emptyset\}$.

Algorithm 2: Inner Product

Step 1. The dot product is calculated between the normal vector to its corresponding *i*-thhyperplane $\mathrm{H}i=[n_{i,1}\ n_{i,2}]$, and all other normal vectors to their corresponding hyperplanes:

$$\mathrm{H1}\square\mathrm{H}k^T=\begin{bmatrix}1.5306\\1.5263\\1.4754\\1.3595\\1.6678\end{bmatrix}\quad\forall\ \ k=1,2,...,6;\ \ k\neq 1$$

$$\mathrm{H2}\square\mathrm{H}k^T=\begin{bmatrix}1.5306\\1.5236\\1.473\\1.3577\\1.6645\end{bmatrix}\quad\forall\ \ k=1,2,...,6;\ \ k\neq 2$$

$$\mathrm{H3}\square\mathrm{H}k^T=\begin{bmatrix}1.5263\\1.5236\\1.4691\\1.3548\\1.659\end{bmatrix}\quad\forall\ \ k=1,2,...,6;\ \ k\neq 3$$

$$\mathrm{H4}\square\mathrm{H}k^T=\begin{bmatrix}1.4754\\1.473\\1.4691\\1.3205\\1.5953\end{bmatrix}\quad\forall\ \ k=1,2,...,6;\ \ k\neq 4$$

$$\mathrm{H5}\square \mathrm{H}k^{T} = \begin{bmatrix} 1.3595 \\ 1.3577 \\ 1.3548 \\ 1.3205 \\ 1.4502 \end{bmatrix} \quad \forall \quad k = 1,2,...,6; \quad k \neq 5$$

$$\mathrm{H6}\square \mathrm{H}k^{T} = \begin{bmatrix} 1.6678 \\ 1.6645 \\ 1.659 \\ 1.5953 \\ 1.4502 \end{bmatrix} \quad \forall \quad k = 1,2,...,6; \quad k \neq 6$$

Step 2. The existing angle between two normal vectors to their corresponding hyperplanes is calculated as follows:

$$\mathrm{H}_{ang(1,k)} = \cos^{-1}\left(\frac{(\mathrm{H1} \bullet \mathrm{H}k)}{\|\mathrm{H1}\|\|\mathrm{H}k\|}\right) = \begin{bmatrix} 0.13626 \\ 0.36113 \\ 3.075 \\ 9.9281 \\ 6.3031 \end{bmatrix} \quad \forall \quad k = 1,2,...,6; \quad k \neq 1$$

$$\mathrm{H}_{ang(2,k)} = \cos^{-1}\left(\frac{(\mathrm{H2} \bullet \mathrm{H}k)}{\|\mathrm{H2}\|\|\mathrm{H}k\|}\right) = \begin{bmatrix} 0.13626 \\ 0.22488 \\ 2.9388 \\ 9.7919 \\ 6.4394 \end{bmatrix} \quad \forall \quad k = 1,2,...,6; \quad k \neq 2$$

$$\mathrm{H}_{ang(3,k)} = \cos^{-1}\left(\frac{(\mathrm{H3} \bullet \mathrm{H}k)}{\|\mathrm{H3}\|\|\mathrm{H}k\|}\right) = \begin{bmatrix} 0.36113 \\ 0.22488 \\ 2.7139 \\ 9.567 \\ 6.6643 \end{bmatrix} \quad \forall \quad k = 1,2,...,6; \quad k \neq 3$$

$$\mathrm{H}_{ang(4,k)} = \cos^{-1}\left(\frac{(\mathrm{H4} \bullet \mathrm{H}k)}{\|\mathrm{H4}\|\|\mathrm{H}k\|}\right) = \begin{bmatrix} 3.075 \\ 2.9388 \\ 2.7139 \\ 6.8531 \\ 9.3782 \end{bmatrix} \quad \forall \quad k = 1,2,...,6; \quad k \neq 4$$

$$\mathrm{H}_{ang(5,k)} = \cos^{-1}\left(\frac{(\mathrm{H5} \bullet \mathrm{H}k)}{\|\mathrm{H5}\|\|\mathrm{H}k\|}\right) = \begin{bmatrix} 9.9281 \\ 9.7919 \\ 9.567 \\ 6.8531 \\ 16.231 \end{bmatrix} \quad \forall \quad k = 1,2,...,6; \quad k \neq 5$$

$$\mathrm{H}_{ang(6,k)} = \cos^{-1}\left(\frac{(\mathrm{H6} \bullet \mathrm{H}k)}{\|\mathrm{H6}\|\|\mathrm{H}k\|}\right) = \begin{bmatrix} 6.3031 \\ 6.4394 \\ 6.6643 \\ 9.3782 \\ 16.231 \end{bmatrix} \quad \forall \quad k = 1,2,...,6; \quad k \neq 6$$

Two normal vectors to their corresponding hyperplanes are considered "parallel" to each other if the angle between them does not exceed five degrees. This yields Table D.4:

Table D.4. Parallel vectors.

Hyperplane vector	**Parallel hyperplane vectors**
H1	H2, H3, H4
H2	H1, H3, H4
H3	H1, H2, H4
H4	H1, H2, H3
H5	0
H6	0

Step 3. The set of planes that must be reduced is S_P = {H1, H2, H3, H4, H5, H6}, while the set of approximant hyperplanes is $S_{AH} = \{\varnothing\}$.

a) Hyperplanes H1, H2, H3 and H4 have an "identical" inclination in the P_G-parameter space with respect to three other different hyperplanes. Without loss of generality, H1 plane is selected as the first approximant plane, which adjusts hyperplanes H2,

H3 and H4. Thus, the resulting new set of hyperplanes to be reduced is S_P = {H5, H6} and the set of approximant hyperplanes is S_{AH} = {H1}.

b) Since H5 and H6 are the only planes that must be approximated and their corresponding normal vectors are not "parallel" to each other, they are automatically included in the set approximant hyperplanes S_{AH} = {H1, H5, H6}, and the set of planes that must be reduced is empty, S_P = {∅}. Thus, the algorithm ends.

Appendix E

E IEEE 54-machine 118-bus System Data

Table E.1: Transmission line parameters.

Buses		*R* (pu)	*X* (pu)	*B*/2 (pu)	Buses		*R* (pu)	*X* (pu)	*B*/2 (pu)
1	2	0.0303	0.0999	0.0254	38	65	0.00901	0.0986	1.046
1	3	0.0129	0.0424	0.01082	64	65	0.00269	0.0302	0.38
4	5	0.00176	0.00798	0.0021	49	66	0.018	0.0919	0.0248
3	5	0.0241	0.108	0.0284	49	66	0.018	0.0919	0.0248
5	6	0.0119	0.054	0.01426	62	66	0.0482	0.218	0.0578
6	7	0.00459	0.0208	0.0055	62	67	0.0258	0.117	0.031
8	9	0.00244	0.0305	1.162	66	67	0.0224	0.1015	0.02682
9	10	0.00258	0.0322	1.23	65	68	0.00138	0.016	0.638
4	11	0.0209	0.0688	0.01748	47	69	0.0844	0.2778	0.07092
5	11	0.0203	0.0682	0.01738	49	69	0.0985	0.324	0.0828
11	12	0.00595	0.0196	0.00502	69	70	0.03	0.127	0.122
2	12	0.0187	0.0616	0.01572	24	70	0.00221	0.4115	0.10198
3	12	0.0484	0.16	0.0406	70	71	0.00882	0.0355	0.00878
7	12	0.00862	0.034	0.00874	24	72	0.0488	0.196	0.0488
11	13	0.02225	0.0731	0.01876	71	72	0.0446	0.18	0.04444
12	14	0.0215	0.0707	0.01816	71	73	0.00866	0.0454	0.01178
13	15	0.0744	0.2444	0.06268	70	74	0.0401	0.1323	0.03368
14	15	0.0595	0.195	0.0502	70	75	0.0428	0.141	0.036
12	16	0.0212	0.0834	0.0214	69	75	0.0405	0.122	0.124
15	17	0.0132	0.0437	0.0444	74	75	0.0123	0.0406	0.01034
16	17	0.0454	0.1801	0.0466	76	77	0.0444	0.148	0.0368
17	18	0.0123	0.0505	0.01298	69	77	0.0309	0.101	0.1038
18	19	0.01119	0.0493	0.01142	75	77	0.0601	0.1999	0.04978
19	20	0.0252	0.117	0.0298	77	78	0.00376	0.0124	0.01264
15	19	0.012	0.0394	0.0101	78	79	0.00546	0.0244	0.00648
20	21	0.0183	0.0849	0.0216	77	80	0.017	0.0485	0.0472
21	22	0.0209	0.097	0.0246	77	80	0.0294	0.105	0.0228
22	23	0.0342	0.159	0.0404	79	80	0.0156	0.0704	0.0187
23	24	0.0135	0.0492	0.0498	68	81	0.00175	0.0202	0.808
23	25	0.0156	0.08	0.0864	77	82	0.0298	0.0853	0.08174
25	27	0.0318	0.163	0.1764	82	83	0.0112	0.03665	0.03796
27	28	0.01913	0.0855	0.0216	83	84	0.0625	0.132	0.0258
28	29	0.0237	0.0943	0.0238	83	85	0.043	0.148	0.0348
8	30	0.00431	0.0504	0.514	84	85	0.0302	0.0641	0.01234
26	30	0.00799	0.086	0.908	85	86	0.035	0.123	0.0276
17	31	0.0474	0.1563	0.0399	86	87	0.02828	0.2074	0.0445
29	31	0.0108	0.0331	0.0083	85	88	0.02	0.102	0.0276
23	32	0.0317	0.1153	0.1173	85	89	0.0239	0.173	0.047
31	32	0.0298	0.0985	0.0251	88	89	0.0139	0.0712	0.01934
27	32	0.0229	0.0755	0.01926	89	90	0.0518	0.188	0.0528
15	33	0.038	0.1244	0.03194	89	90	0.0238	0.0997	0.106
19	34	0.0752	0.247	0.0632	90	91	0.0254	0.0836	0.0214
35	36	0.00224	0.0102	0.00268	89	92	0.0099	0.0505	0.0548
35	37	0.011	0.0497	0.01318	89	92	0.0393	0.1581	0.0414
33	37	0.0415	0.142	0.0366	91	92	0.0387	0.1272	0.03268
34	36	0.00871	0.0268	0.00568	92	93	0.0258	0.0848	0.0218
34	37	0.00256	0.0094	0.00984	92	94	0.0481	0.158	0.0406
37	39	0.0321	0.106	0.027	93	94	0.0223	0.0732	0.01876

37	40	0.0593	0.168	0.042	94	95	0.0132	0.0434	0.0111
30	38	0.00464	0.054	0.422	80	96	0.0356	0.182	0.0494
39	40	0.0184	0.0605	0.01552	82	96	0.0162	0.053	0.0544
40	41	0.0145	0.0487	0.01222	94	96	0.0269	0.0869	0.023
40	42	0.0555	0.183	0.0466	80	97	0.0183	0.0934	0.0254
41	42	0.041	0.135	0.0344	80	98	0.0238	0.108	0.0286
43	44	0.0608	0.2454	0.06068	80	99	0.0454	0.206	0.0546
34	43	0.0413	0.1681	0.04226	92	100	0.0648	0.295	0.0472
44	45	0.0224	0.0901	0.0224	94	100	0.0178	0.058	0.0604
45	46	0.04	0.1356	0.0332	95	96	0.0171	0.0547	0.01474
46	47	0.038	0.127	0.0316	96	97	0.0173	0.0885	0.024
46	48	0.0601	0.189	0.0472	98	100	0.0397	0.179	0.0476
47	49	0.0191	0.0625	0.01604	99	100	0.018	0.0813	0.0216
42	49	0.0715	0.323	0.086	100	101	0.0277	0.1262	0.0328
42	49	0.0715	0.323	0.086	92	102	0.0123	0.0559	0.01464
45	49	0.0684	0.186	0.0444	101	102	0.0246	0.112	0.0294
48	49	0.0179	0.0505	0.01258	100	103	0.016	0.0525	0.0536
49	50	0.0267	0.0752	0.01874	100	104	0.0451	0.204	0.0541
49	51	0.0486	0.137	0.0342	103	104	0.0466	0.1584	0.0407
51	52	0.0203	0.0588	0.01396	103	105	0.0535	0.1625	0.0408
52	53	0.0405	0.1635	0.04058	100	106	0.0605	0.229	0.062
53	54	0.0263	0.122	0.031	104	105	0.00994	0.0378	0.00986
49	54	0.073	0.289	0.0738	105	106	0.014	0.0547	0.01434
49	54	0.0869	0.291	0.073	105	107	0.053	0.183	0.0472
54	55	0.0169	0.0707	0.0202	105	108	0.0261	0.0703	0.01844
54	56	0.00275	0.00955	0.00732	106	107	0.053	0.183	0.0472
55	56	0.00488	0.0151	0.00374	108	109	0.0105	0.0288	0.0076
56	57	0.0343	0.0966	0.0242	103	110	0.03906	0.1813	0.0461
50	57	0.0474	0.134	0.0332	109	110	0.0278	0.0762	0.0202
56	58	0.0343	0.0966	0.0242	110	111	0.022	0.0755	0.02
51	58	0.0255	0.0719	0.01788	110	112	0.0247	0.064	0.062
54	59	0.0503	0.2293	0.0598	17	113	0.00913	0.0301	0.00768
56	59	0.0825	0.251	0.0569	32	113	0.0615	0.203	0.0518
56	59	0.0803	0.239	0.0536	32	114	0.0135	0.0612	0.01628
55	59	0.04739	0.2158	0.05646	27	115	0.0164	0.0741	0.01972
59	60	0.0317	0.145	0.0376	114	115	0.0023	0.0104	0.00276
59	61	0.0328	0.15	0.0388	68	116	0.00034	0.00405	0.164
60	61	0.00264	0.0135	0.01456	12	117	0.0329	0.14	0.0358
60	62	0.0123	0.0561	0.01468	75	118	0.0145	0.0481	0.01198
61	62	0.00824	0.0376	0.0098	76	118	0.0164	0.0544	0.01356
63	64	0.00172	0.02	0.216					

Table E.2: Transformer parameters.

Buses		R_s (pu)	X_s (pu)	Tap T_v	Tap U_v	Buses		R_s (pu)	X_s (pu)	Tap T_v	Tap U_v
8	5	0	0.0267	0.985	1	64	61	0	0.0268	0.985	1
26	25	0	0.0382	0.96	1	65	66	0	0.037	0.935	1
30	17	0	0.0388	0.96	1	68	69	0	0.037	0.935	1
38	37	0	0.0375	0.935	1	81	80	0	0.037	0.935	1
63	59	0	0.0386	0.96	1						

Table E.3: Load parameters.

Bus	P (MW)	Q (MVars)	Bus	P (MW)	Q (MVars)	Bus	P (MW)	Q (MVars)
1	51	27	42	37	23	82	54	27
2	20	9	43	18	7	83	20	10
3	39	10	44	16	8	84	11	7
4	30	12	45	53	22	85	24	15
6	52	22	46	28	10	86	21	10
7	19	2	47	34	0	88	48	10
11	70	23	48	20	11	90	78	42
12	47	10	49	87	30	92	65	10
13	34	16	50	17	4	93	12	7
14	14	1	51	17	8	94	30	16
15	90	30	52	18	5	95	42	31
16	25	10	53	23	11	96	38	15
17	11	3	54	113	32	97	15	9
18	60	34	55	63	22	98	34	8
19	45	25	56	84	18	100	37	18
20	18	3	57	12	3	101	22	15
21	14	8	58	12	3	102	5	3
22	10	5	59	277	113	103	23	16
23	7	3	60	78	3	104	38	25
27	62	13	62	77	14	105	31	26
28	17	7	66	39	18	106	43	16
29	24	4	67	28	7	107	28	12
31	43	27	70	66	20	108	2	1
32	59	23	74	68	27	109	8	3
33	23	9	75	47	11	110	39	30
34	59	26	76	68	36	112	25	13
35	33	9	77	61	28	114	8	3
36	31	17	78	71	26	115	22	7
39	27	11	79	39	32	117	20	8
40	20	23	80	130	26	118	33	15
41	37	10						

Table E.4: Shunt capacitors.

Bus	Q (MVars)	Bus	Q (MVars)
5	-40	74	12
34	14	79	20
37	-25	82	20
44	10	83	10
45	10	105	20
46	10	107	6
48	15	110	6

Table E.5: Power generation bids for the IEEE 118-bus.

Gen	C_{G_i} ($/MWh)	$P_{G_i}^{\max}$ (MW)	Gen	C_{G_i} ($/MWh)	$P_{G_i}^{\max}$ (MW)	Gen	C_{G_i} ($/MWh)	$P_{G_i}^{\max}$ (MW)
1	0.03	0	42	0.03	-59	80	0.03	477
4	0.03	-9	46	0.03	19	85	0.04	0
6	0.03	0	49	0.03	204	87	0.03	4
8	0.03	-28	54	0.03	48	89	0.03	607
10	0.03	450	55	0.03	0	90	0.07	-85
12	0.08	85	56	0.03	0	91	0.03	-10
15	0.03	0	59	0.03	155	92	0.03	0

18	0.03	0	61	0.03	160	99	0.04	-42
19	0.05	0	62	0.05	0	100	0.03	252
24	0.03	-13	65	0.03	391	103	0.03	40
25	0.03	220	66	0.03	392	104	0.03	0
26	0.03	314	69	0.03	0	105	0.03	0
27	0.03	-9	70	0.03	0	107	0.03	-22
31	0.03	7	72	0.03	-12	110	0.09	0
32	0.03	0	73	0.08	-6	111	0.03	36
34	0.06	0	74	0.03	0	112	0.03	-43
36	0.07	0	76	0.04	0	113	0.03	-6
40	0.03	-46	77	0.04	0	116	0.03	-184

Bibliography

[Ajjarapu and Christy, 1992] V. Ajjarapu and C. Christy, "The continuation power flow: A tool for steady state voltage stability analysis", *IEEE Trans. on Power Systems*,Vol. 7, No. 1, February 1992.

[Alsac and Stott, 1974] O. Alsac and B. Stott, "Optimal load flow with steady-state security," *IEEE Trans. Power App. Syst*., vol. PAS-93, no. 3. Pp. 745-751, May 1974.

[Avalos et al., 2008] R. J. Avalos, C. A. Cañizares, and M. F. Anjos, "A practical voltage stability-constrained optimal power flow," in *Proc. 2008 IEEE PES, General Meeting*, pp. 1-6.

[Battistelli et al., 2011] C. Battistelli, C. A. Cañizares, M. Chehreghani-Bozchalui, V. J. Gutierrez-Martinez, and C. R. Fuerte-Esquivel, "Practical Security-Boundary-Constrained Dispatch Models for Electricity Markets," in *Proc. Power Syst. Comp. Conf.*, 2011, pp. 1-7.

[Besanger et al., 2013] Y. Besanger, M. Eremia and N. Voropai, "Major grid blackouts: Analysis, classification, and prevention," in: M. Eremia and M. Shahidehpour, Eds., *Handbook of Electrical Power System Dynamics: Modeling, Stability, and Control.* Hoboken, NJ: Wiley-IEEE press, pp.789- 863, February 2013.

[Bhaskar et al., 2011] M.M. Bhaskar, M. Srinivas, and S. Maheswarapu, "Security constrained optimal power flow (SCOPF)-A comprehensive survey," *IEEETrans. Power Syst.,* vol. 2, pp. 11-20, June 2011.

[Caino de Oliveira et al., 2010] K. R. Caino de Oliveira, L. F. C. Alberto and N. G. Bretas, "A Fast Methodology for Stability Margin Evaluation of Power Systems due to Hopf Bifurcation", *Power and Energy Society General Meeting*, *2010 IEEE*, July 25-29, 2010.

[Cañizares, 2000] C. A. Cañizares, "Power Flow and Transient Stability Models of FACTS Controllers for Voltage and Angle Stability Studies," In Proc. of IEEE/PES Winter Meeting, Singapore, January 2000.

[Cañizares et al., 2001] C. Cañizares, W. Rosehart, A. Berizzi, and C. Bovo, “Comparison of voltage security constrained optimal power flow techniques,” in *Proc. 2001 IEEE PES, Summer Meeting*, pp. 2115-2120.

[Cañizares, 2002] C. A. Cañizares, editor. Voltage stability assessment: Concepts, practices and tools. Technical report, IEEE/PES Power System Stability Subcommittee, August 2002.

[Cañizares and Kodsi, 2006] C. A. Cañizares and S. K. M. Kodsi, “Power system security in market clearing and dispatch mechanisms,” in *Proc. 2006 IEEE PES Power Syst. Conf. Expo.*, pp. 1-6.

[Chattopadhyay and Deqiang, 2000] D. Chattopadhyay and G. Deqiang, “Dispatch optimization incorporating transient and voltage stability constraints,” in *Proc. 2000 IEEE PES Summer Meeting*, pp. 516-521.

[Chiang, 2011] H.-D. Chiang, *Direct Methods for Stability Analysis of Electric Power Systems: Theoretical Foundation*, BCU Methodologies, and Applications, John Wiley &Sons,Inc., New Jersey, 2011.

[Dobson and Lu, 1992] I. Dobson and L. Lu, "Voltage collapse precipitated by the immediate change in stability when generator reactive power limits are encountered," IEEE Trans. on Circuits and Systems-I: Fundamental Theory and Applications, pp. 762-766, September 1992.

[Feng et al., 2000], Z. Feng, V. Ajjarapu and B. Long, “Identification of voltage collapse through direct equilibrium tracing,” IEEE Transactions on Power systems, Vol. 15, No. 1, February 2000, pp. 342-349.

[Flores, Fuerte-Esquivel, Barrera and Carvajal, 2011], J.J.Flores, C.R. Fuerte-Esquivel, J.Barrera, and H.R. Carvajal, “Particle Swarm Optimization Method to Assess a Voltage Stability Region by Multi-Parameter Bifurcation Analysis,” International Review of Electrical Engineering, Vol. 6, No. 6, December 2011, pp. 3102-3110.

[Fourer et al., 2003] R. Fourer, D. M. Gay, and B. W. Kernighan, *AMPL: A Modeling Language for Mathematical Programming*, 2nd ed. Pacific Grove, CA: Thomson, Brooks/Cole, 2003.

[Galiana, 1984] F. D. Galiana, "Load Flow Feasibility and the Voltage Collapse Problem", Proceedings of the 23rd Conference on Decision and Control, Vol. 3, pp. 2098-2103, December 1984.

[Gan et al., 2000] D. Gan, R. J. Thomas, and R. D. Zimmerman, “Stability-constrained optimal power flow,” *IEEE Trans. Power Syst.*, vol.15, no.2, pp.535-540, May 2000.

[Ghasemi and Maria, 2008] H. Ghasemi and A. Maria, "Benefits of Employing an Online Security Limit Derivation Tool in Electricity Markets", in Proc. IEEE-PES General Meeting, July 2008.

[Govaerts, 2000] Willy J. F. Govaerts, *Numerical Methods for Bifurcations of Dynamical Equilibria*, SIAM, 2000.

[Gu et al., 2010] W. Gu, W. Liu and R. Wang, “Study on Prediction-Correction Homotopy Method of Tracking Hopf Bifurcation Point”, *Transmission and Distribution Conference and Exposition, 2010 IEEE PES*, Abril19-22,2010.

[Gu and Cañizares, 2007] X. Gu, and C. A. Cañizares, “Fast Prediction of Loadability Margins Using Neural Networks to Approximate Security Boundaries of Power Systems,” *IET Gen., Trans. Dist.*, vol. 1, no. 3, pp. 466-475, May 2007.

[Gutierrez-Martinez et al., 2011] V.J. Gutierrez-Martinez, C.A. Cañizares, C.R. Fuerte-Esquivel, A. Pizano-Martinez, and X. Gu, "Neural-Network Security-Boundary Constrained Optimal Power Flow," *IEEE Trans. on Power Syst.*, Vol. 26, No.1, pp.63-72, Feb., 2011.

[Gutiérrez-Martínez, 2011-1] V. J. Gutiérrez-Martínez, "Voltage Security Boundary-ConstrainedOptimalPowerFlow," Ph.D. dissertation, Div. de Estudios de Posgrado de la Facultad de Ingeniería Eléctrica, UMSNH, Morelia, Michoacán, México, 2011.

[Guoyun et al., 2005] C. Guoyun, D. J. Hill, and R. Hui, “Continuation of local bifurcations for power system differential-algebraic equation stability model”, *IET Proceedings Generation, Transmission and Distribution*, July 8, 2005.

[Hassard et al., 1981] B. D. Hassard, N. D. Kazarinoff and Y.-H.Wan, *Theory and applications of Hopf bifurcation*, Cambridge University Press, Cambridge, 1981.

[Hill and Mareels, 1990], D. J. Hill and I. M. Y. Mareels, “Stability Theory for Differential/Algebraic Systems with Application to Power System,” IEEE Transactions on Circuits and Systems, Vol. CAS-37, No. 11, 1990, pp. 1416-1423. doi:10.1109/ 31.62415

[Illic and Zaborsky, 2000] M. Illic and J. Zaborsky, *Dynamics and Control of Large Electric Power Systems*, John Wiley & Sons Inc., 2000.

[KNITRO] KNITRO.[Online]. Available: http://www.ziena.com

[Kundur, 1994] P. Kundur, *Power System Stability and Control*, Mc-Graw Hill, 1994.

[Kuznetsov, 1998] Y. A. Kuznetsov, *Elements of Applied Bifurcation Theory*, Second Edition, Springer, 1998.

[Lerm et al., 2003] A. A. P. Lerm, C. A. Cañizares and A. S. e Silva, "Multi-parameter bifurcation analysis of the south brazilian power system," IEEE Trans. on Power Systems, Vol. 18, pp. 737-746, May 2003.

[Makarov et al., 2010] Y. Makarov, P. Du, S. Lu, T. B. Nguyen, X. Guo, J.W. Burns, and J.F. Gronquist. (2010, March). Wide area security region.Pacific Northwest National Lab., USA.[Online]. Available: http://www.pnl.gov/main/ publications/external/technical_reports/PNNL-19331.pdf

[Marsden and McCraken, 1976] J. E. Marsden and M. McCraken, The Hopf Bifurcation and Its Applications. New York: Springer-Verlag, 1976.

[Martínez-Ramos and Quintana, 2009] J. L. Martínez-Ramos and V. H. Quintana, "Optimal and secure operation of transmission systems," in: A. Gómez-Expósito, A. Conejo and C. Cañizares, Eds., *Electric Energy Systems: Analysis and Operation.* Boca Raton, FL:CRC, 2009, pp. 211-264.

[Milano, 2005] F. Milano, "An open source power system analysis toolbox," IEEE Trans. on Power Systems, Vol. 20, No. 3, pp. 1199-1206, August 2005.

[Milano et al., 2005] F. Milano, C. A. Cañizares, and A. J. Conejo, "Sensitivity-based security-constrained OPF market clearing model," *IEEE Trans. Power Syst.*, vol.20, no.4, pp.2051-2060, Nov. 2005.

[Monticelli et al., 1987] A. J. Monticelli, M. V. P. Pereira, and S. Granville, "Security-constrained optimal power flow with post-contingency corrective rescheduling," *IEEE Trans. Power Syst.*, vol. 2, no. 1, pp. 175-182, Feb. 1987.

[Motto et al., 2002] A. Motto, F. Galiana, A. Conejo, and J. Arroyo, "Network-constrained Multiperiod Auction for a Pool-Based Electricity Market," *IEEE Trans. Power Syst.*, vol.17, no. 3, pp. 646-653, Aug. 2002.

[Nayfeh and Balachandran, 1995] A. H. Nayfeh and B. Balachandran, *Applied Nonlinear Dynamics: Analytical, Computational, and Experimental Methods*, Wiley-VCH, 1995.

[Rosehart et al., 1999] W. Rosehart, C. Cañizares, and V. Quintana, "Optimal power flow incorporating voltage collapse constraints," in *Proc. 1999 IEEE PES Summer Meeting*, pp. 820-825.

[Sauer and Pai, 1988] P. W. Sauer and M. A. Pai, *Power system dynamics and stability*. Prentice Hall, 1988.

[Seydel, 1988] R. Seydel, *From Equilibrium to Chaos: Practical Bifurcation and Stability Analysis*, Elsevier Science Ltd, 1988.

[Simon and Blume, 1994] C. P. Simon and L. Blume, *Mathematics for economists.* New York, NY:W.W. Norton& Company, Inc., 1994, pp. 226-230.

[Stott et al., 1987] B. Stott, O. Alsac, and A. Monticelli, "Security analysis and optimization," *Proc. of the IEEE*, Vol. 75, no. 12, pp. 1623-1644, Dec. 1987.

[Stott and Alsac, 2012] B. Stott and O. Alsac, "Optimal Power Flow—Basic Requirements for Real-life Problems and their Solutions," white paper, July 2012. [On Line.] Available: www.ieee.hr/_download/repository/Stott-Alsac-OPF-White-Paper.pdf

[Taylor, 1994] C. W. Taylor, *Power System Voltage Stability*, Mc-Graw Hill, 1994.

[Thompson and Stewart, 1986] J. M. T. Thompson and H. B. Stewart, *Nonlinear Dynamics and Chaos. Chichester*, England: John Wiley & Sons, 1986.

[University of Washington]. Online available: http://www.ee.washington.edu/research/pstca/.

[Van Cutsem and Vournas, 2008] T. Van Cutsem and C. Vournas, *Voltage stability of electric power systems*, Springer, 2008.

[Venkatasubramanian et al., 1995] V. Venkatasubramanian, H. Schättler, and J. Zaborszky, "Local Bifurcations and Feasibility Regions in Differential-Algebraic Systems", *IEEE Trans. on Automatic Control*, Vol. 49, No. 12, December 1995.

[WSCC, 1996] Western Systems Coordinating Council (WSCC), "Power systems outages that occurred in the western interconnection on july 1996", technical report, September 1996.

[Wu and Kumagai, 1982] F. Wu and S. Kumagai, "Steady-state security regions of power systems," *IEEE Trans. Circuits Syst., I: Fund. Theory Appl.,* vol.29, no.11, pp. 703-711, Nov. 1982.